Mechanistic Studies on the Cope Rearrangement and Investigations of Organocatalytic Claisen Rearrangement and Photochemical Reactions

By

HYUNJUNE JUN

Department of Chemistry, McGill University, Montreal

April 2020

A thesis submitted to McGill University in partial fulfillment of the requirements of the degree of Master of Science

TABLE OF CONTENTS

Abstract

Part A

While several catalytic methods of the Claisen rearrangement using Lewis acids and transition metals have been developed in the past years, only one example of an organocatalytic Claisen rearrangement using a hydrogen-bond donor catalyst has been reported. Recently, our research group published the first example of an iminium catalyzed Cope rearrangement using a diazepane carboxylate catalyst, which was shown to be efficient in forming α-substituted iminium ions. Inspired by our success with the Cope rearrangement, we investigated the application of the diazepane carboxylate catalyst in the iminium catalyzed Claisen rearrangement. Our research efforts focused on identifying the appropriate substrates that can undergo Claisen rearrangement under our iminium catalysis conditions. Preliminary studies by Dr. Kaldre showed that the aliphatic Claisen substrates were prone to decomposition under our acidic iminium catalysis conditions. In our studies, the aromatic Claisen substrates were shown to be robust under acidic conditions, and the diazepane carboxylate catalyst was efficient in forming iminium ions with these substrates. However, an unexpected decomposition pathway was identified under our iminium catalysis conditions, and further investigations led us to conclude that the aromatic Claisen substrates are not compatible with our iminium catalysis, potentially due to the formation of highly reactive intermediates or products which are prone to other decomposition pathways.

Part B

In our iminium catalyzed Cope rearrangement, we found that the larger ring sized hydrazide catalyst, particularly the 7-membered ring, was most efficient in catalyzing the Cope rearrangement of a variety of 2-formyl-1,5-hexadienes. In our previous studies, Dr. Häggman showed that the larger ring sized hydrazide catalyst had a lower proton affinity and basicity compared to the small ring congeners. We hypothesized the higher reactivity of the 7-membered hydrazide catalyst was from the reduced proton affinity of the amine, facilitating the proton transfer steps in the iminium ion formation, and we proposed that the iminium ion formation should be the rate-limiting step of our Cope rearrangement. Our density functional theory calculations suggested a stepwise mechanism for this rearrangement, proceeding through an intermediate carbocation. However, Houk's group proposed that the observed reactivity trend has

to do with the relative rigidity/flexibility of the cyclic hydrazide catalyst, and the rate-limiting step is the Cope rearrangement and not the iminium ion formation. This part of the thesis describes our mechanistic experiments performed in collaboration with the Houk research group to determine the mechanism and the origin of rate acceleration by the cyclic hydrazide catalysts. The reaction kinetics for different ring sized hydrazide catalysts have been measured, and the carbon kinetic isotope effect for a model reaction has been experimentally determined to elucidate the reaction mechanism of our Cope rearrangement. Current results suggest that our model reaction proceeds through a concerted mechanism with the Cope rearrangement as the rate-limiting step, but the reaction may also proceed through a stepwise mechanism depending on the substituents.

Part C

The synergistic combination of photoredox catalysis and organocatalysts has enabled the activation of inert substrates towards useful chemical transformations. From our previous investigations, we found that the 7-membered hydrazide catalyst was highly efficient in forming iminium ions compared to other secondary amines. The purpose of this investigation was to merge photoredox catalysis with iminium catalysis, by taking advantage of the high reactivity of the hydrazide catalyst. The two studied reactions were the reductive radical cyclization and the decarboxylative radical cyclization of α, β-unsaturated aldehydes. For the reductive cyclization, current results suggest that the β-enaminyl radicals generated from our hydrazide catalyst may be electron-poor and not nucleophilic enough to undergo the anticipated radical addition pathway. For the decarboxylative radical cyclization, current results suggest that the reactivity is highly dependent on the stability of the alkyl radicals, as well as the reaction solvent used.

Résumé

Partie A

Plusieurs méthodes catalytiques pour le réarrangement de Claisen utilisant des acides de Lewis et des métaux de transitions ont été développées durant les dernières années, tandis qu'il y a eu seulement un exemple de méthode organocatalytique pour le réarrangement de Claisen utilisant un catalyseur par liaison hydrogène. Récemment, notre groupe de recherche a publié le premier exemple de réarrangement de Cope par catalyse iminium utilisant un carboxylate d'éthyl diazépane qui s'est avéré efficace pour la formation des ions iminium α-substitués. Inspiré par notre réussite avec le réarrangement de Cope, nous avons investigué l'application de carboxylate d'éthyl diazépane pour le réarrangement de Claisen par catalyse iminium. Nos efforts de recherche ont été concentrés sur l'identification des substrats appropriés qui peuvent suivre le réarrangement de Claisen sous nos conditions de catalyse iminium. Les études préliminaires par Dr. Kaldre ont démontré que les substrats aliphatiques de Claisen sont sujets à la décomposition sous nos conditions acidiques de catalyse iminium. Dans nos études, les substrats aromatiques de Claisen se sont montrés robustes sous des conditions acidiques, et le carboxylate d'éthyl diazépane a été efficace pour former des ions iminium avec ces substrats. Toutefois, une décomposition inattendue a été identifiée sous nos conditions de catalyse iminium, et d'après nos recherches supplémentaires, nous avons conclu que les substrats aromatiques de Claisen ne sont pas compatibles avec notre catalyse iminium, possiblement en raison de la formation des intermédiaires ou des produits réactifs qui sont sujettes aux autres voies de décomposition.

Partie B

Dans notre réarrangement de Cope par catalyse iminium, nous avons découvert que le catalyseur hydrazide avec la grande taille du cycle, telle que la taille 7, est le plus efficace à catalyser le réarrangement de Cope pour les 2-formyl-1,5-diènes. Dans nos études précédentes, Dr. Häggman a montré que le catalyseur hydrazide avec la grande taille du cycle a une affinité aux protons et une basicité inférieures comparé aux congénères de petite taille. Nous avons émis l'hypothèse que la haute réactivité du catalyseur de taille 7 est causé par l'affinité aux protons réduite de l'amine, et cela facilite les transferts du proton durant la formation d'ion iminium. Nous avons aussi proposé que la formation d'ion iminium devrait être l'étape cinétiquement limitante

de notre réarrangement de Cope. Nos calculs de théorie de densité fonctionnelle ont suggéré un mécanisme réactionnel par étapes impliquant un intermédiaire carbocation. Toutefois, le groupe de Houk a proposé que la réactivité observée a à avoir avec la rigidité/flexibilité du catalyseur hydrazide cyclique, et que l'étape cinétiquement limitante est le réarrangement de Cope et pas la formation d'ion iminium. Cette partie de thèse décrit nos expériences mécanistiques performées en collaboration avec le groupe de Houk pour déterminer le mécanisme et l'origine de la vélocité de la réaction par le catalyseur hydrazide cyclique. Les cinétiques chimiques pour différents catalyseurs cycliques ont été mesurées, et l'effet isotopique cinétique du carbone pour une réaction modèle a été déterminé expérimentalement pour élucider le mécanisme de notre réarrangement de Cope. Les résultats actuels sur notre réaction modèle suggèrent un mécanisme concerté avec le réarrangement de Cope étant l'étape cinétiquement limitante, mais la réaction peut également se procéder par un mécanisme par étapes dépendamment des substituants.

Partie C

La combination synergique de la catalyse photorédox et organocatalyseurs a permit l'activation des substrats inertes pour des transformations chimiques utiles. De nos études précédentes, nous avons découvert que le catalyseur hydrazide de taille 7 est très efficace à former des ions iminium comparé aux autres amines secondaires. L'objectif de cette investigation a été de combiner la catalyse photorédox avec la catalyse iminium en prenant l'avantage de haute réactivité du catalyseur hydrazide. Les deux réactions étudiées sont la cyclisation radicalaire réductrice et la cyclisation radicalaire décarboxylative d'aldéhydes α, β- insaturés. Pour la cyclisation réductrice, les résultats actuels suggèrent que les radicaux β-énaminyle générés par notre catalyseur hydrazide sont pauvres en électrons, et ils ne sont pas assez nucléophiliques pour performer l'addition radicalaire prévue. Pour la cyclisation radicalaire décarboxylative, les résultats actuels suggèrent que la réactivité est fortement dépendante sur la stabilité des radicaux alkyles et le solvant utilisé pour la réaction.

ACKNOWLEDGEMENTS

I would like to first thank my supervisor, Dr. James L. Gleason, for giving me the opportunity to join his research group and work on interesting and rewarding projects. I truly appreciated his support and patience despite my mistakes. His guidance, teaching and knowledge of chemistry were invaluable and they shaped me as a scientist.

I would like to thank Dr. Scott Bohle for introducing me to the area of research during my undergraduate studies, and I really appreciated his support for my graduate school applications. I also want to thank Dr. J-P Lumb for his teaching in organic chemistry and for helpful discussions about chemistry and advices on the career path. Special thanks to all the professors who taught me advanced organic chemistry courses, Dr. J-P Lumb, Dr. C-J Li, and Dr. N. Moitessier.

I would like to thank Chantal Marotte and Sandra Aerssen for their administrative assistances and sending important reminders. Special thanks to Dr. Nadim Saadé and Dr. Alex Wahba for taking time to analyze my compounds in the McGill mass spectrometry facility. Many thanks to Dr. Robin Stein for helpful discussions and setting up NMR methods for my KIE experiments. This project would not have been possible without your help and support.

Since I joined Dr. Gleason's research group, I had a chance to meet amazing and talented lab mates. I will start with the senior students. Thank you, Jon, for teaching the titration method, and Adam for answering my chemistry questions and teaching laboratory techniques. Thank you, Ryan, for helpful discussions and being a great mentor sitting next to me, and Sam for introducing me to the lab in the beginning and kindly answering my questions. Thank you, Josie, for taking charge of the chemical orderings and being a great lab mate, and Ali for your useful advices and kindness. I wish you good luck in your studies in Ottawa. Thank you, Donald, for helpful discussions and funny comments, David for being friendly and knowledgeable in chemistry and other subjects, and Yufei for being a nice lab mate sharing the fume hood with me. Good luck in your future studies. Thank you, Anthony, for asking me questions as well as giving me tips and advices, Zhizhong for being nice and smiley, and Kelly for being very patient with me. Good luck to Charles and Melissa in your undergraduate studies.

Finally, I want to thank my parents for their love and support, and I would not be here today without their endless prayers. Thank you for teaching me important life lessons and

always trusting me in what I do. I would like to thank my big brother for his advices and useful discussions about life in general. You are my great source of inspiration and motivation, and I truly appreciate your support.

List of Figures

List of Schemes

List of Tables

List of Abbreviations

Å	angstrom
Ac	acetyl
aq.	aqueous
Ar	aryl
α	alpha
Bn	benzyl
Boc	di-tert-butyl decarbonate
Bu	butyl
β	beta
cat.	catalytic
CFL	compact fluorescent lamp
cm^{-1}	wavenumber
˚C	Celsius
d	day / doublet
D	deuterated
DABCO	1,4-diazabicyclo [2.2.2] octane
DCM	dichloromethane
DEPT	distortionless enhancement by polarization transfer
dF	difluoro-
DFT	density functional theory
DIBAL-H	diisobutylaluminium hydride
DIPEA	diisopropylethylamine
DMF	dimethylformamide
DME	dimethoxyethane
DMP	Dess-Martin periodinane
DMSO	dimethylsulfoxide
d.r.	diastereomeric ratio
δ	delta / partial charge

E	energy
ΔE	energy difference
E^+	electrophile
ee	enantiomeric excess
equiv.	equivalent
EtOAc	ethyl acetate
ESI	electron spray ionization
Et_2O	diethyl ether
Et	ethyl
eV	electron volts
g	gram
ΔG	Gibb's free energy
γ	gamma
H	hour
ΔH	enthalpy
HOMO	highest occupied molecular orbital
HFIP	hexafluoro isopropanol
HMPA	hexamethylphosphoramide
HRMS	high resolution mass spectrometry
Δ	heat
IBX	2-iodoxybenzoic acid
IR	infrared
J	coupling constant
k	spring constant
kcal	kilocalorie
L	liter
LDA	lithium diisopropyl amine
LED	light emitting diode
LUMO	lowest occupied molecular orbital
m	multiplet / reduced mass
M	molar

*m*CPBA	meta-chlorobenzoic acid
Me	methyl
min	minute
mL	milliliter
mmol	millimole
nm	nanometer
Nu	nucleophile
PCC	pyridinium chlorochromate
p-Ts	para toluenesulfonyl
ph	phenyl
pH	hydrogen ion concentration
rt	room temperature
s	second
TBS	tert-butylsilyl
THF	tetrahydrofuran
TMS	trimethylsilyl
TS	transition structure
ǂ	transition state
TLC	thin layer chromatography
*u*L	microliter
UV	ultraviolet
W	watt

Chapter 1. Effort towards an organocatalytic Claisen rearrangement

1.1 The origin of Claisen and Cope rearrangement

The Claisen rearrangement was first discovered in 1912, and it is the earliest example of a [3,3]-sigmatropic rearrangement, a thermally allowed pericyclic process[1]. A sigmatropic rearrangement is an intramolecular process in which a σ-bond adjacent to a π-system migrates from one position to another, forming a new σ-bond and causing a re-organization of a π-system[2]. In a [3,3]-sigmatropic rearrangement, the numbers in the square brackets denote the order of the rearrangement, and they indicate that the newly formed σ-bond has a 3,3-relationship relative to the old σ-bond (Scheme 1.1 (i)).

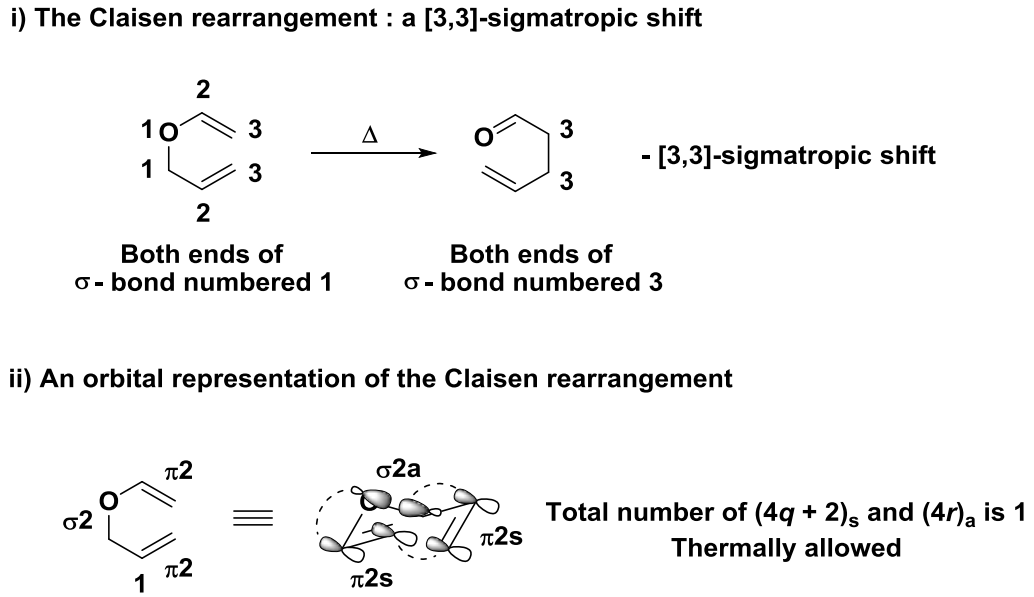

Scheme 1.1 The Claisen rearrangement and the orbital representation

The Claisen rearrangement follows the Woodward-Hoffman's orbital symmetry rules which state that thermal pericyclic reactions are symmetry-allowed when the total number of $(4q + 2)_s$ and $(4r)_a$ components is odd[2]. The terms $(4q + 2)_s$ and $(4r)_a$ represent the number of electron in the component where '*q*' and '*r*' are integers and the subscripts 's' and 'a' stand for suprafacial and antarafacial, respectively. In a suprafacial component, the bond that is made or broken lies on the same face of the reacting system, whereas in an antarafacial component, the newly formed or

broken bond lies on opposite faces of the system. This concept can be visualized using a simple allyl vinyl ether **1** for the Claisen rearrangement (Scheme 1.1 (ii)). The allyl vinyl ether **1** has a total of three ($4q + 2$) components: two π^2 and one σ^2 components, where π and σ denote the type of electron. By joining the orbitals that are forming new bonds, there is a total of one $(4q + 2)_s$ component ($\pi^2{}_s$), which makes the Claisen rearrangement a thermally allowed pericyclic process.

One of the well-known examples of Claisen rearrangement is the thermal rearrangement of allyl phenyl ether **2** to 2-allyl ketone **3** which quickly tautomerizes to 2-allyl phenol **4** (Scheme 1.2 (i)). Allyl vinyl ethers such as **5** are also known to undergo Claisen rearrangement to give γ, δ-unsaturated carbonyl compounds such as **7**, and the reaction proceeds through a chair-like transition state **6** which allows the stereochemical outcomes to be readily predicted (Scheme 1.2 (ii)). Analogously, the Cope rearrangement, which was discovered in 1940[3], is another example of a [3,3]-sigmatropic rearrangement which involves thermal isomerization of 1,5-hexadienes such as **8**, and the reaction also proceeds via the chair-like transition state **9** (Scheme 1.2 (iii)).

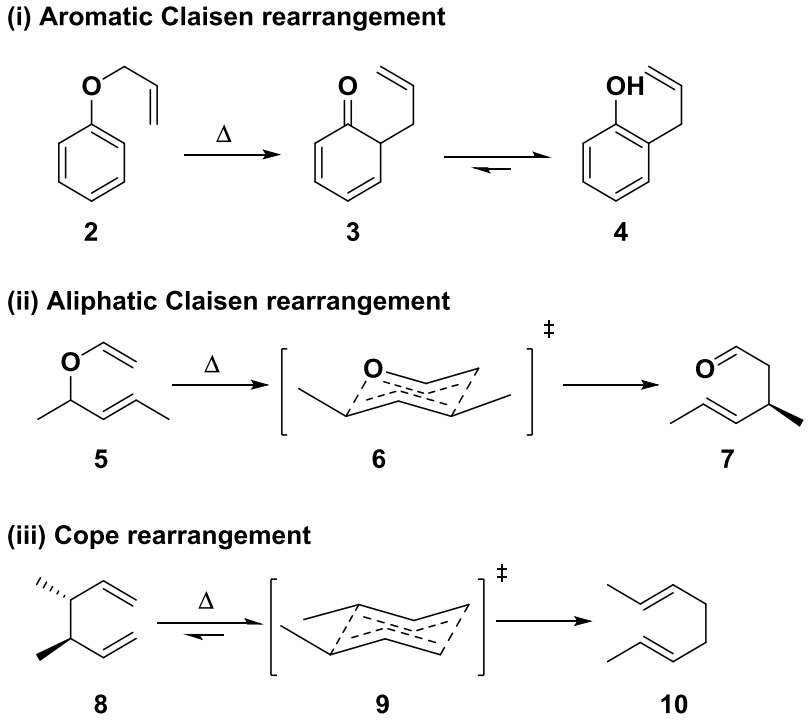

Scheme 1.2 Thermal Claisen and Cope rearrangement

In both Claisen and Cope rearrangement, the uncatalyzed versions typically require harsh thermal conditions to proceed. In the case of the Cope rearrangement, the reaction is reversible,

and the equilibrium lies towards the thermodynamically favored substrate. For the aliphatic Claisen rearrangement, the reaction is irreversible, with the formation of a carbonyl serving as a thermodynamic driving force. One of the examples that employs both of these synthetically useful reactions is the industrial synthesis of citral **15** (Scheme 1.3). The allyl vinyl ether **13** generated by the acid catalyzed condensation of aldehyde **11** and allylic alcohol **12** undergoes sequential thermal Claisen and Cope rearrangement to afford citral **15**.

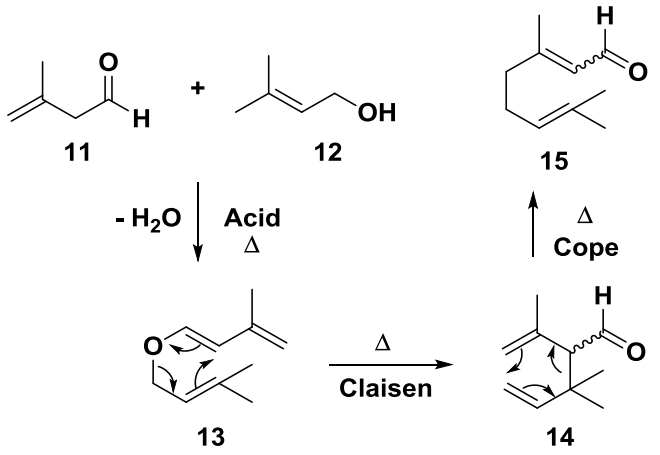

Scheme 1.3 Industrial synthesis of citral using tandem Claisen/Cope sequence

1.2 Variations of Claisen rearrangement

Since its discovery, many variations of the Claisen rearrangement have been developed to expand its scope and applicability in organic synthesis. The Eschenmoser-Claisen rearrangement (1964)[4] is a reaction between an allylic or benzylic alcohol and *N*,*N*-dimethylacetamide dimethyl acetal to generate γ, δ-unsaturated amide (Scheme 1.4 (i)). Upon heating, the allylic alcohol **16** and *N*,*N*-dimethylacetamide dimethyl acetal **17** form the ketene aminal intermediate **18** which subsequently undergoes [3,3]-sigmatropic rearrangement via a chair-like transition state **19** which avoids the destabilizing 1,3-diaxial interaction compared to the transition state **20**, giving (*E*)-alkene **21** as a major product vs. (*Z*)-alkene **22**. During the total synthesis of (+)-pravastatin (1992)[5], Daniewski et al. used Eschenmoser-Claisen rearrangement to generate key intermediate **24** by heating the substrate **23** with acetal **17** at 130 °C for 48 h (Scheme 1.4 (ii)).

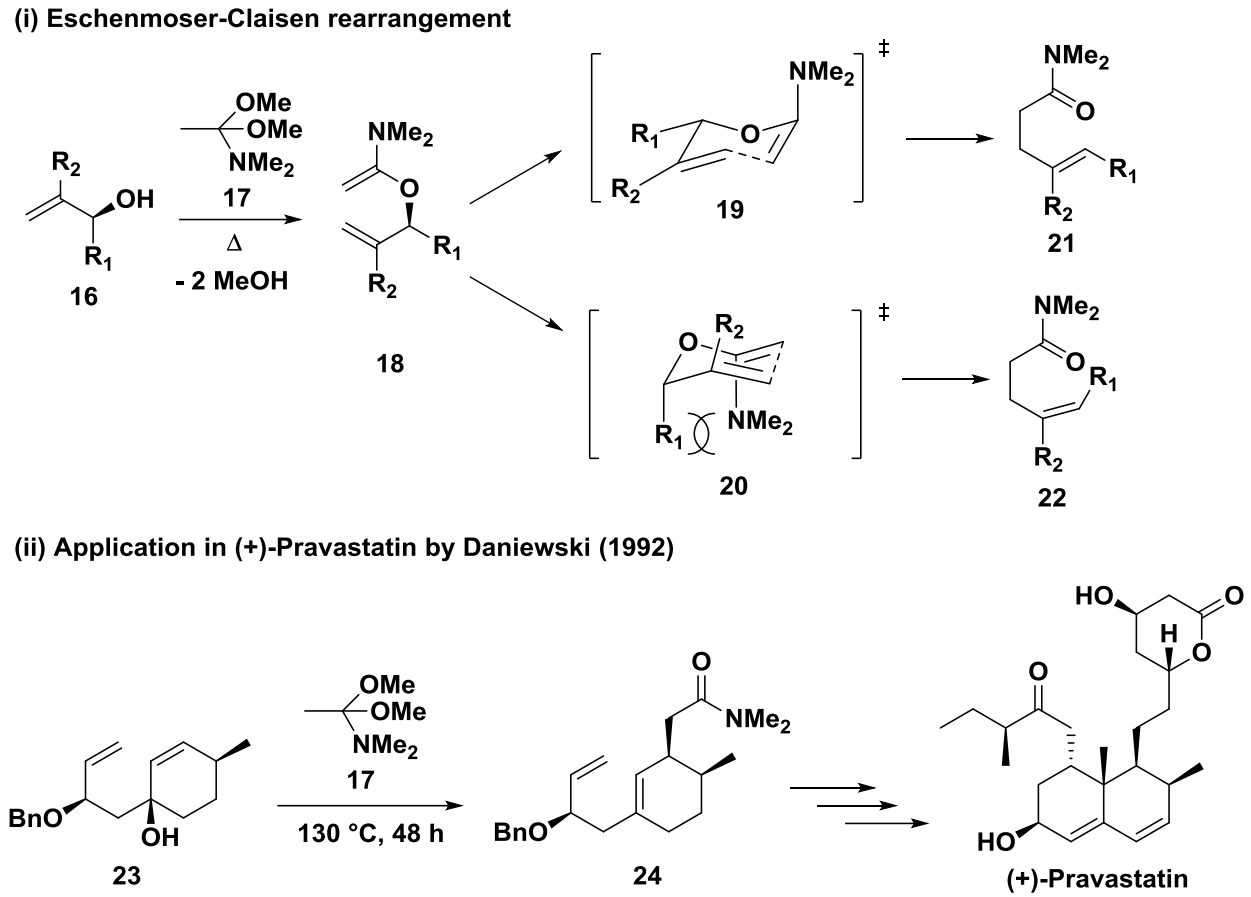

Scheme 1.4 Eschenmoser-Claisen rearrangement and its application by Daniewski

A related variant, the Johnson-Claisen rearrangement, is the reaction between the allylic alcohol **25** and trialkyl orthoacetate **26** to generate the ketene acetal **27**, and the rearrangement produces γ, δ-unsaturated ester **29** as a major product with (*E*)-stereochemistry of the double bond (Scheme 1.5 (i))[6]. Johnson-Claisen / Claisen rearrangement cascade has been used during the total synthesis of (-)-lepenine by Fukuyama in 2014[7]. Heating the allylic alcohol **30** at reflux in triethyl orthoacetate **31** in the presence of 5 mol% of 4-nitrophenol generated the ketene acetal intermediate **32**, and a combination of Johnson-Claisen and aromatic/ Claisen rearrangement proceeded smoothly to afford the product **33** in 85% albeit, with a long reaction time (Scheme 1.5 (ii)).

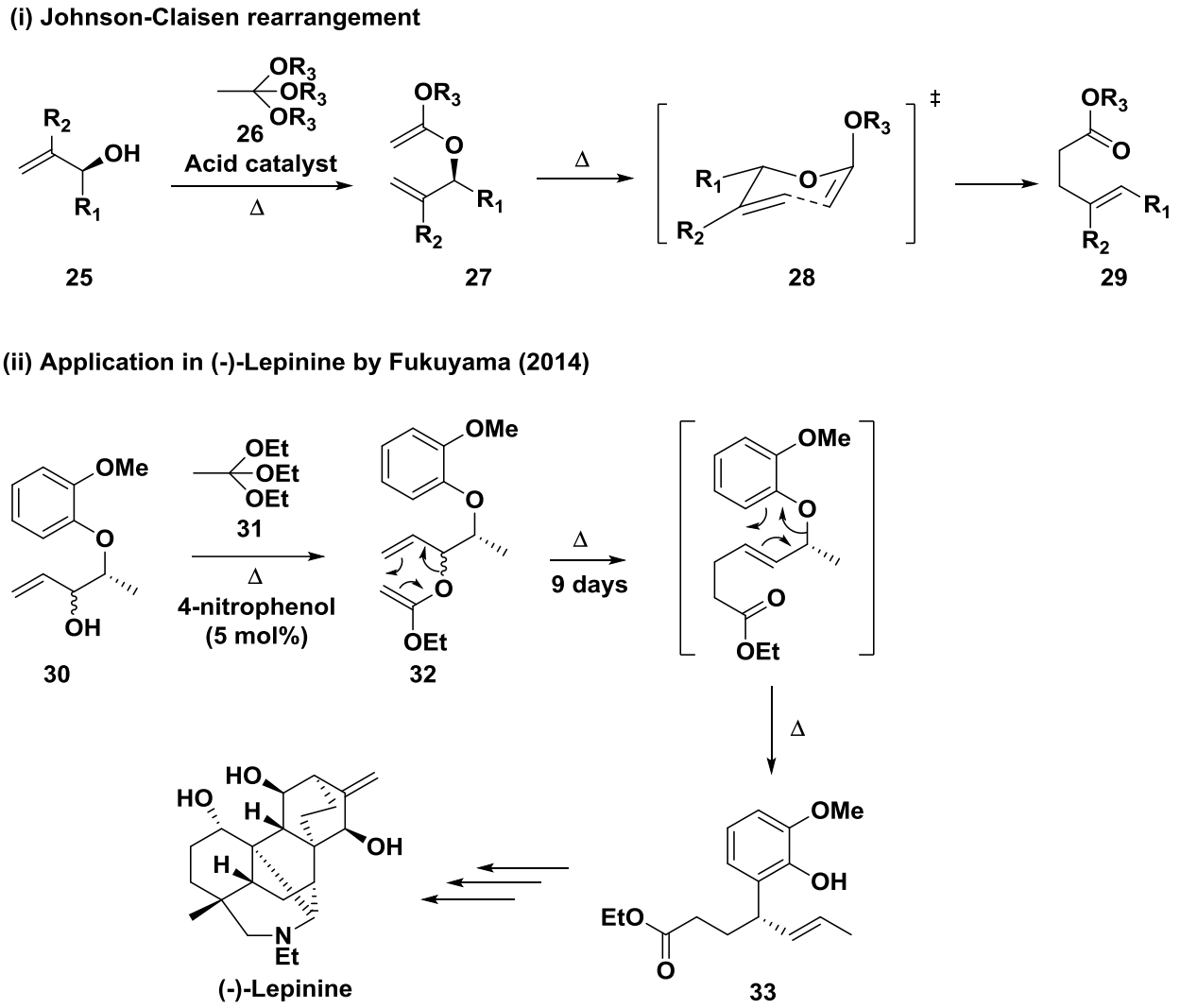

Scheme 1.5 Johnson-Claisen rearrangement and its application by Fukuyama

In 1972, Ireland et al. developed the [3,3]-sigmatropic rearrangement of *O*-trialkylsilylketene acetals to γ, δ-unsaturated carboxylic acids, known as the Ireland-Claisen rearrangement[8] (Scheme 1.6 (i)). This reaction takes place under much milder conditions than regular Claisen rearrangement, typically at a room temperature. The reaction starts with the deprotonation of an allyl ester **34** to make either the (*Z*) or the (*E*) silyl ketene acetals **35** and **36**. The (*Z*) or (*E*) enolate geometry results in an *anti* or *syn* stereochemistry in final products via chair-like transition states **37** or **38** to afford the (*E*)-product **39** or (*Z*)-product **40**. The Ireland-Claisen rearrangement has been used in the formal total synthesis of (+)-zaragozic acid C by Rizzacasa et al. to generate a carbon-carbon bond and two asymmetric centers simultaneously[9] (Scheme 1.6

(ii)). The formation of (*Z*)-silyl enol ether from the ester **41** effected Ireland-Claisen rearrangement via the chair-like transition state **42** to give the product **43** as the major isomer along with three minor isomers in a 3.6:1 ratio.

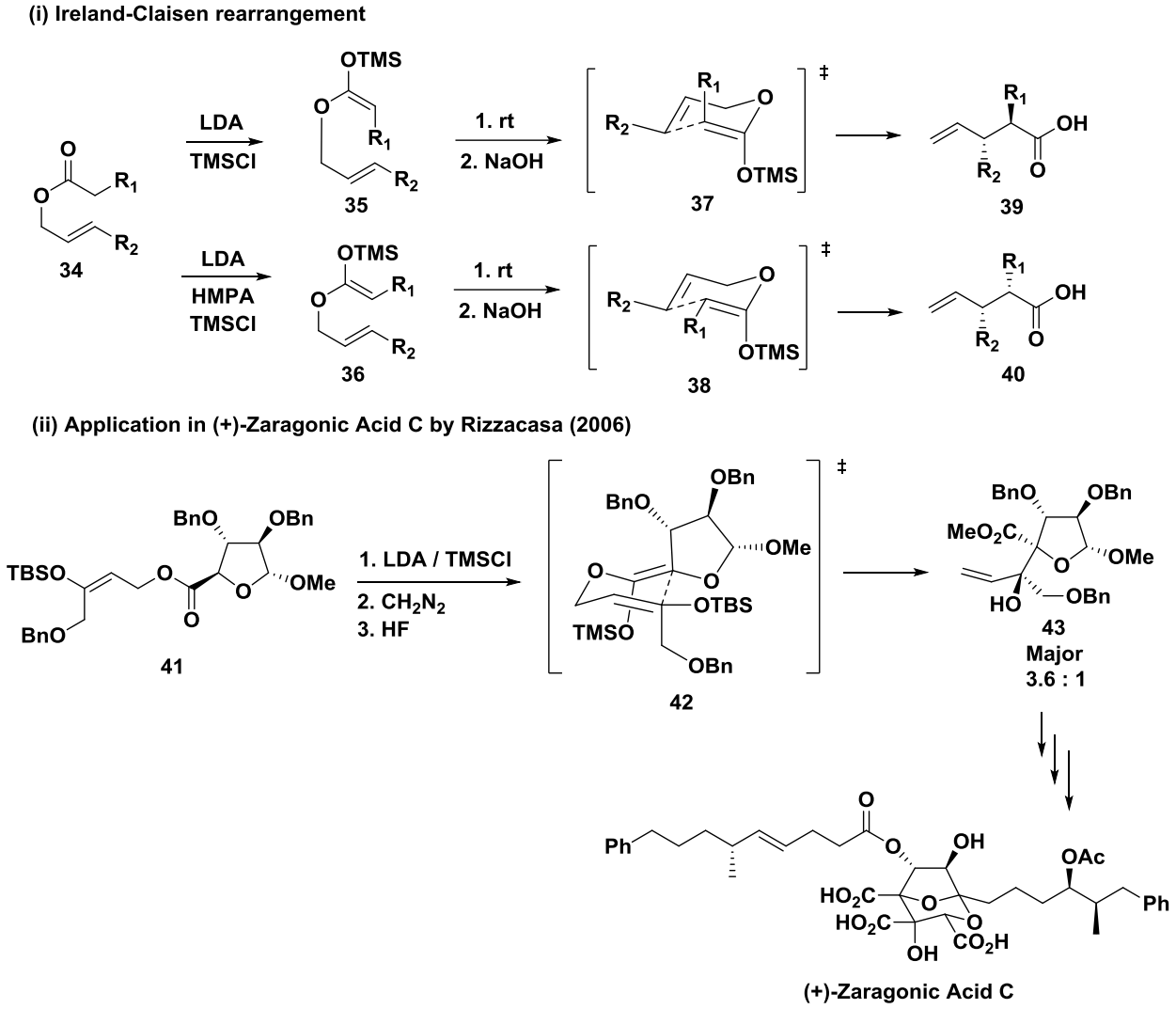

Scheme 1.6 Ireland-Claisen rearrangement and its application by Rizzacasa

Apart from the variants of Claisen rearrangement briefly discussed above, the Bellus-Claisen[10], Gosteli-Claisen[11], Aza/Thio-Claisen[12,13], and many other variations have also been developed to date. As exemplified by their applications in total synthesis, these variants of Claisen rearrangement are useful in building molecular complexity.

1.3 Catalysis of Claisen Rearrangement

Interestingly, Claisen rearrangement is also observed in primary metabolism. Chorismate mutase, which is an enzyme widely found in bacteria, fungi and plants, catalyzes the Claisen rearrangement of chorismate ion **44** to the prephenate ion **46** via the chair-like transition state **45**. Prephenate is an important intermediate in the biosynthesis of phenylalanine and tyrosine[14,15] (Scheme 1.7).

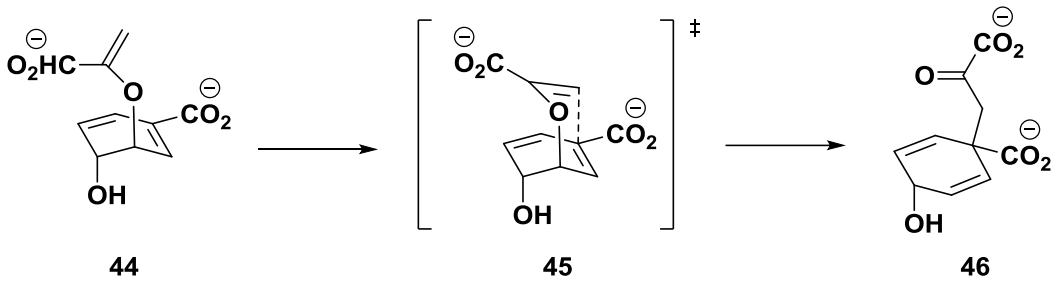

44 **45** **46**

Scheme 1.7 Conversion of chorismate to prephenate via Claisen rearrangement

The x-ray structure of Chorismate mutase in *Escherichia Coli* has been elucidated by Ganem et al.[16] (Figure 1.1). The enzyme catalyzes the reaction by a factor of more than 10^6, and this exceptional rate acceleration can be explained by the formation of enzyme-substrate complex that restricts the substrate to its active conformation, and also by the electrostatic stabilization of transition state via hydrogen bonding interactions between the chorismate ion and the surrounding protein residues[17].

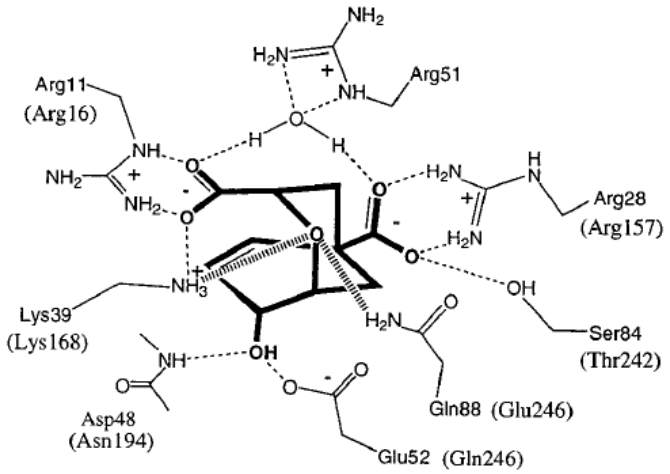

Figure 1.1 Structure of enzyme and substrate at the active site in *Escherichia Coli*

It has previously been observed that the rate of Claisen rearrangement of allyl vinyl ether systems were faster in polar and hydrogen bonding solvents[18,19]. It was viewed that the mechanism of Claisen rearrangement is a concerted, but asynchronous process where the C-O bond breakage and C-C bond formation does not happen at the same time, and this finding has been supported by earlier computational studies and deuterium isotope effects [20,21,22]. Although the extent of C-O bond breakage and C-C bond formation depends on the specific substrate, this asynchronicity suggests that there is a polarization with a slight degree of charge separation in the transition state of Claisen rearrangement. Using quantum mechanical computational methods, Jorgensen advanced a simple model system for the aqueous acceleration of the Claisen rearrangement in water, and he showed that there are hydrogen bonding interactions from two water molecules which stabilize the partial negative charge that is developed on the oxygen atom of allyl vinyl ether during the transition state[23] (Scheme 1.8). These results suggested that potential catalysis could be achieved by the electrostatic stabilization of partial negative charge on the oxygen atom of allyl vinyl ethers during the transition state.

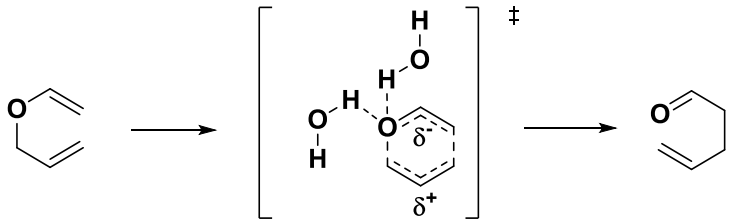

Scheme 1.8 Electrostatic stabilization of transition state by water molecules

Inspired by above findings, current methods for the catalysis of Claisen rearrangement often rely on the activation of oxygen atom of allyl vinyl ether by transition metals or hydrogen-bond donating catalysts. There are also few examples with the activation of olefins with transition metal catalysts.

1.3.1 Lewis acid catalyzed Claisen rearrangements

In Lewis acid catalyzed Claisen rearrangements, the metal typically coordinates to the oxygen atom of allyl vinyl ether which weakens the C-O bond, and it also stabilizes the partial negative charge that develops in the transition state.

The Yamamoto group found that aluminum-based chiral Lewis acids, such as binaphthol **47** can promote the Claisen rearrangement of allyl vinyl ether **48** to afford product **50** in good yield and enantioselectivity (Scheme 1.9 (i))[24, 25]. On binding to **47**, substrate **48** forms a preferable six-membered chair-like transition state **49**. However, the reaction employs stoichiometric amount of the Lewis acid, and some of the substrates such as **51** had issues with the regioselectivity, giving a mixture of [3,3] and [1,3]-sigmatropic rearrangement products **52** and **53** (Scheme 1.9 (ii)).

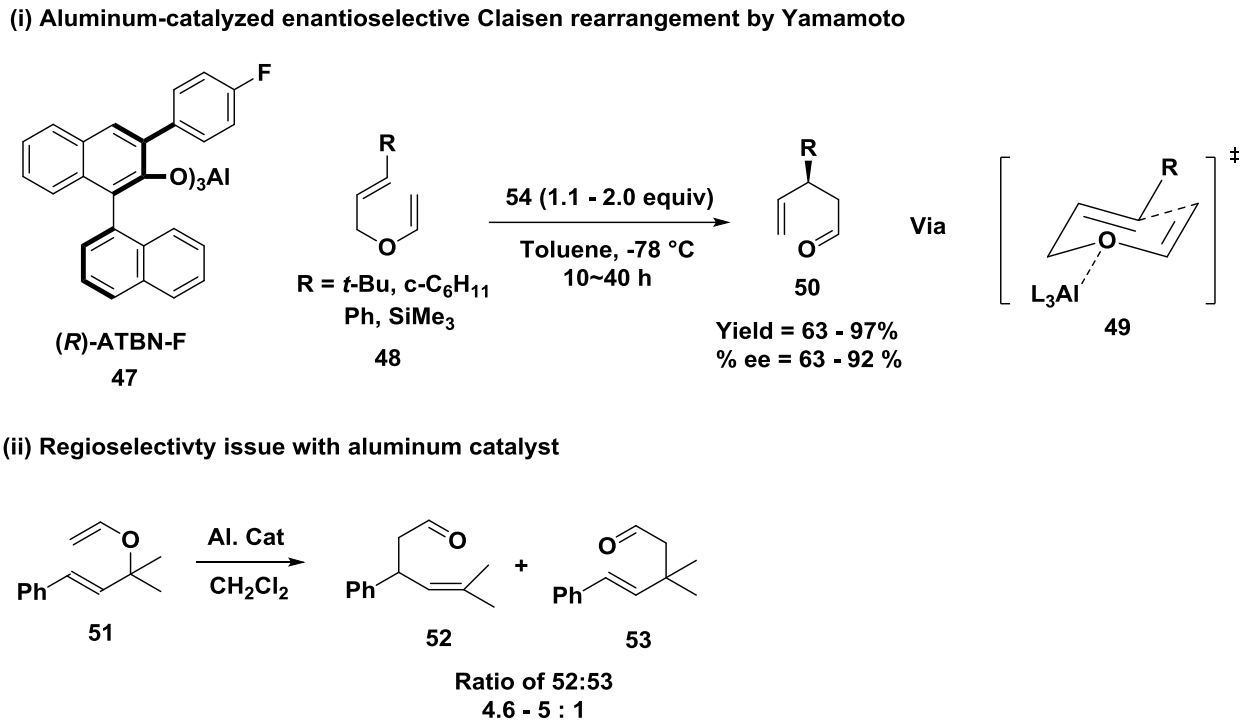

Scheme 1.9 Aluminum-catalyzed Claisen rearrangement by Yamamoto

The Hiersemann group employed chiral Cu(II) complex **54** to catalyze Claisen rearrangement of 2-alkoxycarbonyl-substituted allyl vinyl ethers **55** (Scheme 1.10)[26]. The allyl vinyl ether is coordinated to the chiral Cu(II) ion in a bidentate fashion through a chair-like transition state **57** to generate product **56** in good yield and enantioselectivity. Among Lewis acid

catalyzed asymmetric Claisen rearrangements, this was the first example employing only a catalytic amount of the catalyst.

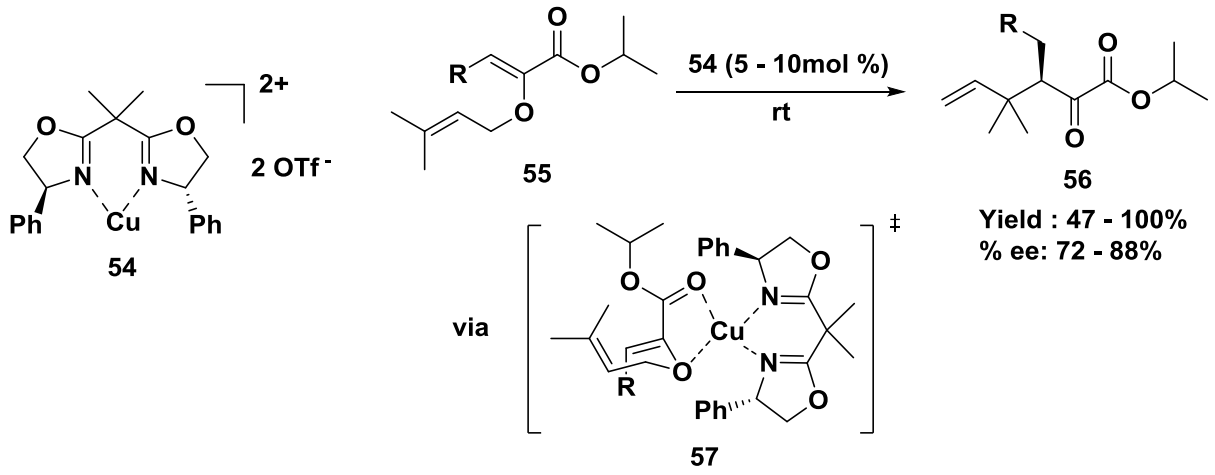

Scheme 1.10 Enantioselective copper-catalyzed Claisen rearrangement by Hiersemann

1.3.2 Olefin activated Claisen rearrangement

Since the seminal investigation by Van Der Baan et al.[27], several reports on palladium catalyzed Claisen rearrangement of allyl vinyl ethers have been published [28,29]. For example, the Nelson group has shown that allyl vinyl ethers **58** can undergo Claisen rearrangement using a palladium catalyst to afford product **59** in good yields and diastereoselectivity, along with the formation of side product **60** (Scheme 1.11 (i))[30]. According to the proposed mechanism, the palladium catalyst activates both olefins of the substrate, forming a Pd(II)-diolefin complex which adopts a boat-type conformation **63** which is presumably lower in energy than the chair conformation **62** (Scheme 1.11 (ii)). This boat-type conformation explains the unexpected anti-stereochemistry obtained in the product. Electron rich enol then adds to the Pd(II) center to form the σ-complex **64** which subsequently undergoes migratory insertion to give intermediate **65**. The β-elimination of the oxocarbenium ion regenerates the catalyst and affords the product **66** with the anti-stereochemistry.

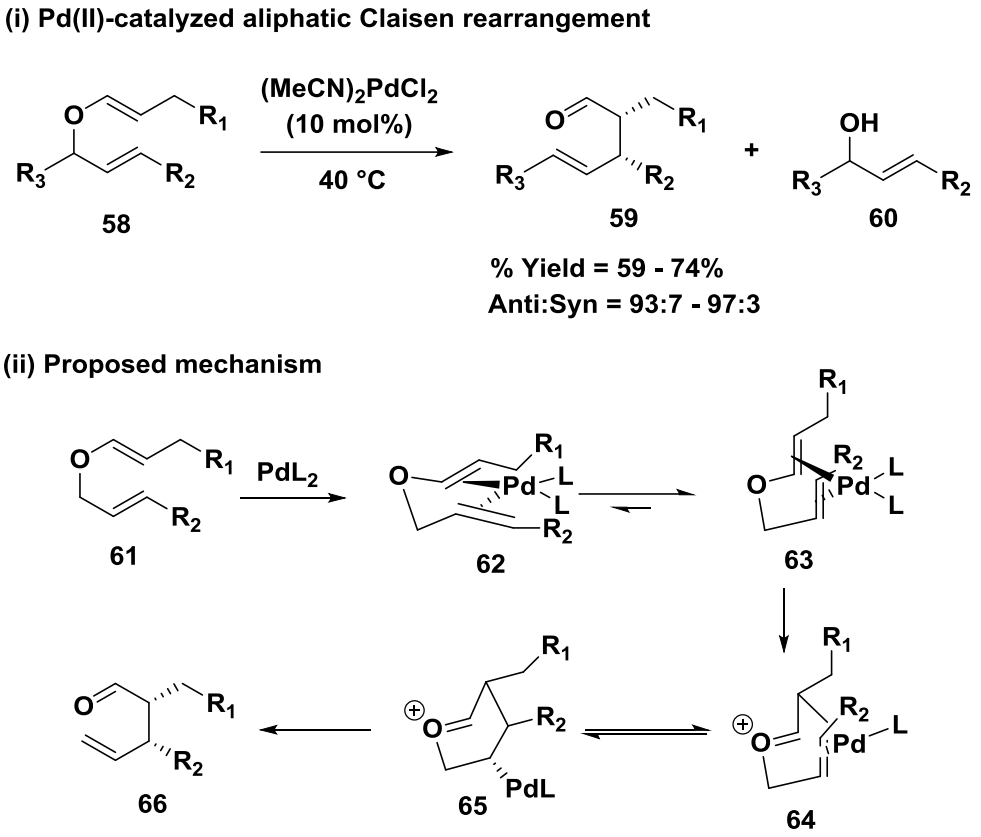

Scheme 1.11 Pd(II)-catalyzed aliphatic Claisen rearrangement by Nelson

The Nelson group also showed that ruthenium and boron can be used as a cooperative transition metal-Lewis acid cocatalyst system to promote the Claisen rearrangement of ally vinyl ether **67** (Scheme 1.12)[31]. The boron Lewis acid associates with the ether oxygen of the substrate to allow oxidative insertion of Ru(II) catalyst. This generates the metal-enolate and allyl cation **68** which recombine to give the rearrangement product **69**. However, since the reaction likely proceeds through a stepwise mechanism, it lacks the intrinsic regiochemical bias that is present in concerted processes, resulting a mixture of [3,3] and [1,3] rearrangement products **69** and **70**. Although the exact mechanism is still under investigation, the transition state may involve a boat-type conformation which results in the anti-stereochemistry in the final products.

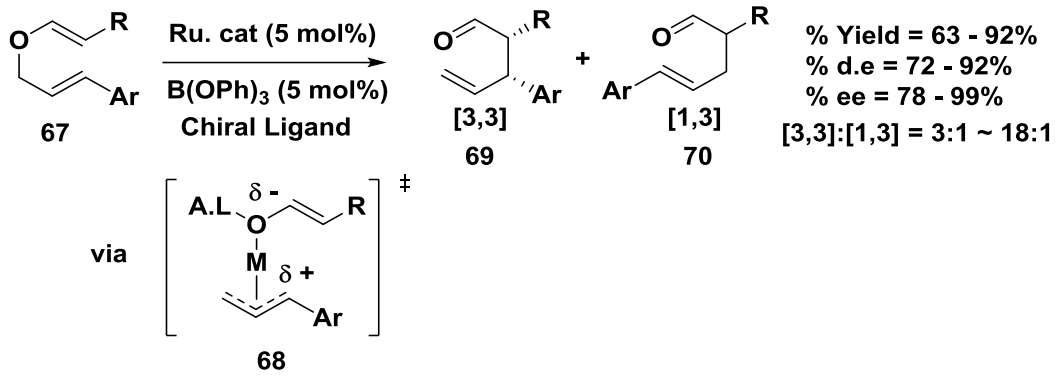

Scheme 1.12 Ru(II)-catalyzed asymmetric Claisen rearrangement by Nelson

1.3.3 Hydrogen-bond-donor catalyzed Claisen rearrangement

Inspired by reports on aqueous acceleration of Claisen rearrangement arising from hydrogen bonding, Jacobsen et al. reported a highly enantioselective Claisen rearrangement catalyzed by guanidinium ion (Scheme 1.13)[32,33]. The guanidinium catalyst such as **71** was effective at catalyzing the rearrangement for substrates such as **72** bearing electron-donating substituents at 4- or 6-position, or **73** which has an electron withdrawing groups at 2-position to give their corresponding products **74** and **75**. These substrates had higher degree of charge separation in the transition structure, and the guanidinium catalyst was able to efficiently stabilize this electrostatic interaction. For *O*-allyl α-ketoester **77**, chiral guanidinium catalyst **76** interacted with the substrate through both the ether oxygen atom and the pendant ester group in a bidentate fashion such as **79** to generate product **78**, similar to Hiersemann's copper catalyzed Claisen rearrangement. Despite excellent yields and enantioselectivity, the reaction required long reaction times ranging from 5 to 14 days.

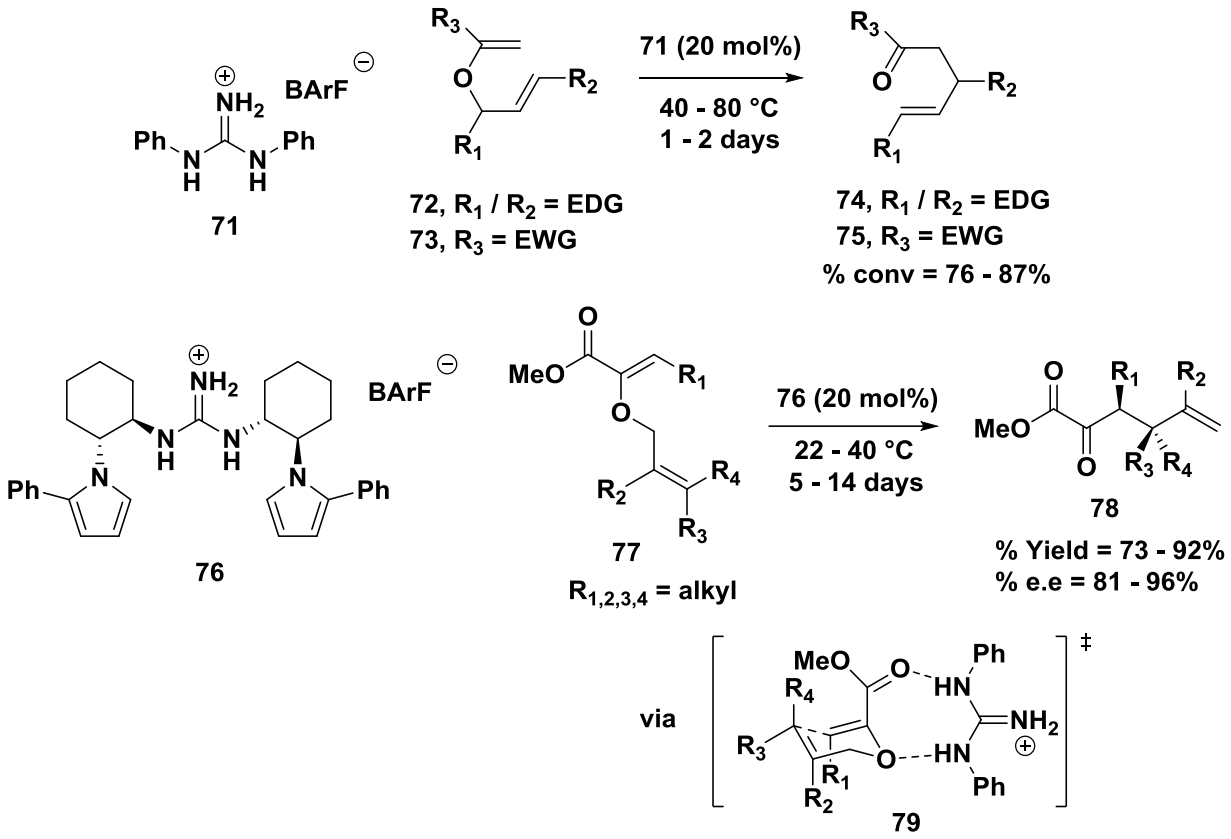

Scheme 1.13 Guanidinium-catalyzed Claisen rearrangement by Jacobsen

1.4 LUMO activation with Lewis acid catalysis

LUMO lowering catalysis involves lowering of the lowest occupied molecular orbital (LUMO) energy of an electrophile in order to reduce the energy difference between the highest occupied molecular orbital (HOMO) of a nucleophile and LUMO of the electrophile (Figure 1.2). This decrease in activation energy results in a significant rate acceleration compared to the non-catalyzed reaction, and it enhances the reactivity of the electrophile towards mild nucleophilic reagents. Typically, this electrophilic activation is applied to carbonyl compounds such as ketones, aldehydes, α, β-unsaturated enones and enals. In 1960, Yates et al. reported the first example of a LUMO lowering activation of a carbonyl compound in a Diels-Alder reaction using a Lewis acid[34]. They observed a significant rate acceleration in the Diels-Alder reaction between anthracene **80** and maleic anhydride **81** using $AlCl_3$, giving quantitative yield of the cycloadduct **82** in 1.5 minutes, whereas the uncatalyzed reaction was estimated to required 4800 hours for 95%

completion (Scheme 1.14 (i)). Later theoretical studies with frontier orbital energy analysis revealed that the complexation of Lewis acid with the Lewis basic lone pair of oxygen was lowering the LUMO energy of the dienophile (Scheme 1.14 (ii))[35].

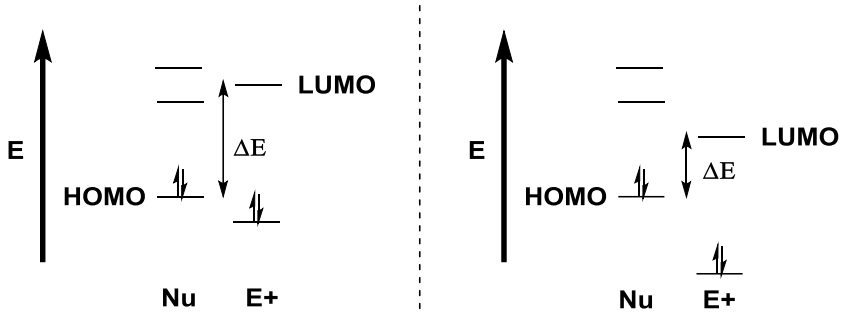

Figure 1.2 Reduction in activation energy by LUMO lowering catalysis

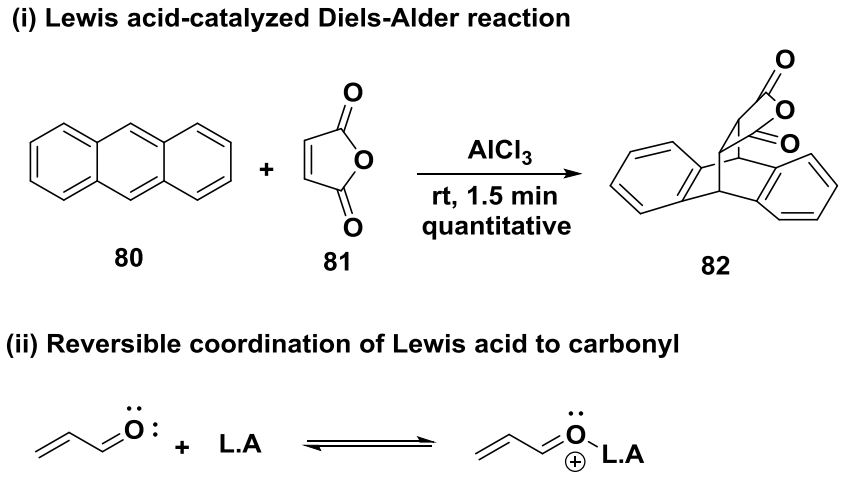

Scheme 1.14 First example of LUMO lowering activation with Lewis acid

Typically, Lewis acid catalysts are based on main group elements such as aluminum, boron, magnesium, and a few *d*-block metals. In order to obtain an efficient catalytic turnover, the Lewis acid catalyst must be able to reversibly coordinate to the substrate and the product, which constitutes one of the challenges in Lewis acid catalysis. Nowadays, asymmetric catalysis can be achieved using a combination of chiral ligands which forms a complex *in-situ* with the metal center of the Lewis acid catalyst. Salen complexes **83**, TADDOL **84**, Bis(oxazoline) **85** and BINOL **86** are among common examples of chiral ligands which have many applications in asymmetric transformations (Scheme 1.15 (i)). For example, Yamamoto et al. showed that BINOL assisted

chiral aluminum complex **87** can catalyze hetero-Diels Alder reaction of diene **88** and aldehyde **89** to give the cycloadduct **90** in good yields and enantioselectivity (Scheme 1.15 (ii))[36].

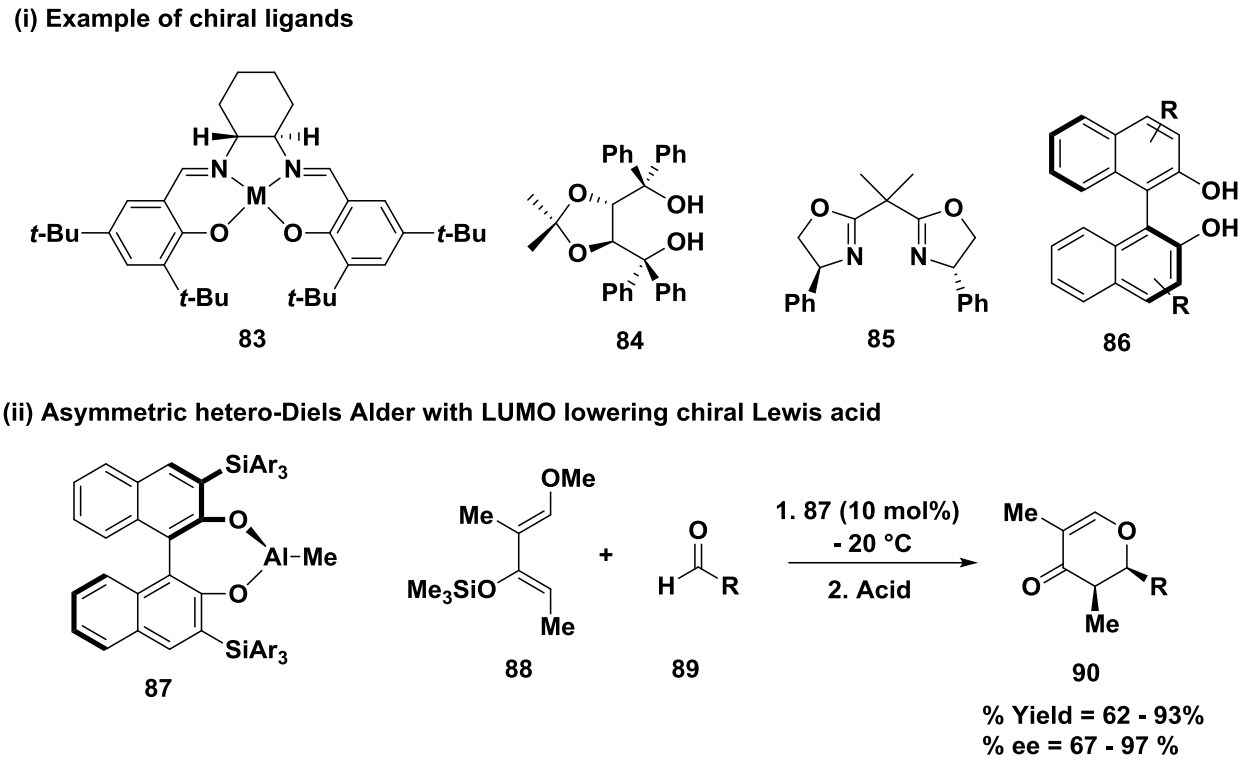

Scheme 1.15 Examples of chiral ligands and an application in asymmetric catalysis

1.5 LUMO activation with iminium catalysis

Since the pioneering work of MacMillan in 2000[37], iminium catalysis is widely viewed as an alternative method to Lewis-Acid catalysis for the LUMO lowering activation of electrophiles. Through the reversible formation of iminium ions from α, β-unsaturated ketones or aldehydes with primary or secondary amines, iminium catalysis can emulate the equilibrium dynamics of Lewis acid catalysis (Scheme 1.16).

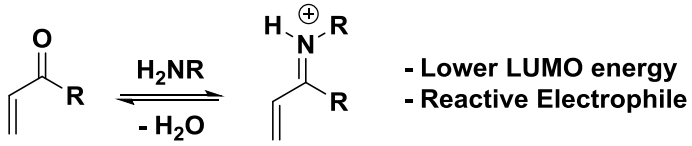

Scheme 1.16 LUMO activation with reversible iminium ion formation

The amine-based organocatalysts have environmental and economic benefits over Lewis acid catalysts which often employ toxic/sensitive metals and expensive ligands. With the widespread availability of enantiopure chemicals from the nature such as amino acids, chiral amine-based organocatalysts can be derived and used to induce asymmetry through the formation of temporary covalent bond with the substrate.

MacMillan is one of the pioneers in the field of iminium catalysis, and he reported the first highly enantioselective organocatalytic Diels-Alder reaction of α, β-unsaturated enals using the imidazolidinone secondary amine catalyst[37]. He showed that the imidazolidinone catalyst **93** can catalyze the Diels-Alder reaction between diene **91** and enal **92** to afford product **94** in good yields and enantioselectivity (Scheme 1.17). The transition state adopts the structure **95** with (*E*)-iminium geometry which avoids steric interactions between the olefin and gem-dimethyl substituents, and the benzyl group effectively shields one face of the dienophile.

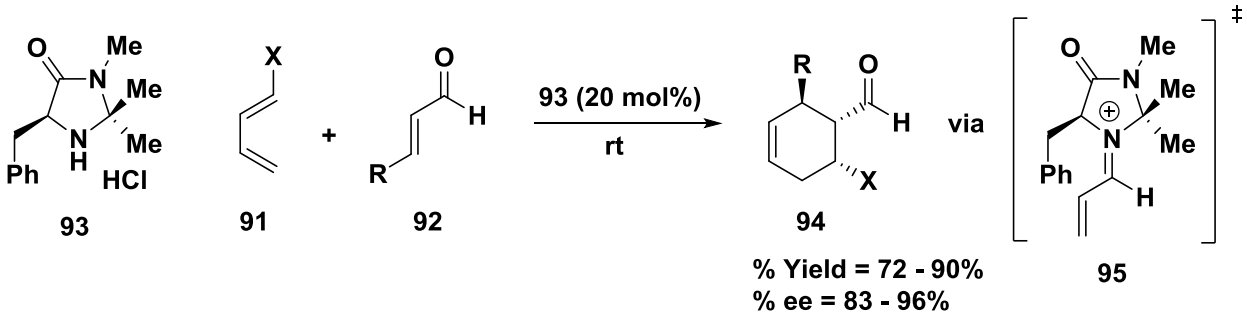

93 91 92 94 95

Scheme 1.17 Imidazolidinone catalyzed Diels-Alder reaction by MacMillan

1.5.1 LUMO activation of α-substituted acroleins with secondary amine catalysts

Unlike with primary amines, the formation of iminium ions from α-substituted enones and acroleins with secondary amines is much more challenging due to the intrinsic presence of allylic 1,3-strain (Scheme 1.18). For this reason, iminium catalyzed reactions involving α-substituted enones and acroleins with secondary amine catalysts are exceedingly rare.

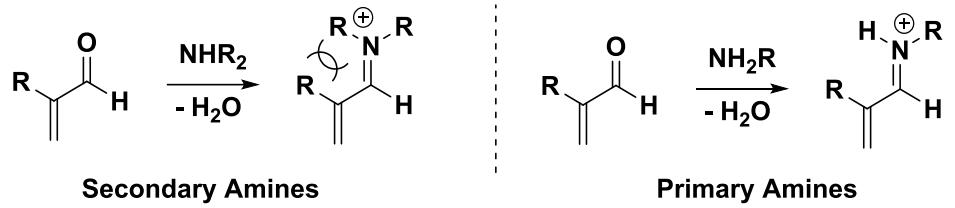

Scheme 1.18 Intrinsic allylic 1,3-strain in iminium ion from secondary amines

In 2016, Hayashi et al. reported the Diels-Alder reaction of α-substituted acroleins **96** and cyclopentadiene **97** catalyzed by prolinol catalyst **98** (Scheme 1.19)[38]. With the electron withdrawing property of trifluoromethyl substituents, diarylprolinol silyl ether catalyst **98** was particularly efficient at catalyzing the reaction, giving the cycloadduct **99** in good yield with high exo and enantioselectivity. Despite the presence of A-1,3-strain, the reaction was proposed to proceed through the iminium ion intermediate **100** with the bulky side chain of the catalyst shielding one face of the iminium ion in order to direct the approach of the diene.

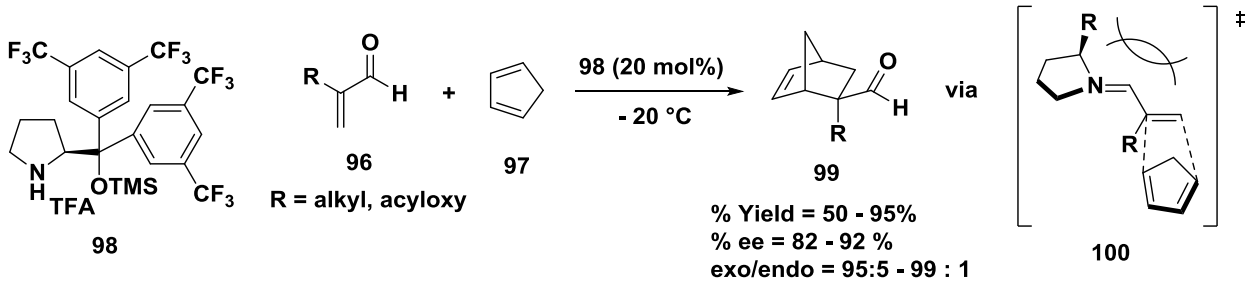

Scheme 1.19 Prolinol-catalyzed Diels-Alder reaction by Hayashi

1.5.2 LUMO activation of α-substituted acroleins with primary amines catalysts

The advantage of primary amine organocatalysts is their effectiveness in forming iminium ions with sterically hindered substrates such as α-substituted ketones and aldehydes. Upon condensation of α-substituted acrolein **101** with a primary amine, the iminium ion adopts the (*E*)-geometry **102** which avoids sterically disfavored allylic 1,3-strain that is present in (*Z*)-isomer **103** (Scheme 1.20).

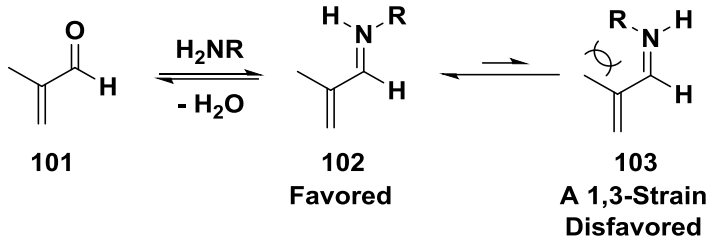

Scheme 1.20 Effect of allylic 1,3-strain on iminium ion geometry

Chiral primary amine organocatalysts have been used in variety of reactions involving α-substituted enals. For example, Maruoka et al. reported the Diels-Alder reaction of α-substituted acrolein **104** with cyclopentadiene **97** with the binaphthyl-based primary amine catalyst **106** (Scheme 1.21)[39]. The product **105** is obtained in good yield and enantioselectivity, and the efficiency of the catalyst **106** is explained by the transition state structure **107**, where the internal hydrogen bonding between the imine and ammonium proton activates the dienophile towards the cycloaddition with the cyclopentadiene**.**

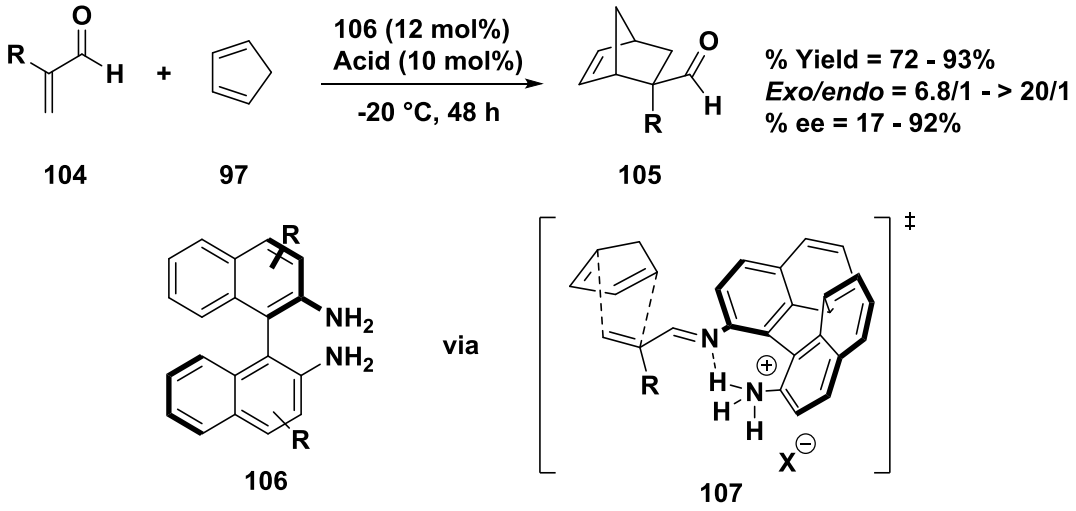

Scheme 1.21 Diels-Alder reaction of α-substituted acrolein by Maruoka

In addition to Diels-Alder reactions, other examples such as Michael addition[40], epoxidation[41], hetero-Michael addition[42] to α-substituted acroleins using primary amine organocatalysts have been developed.

1.6 The α-Effect in iminium catalysis: hydrazide-based organocatalyst

The α-effect is known as the increase in nucleophilicity of a heteroatom that is adjacent to another heteroatom. In terms of molecular orbitals, the interaction between the lone pairs of the nucleophilic heteroatom and its adjacent heteroatom causes a splitting of orbitals into high and low energy states. Therefore, the nucleophilic heteroatom has an increased HOMO energy and it becomes more reactive[2]. Tomkinson et al. utilized the rate accelerating effect of the α-effect in iminium catalyzed Diels-Alder reactions[43]. In a preliminary study, the Tomkinson group discovered that the Diels-Alder reaction between cinnamaldehyde **108** and cyclopentadiene **97** can be accelerated using *N,O*-dimethylhydroxylamine **110**, giving the product **111** in 65% yield after 48 h compared to using dimethylamine **109** which gave 22% yield under the same reaction conditions (Scheme 1.22 (i)). They also synthesized hydrazide catalyst derivatives and showed an example in which the acyclic hydrazide **112** catalyzed the Diels-Alder reaction of methacrolein **101** with cyclopentadiene **97**, affording the product **113** in 98% yield with 83:17 *exo*:*endo* ratio (Scheme 1.22 (ii)).

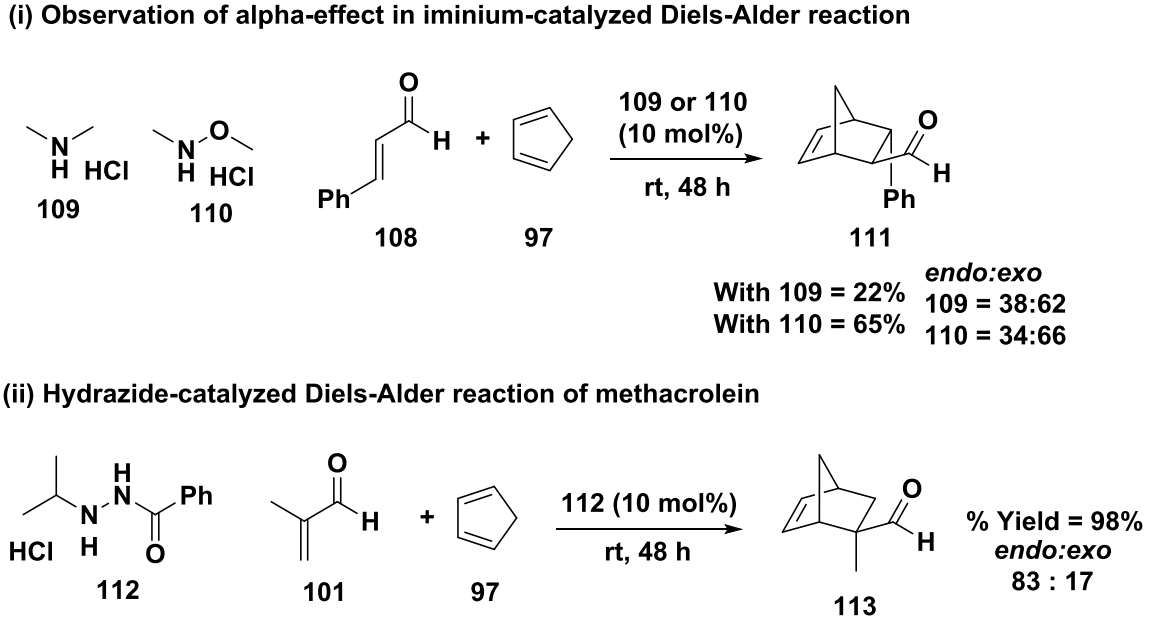

Scheme 1.22 Alpha-effect in hydrazide-catalyzed Diels-Alder reaction

Following Tomkinson's reports, other hydrazide-based organocatalysts have been developed and used extensively in iminium catalyzed Diels-Alder reaction. The Ogilvie group designed the camphor-derived cyclic hydrazide catalyst **115** which was efficient in the Diels-Alder reaction α, β-unsaturated enals **114** with cyclopentadiene **97,** providing good yields and enantioselectivity of product **116** albeit moderate *exo:endo* ratio (Scheme 1.23 (i))[44]. The Suzuki group also developed the exocyclic hydrazide organocatalyst **118** which was also efficient at catalyzing Diels-Alder reaction of α, β-unsaturated enals **117**, affording good yields and enantioselectivity of *endo* isomer **119** (Scheme 1.23 (ii))[45].

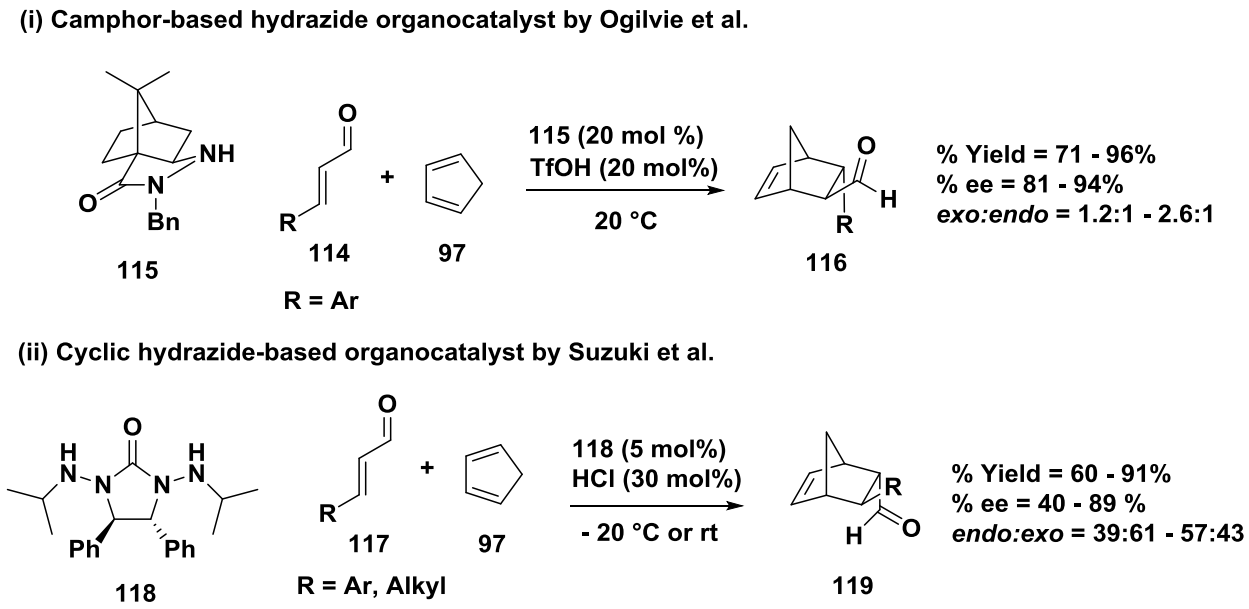

Scheme 1.23 Hydrazide-based organocatalysts by Ogilvie and Suzuki

These studies showed that the hydrazine-based organocatalysts, which generally have an increased reactivity over the secondary amine catalysts, could potentially serve as an efficient platform in iminium catalyzed reactions involving sterically hindered substrates such as α-substituted enals. Our research group became interested in expanding the applications of hydrazine-based organocatalysts in other iminium catalyzed reactions, which later led us to develop the first example of an organocatalytic Cope rearrangement[46].

1.7 Organocatalytic Cope rearrangement using iminium catalysis

In 2016, our group reported the first iminium catalyzed organocatalytic Cope rearrangement[46]. Our previous group member, Dr. Dainis Kaldre who completed the Cope project, showed that the 7-membered ring hydrazide catalyst **121** can efficiently catalyze the [3,3]-sigmatropic rearrangement of variety of 1,5-hexadiene-2-carboxaldehydes **120** to afford product **122** in excellent yield (Scheme 1.24).

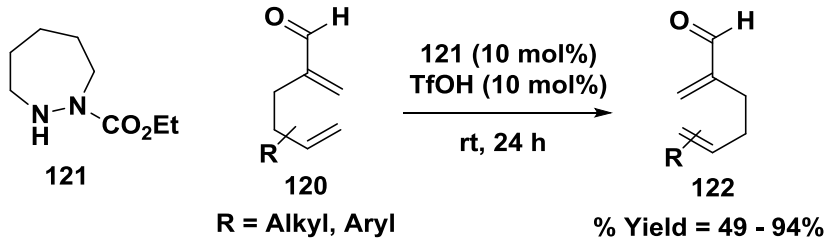

Scheme 1.24 First example of iminium-catalyzed organocatalytic Cope rearrangement

During our initial study, the DFT calculations revealed that the Cope rearrangement of 1,5-hexadiene **123** is predicted to have an activation energy of 35.8 kcal mol^{-1} (Figure 1.3). Incorporation of the aldehyde functionality at the 2-position (**124**) lowered this activation barrier to 30.5 kcal mol^{-1}, and the formation of an iminium ion further reduced the activation energy down to 11.7 kcal mol^{-1} (**125**), and each of these structure had lower calculated LUMO energies than their parent substrate **123** (-2.16 eV for **124** and -6.82 eV for **125).**

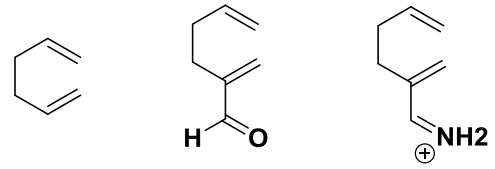

	123	124	125
T.S. energy (kcal/mol)	35.8	30.5	11.7
LUMO energy (eV)	-1.10	-2.16	-6.82

Figure 1.3 DFT calculations for transition state energy and LUMO energy

The substrate **126** was taken as a model substrate for this investigation. Considering the substrate **126** is an α-substituted enal, primary amines were first tested due to their effectiveness in forming iminium ions with hindered substrates. However, all the primary amine tested, such as cyclohexylamine **128**, 1,2-diaminocyclohexane **129**, aniline **130**, benzylamine **131**, *O*-methyl hydroxylamine **132**, failed to deliver any of the rearrangement product **127** at 23°C after 24 h (Scheme 1.25). Switching to secondary amine catalysts such as imidazolidinone **133**, proline **134**, and proline methyl ester **135** also did not show any sign of reactivity (Scheme 1.25). We then looked at the hydrazide catalysts. Interestingly, using secondary amine hydrazide catalyst **136** showed little sign of reactivity, affording the rearrangement product **127** in 13% yield with the remainder being the starting material **126**. Upon investigating secondary amine cyclic hydrazide catalysts, an increased reactivity trend was observed going from 5-membered catalyst **137** to 8-membered catalyst **140** (Scheme 1.25). Although the catalyst **140** showed the best result, its inherent difficult synthetic route prompted us to use the 7-membered catalyst **121** as the preferred catalyst. The use of *N*-methylated 7-membered catalyst **139** shut down the reactivity, suggesting that simple proton catalysis is not driving this rearrangement.

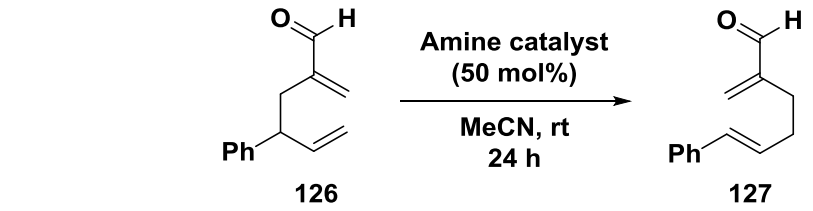

126 127

- Primary amines = No reactivity

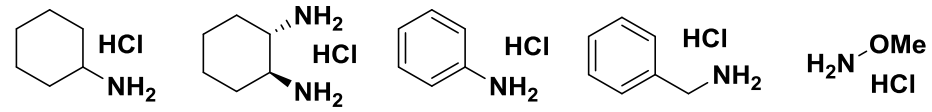

128 129 130 131 132

- Secondary amines = No reactivity

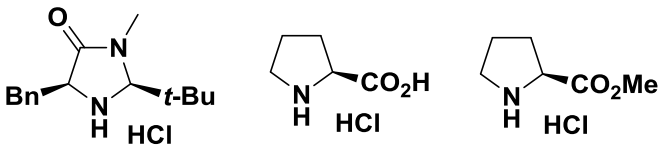

133 134 135

- Hydrazide catalyst

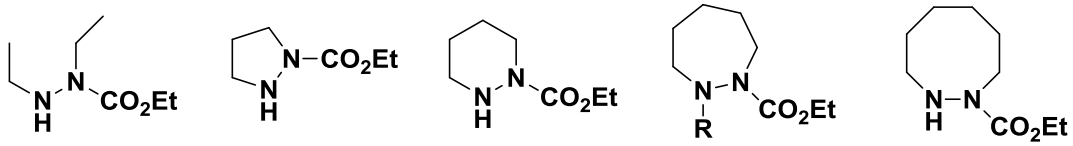

136 137 138 121, R = H 83%* 140
13 %* 6%* 28%* 139, R = Me 0 % 89%*

* ^{1}H NMR Yield (%)

Scheme 1.25 Screening of variety of amine catalysts

According to our DFT calculations, we suggested that our organocatalytic Cope rearrangement was a stepwise process which proceeds through an intermediate cation. The initial conjugate addition of alkene **141** to the α, β-unsaturated iminium ion generates the intermediate cation **142** which fragments to **143** and hydrolyzes to generate the product **127** (Figure 1.4).

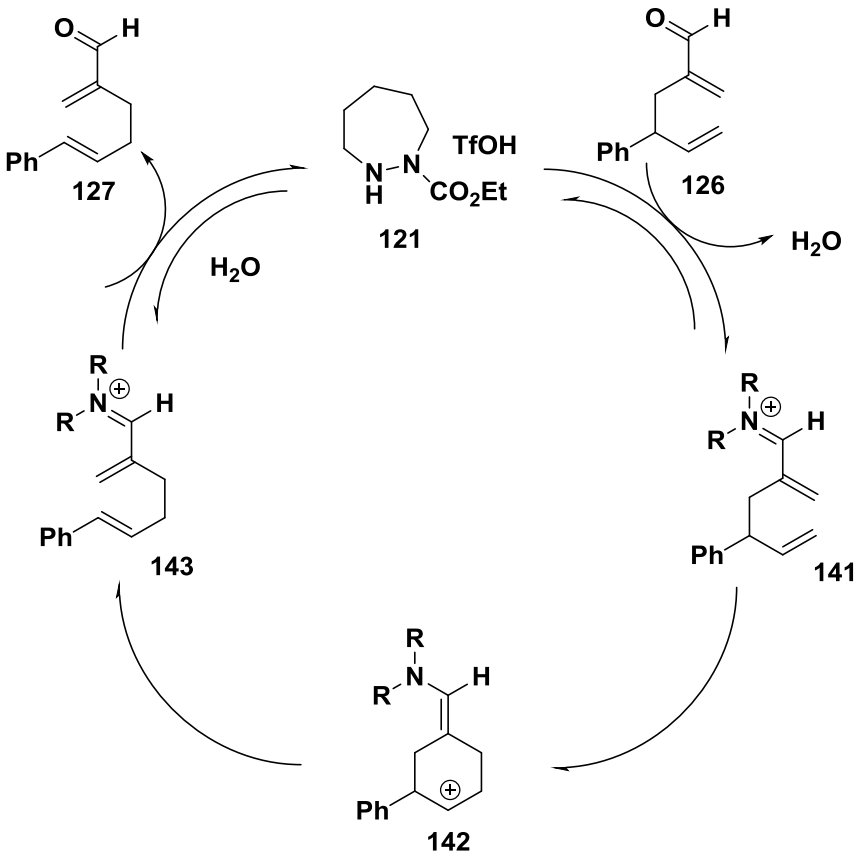

Figure 1.4 Proposed catalytic cycle for the hydrazide-catalyzed Cope rearrangement

The exceptional reactivity of our hydrazide catalyst **121** led us to develop further organocatalytic reactions involving α-substituted enals, such as the Michael addition of indoles[47], Diels-Alder cycloadditions[48], and polyene cyclizations[49].

1.8 Purpose of the investigation and preliminary studies

Inspired by our iminium catalyzed organocatalytic Cope rearrangement, the initial goal of this investigation was to develop an iminium catalyzed aliphatic Claisen rearrangement. Dr. Kaldre first began this project, and using DFT calculations at the B3LYP/6-31G* level (performed by Dr.Gleason), it was found that the Claisen rearrangement for allyl vinyl ether **1** has an activation energy 26.2 kcal/mol. Installing a formyl group at the 5-position (**144**) reduced the activation energy down to 24.2 kcal/mol, and the formation of iminium ion **145** further reduced the activation energy down to 15.9 kcal/mol (Figure 1.5).

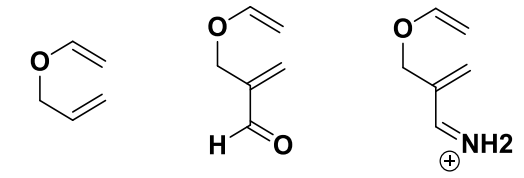

T.S. energy (kcal/mol)	26.2	24.2	15.9

Figure 1.5 DFT Calculations for activation energy of allyl vinyl ether systems

Analogous to our organocatalytic Cope rearrangement, we believe that it is possible to accelerate the aliphatic Claisen rearrangement via iminium catalysis using our hydrazide catalyst **121**. To test our hypothesis, Dr. Kaldre first tested the aliphatic substrate **146**. When the substrate **146** was heated at 80 °C in acetonitrile, it slowly underwent Claisen rearrangement to afford the product **147** in 16% yield along with some decomposition of the starting material (Table 1.1, entry 1). Using the hydrazide catalyst **121** with triflic acid or trifluoroacetic acid as acid co-catalysts led to rapid hydrolysis of the enol ether functionality to its corresponding alcohol **148** (entry 2 and 3). Unfortunately, after numerous trials it was concluded that aliphatic Claisen substrates are incompatible with our iminium catalysis conditions which require strong acid co-catalysts. Further development would therefore require substrates that are robust under acidic and nucleophilic conditions.

Table 1.1 Iminium-catalyzed Claisen rearrangement of 146

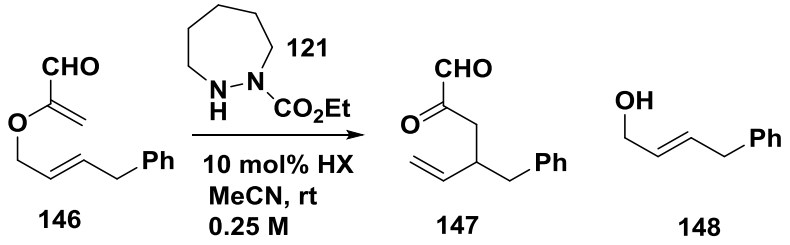

Entry	121 (mol%)	HX (mol %)	Temp (°C)	Time (h)	Yield 146*	Yield 147*	Yield 148*
1	-	-	80	24	71	18	-
2	20	TfOH (10)	rt	2	-	-	85

3	20	TFA (10)	rt	24	24	-	55

* ^{1}H NMR yield according to standard – mesitylene

1.9 Current results and discussions on the aromatic Claisen rearrangement

Having previously identified the stability issue with the aliphatic Claisen substrate, it was clear that the potential substrates had to be robust and acid-stable under our iminium catalysis conditions. This led us to investigate the aromatic Claisen substrates, which are easier to prepare and handle than aliphatic Claisen substrates bearing labile enol ethers. The goal of my project was to develop an iminium catalyzed aromatic Claisen rearrangement, and my research efforts focused on synthesizing a variety of aromatic Claisen substrates and screening them under our iminium catalysis conditions to check whether the hydrazide catalyst **121** can efficiently promote the Claisen rearrangement.

To start this investigation, 2-(phenoxymethyl)acrylaldehyde **153** was chosen as the model substrate, which was prepared in three steps from 2-methylenepropane-1,3-diol **179** (Scheme 1.26). Treatment of 2-methylenepropane-1,3-diol **149** with thionyl chloride gave cyclic dioxathiane **150** in 63% yield which was opened with phenoxide anion **151** to give allylic alcohol **152** in 40% yield. Oxidation of **152** with Dess-Martin periodinane (DMP) gave the model substrate **153** in 90% yield.

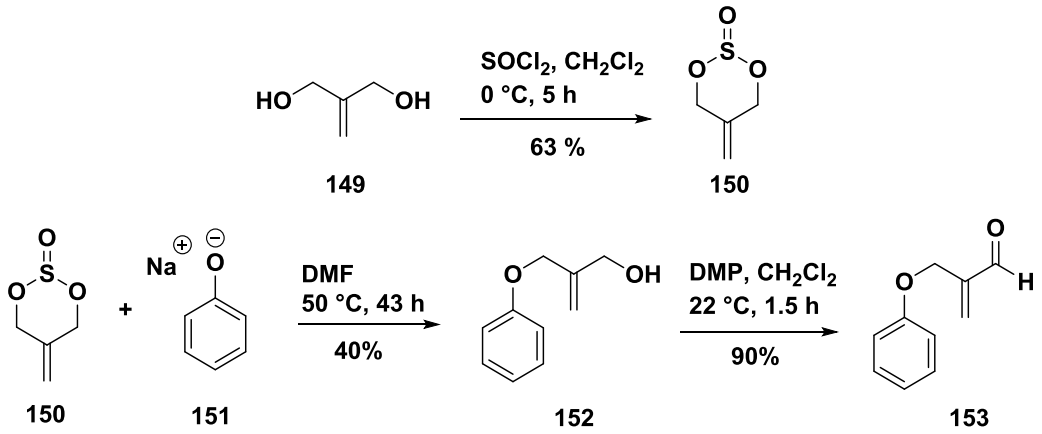

Scheme 1.26 Synthesis of model substrate 130

Substrate **153** was subjected to the catalytic conditions similar to our organocatalytic Cope rearrangement. Treatment of **153** with 20 mol% of catalyst **121** as HCl salt in acetonitrile produced

phenol **154** as a major product along with unstable α, β-unsaturated aldehyde **155** which slowly underwent decomposition upon storage (Table 1.2, entry 1). We believe that these decomposition products are formed via conjugation addition of water or nucleophilic catalyst **121** to the α, β-unsaturated iminium ion **156** followed by the elimination of **157** (Scheme 1.27).

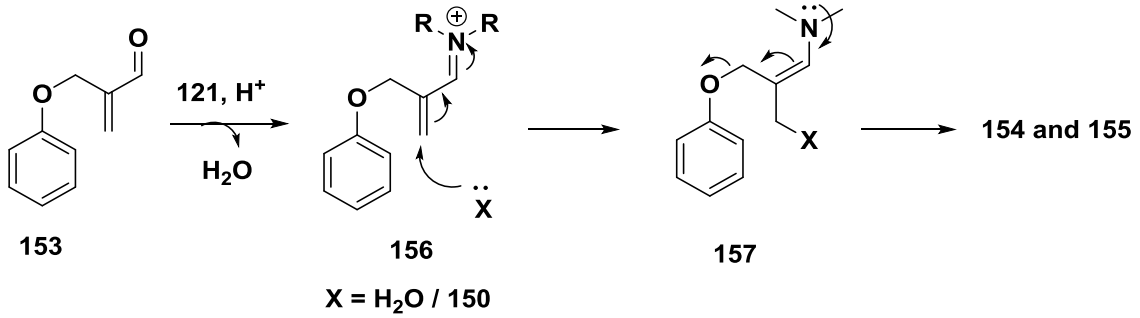

Scheme 1.27 Proposed decomposition pathway of substrate 153

Switching the solvent to nitromethane (entry 2) or the counter acid to triflic acid (entry 3) gave the same result. To test the stability of the substrate under acidic condition, **153** was treated with 100 mol% of methanesulfonic acid (entry 4), and the substrate **153** remained stable indefinitely, producing only trace amount of phenol **154** as the byproduct of hydrolysis.

To confirm the formation of iminium ion, substrate **153** was treated with 20 mol% of catalyst **121**, 10 mol% of perchloric acid and excess of cyclopentadiene **97**, and we were able to obtain the corresponding Diels-Alder product **158** in 71% yield (Scheme 1.28).

In order to confirm whether the thermal Claisen rearrangement of **153** can cleanly proceed, we attempted the thermal reaction of **153** in toluene at 100 °C for two days (entry 5) which showed no reactivity, but increasing the reaction temperature up to ~ 200 °C in toluene (entry 6) led to a complex mixture of rearrangement products. It is known that aromatic Claisen substrates bearing a carbonyl functionality such as an ester or a carboxylic acid at the 5-position undergo complex thermal reactions after the Claisen rearrangement[50]. Thermal reaction of **153** in DMSO at ~ 180 °C led to complete decomposition of the starting material (entry 7).

Table 1.2. Iminium-catalyzed Claisen rearrangement of 153

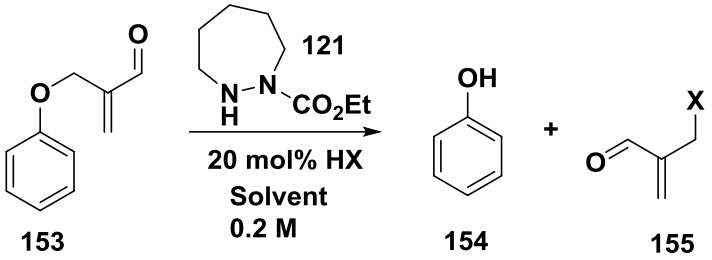

Entry	121 (mol%)	HX	Temp (°C)	Solvent	Time (h)	Products
1	20	HCl	rt	MeCN	24	**154** + **155**
2	20	HCl	rt	$MeNO_2$	24	**154** + **155**
3	20	TfOH	rt	MeCN	24	**154** + **155**
4	-	MsOH	Rt	MeCN	< 7 days	**153** + **154**
5	-	-	100	Toluene	2 days	**153**
6	-	-	200	Toluene	72	Complex Mixture
7	-	-	180	DMSO	24	Decomp.

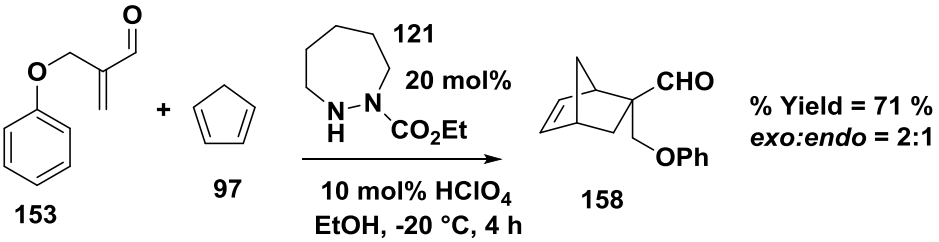

Scheme 1.28 Iminium-catalyzed Diels-Alder reaction of 153

The inability to isolate any products from thermal reactions caused us to question the stability of the expected products. We thus decided to synthesize the authentic sample of the expected product **162** (Scheme 1.29). Thermal Claisen rearrangement of allylic alcohol **152** in toluene at 220 °C for 8 days gave **159** in 79% yield. Attempt to oxidize **159** with DMP or IBX only led to decomposition. Suspecting that the phenol might be complicating the oxidation, it was protected with TBS group, and the oxidation of allylic alcohol **160** with DMP gave the precursor **161**. Careful deprotection of O-TBS group with TBAF gave the expected Claisen product **162** in moderate 35% yield which was stable upon storage at – 20 °C and slowly decomposed in ambient

temperature. In all of the reaction conditions tested in table 1.2, not a trace amount of product **162** could be observed by NMR, and we hypothesized that the main issue was the conjugate addition of nucleophiles to α, β-unsaturated iminium ion shown in scheme 1.27.

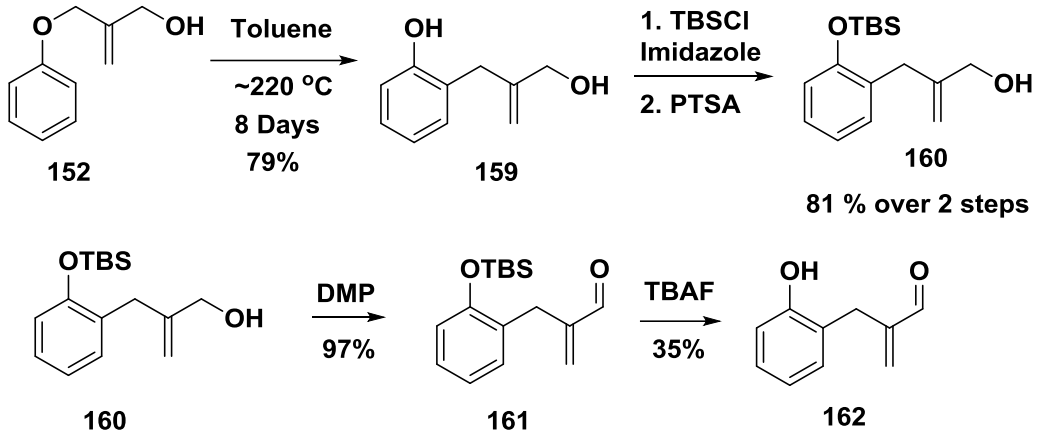

Scheme 1.29 Synthesis of Claisen rearrangement product 162

Next, we considered substrate **166** bearing the geminal dimethyl group at the termini of the olefin which we expected would prevent or slow-down the undesired conjugate addition of nucleophiles. Synthesis of **166** began with the alkylation of phenol **154** with bromo acrylate **163** to afford **164** in 88% yield (Scheme 1.30). Treating ester **164** with MeLi in the presence cerium trichloride gave exclusively the 1,2-addition product **165** in 86% yield. In the absence of cerium trichloride, MeLi addition led to rapid decomposition of **164** to phenol **154**, giving poor yield of the desired product. Alcohol **165** underwent oxidative 1,3-transposition with PCC to give the final substrate **166** in 31% yield.

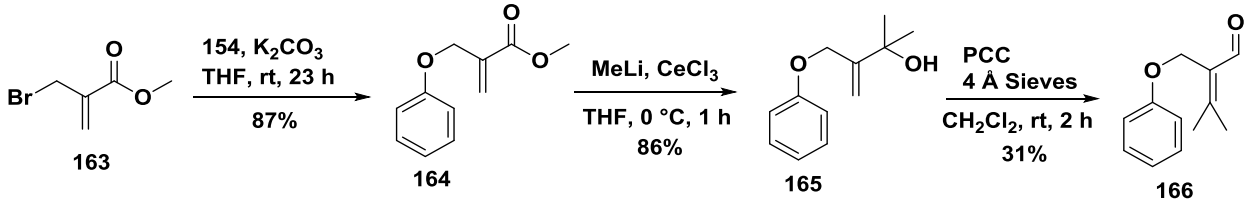

Scheme 1.30 Synthesis of substrate 166

When the substrate **166** was subjected to our catalytic condition using 20 mol% of catalyst **121** as HCl salt in MeCN (Table 1.3, entry 1), the rate of substrate decomposition was much

slower, but no Claisen reactivity was observed even with prolonged reaction times. Changing the amount of acid co-catalyst (entry 2) had no impact, and the attempt at a thermal Claisen rearrangement was also unsuccessful (entry 3).

Table 1.3 Iminium-catalyzed Claisen rearrangement of 166

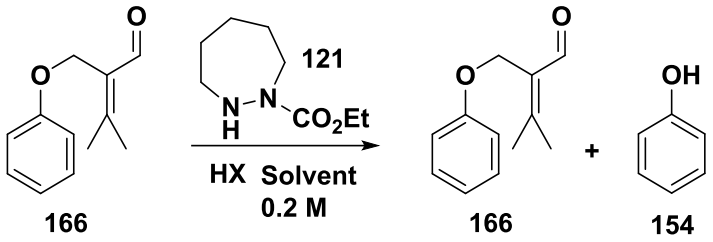

Entry	121 (mol%)	HX	Temp (°C)	Solvent	Time (h)	Products
1	20	HCl (20 mol%)	rt	MeCN	24	**154** + **166**
2	20	HCl (10 mol%)	rt	$MeNO_2$	24	**154** + **166**
3	-	-	180	Toluene	5 days	**154** + **166**

Treating **166** with cyclopentadiene **97** under our catalytic condition using **121** still gave the Diels-Alder adduct **167** in 16% yield after 10 days, despite being a sterically hindered dienophile (Scheme 1.31). With the methylated catalyst **139**, no reactivity was observed, which confirmed that the Diels-Alder reaction proceeded through iminium catalysis and not via proton catalysis.

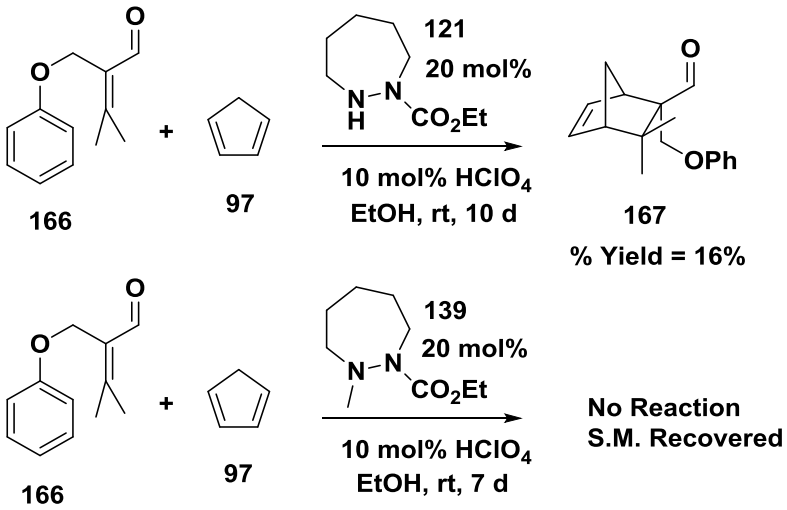

Scheme 1.31. Iminium-catalyzed Diels-Alder reaction of 166

According to our proposed mechanism of the organocatalytic Cope rearrangement presented in the previous section (Figure 1.4), the reaction essentially begins with the conjugate addition of alkene to an α, β-unsaturated iminium ion. We thought that by introducing electron donating groups to the aromatic system of our Claisen substrates, we could increase the nucleophilicity of the arene, thereby initiating the conjugate addition of arene to α, β-unsaturated iminium ion. We thus considered three substrates, **171**, **173** and **177** each bearing methoxy groups at 3- and 5- position of the arene. Substrate **171** and **173** were synthesized starting from 3,5-dimethoxy phenol **168** (Scheme 1.32 (i)). Alkylation of **168** with bromo acrylate **163** gave **169** in 69 % yield. DIBAL reduction of **169** followed by DMP oxidation gave the substrate **171** in 39 % yield over two steps. 1,2-addition of MeLi to **169** in the presence of cerium trichloride gave **172** in 35% yield (84% brsm), and the oxidative 1,3-transposition of **172** with PCC gave the substrate **173** in moderate 22% yield. For substrate **177**, the synthesis began with Heck coupling of 3,5-dimethoxy iodobenzene **174** with 3-buten-1-ol **175** to generate **176** in 56% yield. Organocatalytic α-methynylation of **176** with formaldehyde gave the substrate **177** in 71% yield.

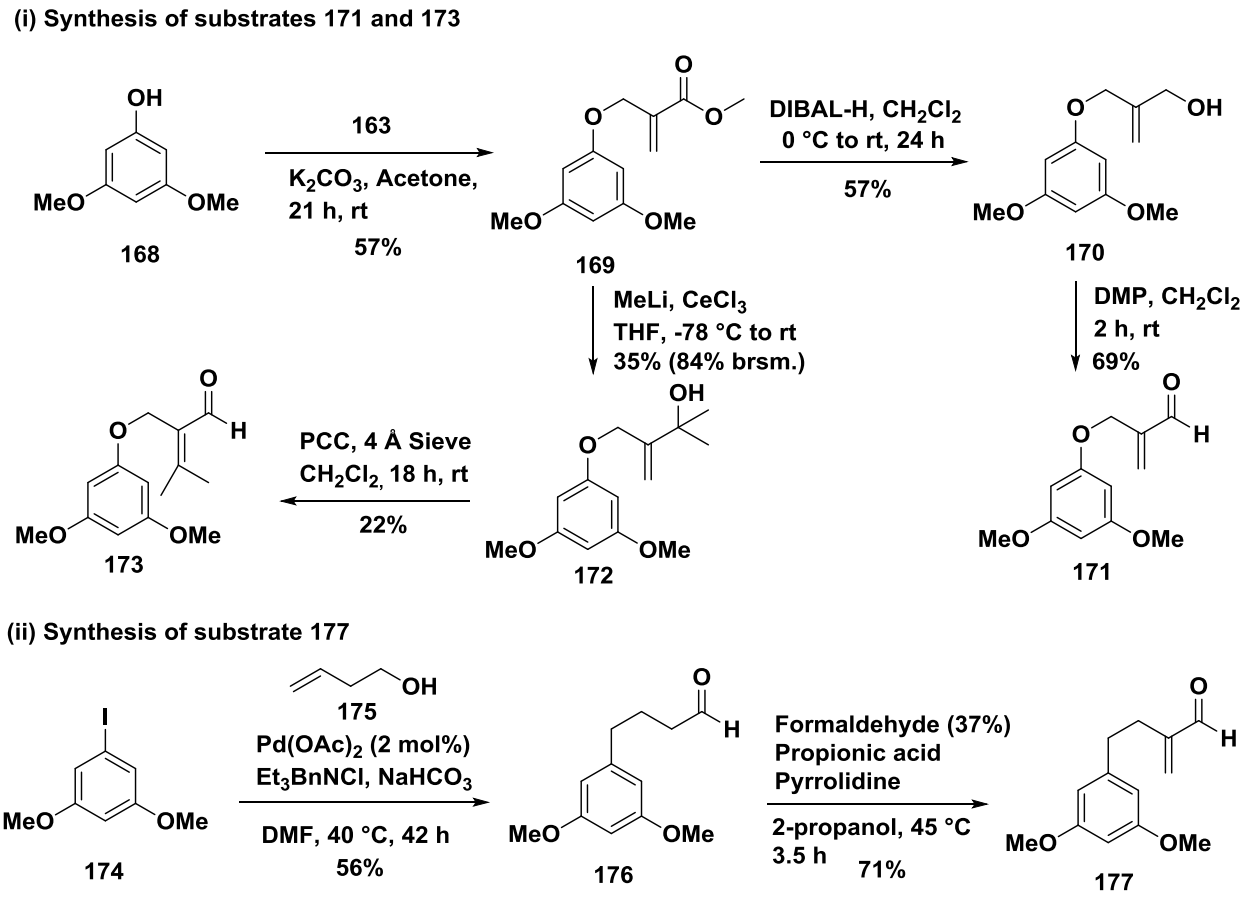

Scheme 1.32 Synthesis of substrates 201, 203 and 207

When the substrates **171** and **173** were subjected to the catalytic conditions using 20 mol% of catalyst **121** as a HCl salt in MeCN, both substrates underwent complete decomposition in less than 0.5 h, and no sign of product formation could be observed by NMR (Scheme 1.33 (i)). However, when substrate **177** was subjected to the reaction condition using 20 mol% of catalyst **121** as a HCl salt in $MeNO_2$, the reaction was completed within 0.5 h and gave 50% yield of cyclized product **179** along with trace amounts of unknown impurities (Scheme 1.33 (i)). For the substrate **177**, we hypothesize that after the conjugate addition of the arene to the α, β-unsaturated iminium ion, the intermediate cation **178** is protonated upon workup, giving the cyclized product **179** (Scheme 1.33 (ii)). In the case of **171** and **173**, the reason for their rapid decomposition is unclear, but we speculate that after the conjugate addition of the arene to the α, β-unsaturated iminium ion, the resulting chromane intermediate **180** or the product may be highly reactive or unstable, undergoing polymerizations and various decomposition pathways (Scheme 1.33 (iii)).

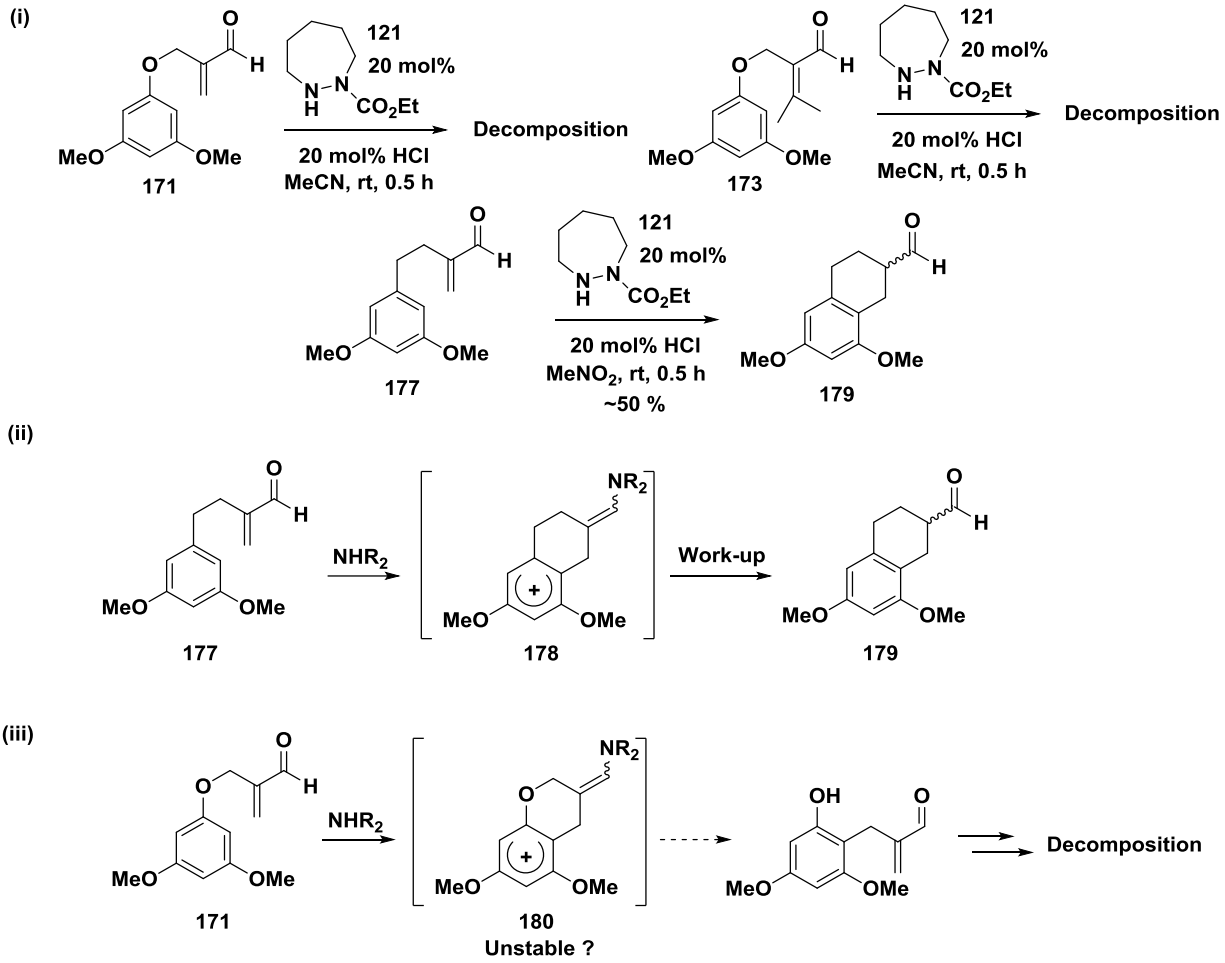

Scheme 1.33 Iminium-catalyzed Claisen rearrangement of 171, 173 and 177

1.10 Conclusions and future directions

Inspired by our success in organocatalytic Cope rearrangement, we attempted to develop an organocatalytic aromatic Claisen rearrangement. Our hydrazide catalyst **121** was efficient at forming iminium ion with our substrates, and we were able to confirm the formation of iminium ions by reacting them with a dienophile to generate the Diels-Alder adducts. However, our iminium catalysis conditions failed to promote the Claisen rearrangement. Aromatic Claisen substrates were more robust under acidic conditions compared to the aliphatic substrates, but they still slowly underwent decomposition and hydrolysis under our catalytic condition. Based upon our mechanistic proposal on Cope rearrangement, we attempted to promote conjugate addition of

arene to α, β-unsaturated iminium ion by increasing the nucleophilicity of the aromatic ring. However, these substrates underwent rapid decomposition under our catalytic condition. We hypothesize that the resulting intermediate or product are highly reactive, and they quickly undergo polymerization and other decomposition pathways. Interestingly, structurally similar carbon analogue **177** underwent successful cyclization in moderate yield, which suggests that the oxygen atom of the phenoxy group in aromatic Claisen substrates may be the issue. As a future direction, the catalytic reactions for substrates **171** and **173** could be run at a cryogenic temperature to see whether we can slow down the decomposition and isolate any intermediates which may give us a clue about the potential decomposition pathway. In addition, we could also test Lewis acid and hydrogen-bonding catalysts to check the compatibility of our substrates with other mode of activations.

1.11 References

1. Claisen, L. (1912). Berichte der deutschen chemischen Gesellschaft **45**(3): 3157-3166.
2. Clayden, J., et al. (2012). Organic chemistry. Oxford ;, Oxford University Press.
3. Cope, A. C. and E. M. Hardy (1940). Journal of the American Chemical Society **62**(2): 441-444.
4. Wick, A. E., et al. (1964). Helvetica Chimica Acta **47**(8): 2425-2429.
5. Daniewski, A. R., et al. (1992). The Journal of Organic Chemistry **57**(26): 7133-7139.
6. Johnson, W. S., et al. (1970). Journal of the American Chemical Society **92**(3): 741-743.
7. Nishiyama, Y., et al. (2014). Journal of the American Chemical Society **136**(18): 6598-6601.
8. Ireland, R. E. and R. H. Mueller (1972). Journal of the American Chemical Society **94**(16): 5897-5898.
9. Bunte, J. O., et al. (2006). Angewandte Chemie International Edition **45**(38): 6376-6380.
10. Malherbe, R. and D. Belluš (1978). Helvetica Chimica Acta **61**(8): 3096-3099.
11. Gosteli, J. (1972). Helvetica Chimica Acta **55**(2): 451-460.
12. Hill, R. K., Gilman, N. W. *Tetrahedron Lett.* **1967**, 1421-1423.
13. Kwart, H. and C. M. Hackett (1962). Journal of the American Chemical Society **84**(9): 1754-1755.
14. Andrews, P. R., et al. (1973). Biochemistry **12**(18): 3492-3498.

15. Goerisch, H. (1978). Biochemistry **17**(18): 3700-3705.
16. Lee, A. Y., et al. (1995). Journal of the American Chemical Society **117**(12): 3627-3628.
17. Khanjin, N. A., et al. (1999). Journal of the American Chemical Society **121**(50): 11831-11846.
18. Goering, H. L. and R. R. Jacobson (1958). Journal of the American Chemical Society **80**(13): 3277-3285.
19. White, W. N. and E. F. Wolfarth (1970). The Journal of Organic Chemistry **35**(7): 2196-2199.
20. Dewar, M. J. S. and E. F. Healy (1984). Journal of the American Chemical Society **106**(23): 7127-7131.
21. Vance, R. L., et al. (1988) Journal of the American Chemical Society **110**(7): 2314-2315.
22. Gajewski, J. J. and N. D. Conrad (1979). Journal of the American Chemical Society **101**(10): 2747-2748.
23. Severance, D. L. and W. L. Jorgensen (1992). Journal of the American Chemical Society **114**(27): 10966-10968.
24. Maruoka, K., et al. (1995). Journal of the American Chemical Society **117**(3): 1165-1166.
25. Saito, S., et al. (1996). Synlett **1996**(08): 720-722.
26. Abraham, L., et al. (2001). Angewandte Chemie International Edition **40**(24): 4700-4703.
27. van der Baan, J. L. and F. Bickelhaupt (1986). Tetrahedron Letters **27**(51): 6267-6270.
28. Nevado, C. and A. M. Echavarren (2004). Tetrahedron **60**(43): 9735-9744.
29. Cao, T., et al. (2012). The Journal of Organic Chemistry **77**(24): 11034-11055.
30. Kerrigan, N. J., et al. (2008). Tetrahedron **64**(29): 6863-6869.
31. Geherty, M. E., et al. (2010). Journal of the American Chemical Society **132**(34): 11875-11877.
32. Uyeda, C. and E. N. Jacobsen (2008). Journal of the American Chemical Society **130**(29): 9228-9229.
33. Uyeda, C. and E. N. Jacobsen (2011). Journal of the American Chemical Society **133**(13): 5062-5075.
34. Yates, P. and P. Eaton (1960). Journal of the American Chemical Society **82**(16): 4436-4437.

35. Houk, K. N. and R. W. Strozier (1973). Journal of the American Chemical Society **95**(12): 4094-4096.
36. Maruoka, K., et al. (1988). Journal of the American Chemical Society **110**(1): 310-312.
37. Ahrendt, K. A., et al. (2000). Journal of the American Chemical Society **122**(17): 4243-4244.
38. Hayashi, Y., et al. (2016). Chemistry – A European Journal **22**(44): 15874-15880
39. Kano, T., et al. (2009). Chemical Communications(15): 1956-1958.
40. Fu, N., et al. (2011). Angewandte Chemie International Edition **50**(48): 11451-11455.
41. Lifchits, O., et al. (2010). Journal of the American Chemical Society **132**(30): 10227-10229.
42. Fu, N., et al. (2014). Organic Letters **16**(17): 4626-4629.
43. Cavill, J. L., et al. (2003). Chemical Communications(6): 728-729.
44. Lemay, M. and W. W. Ogilvie (2005). Organic Letters **7**(19): 4141-4144.Ishihara, K. and
45. Suzuki, I., et al. (2011). Organic & Biomolecular Chemistry **9**(8): 3033-3040.
46. Kaldre, D. and J. L. Gleason (2016). Angewandte Chemie International Edition **55**(38): 11557-11561.
47. Larnaud, F., et al. (2017). European Journal of Organic Chemistry **2017**(18): 2637-2640.
48. Häggman, N. O., et al. (2018). European Journal of Organic Chemistry **2018**(39): 5412-5416.
49. Plamondon, S. J., et al. (2020). Angewandte Chemie International Edition **59**(1): 253-258.
50. Gopalan, B., et al. (1985). Tetrahedron **41**(15): 3153-3159.

Chapter 2. Mechanism and origin of rate acceleration in hydrazide catalyzed Cope rearrangement

2.1 Mechanism of Cope rearrangement

Since the discovery of the Cope rearrangement by Cope and Hardy in 1940, a number of experimental and theoretical studies have been conducted in order to elucidate its mechanism. According to Woodward and Hoffman's molecular orbital theory, the Cope rearrangement is a thermally allowed [3,3] sigmatropic rearrangement that can occur with suprafacial-suprafacial geometries through either a six-membered chair-like or boat-like transition state[51] (Figure 2.1 (i)). Generally, Cope rearrangement has a strong conformational bias towards a chair-like transition state which avoids the unfavorable steric repulsion between substituents and the angle strains that are present in a boat-like transition state. In terms of orbital interactions, Fukui utilized the next lowest unoccupied molecular orbital (NLUMO) and the next highest occupied molecular orbital (NHOMO) to propose that the boat conformation is slightly disfavored due to the presence of a secondary anti-bonding orbital interaction[52] (Figure 2.1 (ii)). In another report, Dewar et al. stated that the π-orbital overlap in chair-conformation is equivalent to an aromatic benzene (**181**), whereas in the boat-conformation it is equivalent to bicyclo-hexatriene **182** which is less aromatic due to two antiaromatic cyclobutadiene rings (Figure 2.1 (iii)[53]. Based on the degree of aromaticity, Dewar et al. proposed that the chair-conformation is energetically favored compared to the boat-conformation.

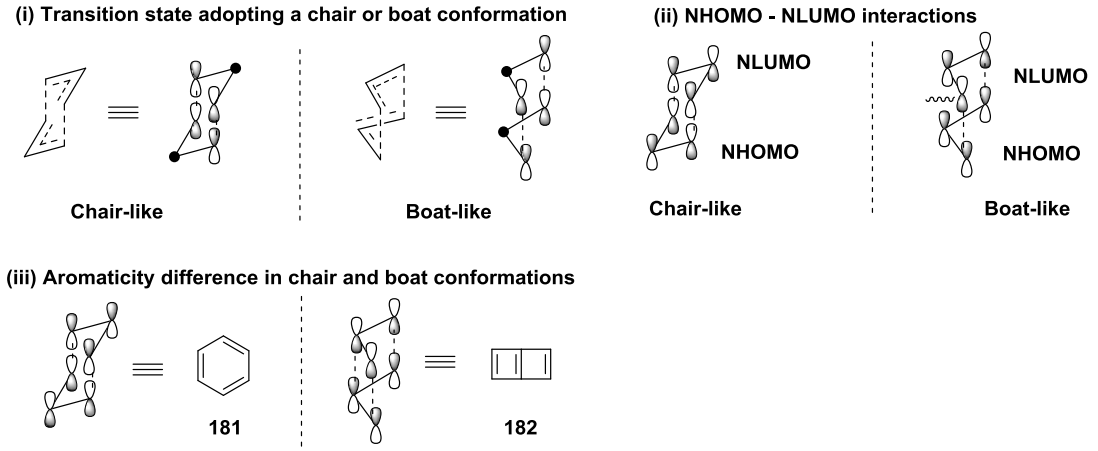

Figure 2.1 Possible chair and boat conformers for the Cope transition state

Doering and Roth experimentally confirmed that for simple 1,5-diene systems, the Cope rearrangement proceeds via a chair-like transition state[54]. When *meso*-3,4-dimethylhexa-1,5-diene **183** underwent Cope rearrangement, the product **185** was obtained in 99.7% yield, via the chair-like transition state **184** (Scheme 2.1). Only a trace amount of the product **187** arising from the boat-conformation **186** was obtained, and the strained product **189** (from conformation **188**) was not detected. Based on the ratio of product **187** and **188**, Doering and Roth estimated that the difference in free energy of activation between the chair and boat conformation is at least 5.7 kcal/mol.

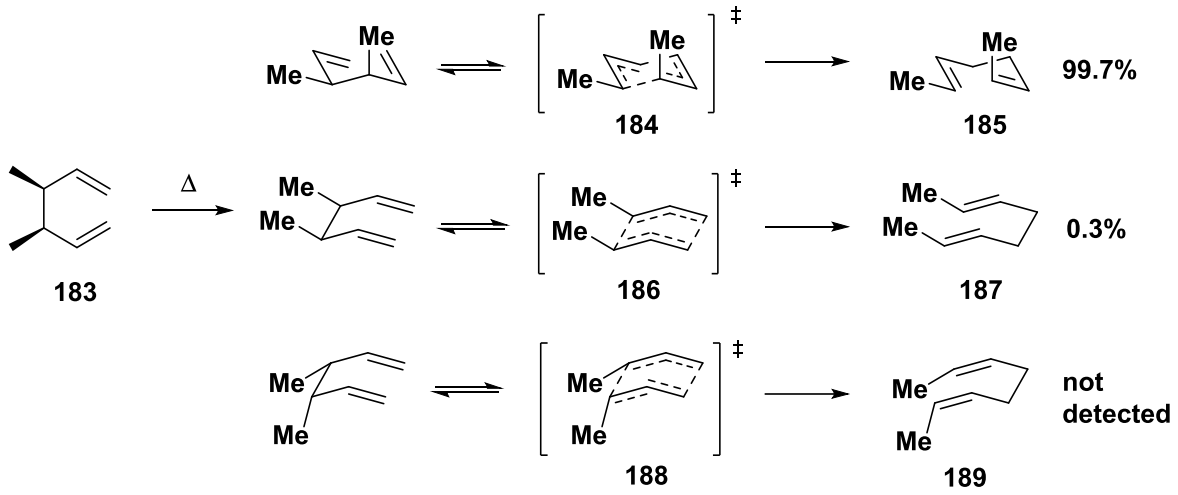

Scheme 2.1 Stereochemistry in the Cope rearrangement of 183

It is important to note that for geometrically constrained substrates with lesser structural flexibility such as *cis*-1,2-divinylcyclopropane **190**, the Cope rearrangement proceeds via the boat transition state **191** to give the rearrangement product **192** (Scheme 2.2)[55]. Overall, the stereochemistry observed in the final products suggests that the Cope rearrangement occurs in a concerted fashion.

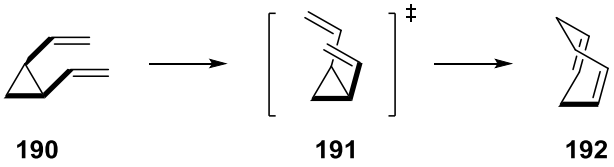

Scheme 2.2 Boat transition state for the cyclopropane 190

Although the Cope rearrangement are generally thought to proceed via a concerted chair or boat-type transition state, there are continuous disputes over the possibility of a stepwise mechanism involving the radical intermediates. The experimental activation barrier for the Cope rearrangement of 1,5-hexadiene **123** proceeding through a synchronous aromatic transition state **193** was calculated to be 33.5 kcal/mol according to Doering et al.[56]. Other proposed transition states arising from a stepwise pathway are 1,4-diyl radical **194** and two allyl radicals **195** which have activation energies of 42.1 and 59.7 kcal/mol, respectively [57,58] (Scheme 2.3). Based on these energetic values, it is clear that the mechanism is likely to proceed via the concerted synchronous aromatic transition state **193** which has the lowest activation barrier. However, the Cope rearrangement of substituted 1,5-hexadiene systems displays interesting behaviors compared to the parent system **123**.

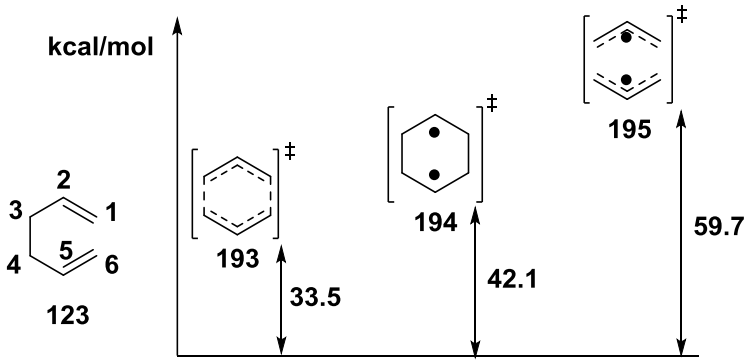

Scheme 2.3 Calculated activation energy for the proposed transition states

2.1.1 Substituent effects on the mechanism of Cope rearrangement

A number of experimental studies have been conducted in order to determine the effect of substituents on the mechanism of Cope of rearrangement. In 1973, Dewar and Wade measured the relative rate of Cope rearrangement for substrates **196** bearing a phenyl group at 3-position, **197** bearing a phenyl group at 2-position, and **198** bearing phenyl groups at both 2- and 5-position of parent system **123** (Scheme 2.4)[59]. For **196**, the rate was 18 times faster than the parent system **123**, suggesting that the "bisallyl radical" intermediate **195** which is stabilized by a phenyl group may be involved in the mechanism. For **197** and **198**, they showed a cumulative accelerating effect, and their relative rate was 41 times and 2000 times faster than the parent system **123**, suggesting

that the "biradical" intermediate **194** which stabilized by the phenyl groups may be involved in the mechanism.

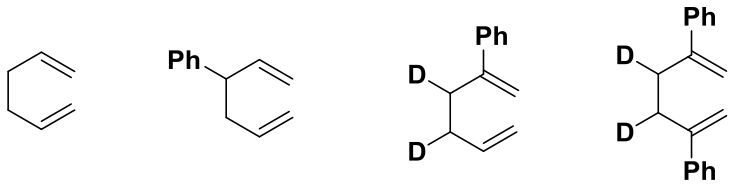

123 **196** **197** **198**

Substrate	Relative Rate of Cope
123	1
196	18
197	41
198	2000

Scheme 2.4 Substituent effect on relative rates of Cope rearrangement

Gajewski and Conrad also supported Dewar and Wade's experimental observations by determining the bond making (BMKIE) and bond breaking (BBKIE) secondary kinetic isotope effects (KIE) for substrates bearing radical-stabilizing substituents at different positions[60]. With their experimental KIE values, their ratio has been used to determine the relative extents of bond formations and dissociation during the transition state of Cope rearrangement (Scheme 2.5). With the introduction of a phenyl group at the 2-position (**201 – 202**), the ratio of BMKIE over BBKIE increases to 3.3 compared to the parent system **199 – 200**, where the ratio is 1.8. Substituent with phenyl groups at both 2- and 5-position (**203 – 204**) further increased the ratio to 8.1, which correlates with a greater degree of bond formation in the transition state. For dicyano-substrates (**205 – 206**), the ratio of BMKIE over BBKIE was only 0.31, suggesting a higher degree of bond dissociation in the transition state.

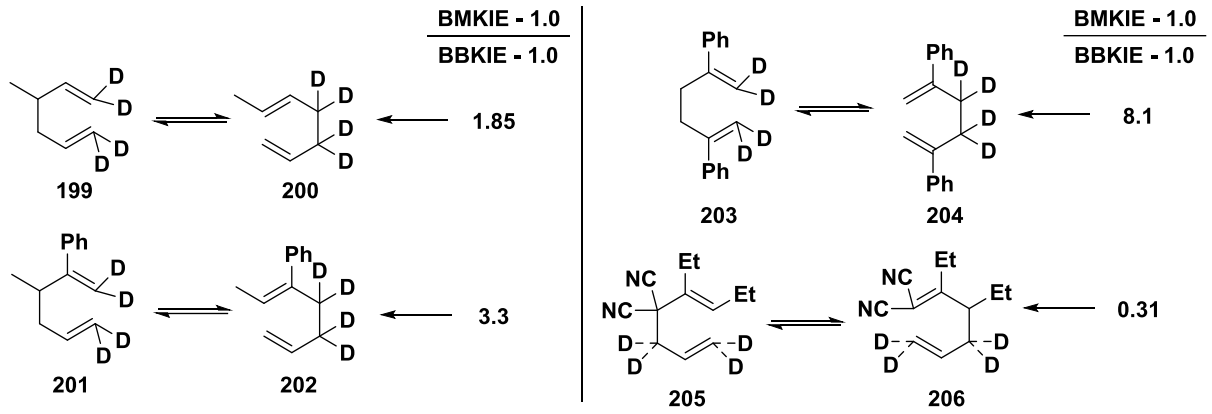

Scheme 2.5 Determination of bond making / breaking secondary kinetic isotope effect

Unfortunately, attempts to trap the "biradical" intermediates in the presence of hydroquinone, thiols, other reagents were unsucessful[61], and no crossover products that would argue for the "bisallyl radical" intermediate have been found[62]. This suggests that the Cope rearrangement is concerted, but the extent of the bond formation and dissociation is not synchronous when radical-stabilizing substituents are present.

Meanwhile, a stepwise mechanism involving ionic intermediates has also been considered by Wigfield et al[63]. They proposed that the mechanism for the Cope rearrangement of **207** might involve a heterolytic cleavage to a highly stabilized malonitrile anion and an allyl cation **208** which recombine to give the product **209** (Scheme 2.6). If the Cope rearrangement of **207** involves an ionic mechanism, the solvent polarity would exert a great influence on the rate of isomerization; however, no drastic change in the rate of isomerization has been observed in going from cyclohexane to ethanol-water mixture as the reaction solvent. These experimental results rendered the ionic mechanism highly unlikely.

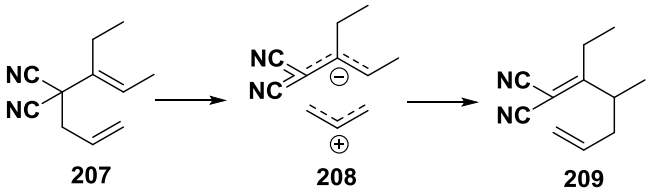

Solvent	Relative rate of Cope
Cyclohexane	1
1,4-Dioxane	11.2
Ethanol	11.7
1:1 Ethanol-water	16.7

Scheme 2.6 Solvent effect on the mechanism of Cope rearrangement

In the case where the double bond of **C5** and **C6** is in conjugation with the *p*-methoxyphenyl group such as **210**, Wigfield et al. observed that the thermal isomerization gave exclusively the [1,3]-shift product **211** and none of the product **212** which would be expected from a concerted Cope rearrangement (Scheme 2.7 (i))[64]. Chemically induced dynamic nuclear polarization (CIDNP) did not detect any short-lived free radical intermediates, thus rendering the radical mechanism unlikely. By conducting an ion trapping experiment, Wigfield et al. were able to trap the cationic intermediate using sodium borohydride, and they detected anethole **213** and dinitrile **214** by gas-liquid chromatography (GLC) mass spectrometry (Scheme 2.7 (ii)). Although this is no longer a Cope rearrangement but rather a [1,3]-shift, this result opened up the possibility of an ionic mechanism for the Cope rearrangement. However, substrates demonstrating an ionic [3,3]-sigmatropic shift were exceedingly rare, and the emphasis has been focused on studying mechanisms involving radical intermediates.

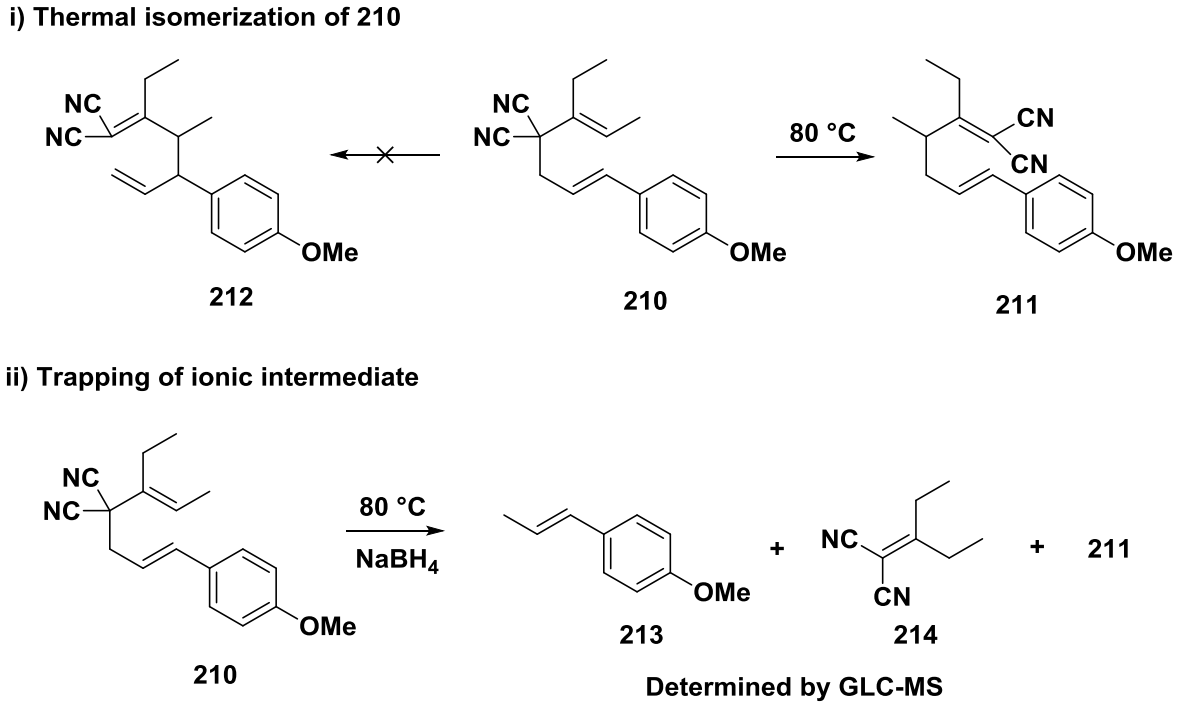

Scheme 2.7 Thermal isomerization and trapping of ionic intermediates

The More O'Ferrall-Jencks plot uses the three resonance contributors to show the substituent dependency of the Cope rearrangement (Figure 2.2). When the substrate contains radical-stabilizing group at 1-, 3-, 4- or 6- position (called active positions), the transition state will

have more of a "bisallyl radical" character, whereas with radical-stabilizing group at 2- and 5-position (called nodal positions), the transition state will show more of a "biradical" character. However, in the case in which the substituents are in mixed positions (e.g., 2,4-substituted systems), two important questions arise: 1) would there be a preference for one of the three resonance contributors in the transition state, and 2) whether the stabilizing effect by the substituent at each position adds up or competes against each other. To address these questions, Doering et al. proposed the "centauric" and "chameleonic" models for the transition state depending on the substitution patterns[65]. In "centauric" model, we assume that for some substitution patterns the transition structure is a half allyl radical-half secondary radical, and the substituent effects are additive. In contrary, the "chameleonic" model assumes that for different substitution patterns the transition structure favors only one of the three resonance contributors, and substituent effects are either cooperative or competitive.

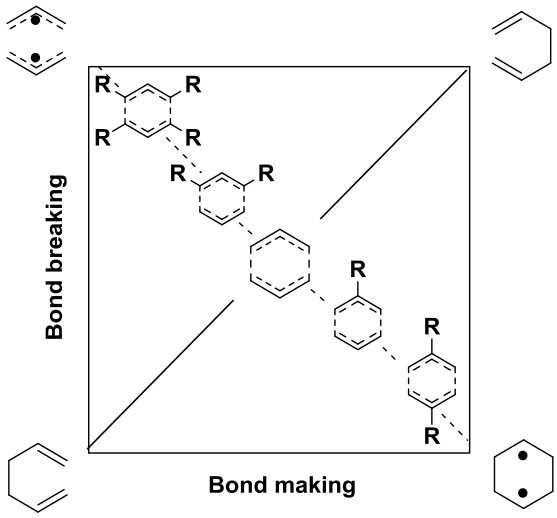

Figure 2.2 More O'Ferrall-Jencks plot of substituent effects on Cope rearrangement

The effect of phenyl substituents on the Cope rearrangement of 1,5-hexadienes has been studied in depth both computationally and experimentally by Dewar, Doering and Houk[61,66,67]. First, the calculated activation enthalpy of 2-phenyl-1,5-hexadienes **215** using unrestricted-B3LYP was 29.4 kcal/mol, which is 3.8 kcal/mol lower compared to the parent system **123** (33.2 kcal/mol) (Table 2.1, entry 1 and 2). Next, the calculated activation enthalpy for 2,5-diphenyl-1,5-hexadiene **216** was 21.3 kcal/mol which was in excellent agreement with the experimental value (entry 3)

(experimental value is 21.3 ± 0.3 kcal/mol)[66]. If the substituent effect was additive, the second phenyl group should have also lowered the activation enthalpy of **216** by 3.8 kcal/mol from **215**. Instead, the experimental activation enthalpy was lowered by a much greater value of 8.1 kcal/mol, which suggests that the substituent effect is cooperative as the "chameleonic" model would predict. This trend was also observed for systems with substitutions at active positions, such as 1,3-diphenyl-1,5-hexadiene **217** and 1,3,4,6-tetraphenyl-1,5-hexadiene **218** (entry 4 and 5). For the system with substituents at "mixed" positions such as 1,3,5-triphenyl-1,5-hexadiene **219** (entry 6), substituent effect additivity predicts the enthalpy value to be 27.4 kcal/mol. The B3LYP calculated enthalpy is 29.2 kcal/mol, which indicates a negative deviation of 1.8 kcal/mol from substituent effect additivity. This is due to the occurrence of competitive effect in which the phenyl group stabilizes different diradical contributors. Although the value predicted from substituent effect additivity is closer to the experimental value, the deviation observed from B3LYP calculation is within the range of experimental error.

Table 2.1 Activation enthalpy of Cope rearrangement for phenyl-substituted systems

Entry	Substrate	Method	Calc. $\Delta H^{\ddagger}$ (kcal/mol)	R^{*} (Å)
1	1,5-hexadiene (**123**)	B3LYP	33.2	1.965
2	2-phenyl-1,5-hexadiene (**215**)	UB3LYP	29.4	1.837, 1.821
3	2,5-diphenyl-1,5-hexadiene (**216**)	UB3LYP	21.3	1.794, 1.680
4	1,3-diphenyl-1,5-hexadiene (**217**)	B3LYP	30.2	2.218
5	1,3,4,6-tetraphenyl-1,5-hexadiene (**218**)	B3LYP	19.1	2.649
6	1,3,5-triphenyl-1,5-hexadiene (**219**)	B3LYP	29.2	2.113, 2.106

* Length of the forming bond and breaking bond respectively

Houk et al. used the transition structure geometries to explain the observed cooperative and competitive substituent effects[67]. For the cases in which the phenyl substituent is at the nodal position such as in 2-phenyl-1,5-hexadiene **215**, the phenyl substituent causes an average shortening of 0.14 Å for the forming and breaking single bonds in the B3LYP transition structure compared to the parent system **123** (Table 2.1, entry 1 and 2). With the second phenyl substituent in **216**, the bonds are further contracted by ~ 0.09 Å (entry 3). These bonds contractions reflect a

diradical-like transition structure geometry. On the other hand, for substrates with phenyl groups at bond forming/breaking positions such as **217** and **218**, an average of ~ 0.25 and ~ 0.68 Å in bond lengthening is observed, consistent with a bisallyl radical-like transition structure geometry (entry 4 and 5). For the substrate with phenyl groups at mixed position such as 1,3,5-triphenyl-1,5-hexadiene **219**, the average bond length is ~ 2.11 Å, which is ~ 0.11 Å shorter than 1,3-diphenyl-1,5-hexadiene **217** (entry 6).

Multiple phenyl substituents at the same type of carbon causes the transition structure to adopt more diradical-like or bisallyl radical-like geometry, and it is this ideal geometry that allows additional phenyl substituents to have cooperative effects in order to maximize the stabilization. However, in the case of phenyl substituents at mixed position such as with **219**, each substituent stabilizes different diradical contributors to it. Therefore, there is a competitive stabilization, and the optimal transition structure geometry is a compromise between the two operating diradical contributors. This explains why the average bond length of **219** is shorter than **217**. Since the substituent patterns of **219** lead to an overall elongation in the interallylic distance compared to the unsubstituted parent system, substrate **219** adopts the transition structure that is bisallyl radical-like.

Based upon all the experimental and computational data, currently the "chameleonic" model best describes the transition structure of substituted Cope rearrangements.

2.2 Proposed mechanism for our organocatalytic Cope rearrangement

In a simple model system, we performed DFT calculations in order to investigate the mechanism of our iminium-catalyzed Cope rearrangement (Figure 2.3). We initially identified transition state **221** in which a significant amount of bond formation has occurred. Using intrinsic reaction coordinate (IRC) studies, we followed the reaction path from this transition state. The reaction proceeded to an intermediate which was lower in energy by 0.4 kcal/mol. This shallow-energy intermediate was revealed to be carbocation **222** which possessed C-C bond lengths of 1.72 Å for the bonds that are formed and broken during the Cope rearrangement. These calculations suggested that the reaction may occur in a stepwise fashion by conjugate addition followed by

fragmentation, and we realized that this mechanism was related to the palladium and gold catalyzed Cope rearrangement by Overman and Gagné groups.

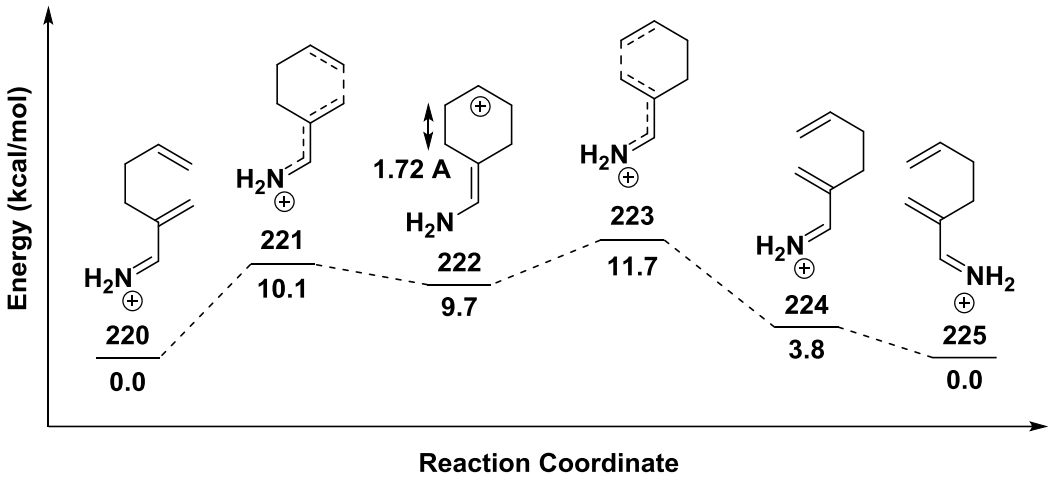

Figure 2.3 IRC calculations of the rearrangement pathways

Previously, Overman et al. reported the palladium-catalyzed Cope rearrangement of 1,5-hexadiene **226** to the products **228** and **229**, and they proposed a stepwise mechanism in which the palladium catalyst activates the olefins of **226** to generate the carbocation intermediate **227** (Scheme 2.8 (i))[68]. In 2012, Gagné et al. reported the gold-catalyzed asymmetric Cope rearrangement of acyclic diene **230** to **234**, which was aided by the strain release of the methylenecyclopropane moiety (Scheme 2.8 (ii))[69].

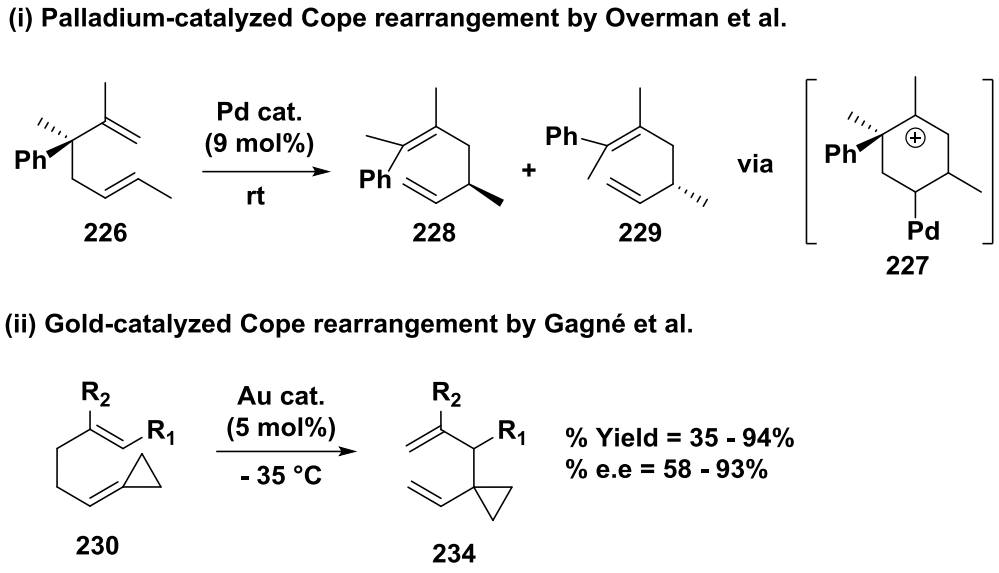

Scheme 2.8 Pd and Au-catalyzed Cope rearrangement via carbocation intermediate

Supported by the DFT calculations, Gagné et al. proposed that the reaction was proceeding through a tertiary carbocation intermediate **232** which was lower in energy by 3.2 kcal/mol compared to the next transition structure **233** (Figure 2.4).

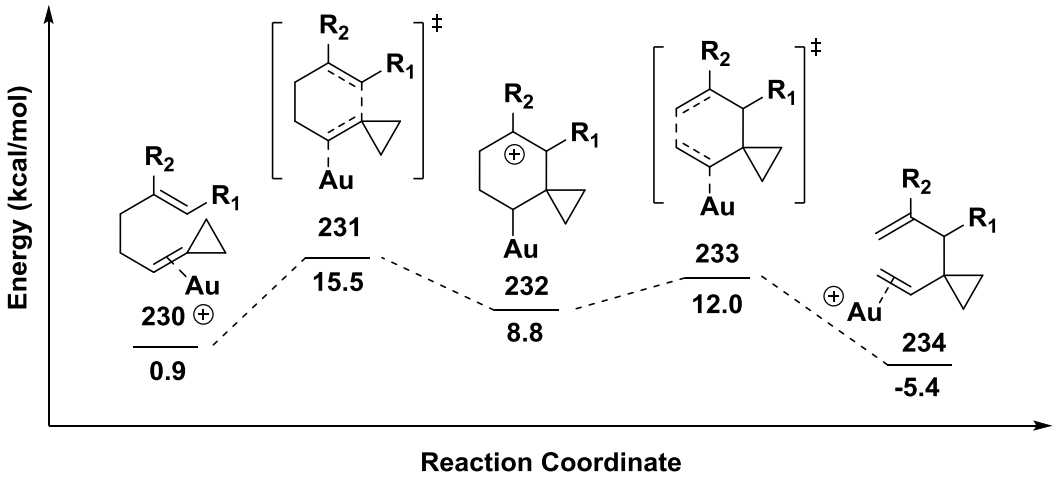

Figure 2.4 DFT calculations for proposed intermediates and transition structure

We propose that our Cope rearrangement also proceed in a stepwise mechanism with a carbocation intermediate, similar to Overman and Gagné's reactions. Thus far, our only evidence

for a stepwise mechanism is computational, thus we need to perform more detailed mechanistic experiments to determine the real mechanism of our Cope rearrangement.

2.3 Proposed origin of rate acceleration for cyclic hydrazide catalysts

In addition to our computational study of the mechanism, we are also interested in understanding the differences in rate between the 5-7 membered ring catalysts. DFT calculations predict that the C-N-N bond angle of the iminium ion increases from 108.7° to 119.3° as the ring sizes increases from 5 to 7. Due to the larger C-N-N bond angle, A-1,3 strain is increased, and the calculated energy of the 7-membered iminium ion increases by 3.7 kcal/mol (Scheme 2.9 (i)). Thus, the formation of 7-membered iminium ion might be expected to be least favored, yet it is the most active of the three cyclic catalysts.

We hypothesized that the stability of the iminium ion is not key to the reactivity, but rather the formation of the iminium ion. One of the key steps in the formation of iminium ions is the proton transfer from the protonated ammonium catalyst to the carbonyl, and another proton transfer to the hydroxyl group at the tetrahedral intermediate, leading to the loss of water. We proposed that the less basic catalyst, which forms a more acidic ammonium with a lower proton affinity, would promote those key events. Our DFT calculations of proton affinity and experimental pKa analysis (performed by Dr. Häggman) on catalysts **137**, **138**, and **121** showed a decreasing trend in proton affinity and basicity in going from the 5 to 7-membered ring catalyst (Scheme 2.9 (ii)). Tomkinson's computational study on the formation of iminium ion revealed that the initial deprotonation of the protonated amine catalyst is the key rate-determining step[70]. They observed a general correlation in which the amine catalyst with lower proton affinity had lower energy barrier for the rate-determining step. Our 7-membered hydrazide catalyst **121** has the lowest proton affinity, thus it would also have the lowest energy barrier for the rate-determining step of the iminium ion formation. Our observed reactivity trend was consistent with this proton affinity/basicity argument, and therefore, it was reasonable to postulate that the iminium ion formation would be the rate-limiting step in our Cope rearrangement.

(i) Calculated ring C-N-N angles and energy of iminium

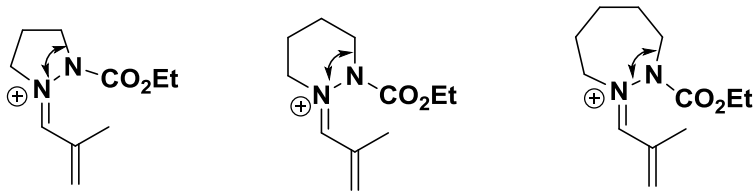

Ring C-N-N angle	**108.7 °**	**114.9 °**	**119.3 °**
Energy (kcal/mol)	**0**	**2.5**	**3.7**

(ii) Calculated proton affinity and experimental pKa

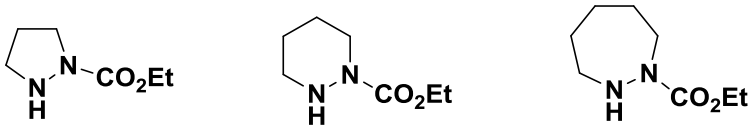

	137	**138**	**121**
Relative proton affinity (kcal/mol)	**0**	**-0.8**	**-1.4**
Experimental pKa	**3.4**	**3.0**	**2.7**

Scheme 2.9 Calculated bond angles and proton affinity of hydrazide catalysts

2.4 Purpose of the investigation

The purpose of this investigation was to experimentally and computationally validate the mechanism of our Cope rearrangement and determine the origin of rate acceleration of our hydrazide catalysts. Based on our previous experiments, we hypothesized that our Cope rearrangement proceeded in a stepwise mechanism via an intermediate carbocation with the formation of iminium ion as the rate-limiting step. In addition, we believe that the lower proton affinity and basicity of the larger ring hydrazide catalyst are the reasons for the observed rate acceleration in our Cope rearrangement. Meanwhile, the Houk research group were also interested in studying the mechanism and the rate accelerating effect of the hydrazide catalysts in our Cope rearrangement. This project was performed in collaboration with the research group of Professor K. N. Houk, and it is still in the progress. All the computational analysis has been performed by Dr. Sanders and Mr. Yu, and we conducted all the experimental work in the laboratory of Professor

James L. Gleason. Due to time constraints, the computational analysis is not yet completed, and the data provided may require further modifications.

2.4.1 Results and discussion on the origin of rate acceleration

Unlike our hypothesis, Houk's group proposed that the observed reactivity trend has more to do with the relative rigidity/flexibility of the cyclic hydrazide catalysts. The Houk group performed calculations on three different hydrazide catalysts (**235**, **236**, and **237,** Figure 2.5) and determined the activation energy of the intermediates and transition states along the reaction coordinate.

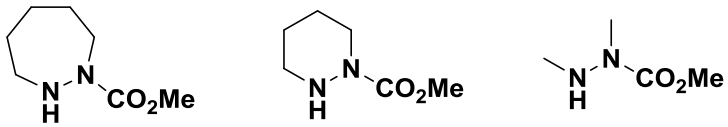

235 **236** **237**

Figure 2.5 Hydrazide catalysts used for the calculations

The catalyst **237** was chosen as a model acyclic system to allow for conformational flexibility, and it was used to predict the preferred conformations of intermediates and transition states in the absence of a ring system. According to the calculations, the activation energy for the transition states was the highest for the 6-membered ring catalyst **236**, next followed by the acyclic catalyst **237**, and then the 7-membered ring catalyst **235** (Figure 2.6).

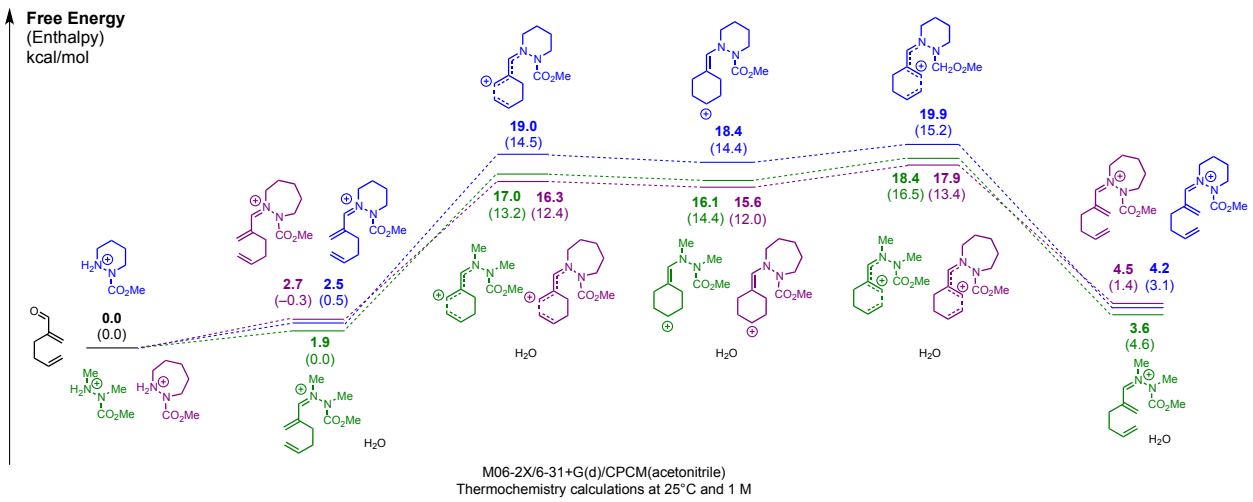

Figure 2.6 The calculated activation energy of transition states for different catalysts

To explain the differences in the activation energy between the 6- and 7-membered ring catalysts, the Houk group looked at their conformations of the highest-energy transition states, as well as their conformations of the starting ammonium catalysts.

First, the highest-energy transition states of the 6- and the 7-membered ring system had slightly different conformations. When these conformations have been compared with the one from the model acyclic catalyst, it was found that the transition state of the 7-membered ring catalyst adopted a conformation that was close to the transition state of acyclic ring system when compared to the 6-membered ring system. This suggests that 7-membered ring system adopts the most ideal transition state geometry. On the other hand, the transition state of the 6-membered ring system was distorted out of the ideal conformation of the model acyclic catalyst. Therefore, the Houk group proposed that in the 6-membered ring system, the distortion from the ideal geometry causes a destabilization of the transition state, which results in a higher activation barrier compared to the 7-membered and the model acyclic system.

Secondly, when looking at the geometry of the iminium ions from the 6- and the 7-membered rings, they again had slightly different conformations. This time, the 6-membered ring catalyst adopted a conformation that was close to the acyclic catalyst, and the conformation of the 7-membered ring catalyst was distorted out of the ideal conformation. The Houk group proposed that with the 7-membered ring catalyst, its distortion out of the ideal geometry causes it to be destabilized and become less rigid than the 6-membered ring catalyst, which results in a lower

activation barrier compared to the other catalyst. Overall, this Houk's group proposal suggest that the rate-liming step is the Cope rearrangement, not the iminium ion formation.

In order to experimentally validate the proposal by the Houk group, we decided the measure the reaction kinetics for the Cope rearrangement using the catalysts **235**, **236**, and **237**. Although the relative rates of the Cope rearrangement have been previously measured with the ethyl carbamate version of our hydrazide catalysts, the computational calculations have been performed using methyl carbamate version of our hydrazide catalyst. Thus, for accuracy reason, we decided to re-measure the reaction kinetics using the catalyst **235**, **236**, and **237**. To start, our model substrate for the Cope rearrangement, 2-methylene-4-phenylhex-5-enal **126**, was synthesized in 6 steps starting from (*E*)-4-phenylbut-3-en-2-one **238**, as has been previously published in the literature (Scheme 2.10)[46].

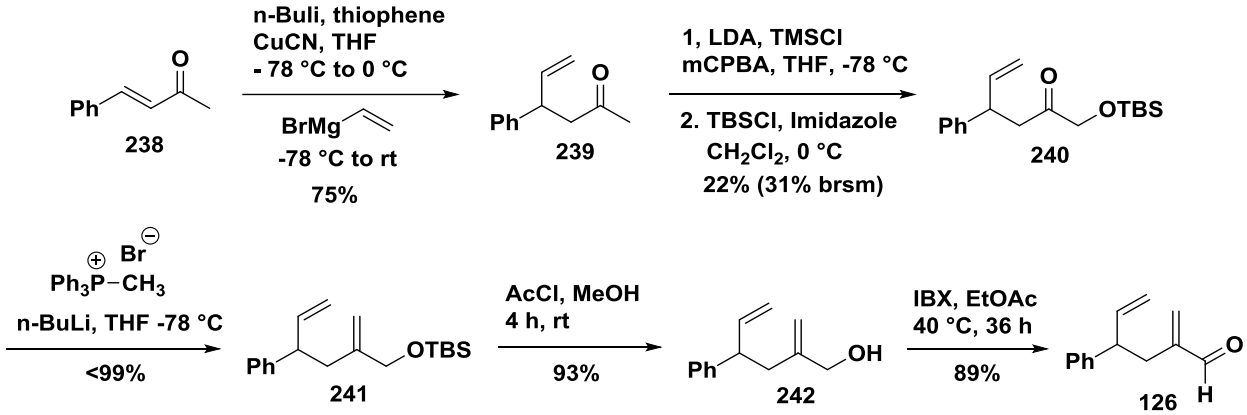

Scheme 2.10 Synthesis of the model substrate 155

The hydrazide **235**, **236**, and **237** were all prepared starting from 1-(*tert*-butyl) 2-methyl hydrazine-1,2-dicarboxylate **243** (Scheme 2.11)[46]. For the synthesis of catalyst **235**, the formation of 7-membered ring from **243** with NaH/1,5-dibromobutane in DMF afforded **244** in 67% yield, and the N-Boc deprotection with AcCl in methanol afforded the free base of the catalyst **235** in 91% yield after the basic work-up (Scheme 2.11 (i)). For the synthesis of catalyst **236**, the formation of 6-membered ring from **243** with NaH/1,4-dibromobutane in DMF afforded **245** in 89% yield, and the N-Boc deprotection with AcCl in methanol gave the free base of **236** in 86% yield after the basic work-up. For the acyclic catalyst **237**, di-methylation of **243** with NaH/MeI in DMF afforded **246** in 89% yield, and N-Boc deprotection of **246** with AcCl in methanol gave the

acyclic catalyst **237** as a HCl salt in nearly quantitative yield (Scheme 2.11 (ii)). The free base of **237** was very unstable and volatile, so it used directly as a HCl salt.

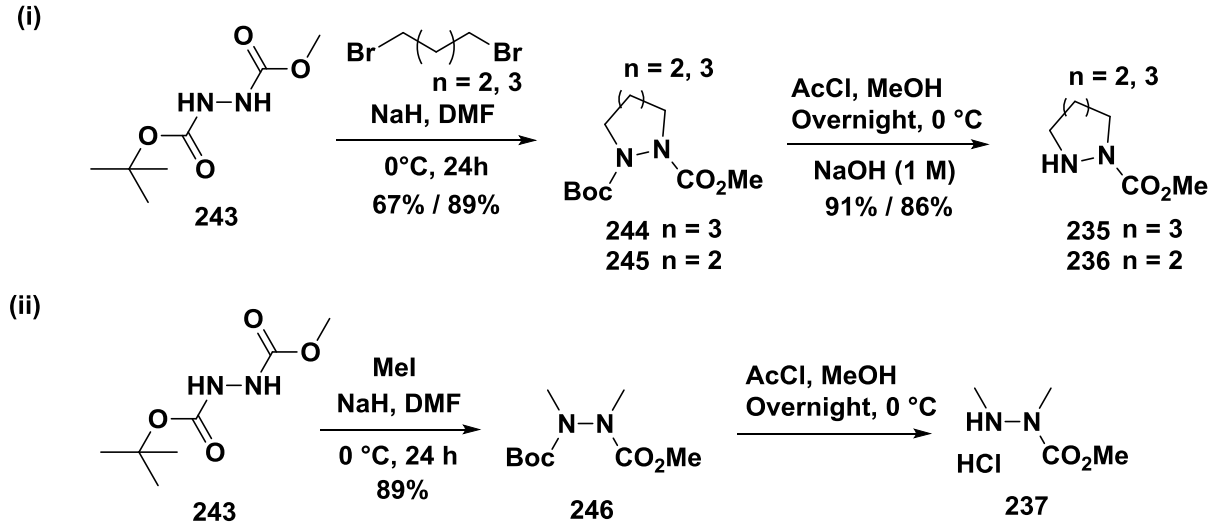

Scheme 2.11 Synthesis of hydrazide catalysts 235, 236 and 237

The reaction kinetics for the model Cope rearrangement were measured by NMR, using 10 mol% of each catalyst as HCl salt in CD_3CN at a concentration of 0.25M relative to the starting material, and the results are summarized in figure 2.7.

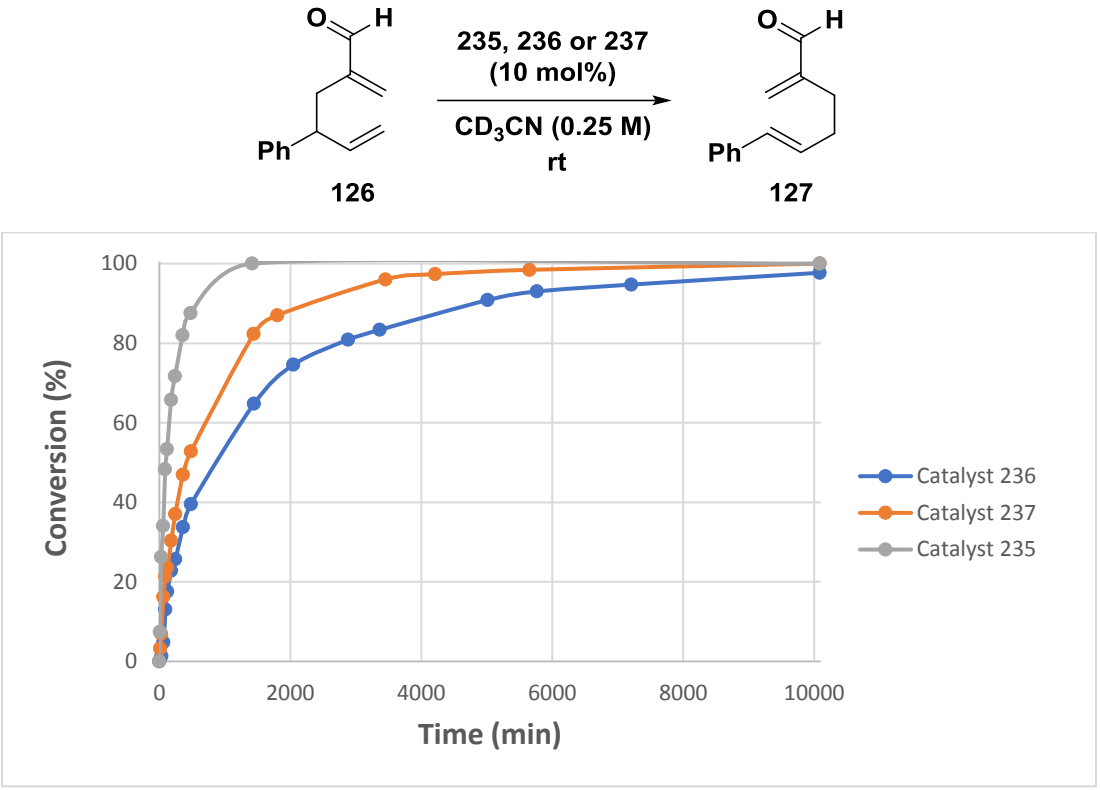

Figure 2.7 The graph of the kinetics measurement

According to our kinetics measurements, the relative rate of Cope rearrangement goes as 7-membered (**235**) > acyclic (**237**) > 6-membered (**236**), which is fairly consistent with the activation energy calculations performed by the Houk group (Figure 2.6). Meanwhile, more computational calculations are being performed by the Houk group in order to optimize transition state structures.

2.4.2 Elucidation of reaction mechanism through kinetic isotope effect

Isotopes are the same element that have different molecular weights. If a site that is involved in the change of bond order is labeled with isotopes, a difference in a reaction rate occurs. The kinetic isotope effect (KIE) measures the change in reaction rate that occurs upon isotopic substitution, and it is a useful tool for elucidating reaction mechanism.

2.4.3 Basic theory of kinetic isotope effect[71, 72]

There are two kinds of kinetic isotope effects: the primary KIE, and the secondary KIE. In primary KIE, the bond to the isotopically labeled atom is made or broken, causing a change in the rate of a reaction. In secondary KIE, the isotopically labeled atom is not directly involved in the bond formation or breakage, but the bond character such as the hybridization changes along the reaction coordinate. The potential energy surface diagram is commonly used to explain these concepts (Figure 2.8). First, every atom has its own zero-point vibrational energy (ZPVE) which is dependent on the vibrational frequency. The equation for the vibrational frequency is given by:

$$v = \frac{1}{2\pi}\sqrt{\frac{k}{m}} \tag{1.1}$$

where *k* is the spring force constant, and *m* is the reduced mass of the atom. Taking protium and deuterium as examples, the value of *m* would be roughly 1 and 2 respectively. According to the equation (1.1), the vibration frequency for deuterium will be smaller than protium, which subsequently results in a lower zero-point vibrational energy (denoted as **(A)** and **(B)** in Figure 2.8). Therefore, protium starts from a higher energy level than deuterium, so it requires less activation energy to reach the barrier where the bond is broken (denoted as **(C)** which is the transition state). This results in an overall change in the rate of a reaction in protium vs. deuterium-labeled compounds.

The same concept applies to the isotopes of other elements such as carbon, oxygen and nitrogen. However, the observed KIE from those elements will be much smaller than deuterium KIE values, because their relative weight difference between the normal and heavier isotope is smaller, which results in small differences in zero-point vibrational energy between the isotopes.

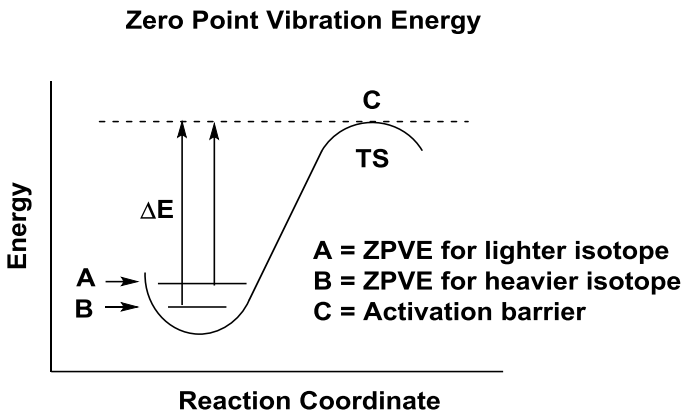

Figure 2.8 The zero-point vibration energy for primary KIE

Secondary KIE can be observed when the bond to the isotopically labeled atom undergoes a change in hybridization along the reaction path (Figure 2.9). For example, in an S_N2 reaction the bond hybridization goes from sp^3 to nearly-sp^2 in the transition state. The transition state will have a higher vibrational frequency because it has more s-characters. A higher vibrational frequency means that the spring force constant *k* becomes larger, so the change in reduced mass *m* becomes more significant (equation (1.1)). With a larger spring force constant *k*, the zero point energy for the lighter atom in the transition state is much higher in energy than the heavier atom in the transition state. In consequence, for the reactant with lighter isotope to reach that zero point energy in the transition state (from **A** to $\mathbf{A}^{\ddagger}$), it requires more energy compared to the reactant with heavier isotope (from **B** to $\mathbf{B}^{\ddagger}$). In this is case, the lighter isotope would react slower than the heavier isotope.

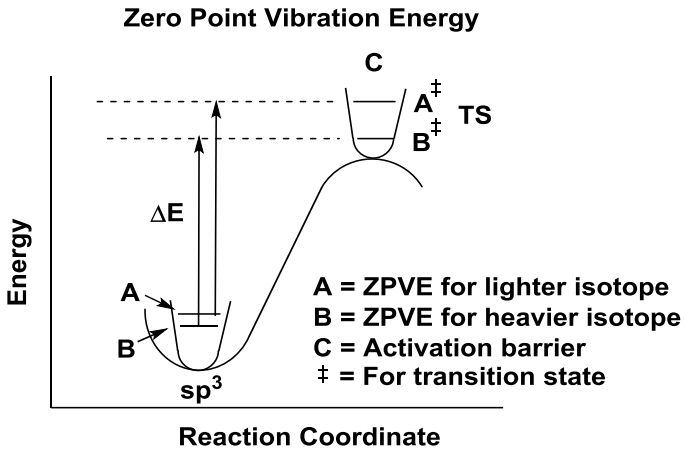

Figure 2.9 The zero point vibration energy for secondary KIE

2.4.4 Experimental determination of KIE: Singleton's method

The primary ^{2}H KIE provides useful information on whether the formation or breakage of C-H bond is involved in the rate determining step of a reaction, and the secondary ^{2}H KIE tells us if a change in hybridization occurs at the adjacent carbon center along the reaction path. Since organic reactions involve making or breaking bonds to a carbon, ^{13}C KIE can also provide useful insights on the reaction mechanisms in which bonding changes occur on carbon atoms in the rate determining step.

One of the experimental methods to determine ^{2}H or ^{13}C KIE is to synthesize isotopically-labeled analogues and analyze the deuterium or ^{13}C content of the starting material or the product by high-resolution NMR. However, the synthesis of isotopic analogues is often very costly and difficult. To overcome this issue, Singleton et al. reported a method to determine ^{2}H or ^{13}C KIE using the heavy isotope content present at natural abundance[73]. As any reaction proceeds, the starting material becomes fractionatively enriched in heavy isotopes which reacts slower than lighter isotopes due to the normal KIE. By taking the reaction to a very high conversion and recovering the starting material, one can compare the isotopic component of the recovered starting material with an unreacted starting material and calculate the corresponding heavy atom KIE. Therefore, the fractional conversion of the reactants is the most important parameter, and with higher conversions, the obtained KIE values becomes much more accurate with a smaller associated uncertainty. The natural abundance of deuterium is only ~ 0.00115% whereas for ^{13}C it

is ~ 1.1 %, thus for ^{2}H KIE analysis, much larger amount of the sample is required compared to the ^{13}C KIE analysis.

Singleton et al. demonstrated the applicability of their method with the Diels-Alder reaction of isoprene **247** with maleic anhydride **248** (Scheme 2.12 (i)). The reaction was taken to 98.9% completion relative to the isoprene **247**, and the unreacted isoprene **247** was recovered for KIE analysis. The ^{13}C KIE has been observed at **C1** (1.022) and **C4** (1.017) which are reacting carbon centers, and the ^{13}C KIE were very small for nonreacting carbon centers **C2** (1.001) and **C4** (1.000) (Scheme 2.12 (ii)). This result indicates that **C1** and **C4** are involved in the rate determining step as one would expect in this Diels-Alder reaction. For the ^{2}H KIE, the "inside" hydrogens of **C1** and **C4** experienced more pronounce KIE (0.908 and 0.938) compared to the "outside" hydrogens (0.956 and 0.968), which suggested that this Diels-Alder reaction proceeds through an asynchronous mechanism.

(i) Diels-Alder reaction between isoprene and maleic anhydride

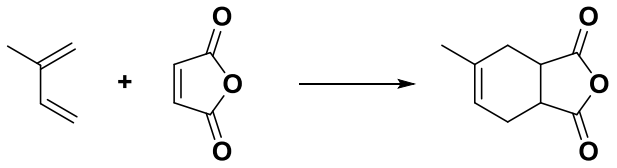

247 **248** **249**

(ii) Observed ^{2}H and ^{13}C KIE on isoprene at 98.9% conversion

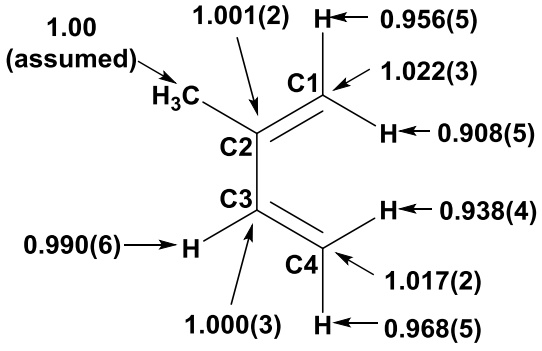

*** standard deviation in parenthesis**

Scheme 2.12 Determination of ^{2}H and ^{13}C KIE in Diels-Alder reaction

For a proper determination of KIE from this method, the reaction must be irreversible, the reaction mechanism must not change over the course of the reaction, and it must be insensitive to impurities in the analyzed product. In addition, in the case of ^{2}H KIE the reaction must be highly scalable to allow recovery of sufficient amount of starting material because of much lower natural abundance of deuterium compared to ^{13}C as mentioned previously. A part from Diels-Alder reactions, Singleton's method has been used to determine the experimental KIEs for many other reactions such as dihydroxylation[74], epoxidation[75] and Baeyer-Villiger oxidation[76], and the obtained experimental values correlated well with the computed data.

2.4.5 Experimental determination of KIE: DEPT spectroscopy method

In 2016, Kwan and Jacobsen reported an extension of Singleton's experimental determination of ^{13}C KIE using distortionless enhancement by polarization transfer (DEPT) spectroscopy[77]. The DEPT method takes advantage of larger gyromagnetic ratio of ^{1}H (42.6 MHz T^{-1}) over ^{13}C (10.7 MHZ T^{-1}), which theoretically results in up to a 4-fold improvement in sensitivity and 16-fold reduction in experimental time compared to the single-pulse ^{13}C NMR method that has been employed in Singleton's method. With this methodology, the amount of sample required for the NMR analysis can be significantly reduced, therefore it is a particularly attractive option for analyzing ^{13}C KIE of reactions in which the reacting starting materials require long synthesis, or expensive catalysts and reagents are used. To test the validity of this method, Kwan and Jacobsen ran the same Diels-Alder reaction of isoprene **247** and maleic anhydride **248** as in Singleton's report[77], and the ^{13}C KIE analysis of the resulting product **249** revealed that the obtained values were very consistent with the reported values by Singleton et al.

2.4.6 Results and discussions on the mechanism of our Cope rearrangement:

We first performed deuterium exchange experiment with the 7-membered ring catalyst **121**. With the DCl salt of our deuterated 7-membered ring catalyst, we measured the reaction kinetics using the same conditions above, but no notable difference in the reaction rate has been observed between the protiated and deuterated catalysts, which might suggest that the iminium ion formation is not the rate-limiting step in our Cope rearrangement.

We next performed the ^{13}C KIE analysis on the Cope rearrangement in order to determine the carbons that experience significant changes in bond order at the rate-determining step. The goal of this experiment was to distinguish between iminium ion formation and the Cope rearrangement as the rate-determining step, as this was a key difference between our original hypothesis and the computations of the Houk group. We used Jacobsen's DEPT method for the ^{13}C KIE analysis owing to its enhanced sensitivity, reduction in NMR running times, and lesser amount of material required for the analysis compared to the single pulse ^{13}C NMR method by Singleton et al.

In order to test for the reproducibility of the DEPT method, we ran the Diels-Alder reaction of isoprene **247** and maleic anhydride **248**, and the obtained ^{13}C KIE value was consistent with the reported values by Singleton and Jacobsen (Scheme 2.13)

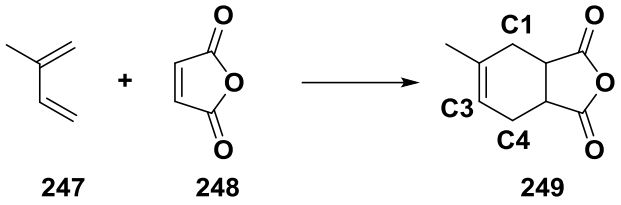

	C1	C3	C4
DEPT (exp. run 1)	1.023(3)	1.005(3)	1.017(3)
DEPT (exp. run 2)	1.021(3)	1.000(3)	1.018(3)
Singleton[73]	1.022(3)	1.000(3)	1.017(2)
Jacobsen[77]	1.023(3)	1.002(3)	1.019(3)

Scheme 2.13 The comparison of experimental ^{13}C KIEs

Next, we measured the ^{13}C KIEs for our Cope rearrangement. The reaction was run to ~25% conversion (run 1) and ~15% conversion (run 2), each relative to the starting material **126,** using 10 mol% of catalyst **235**, and the isolated product **127** from each reaction (which is lower in ^{13}C isotope) was compared with the full 100% conversion product **156** (which contains natural abundance of ^{13}C isotope) to calculate the experimental ^{13}C KIE. The results are summarized in Scheme 2.14, along with the computed values provided by the Houk group.

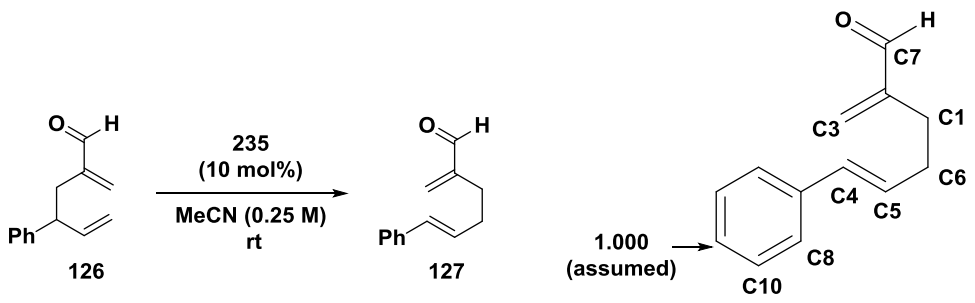

	C1	C3	C4	C5	C6	C7	C8	C10
Run 1 (25% conv.)	1.021(7)	1.012(7)	1.010(8)	1.004(7)	1.024(8)	1.011(7)	0.998(6)	0.999(6)
Run 2 (15% conv.)	1.033(4)	1.021(4)	1.016(4)	1.003(4)	1.030(4)	1.007(4)	1.000(4)	0.999(4)
Houk	1.037	1.011	1.012	1.006	1.033	1.002	-	-

Scheme 2.14 The experimental and computed ^{13}C KIEs for the Cope rearrangement

Looking at the experimental ^{13}C KIEs, the **C1** / **C6** which are the two carbons of the breaking bond in the Cope rearrangement experience the most significant KIEs of 1.021 and 1.024, while **C3** / **C4**, which are the bond forming carbons have substantial KIEs of 1.012 and 1.010 which suggest that they must be involved in the rate-determining step. There is also a non-unity KIE on the aldehyde carbon **C7** which also suggest that it may also be part of the rate-determining step. The computational results by the Houk group agree qualitatively with the experiment. They also predicted significant KIEs of 1.037 and 1.033 at the bond breaking carbons **C1** and **C6**, and substantial KIEs of 1.011 and 1.012 and at the bond forming carbons **C3** and **C4**. These KIE results are consistent with a rate-limiting Cope rearrangement with an early transition state in which the degree of bond formation is greater than the degree of bond breaking, and they highlight that the Cope rearrangement for our model substrate **155** proceeds via a concerted mechanism. However, the Houk group proposed that the mechanism of our Cope rearrangement may change depending on the substituents. With a phenyl group at **C4** as in substrate **155**, the reaction was predicted to be concerted, which has been validated by our KIE experiments. For the unsubstituted system, their computational calculations suggested a stepwise mechanism proceeding through an intermediate cation. For substrate **155**, the conjugation of **C4-C5** double bond with the phenyl group may act as a driving force for a concerted mechanism, whereas this driving force is absent for the unsubstituted system.

2.5 Conclusion and future directions

In collaboration with the Houk group, we performed detailed mechanistic works on our organocatalytic Cope rearrangement. As for the origin of rate acceleration, the Houk group proposed that the conformational flexibility of the larger ring catalyst allows the highest-energy transition state to adopt the ideal geometry that is lower in energy compared to the 6- and acyclic catalyst. In addition, the 7-membered ring ammonium catalyst adopts a conformation that is less rigid than the 6-membered ring ammonium catalyst, and this lowers the activation barrier. So far, our kinetic measurements are in alignment with Dr. Houk's proposals.

In addition, we experimentally determined the ^{13}C KIEs for our Cope rearrangement, and the results suggest that the rate-determining step is the Cope rearrangement and not the formation of iminium ion. Our ^{13}C KIE study also confirmed that the Cope rearrangement of the model system **126** proceeds through a concerted mechanism as proposed by the Houk group. However, their computational calculations suggest that the Cope rearrangement proceeds via a stepwise mechanism for the unsubstituted system. Therefore, the substituent effect seems to have a great influence on the mechanism of our Cope rearrangement. Meanwhile, the Houk group is performing further computational calculations to optimize some of the results.

2.6 References

51. Hoffmann, R. and R. B. Woodward (1965). Journal of the American Chemical Society **87**(19): 4389-4390.
52. Fukui, K. (1971). Accounts of Chemical Research **4**(2): 57-64.
53. Dewar, M. J. S. (1971). Angewandte Chemie International Edition in English **10**(11): 761-776.
54. E. Doering, W. v. and W. R. Roth (1962). Tetrahedron **18**(1): 67-74.
55. Schneider, M. P. and A. Rau (1979). Journal of the American Chemical Society **101**(15): 4426-4427.
56. von E. Doering, W., et al. (1971). Tetrahedron **27**(22): 5299-5306.
57. Roth, W. R., et al. (1990). Journal of the American Chemical Society **112**(5): 1722-1732.

58. Graulich, N. (2011). WIREs Computational Molecular Science **1**(2): 172-190.
59. Dewar, M. J. S. and L. E. Wade (1973). Journal of the American Chemical Society **95**(1): 290-291.
60. Gajewski, J. J. and N. D. Conrad (1979). Journal of the American Chemical Society **101**(22): 6693-6704.
61. Doering, W. v. E., et al. (2000). Journal of the American Chemical Society **122**(2): 193-203.
62. Sunko, D. E., et al. (1970). Journal of the American Chemical Society **92**(22): 6534-6538.
63. Wigfield, D. C. and S. Feiner (1970). Canadian Journal of Chemistry **48**(5): 855-858.
64. Wigfield, D. C., et al. (1974). Tetrahedron **30**(16): 2949-2959.
65. Doering, W. v. E. and Y. Wang (1999). Journal of the American Chemical Society **121**(43): 10112-10118.
66. Dewar, M. J. S. and L. E. Wade (1977). Journal of the American Chemical Society **99**(13): 4417-4424.
67. Hrovat, D. A., et al. (2000). Journal of the American Chemical Society **122**(31): 7456-7460.
68. Overman, L. E. and E. J. Jacobsen (1982). Journal of the American Chemical Society **104**(25): 7225-7231.
69. Felix, R. J., et al. (2012). Nature Chemistry **4**(5): 405-409.
70. Evans, G. J. S., et al. (2006). Organic & Biomolecular Chemistry **4**(13): 2616-2627.
71. Lowry, T. H. and K. S. Richardson (1976). Mechanism and theory in organic chemistry : (by) thomas H. Lowry and kathleen schueller richardson. New York, Harper and Row.
72. Cohen, S. G., et al. (1963). Progress in physical organic chemistry. Volume 1. New York, Wiley.
73. Singleton, D. A. and A. A. Thomas (1995). Journal of the American Chemical Society **117**(36): 9357-9358.
74. DelMonte, A. J., et al. (1997). Journal of the American Chemical Society **119**(41): 9907-9908.
75. Singleton, D. A., et al. (1997). Journal of the American Chemical Society **119**(14): 3385-3386.

76. Singleton, D. A. and M. J. Szymanski (1999). Journal of the American Chemical Society **121**(40): 9455-9456.

77. **Kwan**, E. E., et al. (2017). Journal of the American Chemical Society **139**(1): 43-46.

Chapter 3. Effort towards a dual photoredox and iminium organocatalysis

3.1 Basic theory of photoredox catalysis

Since the late 2000's, photoredox catalysis has receive a lot of attention from synthetic chemists, and there has been a significant increase in the number of research publications employing this novel mode of activation in various organic transformations[78]. In photoredox catalysis, a photocatalyst selectively absorbs photons from visible light to enter an excited state, and it engages in single-electron transfer (SET) with an organic substrate to generate a reactive open-shell radical intermediate. Compared to traditional radical chemistry which requires highly reactive radical initiators, photoredox catalysis only uses small amount of photocatalyst (often 1 mol%) that is bench stable and inert under standard conditions. In addition, upon irradiation with simple household light bulbs or blue LEDs, the excited photocatalysts have the unique ability to act both as an oxidant and a reductant in the same reaction vessel, thus providing access to previously inaccessible reaction platforms[79].

Ruthenium or iridium-based polypyridyl complexes such as $Ru(bpy)_3^{2+}$ (**250**) and $Ir(ppy)_3$ (**251**), and organic dyes such as Eosin Y (**252**) and mes-acr (**253**) are among widely used and readily accessible photocatalysts (Scheme 3.1).

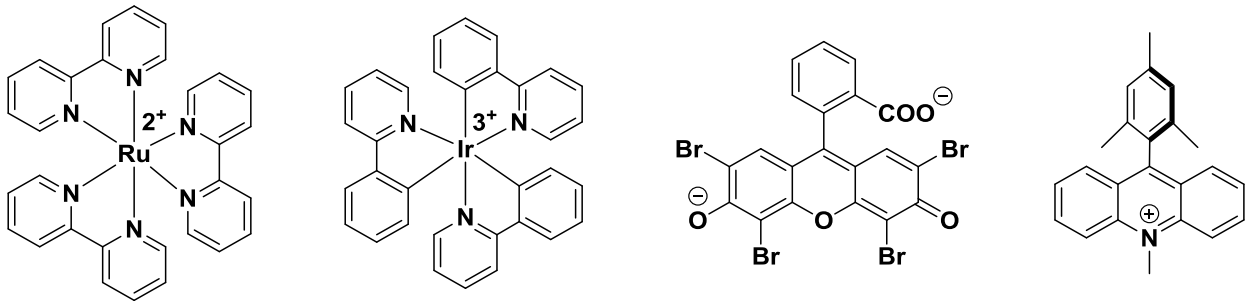

250 **251** **252** **253**

Scheme 3.1 Metal polypyridyl complexes and organic dyes used as photocatalysts

3.1.1 Photochemistry of $Ir(ppy)_3$ photoredox catalyst

Before discussing a variety of unique reactions enabled by photoredox catalysis, it is important to understand the concepts behind the photochemistry of a chromophore absorbing visible-light. For instance, a commonly used photoredox catalyst $Ir(ppy)_3$ **251** can be used as a standpoint to explain this concept using a simplified molecular orbital diagram (Figure 3.1).

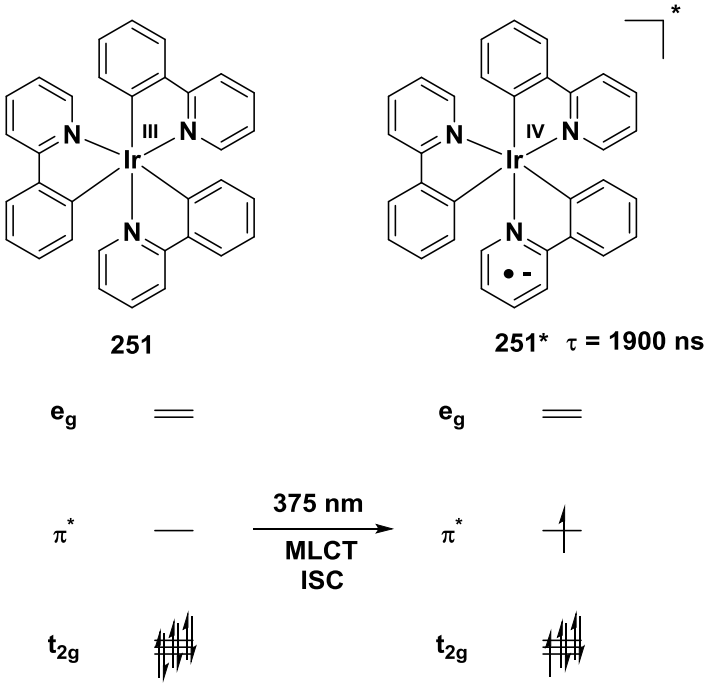

Figure 3.1 Molecular orbital diagram of iridium complex absorbing visible-light

Compact fluorescent light (CFL) and LEDs both provide irradiation over a broad range of wavelength, typically from 250 to 800 nm, and a typical photoredox catalyst such as **251** can absorb light in this visible spectrum range (maximum excitation wavelength of **251** is 375 nm)[80, 81]. When **251** absorbs a photon, it undergoes a metal to ligand charge transfer (MLCT), an event in which an electron from the d-orbital (t_{2g}) of the metal center is excited to the π^* orbital of the ligand (Figure 3.1). This causes an oxidation of Ir(III) to Ir(IV), and a single electron reduction of the phenylpyridine ligand framework (**251***) (the overall oxidation state of the metal complex still remains the same). The initially excited electron occupies the singlet MLCT state, but it can further relax to the lowest-energy triplet MLCT state via a process called intersystem crossing (ISC). This

triplet state has a long enough of a lifetime (1900 ns for the excited state $Ir(ppy)_3$ complex) that it can undergo electron-transfer as a relaxation pathway before it decays to the singlet ground state via phosphorescence. The reason for a long lifetime of the excited triplet state comes from the fact that the direct decay to the singlet ground state is spin-forbidden, therefore the spin must be first inverted back to the spin-allowed singlet excited state via phosphorescence (Figure 3.2).

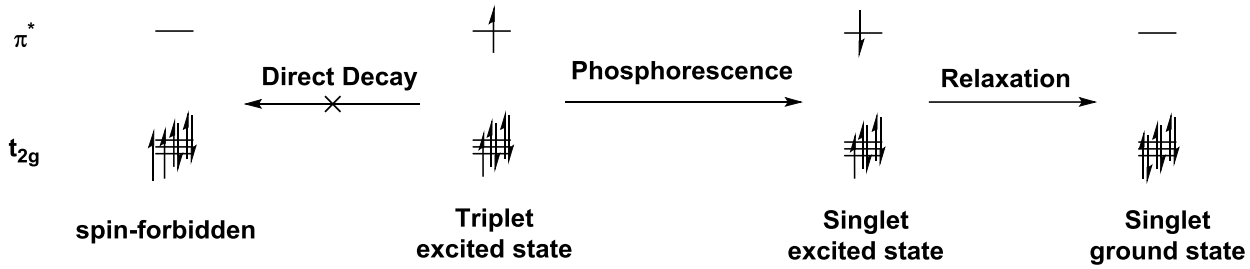

Figure 3.2 Relaxation pathway of triplet excited state to the ground state

The higher-energy electron in the π^* orbital of the excited $Ir(ppy)_3$ **251*** can either be donated to a substrate, thus acting as a reductant ($Ir(III)^*/Ir(IV)$ = -1.73V), or the empty lower-energy t_{2g} orbital can accept an electron from a substrate to act as an oxidant ($Ir(III)^*/Ir(II)$ = 0.31V) (Figure 3.1). Because of this dual redox property, the excited $Ir(ppy)_3$ **251*** can either be quenched via an oxidative or a reductive cycle (Figure 3.3)[78,79,82].

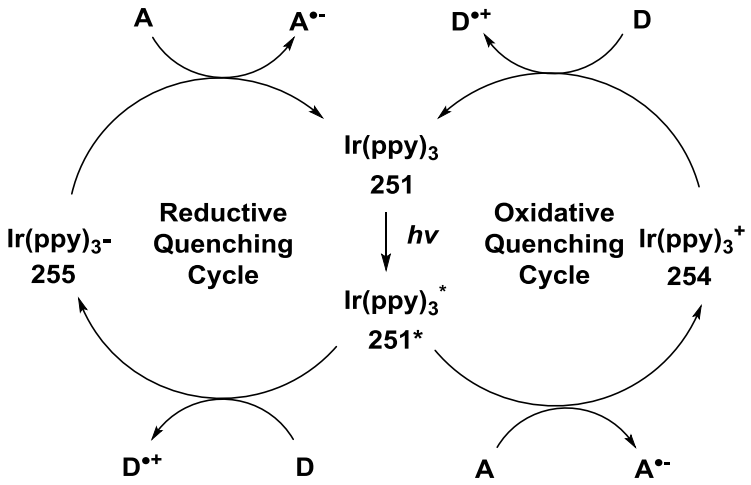

Figure 3.3 Oxidative and reductive quenching cycle of $Ir(ppy)_3$

In the oxidative cycle, **251*** donates a single electron to an acceptor **A** to generate the radical anion of **A** and the oxidized $Ir(ppy)_3^+$ **254**. Now $Ir(ppy)_3^+$ **254** is a strong oxidant (Ir(IV)/Ir(III) = 0.77V) and it can readily accept an electron from a donor **D** to give the radical cation of **D** and regenerate the ground state photocatalyst **251**.

In the reductive cycle, **251*** accepts a single electron from a donor **D** to generate the radical cation of **D** and the reduced $Ir(ppy)_3^-$ **255**. The reduced **255** is now a strong reductant that can donate a single electron to an acceptor **A** to generate the radical anion **A** and the ground state photocatalyst **251**.

For each of these single-electron transfer events to occur, the standard redox potential (*E*) of the donor must match the redox properties of the acceptor[80]. The Gibbs free energy for a ground-state electron transfer between a donor **D** and an acceptor **A** is given by the equation **2.1**:

$$\Delta G_{SET} = E^{ox}(D^+/D) - E^{red}(A/A^-) + \Delta E_{Coulomb} \quad (\mathbf{2.1})$$

The Coulombic charge interactions are often negligible when polar solvents are used, thus for the single-electron transfer events to be thermodynamically favored (i.e. $\Delta G_{SET} < 0$), the oxidation potential of the donor **D** ($E^{ox}(D^+/D)$) must be lower than the reduction potential of the acceptor **A** ($E^{red}(A/A^-)$). In order to tune the redox properties of the transition metal-based photocatalyst, one can alter the substituents on the ligands. As a general rule, electron-donating substituents on the ligands make the metal-complex more reducing, whereas the electron-withdrawing substituents make the metal-complex more oxidizing[83]. Although both ruthenium and iridium have the same electronegativity of 2.2, the iridium complexes are more potent reductants and oxidants than the ruthenium complexes due to their differences in spectroscopic properties of the metal center.

3.2 Earliest applications of photoredox catalysis in organic chemistry

The earliest example of photoredox catalysis of an organic reaction was reported by Kellogg et al. in 1978[84,85]. The reduction of phenacyl sulfonium salts **256** to the desulfurized product **259** could be significantly accelerated by using 1 mol% of $Ru(bpy)_3Cl_2$ **257** as a photocatalyst and a stoichiometric amount of *N*-Me Hantzsch ester **258** as a terminal reductant in

acetonitrile under visible-light (Scheme 3.2 (i)). The Hantzsch ester **258** can absorb in the visible region to get into the photoexcited state **258***, and it can react as a single electron reductant with **256** to generate acyl radical **256-A** and the oxidized Hantzsch ester **258-A** (Scheme 3.2 (ii)). The acyl radical **256-A** can either abstract a proton from **258-A** to generate the pyrinidium byproduct **258-C** and **259** (Path A), or it can abstract a proton from **258** to generate Hantzsch ester radical **258-B** which can enter the photoredox cycle (Path B). The excited $Ru(bpy)_3^{2+}$ **257*** acts as an oxidant and reacts with **258-B** to generate a highly reducing $Ru(bpy)_3^{+}$ **257-A** which reacts with the substrate **256** to generate acyl radical **256-A** and the ground state catalyst **257** which re-enters the catalytic cycle.

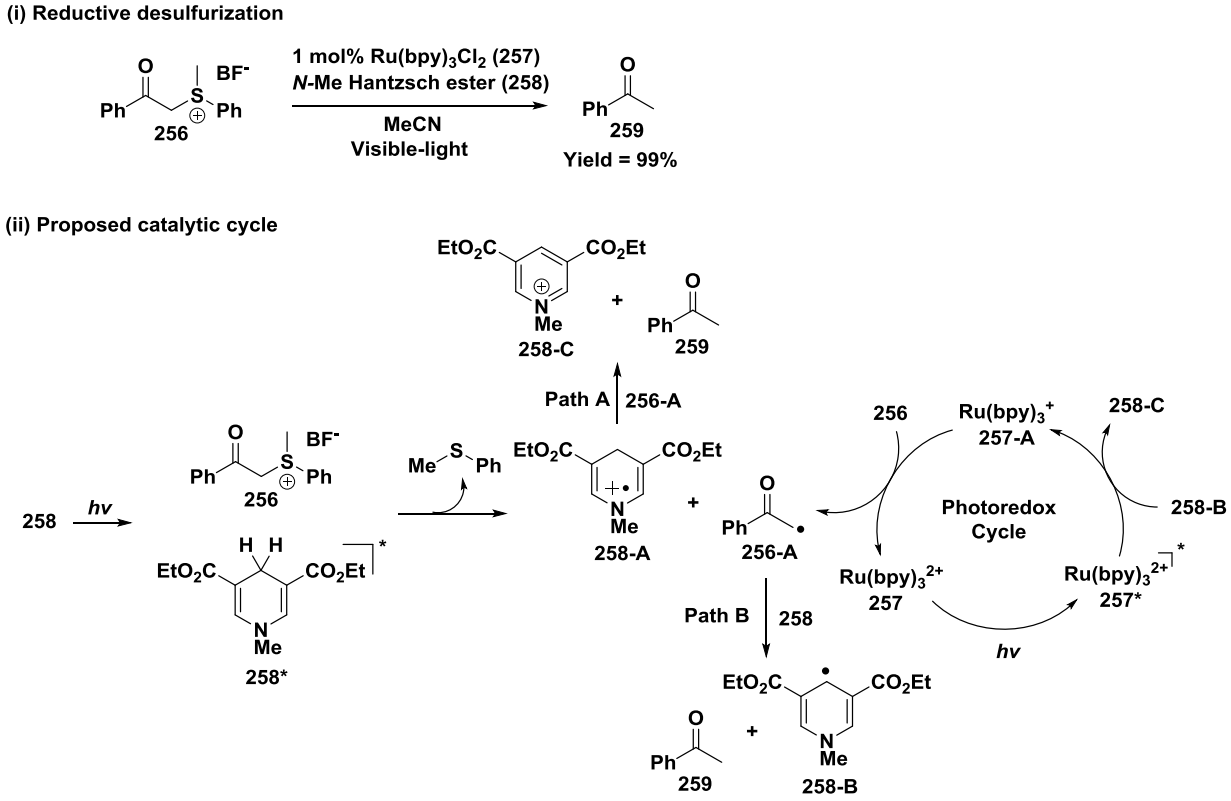

Scheme 3.2 Reductive desulfurization with photoredox catalysis by Kellogg et al.

In 1991, Okada et al. reported a decarboxylative conjugate addition of alkyl radicals to electron deficient olefins via photoredox catalysis[86]. In the presence of 2 mol% $Ru(bpy)_3Cl_2$ **257** and 1-benzyl-1,4-dihydronicotinamide (BNAH, **260**), alkyl radicals generated from *N*-(acyloxy)phthalimides **261** underwent 1,4-addition to electron deficient olefins **263** to give

products **264** in 45 – 69% yield (Scheme 3.3 (i)). The mechanism follows a reductive quenching cycle in which the excited $Ru(bpy)_3Cl_2$ **257*** is reductively quenched by BNAH (**260**) to generate highly reducing $Ru(bpy)_3^+$ **257-A** and the radical cation of BNAH (**260-A**) (Scheme 3.3 (ii)). *N*-(acyloxy)phthalimide **261** is reduced by **257-A** to produce radical anion **261-A**, which is quickly decarboxylated to generate phthalimide **262** and alkyl radical **261-B**. The free radical **261-B** adds to the electron deficient olefins **263** and a proton transfer from **260-A** yields the final product **264**.

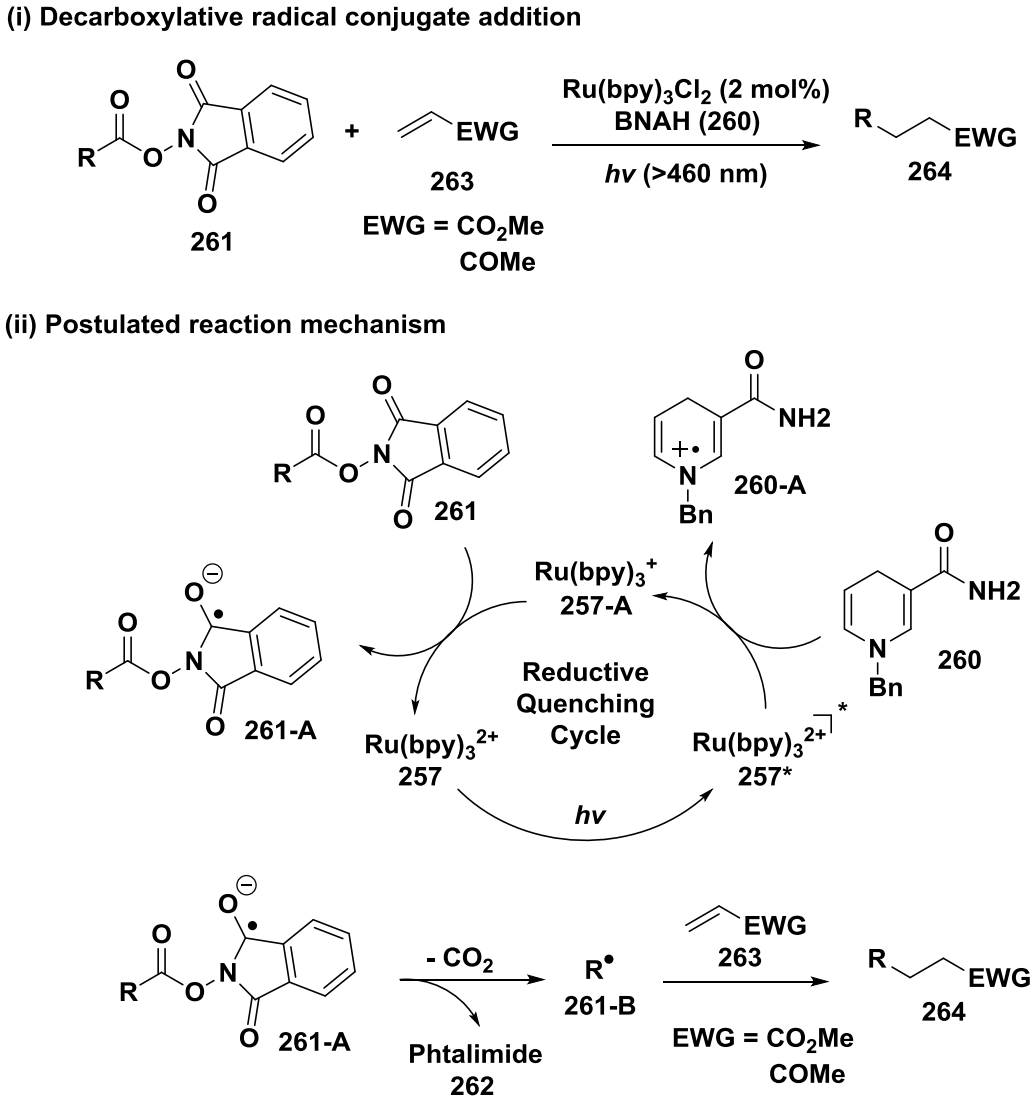

Scheme 3.3 Photocatalysis of decarboxylative radical conjugate addition by Okada

Despite the earlier works that showcased the potential of photoredox catalysis in synthetic chemistry, not much progress was made in this field until late 2000s.

3.3 Recent progress of photoredox catalysis in organic chemistry

Since the seminal reports by Yoon[87], MacMillan[88] and Stephenson[89] in 2008 and 2009, photoredox catalysis has received a lot of attention from synthetic chemists in both academia and industry. It has become a rapidly-growing field of research in organic chemistry as demonstrated by the exponential increase in number of publications in the past 10 years. While photoredox catalysis on its own enabled a variety of unique reactivity that was complementary to the traditional closed-shell pathways, synthetic chemists also recognized that photoredox catalysis could be combined with other activation modes to achieve synergistic catalysis[90]. In the case where a substrate is unreactive under photoredox conditions alone, the addition of a co-catalyst can activate the inert substrate so it can engage in single-electron transfer. Nowadays, Lewis/Brønsted acids, transition metal complexes, and organocatalysts are often used in combination with the photoredox catalyst to either 1) activate a single substrate, or 2) to interact with multiple substrates at once, where each catalyst perform a distinct role in its own discrete catalytic cycle which may or may not interweave with each other in the reaction mechanism. In addition, as the photocatalyst is not covalently or ionically associated with the open-shell radical intermediates it generates, there is an intrinsically lack of stereochemical control which can be overcome using complementary chiral catalysts [90].

3.3.1 Dual photoredox and Lewis acid catalysis

In 2008, Yoon et al. reported the first photoredox and Lewis acid catalyzed [2+2] cycloadditions of enones with visible-light[87]. With 2.5 mol% of $Ru(bpy)_3Cl_2$ **257**, $LiBF_4$ **266** as Lewis acid and Hünig's base **267** as a terminal reductant, a variety of substituted bis-enones **265** efficiently underwent cycloaddition to give product **268** in good yields and diastereoselectivity (Scheme 3.4 (i)). Each reaction component was necessary, and the replacement of $LiBF_4$ **266** with other additives such as Bu_4NBF_4 or $NaBF_4$ suppressed the reaction, suggesting that the lithium cation functions as a Lewis acid to activate the enone **265** towards single-electron reduction.

The mechanism starts with a reductive quenching of the excited $Ru(bpy)_3^{2+}$ **257*** with Hünig's base **267** to generate highly reducing $Ru(bpy)_3^{+}$ **257-A** (Scheme 3.4 (ii)). The substrate **265,** activated by a lithium cation, undergoes a single-electron reduction with **257-A** to generate

the radical **265-A** which subsequently undergo radical conjugate addition followed by cyclization to give **265-B**. One-electron oxidation of **265-B** by the radical cation **267-A** generates the product **268**.

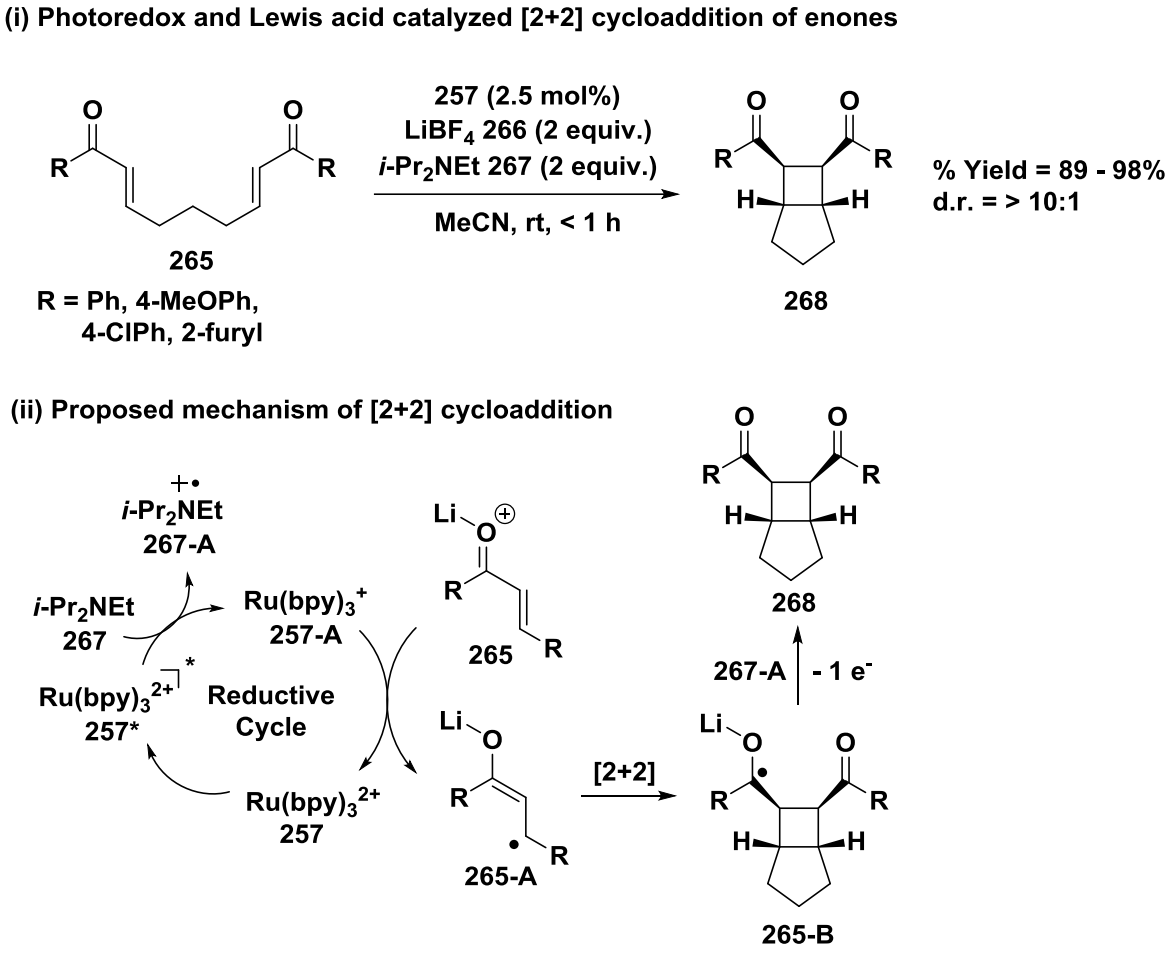

Scheme 3.4 Photocatalytic of [2+2] cycloaddition of bis-enones by Yoon

The asymmetric intermolecular variant of the [2+2] cycloaddition was also reported by the Yoon group later in 2014. Using the combination of europium Lewis acid **271** and chiral dipeptide ligands **272** or **273**, a range of aryl enone **269** and aliphatic enones **270** cyclized to the *cis* or *trans* cyclobutane product **274** in good yields and enantioselectivity (Scheme 3.5 (i))[91]. The reaction takes advantage of the selective bonding of the Lewis acid to the aryl enone **269**, inducing a significant difference in the reduction potential compared to the unbound aliphatic substrate **270**. This difference in reduction potential allows highly selective single-electron reduction of aryl

enones **269** in the presence of aliphatic enones **270**, and the undesired background reaction leading to the racemic products is avoided.

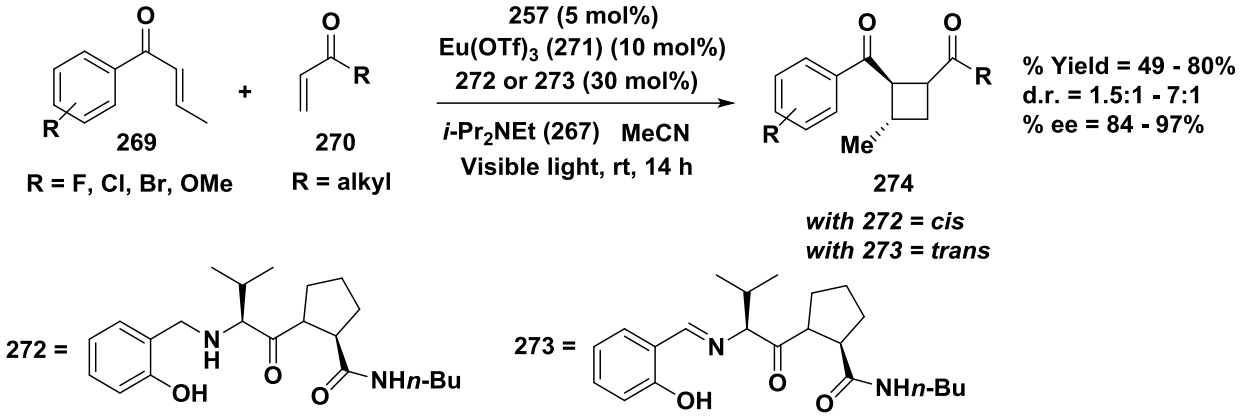

Scheme 3.5 Photocatalysis of intermolecular [2+2] cycloaddition of enones by Yoon

The combination of photoredox catalysis with Lewis acid allows a selective activation of substrates towards single-electron reductions by drastically increasing their reduction potential. Among many other examples, dual photoredox and Lewis acid catalysis has also seen applications in [3+2] cycloadditions[92], Mannich reactions[93] and heterocycles synthesis[94].

3.3.2 Dual photoredox and Brønsted acid catalysis

During the seminal work on photocatalytic [2+2] cycloadditions, Yoon et al. observed a major difference in reactivity when a Brønsted acid was used instead of a Lewis acid. Upon screening a variety of Brønsted acids, it was found that the bis-enone **275** could undergo a 5-*exo*-trig cyclization in the presence of a 2.5 mol% of $Ru(bpy)_3Cl_2$ **257**, 5 equivalents of formic acid **276** and 10 equivalents of amine **267** to afford product **277** in good yields and diastereoselectivity (Scheme 3.6 (i))[95]. As with the [2+2] cycloaddition, the excited photocatalyst **257*** is reductive quenched by the amine **267** to generate a highly reducing $Ru(bpy)_3^+$ **257-A** (Scheme 3.6 (ii)). In the presence of formic acid **276**, the excited photocatalyst **257-A** reduces the bis-enone **275** to the neutral radical **275-A** which performs a 5-*exo*-trig cyclization to give the radical intermediate **275-B**. A proton abstraction (or hydrogen atom transfer) from the amine radical cation **267-A** affords

the final product **277**. Compared to the [2+2] cycloadditions which are net redox-neutral, this reaction is a reductive cyclization involving an overall two-electron reduction of one of the enones.

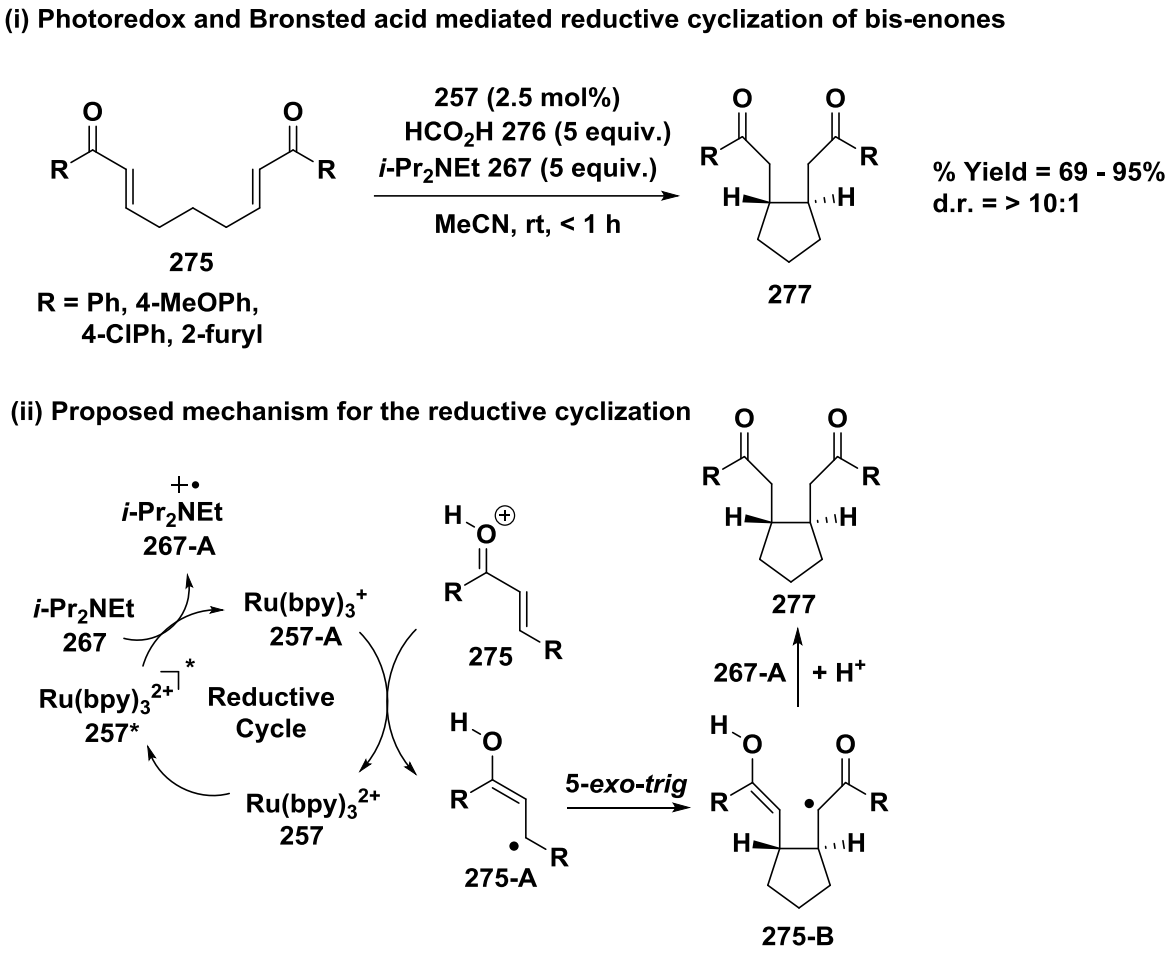

Scheme 3.6 Photocatalysis of reductive cyclizations by Yoon

Multisite proton-coupled electron transfer (MS-PCET) was potentially operative in Yoon's reductive cyclization of enones, as the presence of the formic acid was crucial for the optimal reactivity[90]. MS-PCET is a redox process in which the electron and proton from two separate sources are exchanged in a concerted elementary step, while avoiding high-energy intermediates involved in sequential pathways (Figure 3.4)[96]. The MS-PCET has been used to activate variety of functional groups such as ketones[97], alcohols[98], amines[99] and sulfonamides[100].

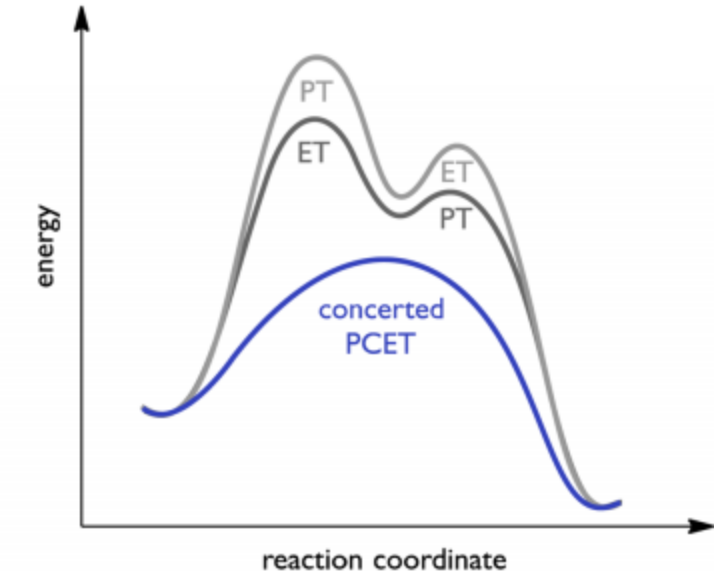

Figure 3.4 Energetic advantage of concerted PCET versus sequential pathways

3.3.3 Dual photoredox and amine organocatalysis

As discussed in the previous chapter, organocatalysis represents one of the most widely used substrate activation modes in organic chemistry. In addition, as shown by the number of examples in this chapter, photoredox catalysis can be combined with other complementary activation modes, and the merger of photoredox and organocatalysis has also been extensively researched in the past years. Indeed, one of the seminal reports by the MacMillan group that rapidly popularized the field of photoredox catalysis involved a dual photoredox-enamine catalysis[88].

Despite recent progress, the activation of α, β-unsaturated carbonyl compounds using the combination of photoredox and iminium catalysis remains a challenging and underdeveloped research area. In 2016, the Melchiorre group reported the first iminium-catalyzed enantioselective radical conjugate addition (RCA) to β-substituted enones to build quaternary carbon stereocentres[101]. The β-substituted cyclic enones **278** successfully underwent RCA with the radical partner **279** to afford product **282** in good yield and enantioselectivity (Scheme 3.7 (i)). The main challenge associated with RCA is that the resulting α-iminyl radical cations from the radical addition are short-lived, and they tend to undergo radical elimination to re-form the more stable iminium and radical ion. To address this issue, Melchiorre group used the electron-relay strategy in which the α-iminyl radical cation is rapidly reduced to its enamine by the redox-active electron-

rich moiety in order to avoid the undesired elimination pathway. The primary amine catalyst **280** has been specifically designed to introduce a redox-active carbazole moiety which acts as both as a single-electron reductant and stereo-defining component.

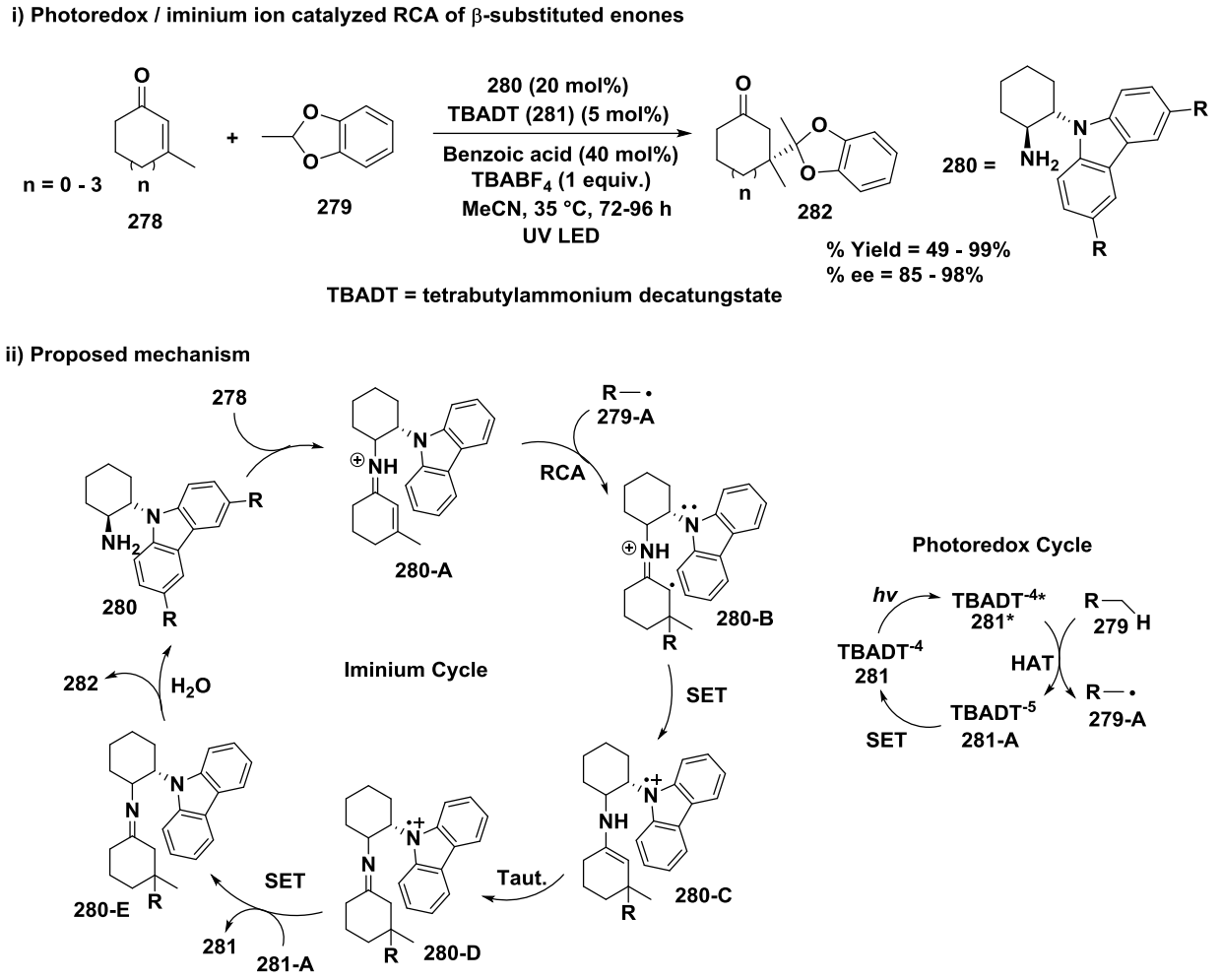

Scheme 3.7 Radical conjugate addition of β-substituted enones by Melchiorre

For the mechanism, the iminium ion **280-A** undergoes RCA with **279-A** to generate α-iminyl radical cation **280-B**, which is quickly reduced by the proximity carbazole moiety to its enamine **280-C** and tautomerized to imine **280-D** to avoid the back-electron transfer (BET) process that would re-form **280-B** (Scheme 3.7 (ii)). The redox state of the carbazole radical cation is restored by the external photocatalyst **281-A** to obtain imine **280-E**, and the final product **282** is generated upon hydrolysis. As demonstrated from the mechanism, each step was carefully designed to avoid undesired reaction pathways.

In 2017, Melchiorre et al. performed the β-alkylation of cinnamaldehyde derivatives catalyzed by the excited-state iminium ion[102]. Using 20 mol% of fluorinated prolinol catalyst **285**, a range of cinnamaldehyde derivatives **283** underwent β-alkylation with benzyl silanes **284** to afford product **286** in good yield and enantioselectivity (Scheme 3.8 (i)). Silanes **284** were chosen as the radical sources due to their relatively low oxidation potential (E_{ox} (**284**$^{\cdot+}$/**284**) = +1.74 V vs. Ag/Ag$^+$) and the tendency of its radical cation to desilylate even with weak nucleophile. The amine catalyst **285** was chosen for its ability to induce high enantioselectivity in thermal reactions, and for its high oxidation potential E_{ox} (**285**$^{\cdot+}$/**285**) = +2.40 V vs. Ag/Ag$^+$) which makes it less prone to single-electron oxidation by the excited iminium ion which leads to an undesired catalyst degradation path. Interestingly in this reaction, the iminium ion has been used as a catalytic organic photocatalyst, instead of a traditional LUMO-lowered electrophile.

The mechanism involves photo-excitation of ground-state iminium ion **285-A** to **285-A*** which is a strong oxidant that can trigger single-electron oxidation of silane **284** to generate β-enaminyl radical **285-B** and silane radical cation **284-A** (Scheme 3.8 (i)). Solvent acts as a nucleophile that desilylate **284-A** to produce alkyl radical **284-B**, which undergo radical-radical recombination with **285-B** to afford enamine **285-C**, and hydrolysis of **285-C** yield the final product. The possibility of radical propagation mechanism was rejected, as single-electron oxidation of **284** ((E_{ox} (**284**$^{\cdot+}$/**284**) = +1.74 V vs. Ag/Ag$^+$) by the α-iminyl radical cation **285-D** (E_{red}(**285-D/285-C**) ~ + 0.9 V vs. Ag/Ag$^+$) is an endergonic process.

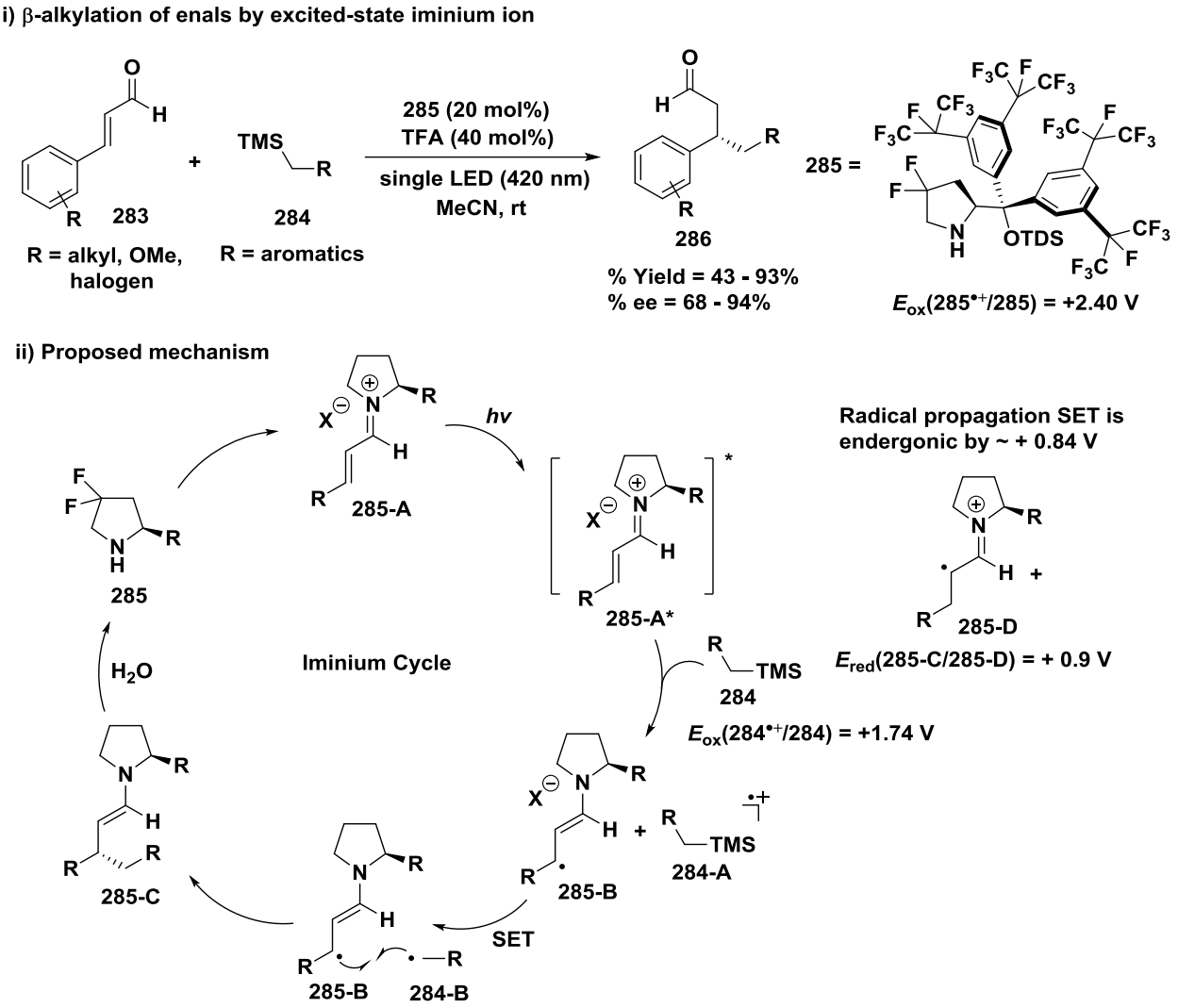

Scheme 3.8 β-alkylation of enals catalyzed by the excited state iminium ion

In addition to examples above, the Melchiorre group employed excited-state iminium ion catalysis to perform an asymmetric β-alkylation of enals via photocatalytic C-H functionalization of toluene[103], a β-functionalization of enals by allene radical addition[104], and they also developed an acyl radical addition to enals catalyzed by traditional LUMO-lowering iminium catalysis[105].

3.4 Investigation of reductive cyclization of enals using photoredox/iminium catalysis

In our previous investigations on the iminium catalyzed pericyclic reactions, we found that our 7-membered ring hydrazide catalysts were very efficient at forming iminium ions with the α-

substituted/unsubstituted enals, and the kinetics for the iminium ion formation was extremely fast compared to other secondary amines. Therefore, we wanted to take advantage of this reactivity and merge it with the photoredox catalysis. Inspired by Yoon's reductive cyclization of enones by photoredox and Brønsted acid dual catalysis (Scheme 3.6), we first became interested in performing similar reaction by using the iminium catalysis. The goal of my project was to achieve single-electron reduction of α, β-unsaturated iminium ions to generate reactive radical intermediates which could engage in radical addition reactions. To start, we planned the following catalytic cycle and chose the substrate **287** as the starting point for this investigation (Scheme 3.9). We anticipated that the α, β-unsaturated iminium ion **288** generated from the condensation of **287** with an amine catalyst could be readily reduced by an external reductant to generate the β-enaminyl radical **289**. The radical **289** could undergo intramolecular radical conjugate addition to the electron-deficient olefin to generate intermediate **290**, and HAT from a proton donor would produce enamine **291** which could hydrolyze to give the desired product **292**.

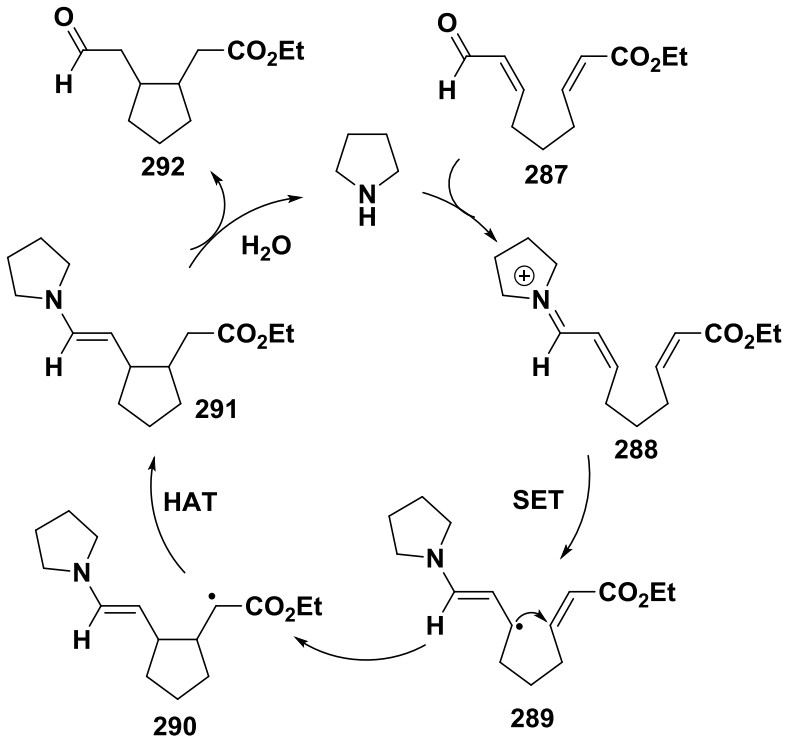

Scheme 3.9 Design for the reductive cyclization of α, β-unsaturated enals

Although a single-electron reduction of a ground-state α, β-unsaturated iminium ion to a β-enaminyl radical is currently unknown, the Gaunt group showed that a simple iminium ion can be reduced to an α-amino radical which can undergo olefin hydroaminoalkylation (Scheme 3.10) [106]. In their proposed mechanism, the iminium ion **296** undergoes SET with the iridium reductant to generate α-amino radical **297**. The radical **297** performs a conjugate addition to an electron deficient olefin **295** to generate the radical intermediate **298**, which undergoes a 1,5-HAT followed by a proton abstraction to release the product **299**. This example is similar to the reaction we are trying to perform, except that an α-amino radical is generated instead of a β-enaminyl radical. Likewise, we believe that by activating an olefin with the iminium catalysis and using an appropriate single-electron reductant, we could generate the desired β-enaminyl radical.

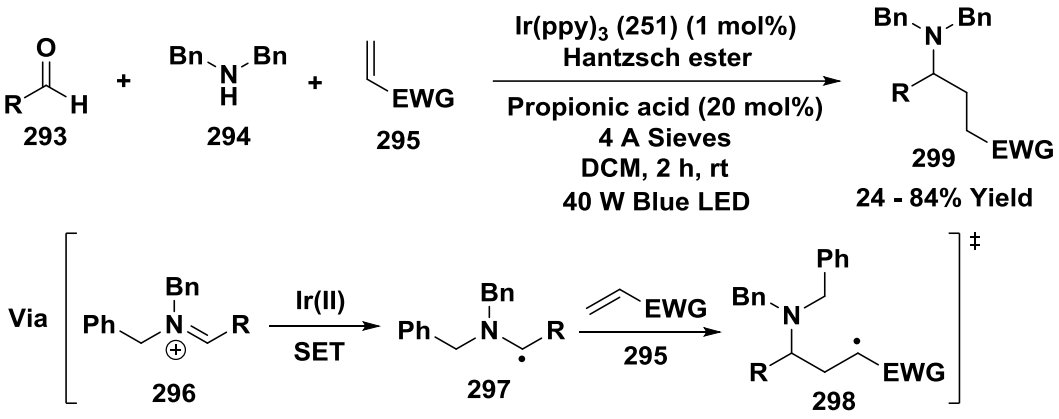

Scheme 3.10 Olefin hydroaminoalkylation by Gaunt

In addition, MacMillan et al. showed that electron-rich β-enaminyl radicals **302** (generated via a different method in his work) can be readily intercepted by an electrophilic olefin **301** to generate β-alkylation products **304** (Scheme 3.11)[107]. This example shows that our anticipated radical conjugate addition of β-enaminyl radical is a viable reaction pathway.

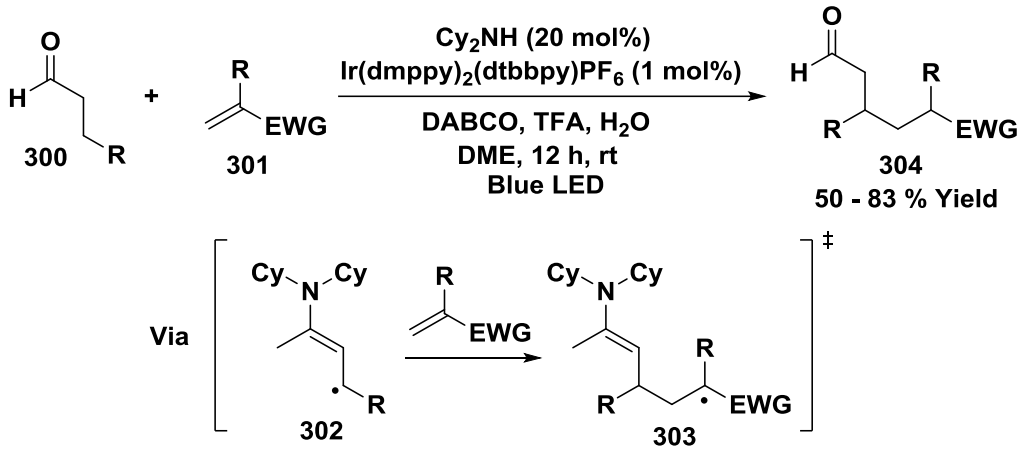

Scheme 3.11 β-Alkylation of aldehydes by MacMillan

3.4.1 Results and discussions

To start, the substrate **287** was synthesized starting from glutaric dialdehyde **305**. Wittig olefination of **305** with (triphenylphosphoranylidene)acetaldehyde followed by a second Wittig olefination with triphenylcarbethoxymethylenephosphorane afforded **287** in 28% yield over two steps (Scheme 3.12). The order of Wittig olefination was important to avoid the formation of inseparable dienal.

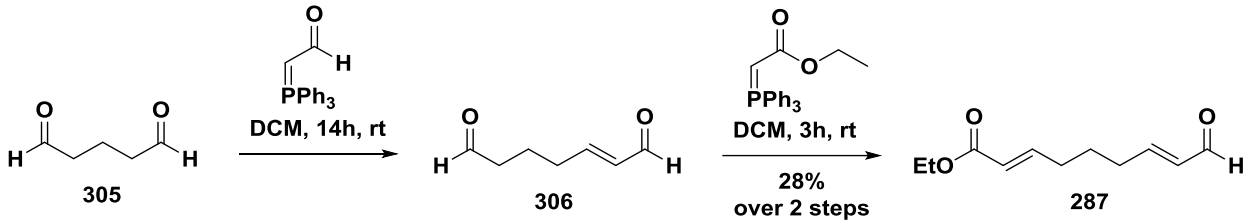

Scheme 3.12 Synthesis of the model substrate 287

We first tested out a list of available stoichiometric single-electron reductants with or without the 7-membered hydrazide catalyst **235**. When substrate **287** was treated with SmI_2 in THF in the presence or absence of the hydrazide catalyst **235**, the substrate quickly underwent complete decomposition within 1 h, and no product could be seen or isolated (Table 3.1, entry 1 and 2). Using lithium 4,4-di-tert-butylbiphenylide (LiDBB) with or without the hydrazide catalyst also led to a rapid decomposition of the starting material **287** within 30 min (entry 3 and 4). Lastly, we

looked at tetrakis(dimethylamino)ethylene (TDAE), an organic electron donor used in some radical coupling reactions[108,109]. The substrate **287** was allowed to react with TDAE in MeCN at room temperature or at 60 °C for extended period of time, but no reactivity was observed (entry 5 and 6). The presence of the hydrazide catalyst **235** had no impact (entry 7 and 8), and the neutralization of acid-co catalyst by the basic TDAE was observed, preventing the formation of iminium ion.

Table 3.1 Iminium catalyzed single electron reduction of 287

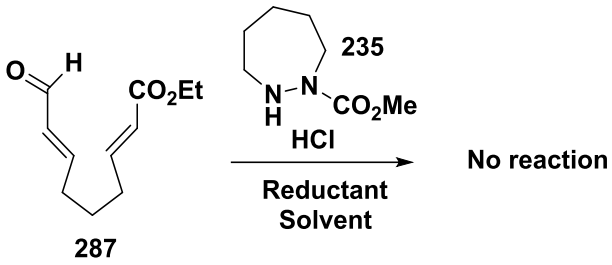

Entry	235 (mol %)	Reductant	Solvent	Temp (°C)	Time (h)	Product
1	-	SmI_2	THF	-78	1	Decomp.
2	100	SmI_2	THF	-78	1	Decomp.
3	-	LiDBB	THF	-78	0.5	Unknown mixtures.
4	100	LiDBB	THF	-78	0.5	Unknown mixtures.
5	-	TDAE	MeCN	rt	24	No Rxn.
6	-	TDAE	MeCN	60	24	No Rxn.
7	100	TDAE	MeCN	rt	24	No Rxn.
8	100	TDAE	MeCN	60	24	No Rxn.

We next looked at iridium- and ruthenium-based photocatalysts, and we closely followed Yoon's protocol for the reductive cyclization of bis-enone[95]. Substrate **287** was first treated with the 2.5 mol% of $[Ir(dtbbpy)(ppy)_2]PF_6$ (**307**), 10 equivalence of DIPEA (**267**), 5 equivalence of formic acid as a Brønsted acid in acetonitrile, and the mixture was irradiated with 23 W CFL (Table 3.2, entry 1). The reaction was completed within 3 hours, delivering 64% yield of the desired product **292** as a mixture of diastereomers. Keeping the above conditions, we added 20 – 50 mol%

of the hydrazide catalyst **235** (entry 2 – 3), and we obtained similar yields of the desired product, but without any observable rate acceleration. Reducing the amount of formic acid was not detrimental to the reaction (entry 4), and the absence of formic acid afforded slightly improved yield of the product (entry 5). The presence of both photocatalyst **307** and DIPEA **267** was essential to the reactivity (entry 6, 7 and 8). Based on the observed experimental results and Yoon's mechanistic proposal, DIPEA is an essential component that acts as a terminal reductant for quenching the excited photocatalyst Ir(III)* to highly reducing Ir(II) state, and also as a hydrogen atom donor. The Ir(II) state of **307** is strongly reducing (E_{red}(Ir(III)/Ir(II) = - 1.51 V) that the assistance of a Brønsted acid such as formic acid is not required to generate β-ketoradical. In addition, iminium catalysis was unlikely to be operative in this reaction as no rate acceleration or improvement of yield was observed.

Table 3.2 Reductive cyclization of 361 with iridium photocatalyst

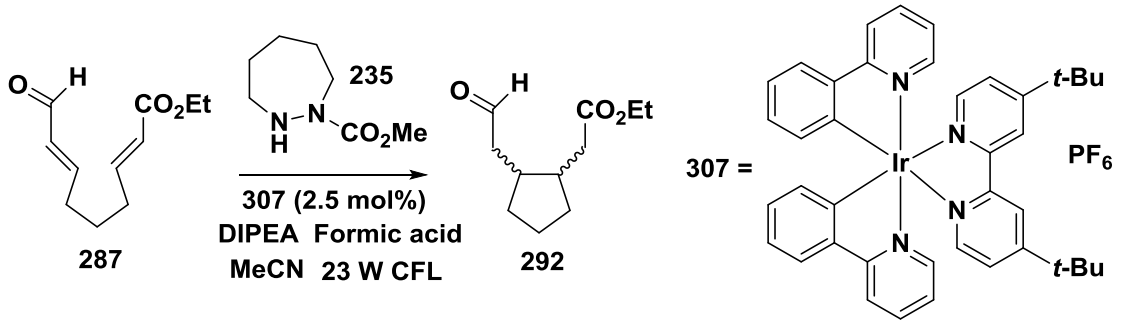

Entry	235 (mol %)	DIPEA (equiv.)	Formic acid (equiv.)	307 (mol %)	Temp. (°C)	Time (h)	% Yield of 292
1	-	10	5	2.5	rt	3	64
2	20	10	5	2.5	rt	3	62
3	50	10	5	2.5	rt	3	64
4	-	10	1	2.5	rt	3	65
5	-	10	-	2.5	rt	3	69
6	-	10	5	-	rt	3	-
7	-	-	5	2.5	rt	3	-
8	50	-	5	2.5	rt	3	Decomp.

Given the iridium photocatalyst **307** is a very strong reductant and it does not require the assistance of a Brønsted acid or an iminium catalysis, we decided to switch to the ruthenium photocatalyst **257** which has a slightly lower reduction potential (E_{red}(Ru(II)/Ru(I)) = - 1.33 V) than **307**. If a less reducing photocatalyst is used, the photocatalyst alone may not be able to reduce the substrate. Therefore, the external activation of a substrate by Brønsted acids or iminium catalysis would become important and beneficial to the photocatalyst. With the ruthenium photocatalyst **257**, the use formic acid was indeed necessary for the reactivity (Table 3.3, entry 1), and in the presence of 2 equivalence of formic acid, the reaction was completed in 24 h, giving 54% yield of the desired product **292** (entry 2). In the presence of 50 mol% of hydrazide catalyst **235**, a similar yield was obtained, but no rate acceleration was observed (entry 3). Reducing the amount of formic acid and DIPEA drastically reduced the reaction rate, delivering only a trace amount of product after 24 h, and the presence of hydrazide catalyst **235** had no impact (entry 4 – 5). As had previously been confirmed, DIPEA was essential for the reactivity (entry 5 – 6). At this point, we hypothesized that DIPEA is too basic and neutralizes all the formic acid which are necessary as an acid-cocatalyst for the formation of iminium ion. Indeed, we experimentally verified that our organocatalytic Cope rearrangement proceeded in the presence of formic acid and hydrazide catalyst **235**, whereas in the presence of DIPEA, the reactivity was suppressed (Scheme 3.13).

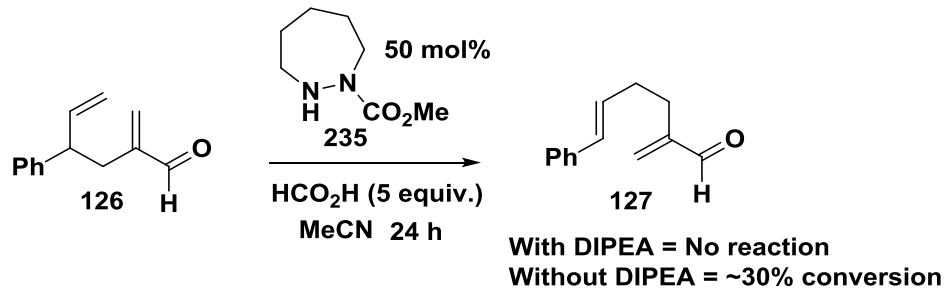

Scheme 3.13 Organocatalytic Cope rearrangement under screening conditions

We tested out different terminal reductants/hydrogen atom donors which are less basic than DIPEA. Using tris(trimethylsilyl)silane **308** showed no reactivity (entry 8) and the substrate decomposed in the presence of the catalyst **235** (entry 9). Use of Hantzsch ester **309** and TEMPO **310** showed the same results (entry 10 – 13). Use of thiophenols **311** and **312** gave no reactivity

(entry 14 and 16), and in the presence of hydrazide catalyst **235** it led to a complex mixture of unknown products (entry 15 and 17). The use of dihydronicotinamide **313** gave poor yield of the product (entry 18), and the presence of hydrazide catalyst **235** was not helpful (entry 19). We also tried the concept of a frustrated Lewis-pairs where the formation of Lewis adduct between acid and base is sterically precluded. Using a bulky Lewis acid tris(tetrafluorophenyl)borane gave moderate yield of the product, but adding our hydrazide catalyst **235** decreased the product yield without any observable rate acceleration (Scheme 3.14).

Table 3.3 Photoredox and iminium catalyzed reductive cyclization of 361

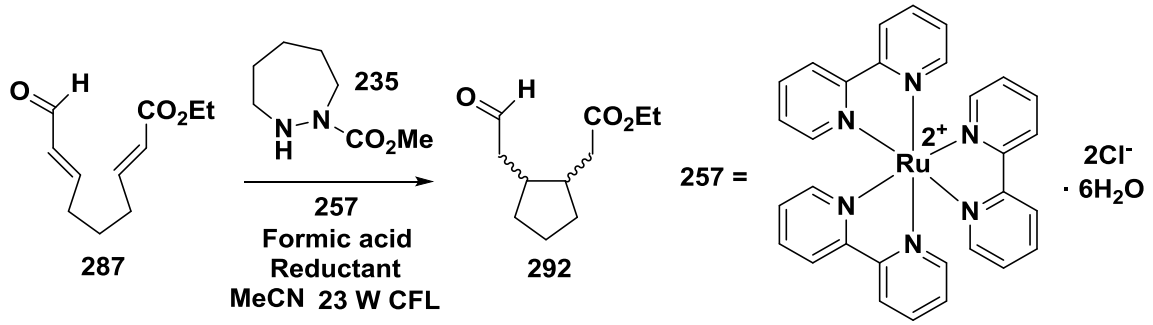

Terminal Reductants

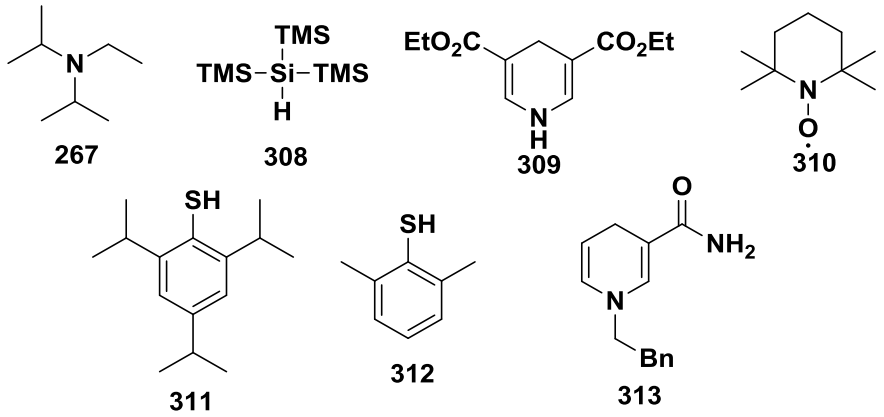

Entry	235 (mol %)	Reductant (equiv.)	Formic acid (equiv.)	257 (mol %)	Temp. (°C)	Time (h)	% Yield of 292
1	-	**267** (10)	-	2.5	rt	24	-
2	-	**267** (10)	2	2.5	rt	24	54

3	50	**267** (10)	2	2.5	rt	24	58
4	-	**267** (2)	0.5	2.5	rt	24	Trace
5	50	**267** (2)	0.5	2.5	rt	24	Trace
6	-	-	1	2.5	rt	24	-
7	50	-	1	2.5	rt	24	Decomp.
8	-	**308** (2)	TFA (1)	2.5	rt	24	-
9	50	**308** (2)	TFA (1)	2.5	rt	24	Decomp.
10	-	**309** (1.5)	1	2.5	rt	24	-
11	50	**309** (1.5)	1	2.5	rt	24	Decomp.
12	-	**310** (1.2)	5	2.5	rt	24	-
13	50	**310** (1.2)	5	2.5	rt	24	Decomp.
14	-	**311** (1.5)	5	2.5	rt	24	-
15	50	**311** (1.5)	5	2.5	rt	24	Mixture
16	-	**312** (1.5)	5	2.5	rt	24	-
17	50	**312** (1.5)	5	2.5	rt	24	Mixture
18	-	**313** (1.5)	5	2.5	rt	24	9
19	50	**313** (1.5)	5	2.5	rt	24	Trace

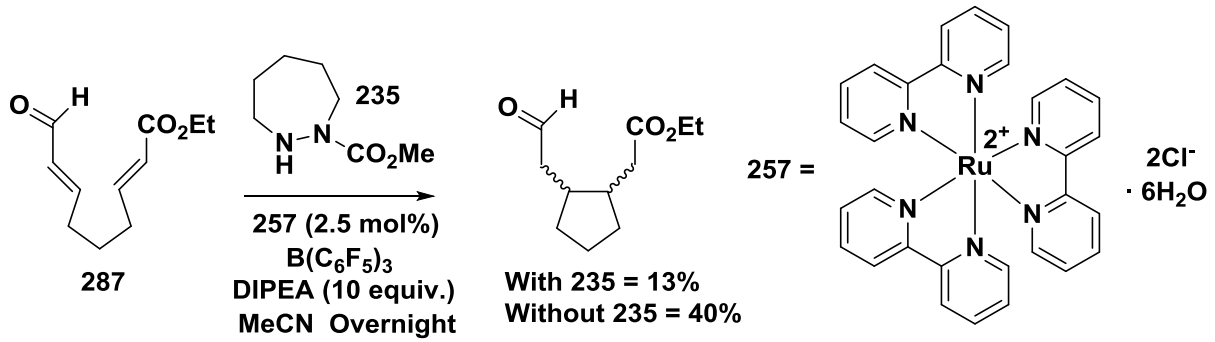

Scheme 3.14 Use of frustrated Lewis pairs with photoredox catalysis

3.4.2 Conclusion and future work

We attempted a reductive radical cyclization of an α, β-unsaturated enal via photoredox/iminium catalysis. Given the strong reduction potential of the iridium photocatalyst

which could reduce the substrate **287** without an additional activation mode, a less reducing ruthenium photocatalyst was used throughout this investigation. One of the major issues in our reaction was the use of basic terminal reductant which neutralized the acid-cocatalyst required for the formation of iminium ion. Although switching to less/non-basic terminal reductants may have solved the acid-base neutralization problem, we were still not able to get our anticipated reaction to work. In Gaunt's hydroaminoalkylation (Scheme 3.10) and MacMillan's β-alkylation of aldehyde (Scheme 3.11), the α-amino radical and β-enaminyl radical are both generated from dialkyl secondary amines, and those radical species may be more nucleophilic than the β-enaminyl radical generated from our hydrazide catalyst. In our hydrazide catalyst **235**, the methyl carbamate group may inductively withdraw electron density from our β-enaminyl radical, rendering it electron-poor and less nucleophilic. Because of this reduced nucleophilicity, the competing back-electron transfer may regenerate the initial α, β-unsaturated iminium ion. We noticed that this iminium ion is not stable for a prolonged time, which may explain the observed decompositions in our experiments. As a future direction, we should screen other non-basic terminal reductants, as well as electron-rich secondary amine catalysts that is not prone to oxidation by a photocatalyst.

3.5 Investigation of decarboxylative cyclization via photoredox/iminium catalysis

In 2014, the MacMillan group developed a decarboxylative conjugate addition of alkyl radicals to electron-deficient olefins via photoredox catalysis (Scheme 3.15)[110]. In this reaction, a mild base ionizes the carboxylic acid **314** to the carboxylate ion, which undergoes a SET oxidation with the iridium photocatalyst followed by a decarboxylation to generate the alkyl radical **315**. The alkyl radical **315** is intercepted by electrophilic acceptors **316** to give radical intermediate **317**, and a subsequent SET with the photocatalyst affords the final product **318**.

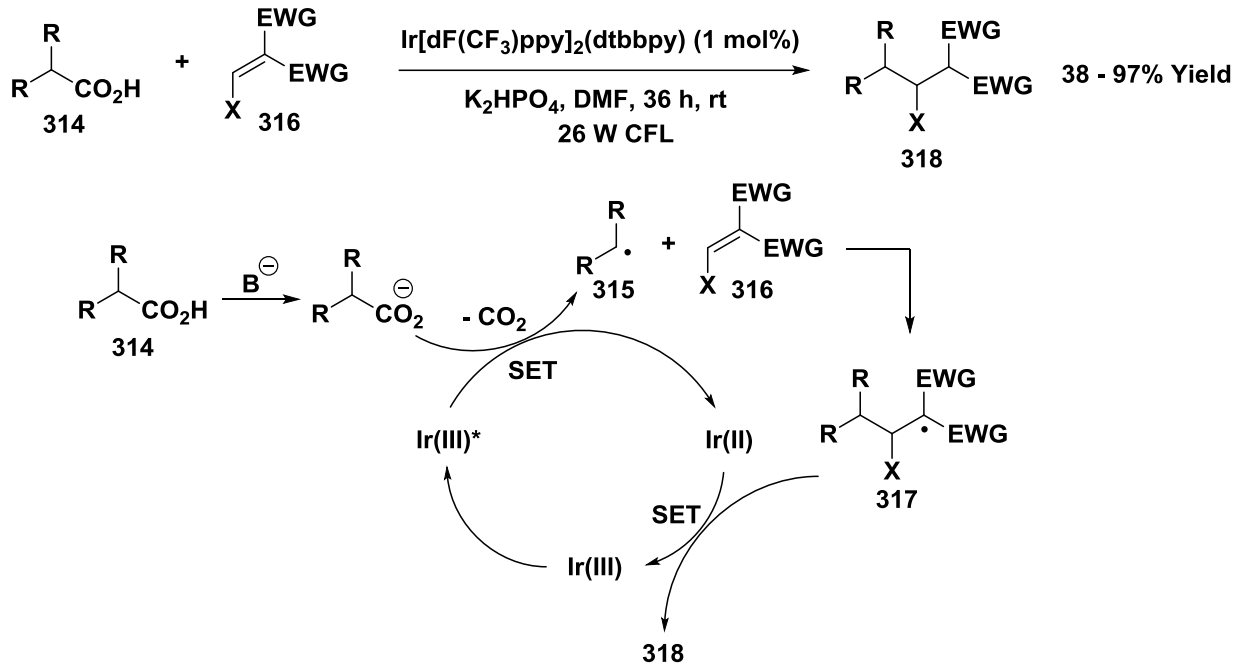

Scheme 3.15 Decarboxylative radical conjugate addition by MacMillan

Interested in this reaction, we decided to investigate the potential application of iminium catalysis using our hydrazide catalyst. The goal of my project was to perform an intramolecular decarboxylative radical addition to α, β-unsaturated enals via LUMO-lowering iminium catalysis. Instead of using an external base as in MacMillan's conditions, we proposed that we could ionize the carboxylic acid by concomitantly forming an iminium ion. To start, we considered the substrate **319** as a starting point. We envisioned that iminium/carboxylate ion **320** could be generated by condensation of hydrazide catalyst **235** with the substrate **319** in which the carboxylic acid moiety acts as an acid-cocatalyst (Scheme 3.16). Since the kinetics for the formation of iminium ion with our hydrazide catalyst is very fast, the carboxylic acid should quickly get ionized to give **320**. The iminium/carboxylate ion **320** could then undergo single-electron oxidation (hexanoate ion, E_{red} = + 1.16 V vs SCE) by a photocatalyst to produce carboxylate radical **321** which decarboxylates to the alkyl radical **322**. The alkyl radical **322** could add onto the α, β-unsaturated iminium ion to generate α-iminyl radical **323**, and a final single-electron reduction of **323** by a photocatalyst would generate the enamine **324** which could hydrolyze to afford the product **325**.

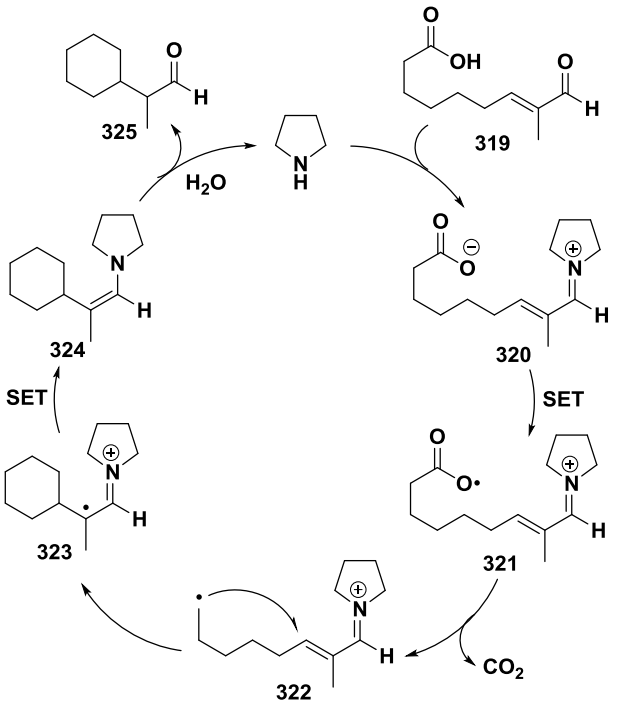

Scheme 3.16 Design of decarboxylative radical cyclization of enal via photoredox and iminium catalysis

3.5.1 Results and discussions

Synthesis of substrate **319** started from cycloheptanone **326**. A one-pot Baeyer-Villiger oxidation of cycloheptanone to 8-membered lactone with potassium persulfate in sulfuric acid followed by ring-opening with ethanol gave the compound **327** in 67 ~ 73% yield (Scheme 3.17). Oxidation of **327** with PCC gave the aldehyde **328** in 43% yield, and Wittig olefination with 2-(triphenylphosphoranylidene)propionaldehyde at reflux in benzene afforded enal **329** in 83% yield. Direct attempts to saponify the ester of **329** with variety of hydroxide source (NaOH, KOH, LiOH) led to the decomposition of the starting material. Thus, enal **329** was reduced to the alcohol **330** with $NaBH_4$ in 93% yield, then the ester was saponified with LiOH monohydrate to give **331** in 96% yield. Final oxidation of the alcohol **331** with Bobbitt's reagent gave the model substrate **319** in 93% yield.

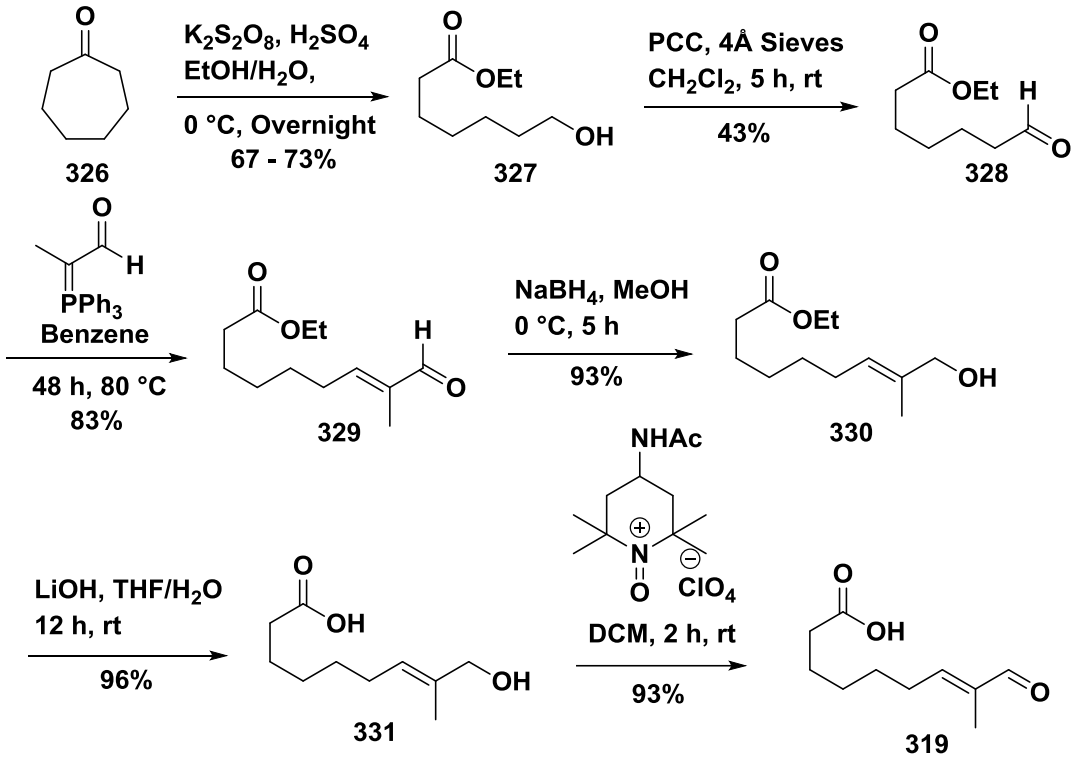

Scheme 3.17 Synthesis of the model substrate 319

With substrate **319** in hand, we tested our hypothesis using our hydrazide catalyst **235** and highly oxidizing iridium photocatalyst Ir[dF(CF_3)ppy]$_2$(dtbbpy)PF_6 (**332**) (E_{ox}(Ir(III)*/(Ir(II)) = 1.21 V). The substrate **319** was irradiated with 23W CFL or blue LED with or without the hydrazide catalyst **235** in DMF for prolonged time (Table 3.4, entry 1 – 4), but no reactivity was observed and the substrate slowly underwent decomposition. Adding weak inorganic bases such as CsOAc, CsF, CsTFA and K_2HPO_4 (entry 5 – 12) with or without the hydrazide catalyst **235** only gave trace amount of the desired product **325** with the remainder being the starting material. In order to confirm that the formation of the iminium ion under our screening condition, **319** was treated with 50 mol% of our hydrazide catalyst **235** and excess of cyclopentadiene **97** (Scheme 3.18). However, only a trace amount of Diels-Alder product was observed by NMR, suggesting that the formation of iminium ion is very slow. In our organocalytic polyene cyclization[49], we found that the slightly acidic mixture of a HFIP/DCM solvent system could accelerate the reaction. Indeed, using 10% HFIP/DCM as the solvent system instead of MeCN gave ~50% conversion of **319** to the Diels-Alder product by NMR after 24 h.

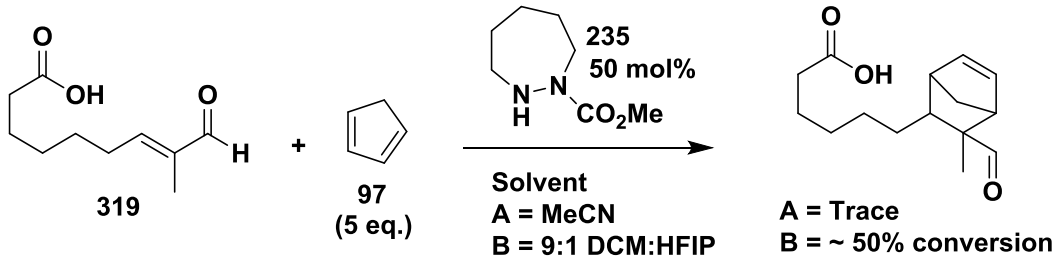

Scheme 3.18 Diels-Alder reaction using hydrazide catalyst in different solvent system

However, switching the solvent system to 10% HFIP/DCM still showed no reactivity (entry 13), and the starting material slowly decomposed in the presence of the hydrazide catalyst (entry 14). As the expected intramolecular reaction did not work, we attempted the intermolecular reaction as with MacMillan's conditions (Scheme 3.15), using 1.2 equivalents of K_2HPO_4, 1 mol% of photocatalyst **332** and 1 equivalent of diethyl 2-ethylienemalonate **333** as the Michael acceptor (Scheme 3.19). In MacMillan's work, these conditions have been used on octanoic acid, which is a primary carboxylic acid structurally similar to **319**, but their reaction only gave 38% yield of the desired product. However, for our substrate **319**, both MacMillan's and our conditions were unsuccessful, giving back most of the starting material. We believe that there is a significant back-electron transfer (BET) that outcompetes the single-electron oxidation of the carboxylate anion to its radical. In addition, the decarboxylation of carboxylate radical may not occur because the primary alkyl radical is too high in energy.

Table 3.4 Decarboxylative RCA of 374 using photoredox and iminium catalysis

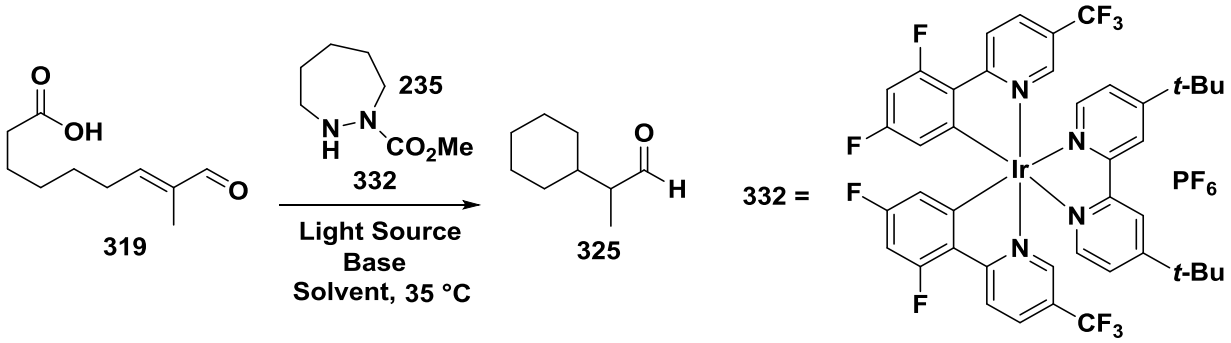

Entry	235 (mol %)	332 (mol %)	Light	Base	Solvent (0.4 M)	Time (h)	% yield 325
1	-	1	23 W CFL	-	DMF	24	S.M.

2	25	1	23 W CFL	-	DMF	24	S.M.
3	-	1	Blue LED	-	DMF	24	S.M.
4	25	1	Blue LED	-	DMF	24	S.M.
5	-	1	23 W CFL	CsOAc	DMF	24	Trace
6	25	1	23 W CFL	CsOAc	DMF	24	Trace
7	-	1	23W CFL	CsF	DMF	24	Trace
8	25	1	23 W CFL	CsF	DMF	24	Trace
9	-	1	23 W CFL	CsTFA	DMF	24	Trace
10	25	1	23W CFL	CsTFA	DMF	24	Trace
11	-	1	Blue LED	K_2HPO_4	DMF	24	Trace
12	25	1	Blue LED	K_2HPO_4	DMF	24	Trace
13	-	2	Blue LED	-	HFIP:DCM (1:9)	24	S.M.
14	25	2	Blue LED	-	HFIP:DCM (1:9)	24	Decomp.

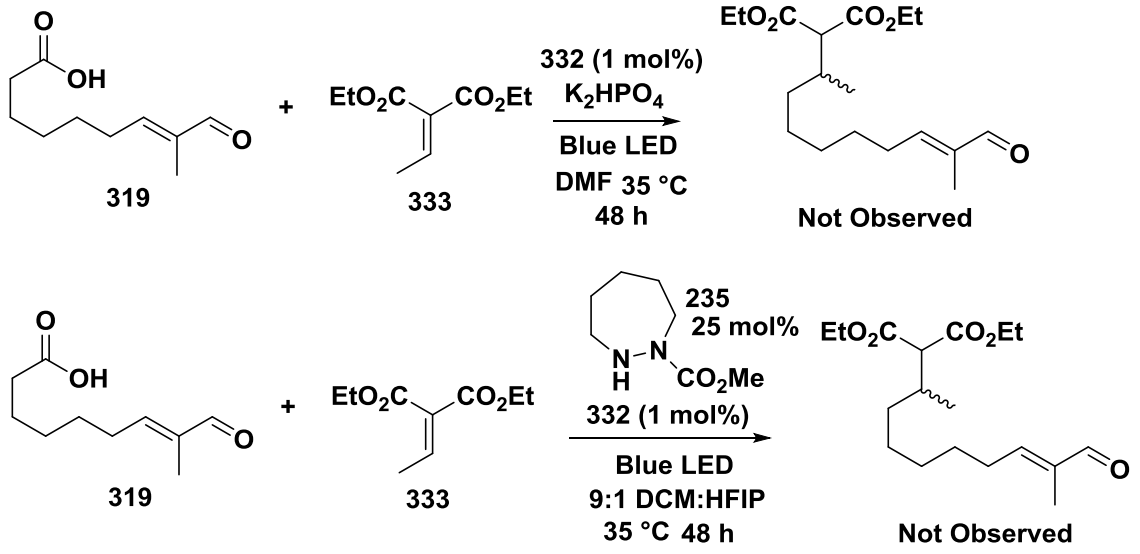

Scheme 3.19 Attempted intermolecular radical conjugate addition of 319

We next looked at secondary and tertiary carboxylic acid substrates **334** and **335** which would generate more stable secondary and tertiary alkyl radicals after the decarboxylation (Scheme 3.20). Synthesis of substrate **334** began with TBS protection of alcohol **327**, affording **336** in 91% yield. The formation of the ester enolate with LDA followed by alkylation with MeI

gave **337** in 97% yield. Ester **337** was deprotected with TBAF to give the alcohol **338** in 98% yield, which was oxidized with PCC to give the aldehyde **339** in 50% yield. Wittig olefination of **339** with 2-(triphenylphosphoranylidene)propionaldehyde gave the enal **340** in 78% yield, and it was reduced to the alcohol **341** with $NaBH_4$ in 91% yield. The ester **341** was saponified to **342** in quantitative yield with LiOH monohydrate, and the final oxidation with Bobbitt's reagent gave substrate **334** in 91% yield.

For substrate **335**, the ester **337** was methylated second time with LDA/MeI, affording **343** in 79% yield. Deprotection of TBS alcohol with TBAF gave **344** in 99% yield, which was oxidized with PCC to give the aldehyde **345** in 71% yield. Wittig olefination with 2-(triphenylphosphoranylidene)propionaldehyde gave the enal **346** in 88% yield, and the reduction of the aldehyde with $NaBH_4$ provided **347** in 99% yield. Saponification of **347** with LiOH monohydrate at reflux in THF/H_2O gave the carboxylic acid **348** in 88% yield, and the final oxidation with Bobbitt's reagent gave substrate **335** in 96% yield.

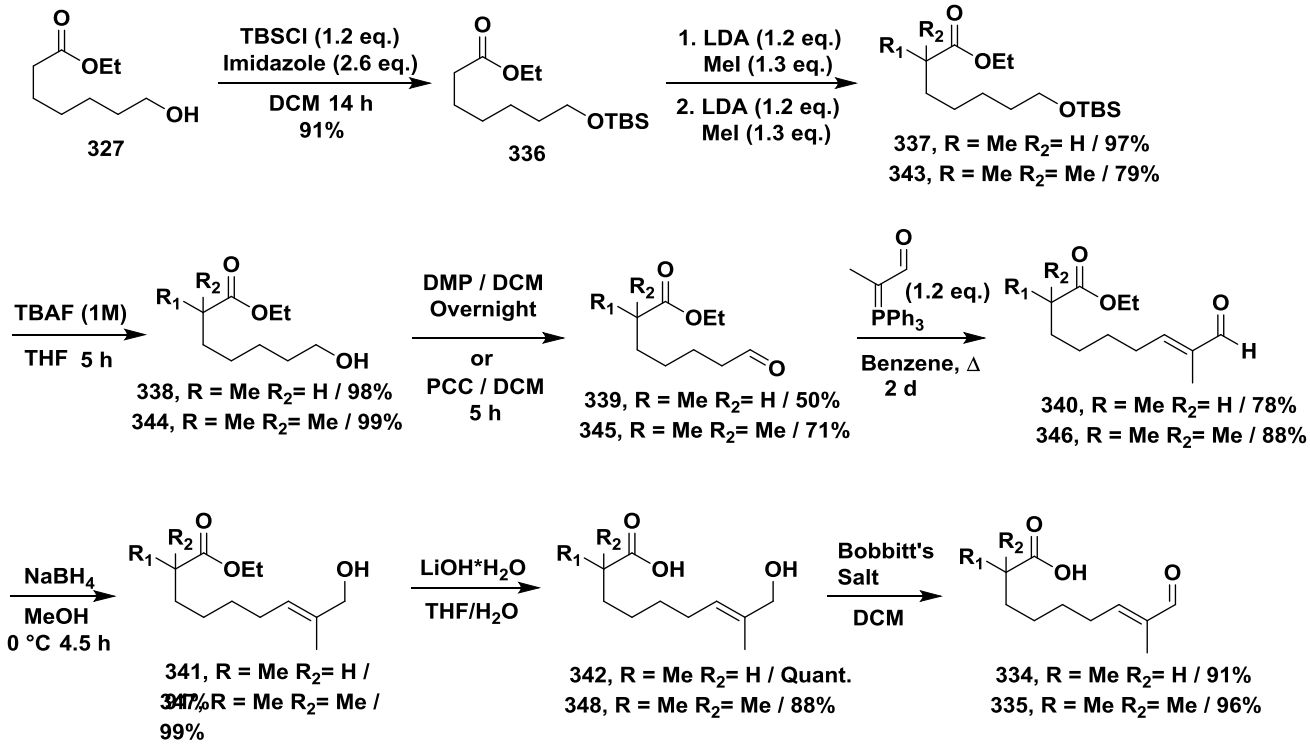

Scheme 3.20 Synthesis of model substrates 334 and 335

In MacMillan's work, his conditions were effective for a variety of secondary carboxylic acid substrates, but the substrates generating α-hetero radicals such as **349** and **350** were mostly high yielding (Scheme 3.21). This suggest that the stability of the generated radical is important to the reactivity. In substrate **334**, the α-methyl group of carboxylic acid should increase the stability of the generated radical and may favor the radical cyclization from Thorpe-Ingold effect. However, when substrate **334** was treated under Macmillan's reaction conditions (Scheme 3.15), only trace amount of the cyclization product **353** was observed by NMR along with unreacted starting materials (Table 3.5, entry 1). The reaction in HFIP/DCM solvent system with our hydrazide catalyst **235** still showed no reactivity, and the starting material slowly decomposed over prolonged reaction time (entry 2). The attempt towards intermolecular radical conjugate addition with diethyl 2-ethylienemalonate **333** under MacMillan's conditions was again unsuccessful, giving instead a trace amount of cyclization product **353** with mostly unreacted starting materials (Scheme 3.22). Similar to the previous cases, significant BET may be preventing this reaction from going forward, and we may need to generate a more stable radical to get an optimal reactivity.

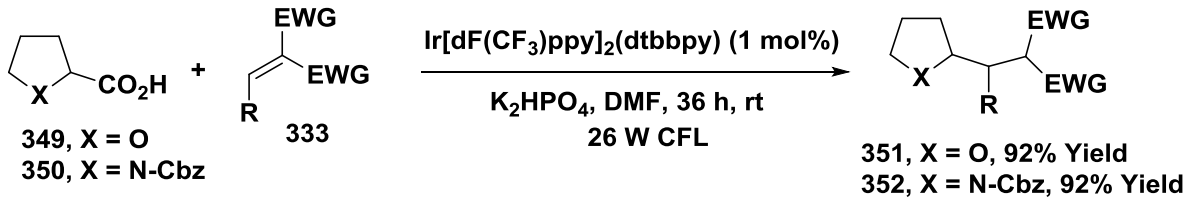

Scheme 3.21 Substrate scopes in MacMillan's decarboxylative radical conjugate addition

Table 3.5 Decarboxylative cyclization of 334 with photoredox and iminium catalysis

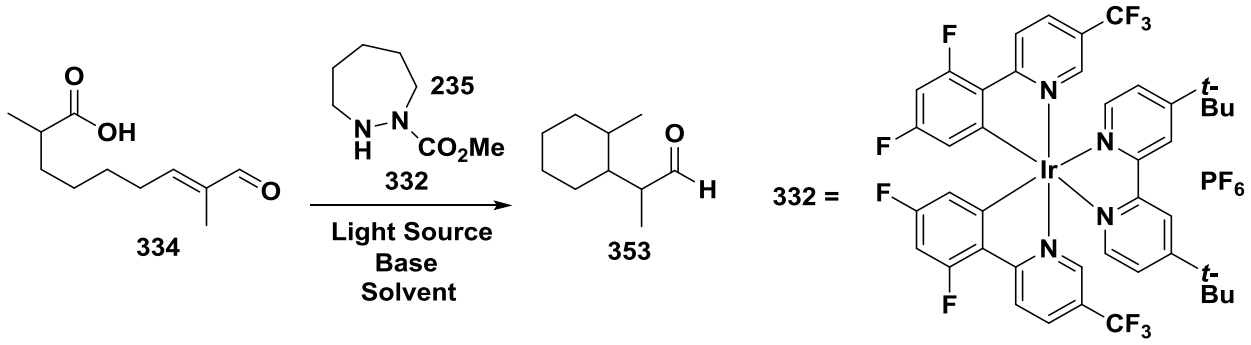

Entry	235 (mol %)	332 (mol %)	Light	Base	Solvent (0.4 M)	Time (h)	% yield 353
1	-	1	Blue LED	K_2HPO_4	DMF	24	Trace
2	25	1	Blue LED	-	HFIP:DCM (1:9)	24	Decomp.

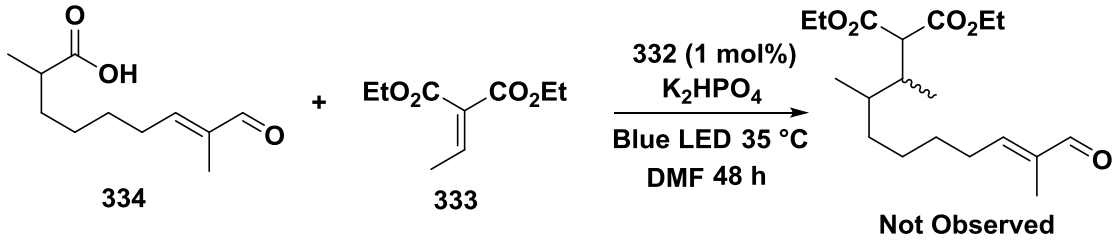

Scheme 3.22 Attempt for intermolecular radical conjugate addition of 334

Lastly, we screened a variety of reaction conditions with the substrate **335**. This time, the reaction under MacMillan's conditions (Scheme 3.15) gave the cyclization product **354** in 42% isolated yield after 72 h (Table 3.6, entry 1). Changing the base to CsOAc also afforded the cyclization product **354** albeit in 24% yield (entry 2). Changing the solvent system from DMF to HFIP:DCM shut down the reactivity, highlighting the importance of using a polar solvent (entry 3). Treating **335** with our hydrazide catalyst **235** in the presence of photocatalyst **332** still showed no reactivity and led to slow decomposition of the starting material over prolonged time (entry 4), and the addition of an external base CsOAc had no effect on the reaction (entry 5). Switching the solvent to DMF in the presence of the hydrazide catalyst **235** still showed no reactivity (entry 6), and the addition of HCl to aid the formation of iminium ion had no effect, leading to slow decomposition of the starting material (entry 7). The use of a Lewis acid such as $Zn(OTf)_2$[103] and an additive such as tetrabutylammonium bromide[111] to promote the formation of iminium ion were also unsuccessful, recovering starting materials back (entry 8 - 11).

Table 3.6 Decarboxylative cyclization of 335 with photoredox and iminium catalysis

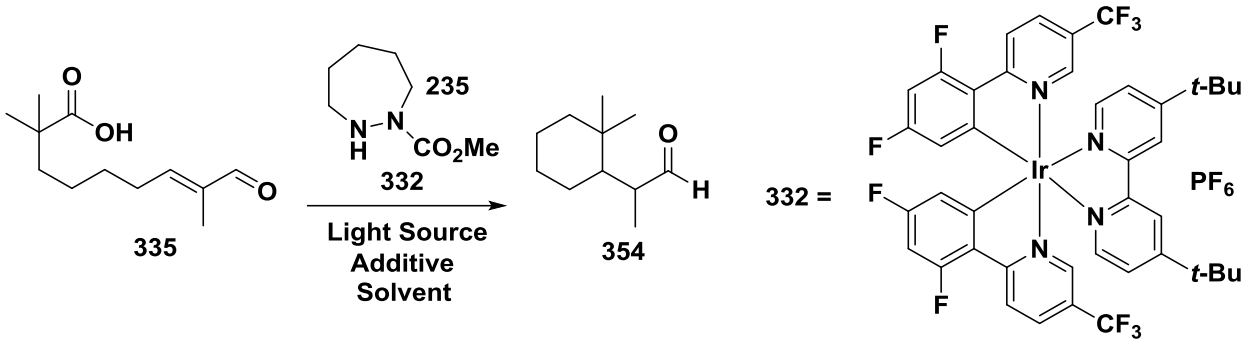

Entry	235 (mol %)	332 (mol %)	Light	Additive (Equiv.)	Solvent (0.4 M)	Time (h)	% yield 354
1	-	1	Blue LED	K_2HPO_4 (1.2)	DMF	72	42
2	-	1	Blue LED	CsOAc (1.2)	DMF	96	24
3	-	1	Blue LED	CsOAc (1.2)	HFIP:DCM (1:9)	72	S.M.
4	25	1	Blue LED	-	HFIP:DCM (1:9)	72	Decomp.
5	25	1	Blue LED	CsOAc (1)	HFIP:DCM (1:9)	72	S.M.
6	25	1	Blue LED	-	DMF	72	S.M.
7	25	1	Blue LED	HCl (0.125)	DMF	72	Decomp.
8	-	1	Blue LED	$Zn(OTf)_2$ (1)	DCM	72	S.M.
9	25	1	Blue LED	$Zn(OTf)_2$ (1)	DCM	72	S.M.
10	-	1	Blue LED	TBAB (1)	DCM	72	S.M.
11	25	1	Blue LED	TBAB (1)	DCM	72	S.M.

3.5.2 Conclusion and future work

We attempted a decarboxylative radical cyclization of α, β-unsaturated aldehydes using photoredox and iminium catalysis. For the primary and secondary carboxylic acid substrates **319** and **334** which showed poor or no reactivity, we believe that there is a significant back-electron

transfer process that prevents the formation of alkyl radicals. The tertiary carboxylic acid substrate **335** gave the most promising result using MacMillan's reaction conditions, and this highlighted the importance of the stability of the generated radical for the reactivity. The reaction was also highly dependent on the solvent system, as switching from DMF to HFIP:DCM completely shut down the reactivity. Unfortunately, despite multiple attempts, no reaction has been observed under our iminium catalysis conditions. Future work for this reaction would be to screen other conditions that can efficiently promote the formation of iminium ion while ionizing the carboxylic acid moiety. In addition, α-unsubstituted enals could also be tested, as the kinetics for the formation of iminium ion would be faster than hindered α-substituted systems.

3.6 References

78. Shaw, M. H., et al. (2016). The Journal of Organic Chemistry **81**(16): 6898-6926.
79. Prier, C. K., et al. (2013). Chemical Reviews **113**(7): 5322-5363.
80. Buzzetti, L., et al. (2019). Angewandte Chemie International Edition **58**(12): 3730-3747.
81. Flamigni, L., et al. (2007). Photochemistry and Photophysics of Coordination Compounds II. V. Balzani and S. Campagna. Berlin, Heidelberg, Springer Berlin Heidelberg**:** 143-203.
82. Bonardi, A.-H., et al. (2018). Beilstein Journal of Organic Chemistry **14**: 3025-3046.
83. Tucker, J. W. and C. R. J. Stephenson (2012). The Journal of Organic Chemistry **77**(4): 1617-1622.
84. Hedstrand, D. M., et al. (1978). Tetrahedron Letters **19**(14): 1255-1258.
85. Van Bergen, T. J., et al. (1979). The Journal of Organic Chemistry **44**(26): 4953-4962.
86. Okada, K., et al. (1991). Journal of the American Chemical Society **113**(24): 9401-9402.
87. Ischay, M. A., et al. (2008) Journal of the American Chemical Society **130**(39): 12886-12887.
88. Nicewicz, D. A. and D. W. C. MacMillan (2008). Science **322**(5898): 77-80.
89. Narayanam, J. M. R., et al. (2009). Journal of the American Chemical Society **131**(25): 8756-8757.
90. Stephenson, C., Yoon, T., MacMillan, D.W.C., Prier, C.K. and MacMillan, D.W.C. (2018). (eds C. Stephenson, T. Yoon and D.W.C. MacMillan).
91. Du, J., et al. (2014). Science **344**(6182): 392-396.
92. Lu, Z., et al. (2011). Journal of the American Chemical Society **133**(5): 1162-1164.

93. Gao, X.-W., et al. (2013). Advanced Synthesis & Catalysis **355**(11-12): 2158-2164.
94. Jackl, M. K., et al. (2017). Organic Letters **19**(17): 4696-4699.
95. Du, J., et al. (2011). Chemical Science **2**(11): 2115-2119.
96. Weinberg, D. R., et al. (2012). Chemical Reviews **112**(7): 4016-4093.
97. Tarantino, K. T., et al. (2013). Journal of the American Chemical Society **135**(27): 10022-10025.
98. Yayla, H. G., et al. (2016). Journal of the American Chemical Society **138**(34): 10794-10797.
99. Musacchio, A. J., et al. (2017). Science **355**(6326): 727-730.
100. Zhu, Q., et al. (2018). Journal of the American Chemical Society **140**(2): 741-747.
101. Murphy, J. J., et al. (2016). Nature **532**(7598): 218-222.
102. Silvi, M., et al. (2017). Nature Chemistry **9**(9): 868-873.
103. Mazzarella, D., et al. (2018). Journal of the American Chemical Society **140**(27): 8439-8443.
104. Perego, L. A., et al. (2020). Advanced Synthesis & Catalysis **362**(2): 302-307.
105. Goti, G., et al. (2019). Angewandte Chemie International Edition **58**(4): 1213-1217.
106. Trowbridge, A., et al. (2018). Nature **561**(7724): 522-527.
107. Terrett, J. A., et al. (2014). Journal of the American Chemical Society **136**(19): 6858-6861.
108. Peng, W., et al. (2004). Tetrahedron Letters **45**(18): 3677-3680.
109. Juspin, T., et al. (2010). European Journal of Medicinal Chemistry **45**(2): 840-845.
110. Chu, L., et al. (2014). Journal of the American Chemical Society **136**(31): 10886-10889.
111. Duce, S., et al. (2012). Chemical Communications **48**(42): 5184-5186.

Chapter 4. Experimental procedures

4.1 General experimental

Materials:

All reactions were performed under an inert argon atmosphere in flame-dried round bottom flask fitted with rubber septa and using magnetic stirring, unless otherwise noted. Liquids and solutions were transferred via syringe or stainless-steel cannula. Tetrahydrofuran (THF) and diethyl ether (Et_2O) were purified by distillation over sodium metal and benzophenone under a nitrogen atmosphere. Dichloromethane (DCM), toluene (PhMe) and *i*-Pr_2NH and *i*-Pr_2NEt were purified by distillation over calcium hydride (CaH_2) under a nitrogen atmosphere. *N,N*-dimethylformamide (DMF) were stored over 3 Å molecular sieves and kept under an argon atmosphere. *n*-Butyllithium (*n*-BuLi) was titrated with *sec*-butanol in PhMe using 2,2'-bipyridine as an indicator. Thin layer chromatography (TLC) was carried out on glass plates, coated with 250 μm of 230-400 mesh silica gel that had been saturated with F-254 indicator. TLC plates were visualized using ultraviolet light and/or by exposure to a basic solution of potassium permanganate followed by heating or an acidic solution of cerium (IV) ammonium molybdate followed by heating. Flash column chromatography was carried out using 230-400 mesh silica gel using reagent grade solvents. All other commercial reagents were used without further purification.

Instrumentation:

NMR spectra were recorded on 400, 500 MHz Varian or 400, 500 MHz Bruker spectrometers. Chemical shifts (δ) were internally referenced to the residual proton resonance in $CDCl_3$ (δ 7.26 ppm), CD_3OD (δ 3.31 ppm), CD_3CN (δ 1.94), $(CD_3)_2CO$ (δ 2.05). Coupling constants are reported in Hertz (Hz). Infrared (IR) spectra were obtained using a Perkin-Elmer Spectrum One FT-IR spectrometer. High-resolution mass spectrometry (HRMS) was conducted by Dr. Alexander Wahba or Dr. Nadim Saadé in the Mass Spectrometry Facility in the Department of Chemistry, McGill University. Photochemical reactions were conducted using 26 W CFL or 34 W blue LED.

4.2 Experimental procedures for chapter 1

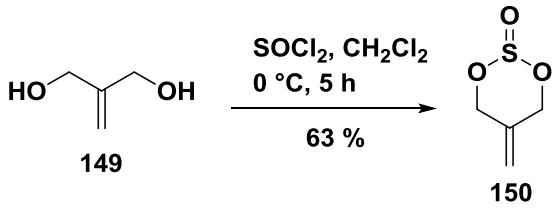

5-methylene-2-oxo[1,3,2]dioxathiane (150): a solution of thionyl chloride (3.04 g, 25.5 mmol, 1.5 equiv) in dichloromethane (4 mL) was added under vigorous stirring to an emulsion of 2-methylenepropane-1,3-diol (1.5 g, 17 mmol, 1 equiv) in dichloromethane (10 mL) at 0 °C. The solution was stirred for 5 h, at which point TLC analysis indicated complete consumption of the starting material. The solvent and excess thionyl chloride was removed under pressure to afford 1.5 g (63%) of **150** as a brown oil which was sufficiently pure for use without further purification. The spectroscopic data is in agreement with that published in the literature[112].

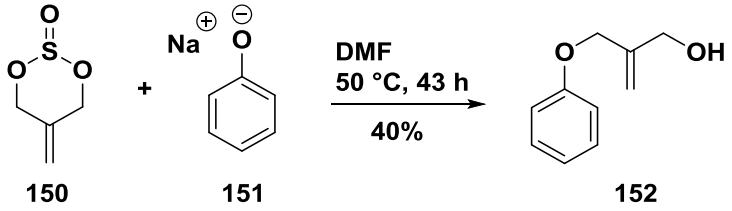

2-(Phenoxymethyl)prop-2-en-1-ol (152): A suspension of sodium hydride (60% dispersion in mineral oil, 0.430 g, 10.7 mmol, 1.2 equiv) in THF (6 mL) was cooled to 0 °C and treated with phenol (1.01 g, 10.7 mmol, 1.2 equiv). After evolution of hydrogen had ceased, the solvent was evaporated under reduced pressure, and the resulting sodium phenolate was dissolved in DMF (5 mL). This solution was added to a solution of dioxathiane **150** (1.20 g, 8.94 mmol, 1 equiv) in DMF (3 mL), and the reaction mixture was stirred at 50 °C. After 43 h, the reaction mixture was quenched with water (80 mL). The aqueous phase was extracted with diethyl ether (3 x 30 mL), and the combined organic fractions were washed with water (4 x 25 mL), brine (25 mL), dried with anhydrous $MgSO_4$, and concentrated under reduced pressure. The residue was purified by chromatography on silica gel using 20% EtOAc:Hexane as eluent to provide alcohol **152** as a clear oil (0.584 g) in 40% yield. The spectroscopic data is in agreement with that published in the literature[112].

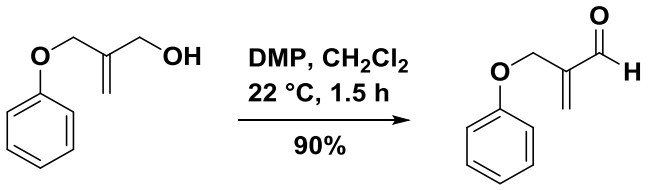

152 153

2-(phenoxymethyl)acrylaldehyde (153): To a solution of **152** (0.40 g, 2.4 mmol, 1 equiv) in 30 mL of dichloromethane was added Dess-Martin periodinane (1.24 g 2.9 mmol, 1.2 equiv) and the resulting mixture was stirred for 1.5 h at room temperature. The reaction mixture was filtered through celite and the solvent was removed under reduced pressure. The product was purified by flash chromatography on silica gel using 20% EtOAc:Hexane as eluent to give **153** as colorless oil (0.355 g) in 90% yield. ^{1}H NMR (400 MHz, Chloroform-*d*) δ 9.69 (s, 1H), 7.36 – 7.29 (m, 2H), 7.02 – 6.94 (m, 3H), 6.68 (d, *J* = 1.9 Hz, 1H), 6.28 (d, *J* = 1.7 Hz, 1H), 4.80 (t, *J* = 1.8 Hz, 2H). ^{13}C NMR (101 MHz, $CDCl_3$) δ 193.1, 158.1, 145.3, 134.5, 129.6, 121.3, 114.7, 63.7. IR (film cm^{-1}) 3067, 2833, 2702, 1687, 1600, 1494 HRMS: calcd for $C_{10}H_{10}O_2Na$ [M+Na] 185.05730, found 185.05757.

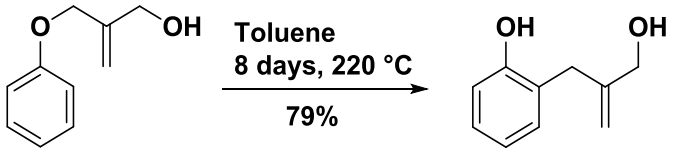

152 159

2-(2-(hydroxymethyl)allyl)phenol (159): A 15 mL pressure reaction vessel was charged with alcohol **152** (100 mg, 0.609 mmol, 1 equiv) and freshly distilled toluene (2.4 mL). The pressure vessel was sealed and heated to 220 °C in a sand bath for 8 days. The reaction mixture was cooled to room temperature, concentrated under reduced pressure, then purified by chromatography on silica gel using 20% EtOAc:Hexane to give product **159** as a white solid (79 mg) in a 79% yield. ^{1}H NMR (500 MHz, Chloroform-*d*) δ 7.18 – 7.09 (m, 2H), 6.92 – 6.84 (m, 2H), 6.34 (s, 1H), 5.08 (dq, *J* = 2.1, 1.0 Hz, 1H), 5.01 (dp, *J* = 2.1, 0.7 Hz, 1H), 4.12 (d, *J* = 4.2 Hz, 2H), 3.46 (s, 2H), 1.92 (t, *J* = 5.4 Hz, 1H). ^{13}C NMR (126 MHz, $CDCl_3$) δ 154.2, 146.9, 130.9, 128.2, 125.2, 120.8,

116.6, 112.9, 65.9, 34.0. IR (film cm^{-1}) 3416, 3142, 2904, 1458, 1262. HRMS: calcd for $C_{10}H_{11}O_2$ [M-H] 163.0765, found 163.0767.

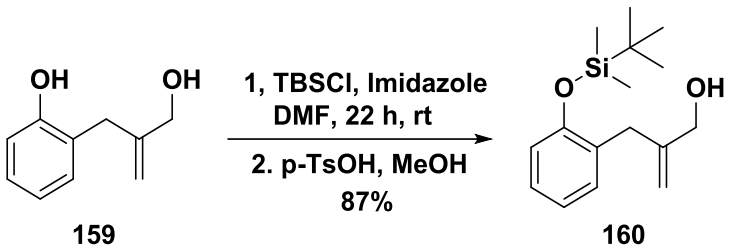

159 160

2-(2-((*tert*-butyldimethylsilyl)oxy)benzyl)prop-2-en-1-ol (160): To a solution of alcohol **159** (21.6 mg, 0.132 mmol, 1 equiv) in DMF (1 mL) was added TBSCl (59.5 mg, 0.395 mmol, 3.00 equiv) and imidazole (44.8 mg, 0.658 mmol, 5.00 equiv), and the mixture was stirred at room temperature for 23 h. Saturated aqueous NH_4Cl (2 mL) was added, and the aqueous layer was extracted with DCM (3 x 7mL), washed with water (10 mL), brine (10 mL) and concentrated under reduced pressure to give the crude residue as a colorless oil. The crude material was re-dissolved in MeOH (2 mL), p-TsOH monohydrate (1.25 mg, 0.00657 mmol, 0.05 equiv) was added, and the solution was stirred for 2 h at room temperature. After evaporation of MeOH under reduced pressure, saturated aqueous NH_4Cl (4 mL) was added and extractred with diethyl ether (3 x 8 mL). Combined organic extracts were washed with brine, dried over $MgSO_4$, and concentrated under reduced pressure. The residue was purified by chromatography on silica gel using 5:1 EtOAc:Hexane as eluent to give **160** as a colorless oil (31.9 mg) in 87% yield. ^{1}H NMR (400 MHz, Chloroform-*d*) δ 7.17 – 7.05 (m, 2H), 6.92 (td, *J* = 7.4, 1.2 Hz, 1H), 6.81 (dd, *J* = 8.1, 1.2 Hz, 1H), 5.07 (dq, *J* = 2.2, 1.1 Hz, 1H), 4.80 (h, *J* = 1.3 Hz, 1H), 4.05 (d, *J* = 6.0 Hz, 2H), 3.40 (s, 2H), 1.61 (t, *J* = 6.4 Hz, 1H), 1.00 (s, 9H), 0.23 (s, 6H). ^{13}C NMR (126 MHz, $CDCl_3$) δ 153.5, 148.0, 130.7, 129.5, 127.3, 121.2, 118.7, 110.7, 65.7, 33.6, 25.8, 18.3, -4.1. IR (film cm^{-1}) 3325, 2932, 2857, 1488, 1252. HRMS: calcd for $C_{16}H_{27}O_2Si$ [M+H] 279.1774 found 279.1778.

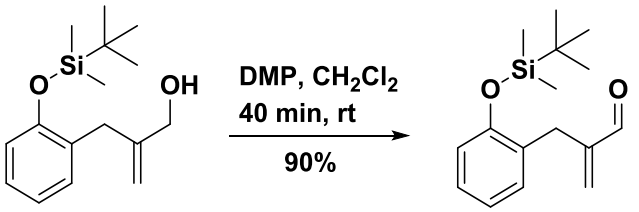

160 161

2-(2-((*tert*-butyldimethylsilyl)oxy)benzyl)acrylaldehyde (161): To a solution of alcohol **160** (29 mg, 0.10 mmol, 1 equiv) in DCM (2 mL) was added DMP (53 mg, 0.13 mmol, 1.2 equiv), and the mixture was stirred for 40 min, at which point TLC analysis indicated complete consumption of the starting material. The reaction mixture was filtered through celite rinsing with DCM (25 mL), concentrated under reduced pressure, and purified by chromatography on silica gel using 10% EtOAc:Hexane as eluent to give **161** as a light yellow oil (25.9 mg) in 90 % yield. ^{1}H NMR (400 MHz, Chloroform-*d*) δ 9.64 (s, 1H), 7.17 – 7.04 (m, 2H), 6.90 (td, *J* = 7.4, 1.2 Hz, 1H), 6.82 (dd, *J* = 8.1, 1.2 Hz, 1H), 6.02 (q, *J* = 1.2 Hz, 1H), 5.92 (q, *J* = 1.3 Hz, 1H), 3.53 (d, *J* = 1.5 Hz, 2H), 0.95 (s, 9H), 0.21 (s, 6H). ^{13}C NMR (126 MHz, $CDCl_3$) δ 194.2, 153.8, 149.2, 134.8, 131.2, 128.5, 127.7, 121.1, 118.5, 28.8, 25.7, 18.2, -4.1. IR (film cm^{-1}) 2956, 2857, 1694, 1490, 1254. HRMS: calcd for $C_{16}H_{25}O_2Si$ [M+H] 277.1618 found 277.1628.

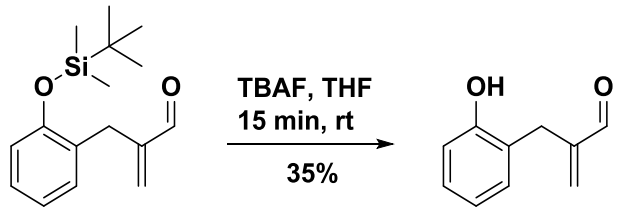

161 162

2-(2-hydroxybenzyl)acryaldehyde (162): To a solution of **161** (12.2 mg, 0.0441 mmol, 1 equiv) in acetonitrile (0.37 mL) was added TBAF (13.8 mg, 0.0503 mmol, 1.2 equiv) and stirred at room temperature for 15 min. Saturated aqueous NH_4Cl (1 mL) was added and mixture was extracted with diethyl ether (3 x 3 mL). The combined organic extracts were dried over $MgSO_4$, concentrated under reduced pressure, and purified by chromatography on silica gel using 100% DCM as eluent to give **162** as a light-yellow oil (2.5 mg) in 35 % yield. ^{1}H NMR (400 MHz, Chloroform-*d*) δ 9.53 (s, 1H), 7.18 – 7.07 (m, 2H), 6.99 (s, 1H), 6.92 – 6.83 (m, 2H), 6.48 (d, *J* = 1.2 Hz, 1H), 6.14 (s,

1H), 3.54 (d, J = 1.0 Hz, 2H). ^{13}C NMR (126 MHz, $CDCl_3$) δ 196.4, 154.0, 148.9, 136.8, 130.6, 128.5, 124.7, 121.0, 117.6, 29.4. IR (film cm^{-1}) 3365, 2924, 2829, 1670, 1488, 1232. HRMS: calcd for $C_{10}H_{10}O_2Na$ [M+Na] 185.0573 found 185.0567.

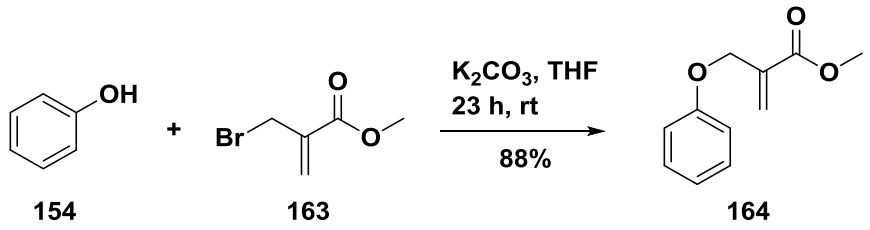

Methyl 2-(phenoxymethyl)acrylate (164): To a stirring solution of **154** (0.884 g, 9.39 mmol, 1 equiv) and acrylate **163** (1.68 g, 9.39 mmol, 1 equiv) in THF (18 mL) was added K_2CO_3 (7.79 g, 56.4 mmol, 6 equiv) in one portion at room temperature. The reaction mixture was stirred for 23 h at which point TLC analysis indicated complete consumption of the starting material. The mixture was filtered through celite, rinsed with diethyl ether (100 mL) and concentrated under reduced pressure. The residue was purified by chromatography on silica gel using 50% DCM:Hexane as eluent to afford **164** as a colorless oil (1.59 g) in 88% yield. ^{1}H NMR (500 MHz, Chloroform-*d*) δ 7.33 – 7.27 (m, 2H), 7.02 – 6.86 (m, 3H), 6.41 (q, J = 1.4 Hz, 1H), 6.02 (q, J = 1.8 Hz, 1H), 4.76 (t, J = 1.7 Hz, 2H), 3.81 (s, 3H). ^{13}C NMR (126 MHz, $CDCl_3$) δ 166.0, 158.3, 135.8, 129.5, 126.5, 121.2, 114.8, 66.0, 52.0. IR (film cm^{-1}) 3035, 2956, 1716, 1597, 1494. HRMS: calcd for $C_{11}H_{12}O_3Na$ [M+Na] 215.0684, found 215.0682.

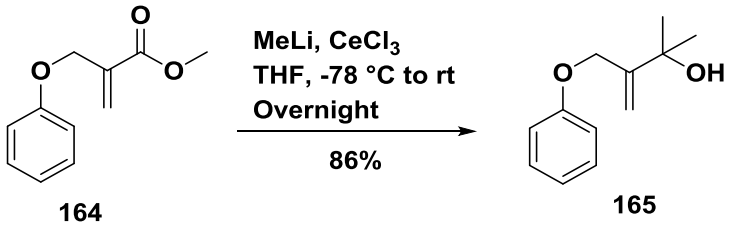

2-methyl-3-(phenoxymethyl)but-3-en-2-ol (165): Oven-dried 250 mL round bottom flask with a magnetic stir bar was charged with powdered cerium(III) chloride heptahydrate (7.70 g, 20.7 mmol, 2.5 equiv), and evacuated to 1.0 mm. The flask was heated at 90 - 100 °C in an oil bath for 2 h then gradually warmed to 140 °C over 30 min and stirred at that temperature overnight. After the flask is back-filled with argon and cooled to 0 °C in an ice-water bath, THF (34 mL) was added

with vigorous stirring and stirred for 6 h, resulting in a gray milky suspension. The suspension was cooled to -78 °C and MeLi (1.6 M in Et_2O, 12.9 mL, 20.7 mmol, 2.5 equiv) was added dropwise over 20 min and stirred for 30 min. A solution of acrylate **164** (1.59 g, 8.27 mmol, 1 equiv) in THF (16 mL) was added slowly to the milky suspension dropwise via cannula over 20 min. The mixture was stirred at -78 °C for 30 min then stirred overnight, allowing gradually to warm to room temperature. The reaction mixture was quenched with an aqueous 5% solution of acetic acid (30 mL) and extracted with ethyl acetate (3 x 50 mL). The combined organic phase was washed with brine (50 mL), dried over anhydrous Na_2SO_4, and concentrated under reduced pressure. The crude product was purified by chromatography on silica gel using 100 % DCM as eluent to give **165** as a colorless oil (1.37 g) in 86% yield. ^{1}H NMR (500 MHz, Chloroform-*d*) δ 7.33 – 7.26 (m, 2H), 7.01 – 6.92 (m, 3H), 5.30 (d, *J* = 0.9 Hz, 1H), 5.25 (q, *J* = 1.2 Hz, 1H), 4.67 (t, *J* = 1.0 Hz, 2H), 1.46 (s, 6H). ^{13}C NMR (126 MHz, $CDCl_3$) δ 158.5, 150.4, 129.5, 121.1, 114.8, 111.9, 72.5, 68.8, 29.7. IR (film cm^{-1}) 3408, 2976, 1597, 1494. HRMS: calcd for $C_{12}H_{16}O_2Na$ [M+Na] 215.1042 , found 215.1046.

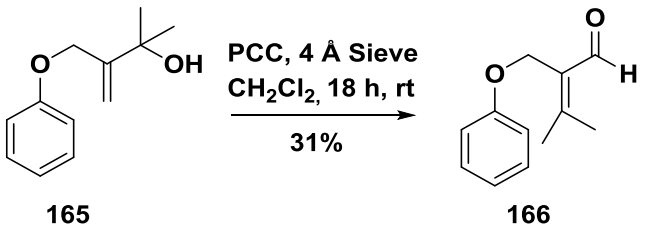

165 166

3-methyl-2-(phenoxymethyl)but-2-enal (166): A solution of alcohol **165** (1.00 g, 5.22 mmol, 1 equiv) in DCM (25 mL) was transferred via cannula to the suspension of PCC (4.45 g, 20.6 mmol, 4 equiv) and 4 Å molecular sieves (4.45 g) in DCM (25 mL). The dark brown reaction mixture was stirred at room temperature for 18 h, at which point TLC analysis indicated complete consumption of the starting material. The mixture was passed through a short pad of silica gel, rinsed with DCM (200 mL) and concentrated under reduced pressure. The brown residue was purified by chromatography on silica gel using 50 to 70% gradient DCM:Hexane to give **166** as a light yellow oil (0.307 g) in 31% yield. ^{1}H NMR (500 MHz, Chloroform-*d*) δ 10.16 (s, 1H), 7.30 – 7.26 (m, 2H), 6.98 – 6.92 (m, 3H), 4.78-4.67 (m, 2H), 2.30 (s, 3H), 2.13 (s, 3H). ^{13}C NMR (126 MHz, $CDCl_3$) δ 189.5, 162.7, 158.6, 132.4, 129.4, 120.9, 114.7, 60.1, 23.9, 19.8. IR (film cm^{-1}) 3067, 2876, 1668, 1597, 1494. HRMS: calcd for $C_{12}H_{14}O_2Na$ [M+Na] 213.0886, found 213.0892.

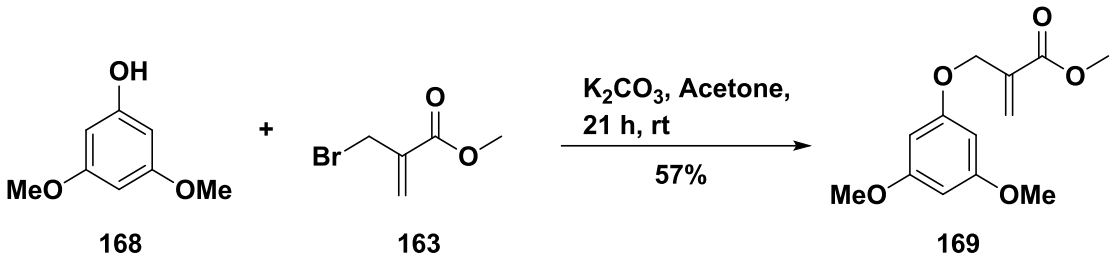

Methyl 2-((3,5-dimethoxyphenoxy)methyl)acrylate (169): To a solution of 3,5-dimethoxyphenol (1.81 g, 11.8 mmol, 1 equiv) and acrylate **163** (2.11 g, 11.8 mmol, 1 equiv) in acetone (24 mL) was added K_2CO_3 (8.14 g, 58.9 mmol, 5.0 equiv) and the reaction was stirred at room temperature for 21 h at which point TLC analysis indicated complete consumption of starting material. The reaction mixture was filtered through celite, rinsed with acetone, and the filtrate was concentrated under reduced pressure. The crude residue was purified by chromatography on silica gel using 80% DCM:Hexane as eluent to give **169** as a colorless oil (1.68 g) in 57% yield. Upon storage at -20 °C, the product crystallized as an off-white solid. ^{1}H NMR (500 MHz, Chloroform-*d*) δ 6.40 (q, *J* = 1.4 Hz, 1H), 6.12 (dd, *J* = 9.7, 2.1 Hz, 3H), 6.00 (q, *J* = 1.8 Hz, 1H), 4.72 (t, *J* = 1.7 Hz, 2H), 3.81 (s, 3H), 3.77 (s, 6H). ^{13}C NMR (126 MHz, $CDCl_3$) δ 165.9, 161.5, 160.2, 135.7, 126.6, 93.7, 93.4, 66.1, 55.4, 52.0. IR (film cm^{-1}) 3002, 2946, 1719, 1592, 1436, 1140. HRMS: calcd for $C_{13}H_{16}O_5Na$ [M+Na] 275.0890 found 275.0886.

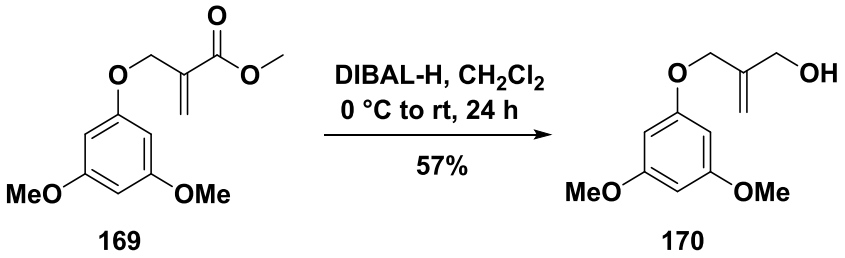

2-((3,5-dimethoxyphenoxy)methyl)prop-2-en-1-ol (170): To a solution of acrylate **169** (600 mg, 2.38 mmol, 1 equiv) cooled at 0 °C in an ice-bath was slowly added DIBAL-H (1M in CH_2Cl_2, 8.3 mL, 2.4 mmol, 3.5 equiv) dropwise. The reaction mixture was allowed to gradually warm to room temperature and stirred for 24 h. The mixture was diluted with diethyl ether (10 mL) and cooled to 0 °C in an ice-bath. The reaction was quenched with water (1.15 mL) and aqueous sodium hydroxide (15%, 0.33 mL), stirred for 30 min, then anhydrous $MgSO_4$ was added and stirred for

another 30 min. The mixture was filtered through celite, concentrated under reduced pressure, and the crude residue was purified by chromatography on silica gel using 20% EtOAc:Hexane, to afford **170** as a colorless oil (302 mg) in 57 % yield. ^{1}H NMR (500 MHz, Chloroform-*d*) δ 6.15 – 6.07 (m, 3H), 5.29 (dq, *J* = 7.3, 1.1 Hz, 2H), 4.56 (t, *J* = 1.0 Hz, 2H), 4.26 (dt, *J* = 6.0, 1.0 Hz, 2H), 3.77 (s, 6H). ^{13}C NMR (126 MHz, $CDCl_3$) δ 161.5, 160.4, 144.1, 113.9, 93.6, 93.3, 69.2, 64.1, 55.4. IR (film cm^{-1}) 3407, 2936, 1590, 1456, 1142. HRMS: calcd for $C_{12}H_{16}O_4Na$ [M+Na] 247.0941 found 247.0944.

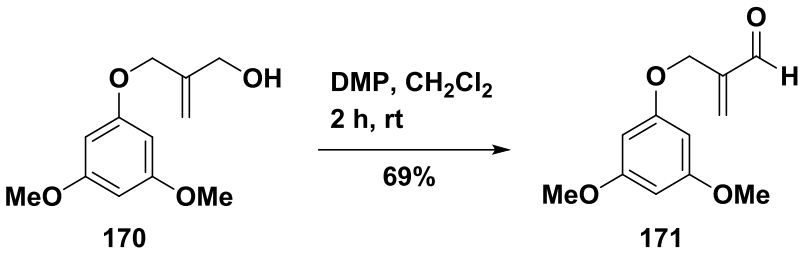

170 171

2-((3,5-dimethoxyphenoxy)methyl)acrylaldehyde (171): To a solution of alcohol **170** (296 mg, 1.32 mmol, 1 equiv) in DCM (13 mL), was added DMP (673 mg, 1.59 mmol, 1.2 equiv), and the mixture was stirred at room temperature for 2 h. The reaction mixture was filtered through celite, and the filtrate was washed with saturated aqueous $Na_2S_2O_4$ (10 mL), aqueous NaOH (15%, 2 x 10 mL), brine, and dried with anhydrous Na_2SO_4. The crude residue was purified by chromatography on silica gel using 20% EtOAc:Hexane as eluent to afford **171** as a colorless oil (203 mg) in 69% yield. ^{1}H NMR (500 MHz, Chloroform-*d*) δ 9.65 (s, 1H), 6.64 (t, *J* = 1.9 Hz, 1H), 6.28 – 6.19 (m, 1H), 6.11 (s, 3H), 4.73 (t, *J* = 1.7 Hz, 2H), 3.77 (s, 6H). ^{13}C NMR (126 MHz, $CDCl_3$) δ 193.0, 161.6, 160.0, 145.3, 134.6, 93.6, 93.6, 63.8, 55.4. IR (film cm^{-1}) 2972, 2845, 1686, 1595, 1150. HRMS: calcd for $C_{12}H_{14}O_4Na$ [M+Na] 245.0784 found 245.0785.

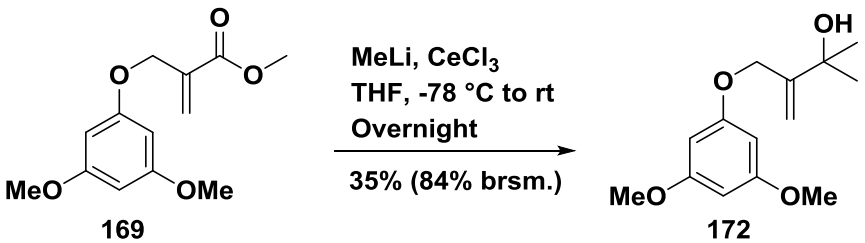

169 172

3-((3,5-dimethoxyphenoxy)methyl)-2-methylbut-3-en-2-ol (172): Oven-dried 250 mL round bottom flask with a magnetic stir bar was charged with powdered cerium(III) chloride heptahydrate (3.69 g, 9.91 mmol, 2.5 equiv), and evacuated to 1.0 mm. The flask was heated at 90 - 100 °C in an oil bath for 2 h then gradually warmed to 140 °C over 30 min and stirred at that temperature overnight. After the flask is back-filled with argon and cooled to 0 °C in an ice-water bath, THF (25 mL) was added with vigorous stirring and stirred for 6 h, resulting in a gray milky suspension. The suspension was cooled to -78 °C and MeLi (1.6 M in Et_2O, 6.2 mL, 9.9 mmol, 2.5 equiv) was added dropwise over 20 min and stirred for 30 min. A solution of acrylate **169** (1.00 g, 3.96 mmol, 1 equiv) in THF (3 mL) was added slowly to the milky suspension dropwise via cannula over 20 min. The mixture was stirred at -78 °C for 30 min then stirred overnight, allowing gradually to warm to room temperature. The reaction mixture was quenched with an aqueous 5% solution of acetic acid (30 mL) and extracted with ethyl acetate (3 x 30 mL). The combined organic phase was washed with brine (50 mL), dried over anhydrous Na_2SO_4, and concentrated under reduced pressure. The crude product was purified by chromatography on silica gel using 20 % EtOAc:Hexane as eluent to give **172** as a light-yellow oil (0.35 g) in 35% (84% brsm) in yield. ^{1}H NMR (500 MHz, Chloroform-*d*) δ 6.13 (d, *J* = 2.1 Hz, 2H), 6.10 (t, *J* = 2.2 Hz, 1H), 5.30 (d, *J* = 0.9 Hz, 1H), 5.24 (q, *J* = 1.2 Hz, 1H), 4.62 (t, *J* = 1.0 Hz, 2H), 3.77 (s, 6H), 1.97 (s, 1H), 1.45 (s, 6H). ^{13}C NMR (126 MHz, $CDCl_3$) δ 161.5, 160.4, 150.3, 112.0, 93.7, 93.3, 72.5, 68,9, 55.4, 29.7. IR (film cm^{-1}) 3448, 2972, 1592, 1474, 1142. HRMS: calcd for $C_{14}H_{20}O_4Na$ [M+Na] 275.1254, found 275.1257

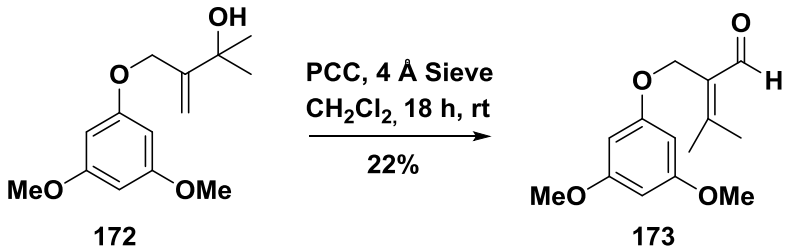

172 173

2-((3,5-dimethoxyphenoxy)methyl)-3-methylbut-2-enal (173): A solution of alcohol **172** (353 mg, 1.40 mmol, 1 equiv) in DCM (14 mL) was transferred via cannula to the suspension of PCC

(1.06 g, 4.91 mmol, 3.5 equiv) and 4 Å molecular sieves (1.06 g) in DCM (25 mL). The dark brown reaction mixture was stirred at room temperature for 18 h, and it was passed through a short pad of silica gel, rinsed with DCM (100 mL) and concentrated under reduced pressure. The brown residue was purified by chromatography on silica gel using 100% DCM to give **173** as a light yellow oil (78 mg) in 22% yield. ^{1}H NMR (500 MHz, Chloroform-*d*) δ 10.15 (s, 1H), 6.13 (d, *J* = 2.2, 2H), 6.09 (t, *J* = 2.2 Hz, 1H), 4.72 (s, 2H), 3.76 (s, 6H), 2.30 (s, 3H), 2.13 (s, 3H). ^{13}C NMR (126 MHz, $CDCl_3$) δ 189.5, 162.9, 161.5, 160.5, 132.3, 93.5, 93.4, 60.1, 55.3, 23.9, 19.8. IR (film cm^{-1}) 2997, 2936, 1666, 1590, 1461, 1142. HRMS: calcd for $C_{14}H_{18}O_4Na$ [M+Na] 273.1097, found 273.1099.

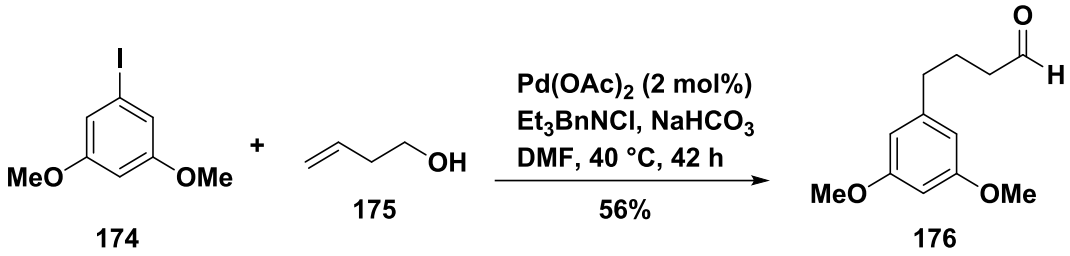

4-(3,5-dimethoxyphenyl)butanal (176): To a solution of iodobenzene **174** (700 mg, 2.65 mmol, 1 equiv) in DMF (7 mL) was added $Pd(OAc)_2$ (11.9 mg, 0.0530 mmol, 0.02 equiv), alcohol **175** (287 mg, 3.98 mmol, 1.50 equiv), benzyltriethylammonium chloride (604 mg, 2.65 mmol, 1 equiv) and sodium bicarbonate (445 mg, 5.30 mmol, 2.00 equiv). The mixture was stirred at 40 °C for 42 h at which point TLC analysis indicated complete consumption of starting material. Saturated aqueous NH_4Cl (10 mL) was added and the mixture was extracted with ethyl acetate (3 x 25 mL). The combined organic extracts were washed with brine, dried with anhydrous Na_2SO_4, concentrated under reduced pressure and purified by chromatography on silica gel using 10% EtOAc:Hexane as eluent to give **176** as a colorless oil (306 mg) in 56% yield. ^{1}H NMR (500 MHz, Chloroform-*d*) δ 9.76 (t, *J* = 1.6 Hz, 1H), 6.36 – 6.29 (m, 3H), 3.78 (s, 6H), 2.66 – 2.54 (m, 2H), 2.46 (td, *J* = 7.3, 1.6 Hz, 2H), 1.96 (p, *J* = 7.4 Hz, 2H). ^{13}C NMR (126 MHz, $CDCl_3$) δ 202.2, 160.9, 143.6, 106.5, 98.0, 55.3, 43.1, 35.3, 23.4. IR (film cm^{-1}) 2940, 2837, 1720, 1593, 1460, 1147. HRMS: calcd for $C_{12}H_{17}O_3$ [M+H] 209.1172 found 209.1169.

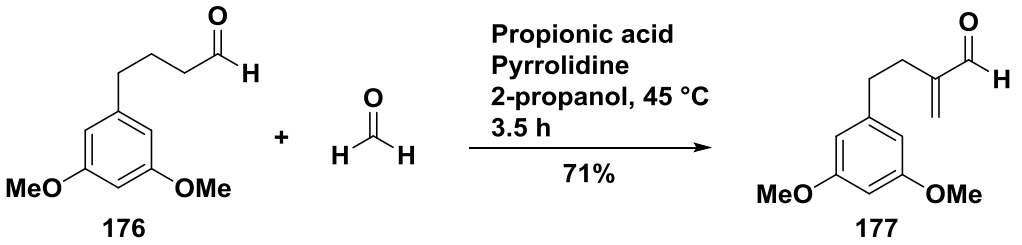

4-(3,5-dimethoxyphenyl)-2-methylenebutanal (177): To a solution of aldehyde **176** (306 mg, 1.47 mmol, 1 equiv) in 2-propanol (1.5 mL) was added formaldehyde solution (37% in water, 0.119 mL, 1 equiv), propionic acid (0.0110 mL, 0.147 mmol, 0.1 equiv), and pyrrolidine (0.0122 mL, 0.147 mmol, 0.1 equiv). The reaction mixture was stirred at 45 °C for 3.5 h. Saturated aqueous $NaHCO_3$ (10 mL) was added, and the mixture was extracted with DCM (3 x 25 mL). The combined organic extracts were washed with brine, dried with anhydrous Na_2SO_4, and concentrated under reduced pressure. The crude residue was purified by chromatography on silica gel using 10% EtOAc:Hexane as eluent to give **177** as a colorless oil (228 mg) in 71% yield. ^{1}H NMR (500 MHz, Chloroform-*d*) δ 9.55 (s, 1H), 6.32 (dd, *J* = 15.1, 2.3 Hz, 3H), 6.22 (q, *J* = 1.1 Hz, 1H), 6.00 (s, 1H), 2.72 (dd, *J* = 9.1, 6.5 Hz, 2H), 2.62 – 2.45 (m, 2H). ^{13}C NMR (126 MHz, $CDCl_3$) δ 194.5, 160.8, 149.2, 143.5, 134.7, 106.5, 98.1, 55.3, 34.3, 29.5. IR (film cm^{-1}) 2936, 2835, 1683, 1592, 1458, 1148. HRMS: calcd for $C_{13}H_{17}O_3$ [M+H] 221.1172 found 221.1171.

General procedure for reaction screening of Claisen rearrangement

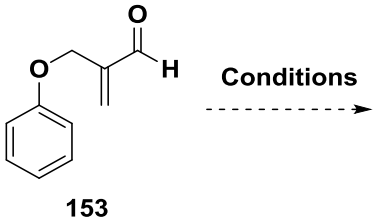

Hydrazide catalyst **121** as HX salt (20 mol%) was dissolved in appropriate solvent at 0.2 M concentration and added to neat aldehyde. An internal standard, mesitylene, was added and the mixture was transferred to an NMR tube. All reactions were monitored by ^{1}H NMR. HCl salt of

121 was prepared by mixing the catalyst free base with methanolic HCl and evaporating excess solvent and HCl under reduced pressure. TfOH salts were prepared by adding corresponding acid to the catalyst in the reaction solvent.

4.3 Experimental procedures for chapter 2

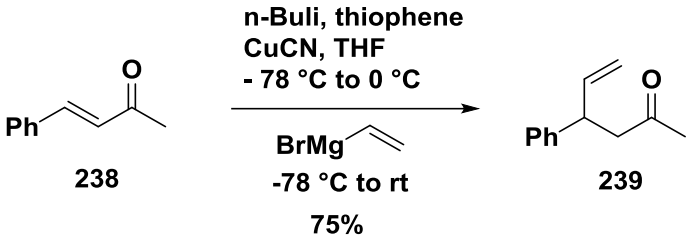

4-phenylhex-5-en-2-one (239): A solution of *n*-butyllithium in hexanes (9.6 ml, 2.5 M, 1.20 equiv) was added to a solution of thiophene (1.92 ml, 24.0 mmol, 1.20 equiv) in THF (90 mL) at -78 °C. After 5 minutes, the mixture was warmed to 0 °C and stirred for additional 30 minutes. The mixture was added, via cannula, to a cold (-78 °C) solution of CuCN (2.15 g, 24.0 mmol, 1.20 equiv) in diethylether (15 mL). The mixture was warmed to 0 °C for 5 minutes and then cooled to -78 °C. Vinnyl magnesium bromide 1.0 M solution in THF (24.0 mL, 1.20 equiv) was added and the mixture was warmed to 0 °C for 5 minutes. The mixture was cooled to -78 °C and (*E*)-4-phenylbut-3-en-2-one **238** (2.92 g, 20.0 mmol, 1 equiv.) was added. Stirring was continued for 2 h at -78 °C and then mixture warmed to rt during 5 h. Saturated aqueous ammonium chloride (30 mL) was added and the resulting mixture was extracted with EtOAc (3 x 30 mL). The combined organic layers were dried over anhydrous sodium sulfate, filtered, and concentrated. The crude residue was purified by chromatography on silica gel using 5% EtOAc/hexanes to afford **239** as a brown oil (2.61 g) in 75 % yield. The spectroscopic data is in agreement with that published in the literature[46].

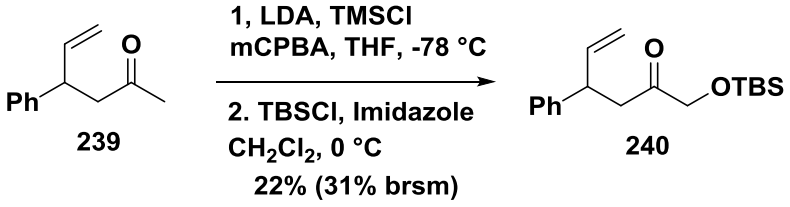

1-((*tert*-butyldimethylsilyl)oxy)-4-phenylhex-5-en-2-one 240: A solution of *n*-butyllithium in hexanes (9.00 mL, 2.5 M, 1.50 equiv) was added to a solution of diisopropylamine (3.17 mL, 22.5 mmol, 1.50 equiv) in tetrahydrofuran (40 mL) at -78 °C. The mixture was stirred 30 minutes at -78 °C and ketone **239** (2.61 g, 15.0 mmol, 1.0 equiv) was added. Finally after 30 minutes freshly distilled TMSCl (3.05 mL, 24.0 mmol, 1.6 equiv) was added and the reaction was allowed to warm to rt during 2 h. Saturated aqueous sodium bicarbonate solution (25 mL) was added and the resulting mixture was extracted with EtOAc (3 x 25 mL). The combined organic layers were dried over anhydrous sodium sulfate, filtered, and concentrated. Crude TMS protected enolate was dissolved in DCM (15 mL), and *m*-CPBA (2.59 g, 15.0 mmol, 1.0 equiv) was added at 0 °C and reaction mixture stirred overnight. Saturated sodium thiosulfate solution (5 mL) was added and the resulting mixture was extracted with EtOAc (3 x 25 mL). Organic layers were washed with 1 M HCl. The combined organic layers were dried over anhydrous sodium sulfate, filtered, and concentrated. Crude 1-hydroxy-4-phenylhex-5-en-2-one (730 mg, 4.2 mmol, 1.0 equiv) was dissolved in dry DCM (15 mL) and imidazole (470 mg, 6.91 mmol, 1.8 equiv) was added followed by TBSCl (694 mg, 4.61 mmol, 1.2 equiv) and reaction stirred at rt overnight. Water (50 mL) was added and the resulting mixture was extracted with DCM (3 x 25 mL). The combined organic layers were dried over anhydrous sodium sulfate, filtered, and concentrated. The crude product was purified by chromatography on silica gel, using 5% EtOAc/hexanes to afford **240** as a colorless oil (1.00 g) in 22% (31% brsm) overall yield. The spectroscopic data is in agreement with that published in the literature[46].

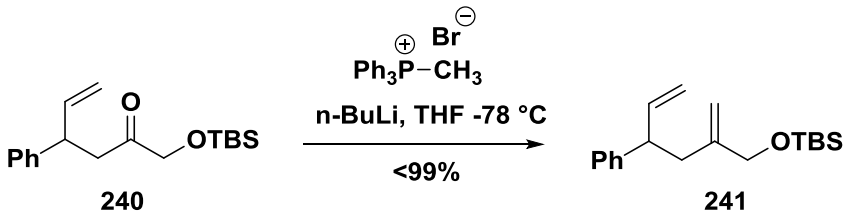

***Tert*-butyldimethylsilyl((2-methylene-4-phenylhex-5-en-1-l)oxy)silane (241):** Triphenylphosphonium bromide (2.13 g, 5.96 mmol, 1.8 equiv) was dissolved in 40 mL dry THF and cooled to -78 °C. A solution of *n*-butyllithium in hexanes (2.25 mL, 2.5 M, 1.7 equiv) was added and mixture was warmed to 0 °C for 2 h. The mixture was cooled to -78 °C and ketone **240**

(1.01 g, 3.31 mmol, 1.0 equiv) was added. The reaction mixture was allowed to warm to rt for 5 hours and stirred overnight. Saturated NH4Cl solution (50 mL) was added and the reaction was extracted with EtOAc (3 x 50 mL). The combined organic layers were dried over anhydrous sodium sulfate, filtered, and concentrated under reduced pressure. The crude residue was purified by chromatography on silica gel, using 5% EtOAc/hexanes as eluent to afford **241** as colorless oil (0.99 g) in 99% yield. The spectroscopic data is in agreement with that published in the literature[46].

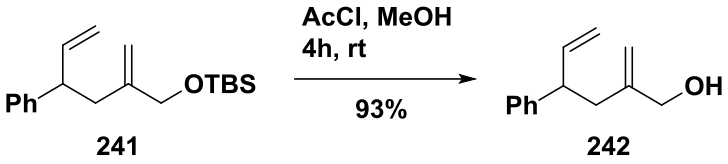

2-methylene-4-phenylhex-5-en-1-ol (242): To a solution of O-TBS protected alcohol **241** (997 mg, 3.30 mmol, 1 equiv) in MeOH (20 mL) was added AcCl (23.5 µL, 0.330 mmol, 0.1 equiv), and the reaction mixture was stirred at room temperature for 4 h. The solvent was evaporated under reduced pressure and the residue was re-dissolved in EtOAc (25 mL), washed with saturated aqueous $NaHCO_3$ (20 mL), brine and dried with anhydrous Na_2SO_4. The organic extract was concentrated under reduced pressure and purified by chromatography on silica gel using 20% EtOAc:Hexane as eluent to give **242** as a colorless oil (576 mg) in 93% yield. The spectroscopic data is in agreement with that published in the literature[46].

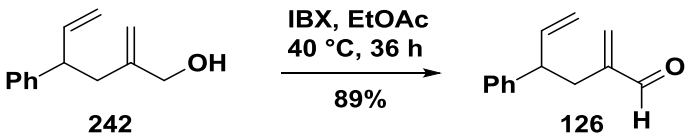

2-methylene-4-phenylhex-5-enal (126): Alcohol **242** (0.576 g, 3.06 mmol, 1 equiv) was dissolved in EtOAc (50 mL) and IBX (1.71 g, 6.11 mmol, 2.0 equiv) was added. The reaction mixture was stirred at 40 °C for 36 h, filtered through celite and concentrated under reduced pressure. The residue was purified by chromatography on silica gel using 5% EtOAc:hexanes as eluent to afford **126** as colorless oil (0.505 g) in 89% yield. The spectroscopic data is in agreement with that published in the literature[46].

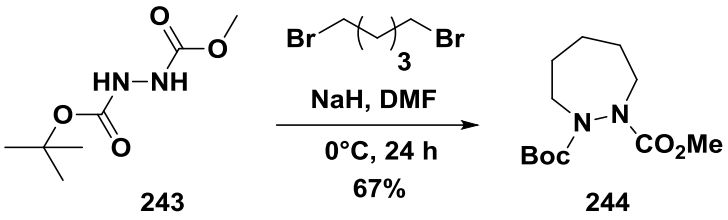

1-(*tert*-butyl) 2-methyl 1,2-diazepane- 1,2-dicarboxylate (244): To a suspension of NaH (0.296 g, 7.40 mmol, 2.35 equiv) in DMF (10.5 mL) cooled at 0 °C in an ice-bath, was added 1-(*tert*-butyl) 2-methyl hydrazine-1,2-dicarboxylate **243** (0.600 g, 3.15 mmol, 1 equiv) in small portions. After evolution of hydrogen had ceased, 1,5-dibromopentane (0.47 mL, 3.5 mmol, 1.1 equiv) was added, and the mixture was stirred for 24 h, gradually warming up to room temperature overnight. Saturated aqueous NH_4Cl (15 mL) was added to the reaction mixture and extracted with EtOAc (3 x 20 mL). The combined organic extracts were washed with water (3 x 25 mL), brine, dried with anhydrous Na_2SO_4 and concentrated under reduced pressure. The residue was purified by chromatography on silica gel using 8:3 Hexane:EtOAc as eluent to give **244** as a colorless oil (0.548 g) in 67% yield. ^{1}H NMR (500 MHz, Chloroform-*d*) δ 4.07 – 3.78 (m, 2H), 3.73 (m, 3H), 3.41 – 2.93 (m, 2H), 1.87 – 1.37 (s, 15H). For major rotamer: ^{13}C NMR (126 MHz, $CDCl_3$) δ 156.4, 154.5, 80.7, 53.0, 49.2, 48.7, 28.3, 27.4, 27.0, 25.9. IR (film cm^{-1}) 2931, 1704, 1446, 1362, 1145. HRMS: calcd for $C_{12}H_{22}N_2O_4Na$ [M+Na] 281.1472, found 281.1483.

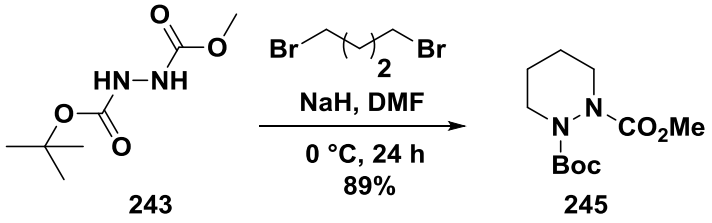

1-(*tert*-butyl) 2-methyl tetrahydropyridazine-1,2-dicarboxylate (245): To a suspension of NaH (79.0 mg, 1.97 mmol, 2.35 equiv) in DMF (2.8 mL) cooled at 0 °C in an ice-bath, was added 1-(*tert*-butyl) 2-methyl hydrazine-1,2-dicarboxylate **243** (159 mg, 0.837 mmol, 1 equiv) in small portions. After evolution of hydrogen had ceased, 1,5-dibromobutane (0.11 mL, 0.92 mmol, 1.1 equiv) was added, and the mixture was stirred for 24 h, gradually warming up to room temperature

overnight. Saturated aqueous NH_4Cl (5 mL) was added to the reaction mixture and extracted with EtOAc (3 x 10 mL). The combined organic extracts were washed with water (3 x 10 mL), brine, dried with anhydrous Na_2SO_4 and concentrated under reduced pressure. The residue was purified by chromatography on silica gel using 20% EtOAc:Hexane as eluent to give **245** as a yellow oil (178 mg) in 89% yield. ^{1}H NMR (500 MHz, Chloroform-*d*) δ 4.10 – 4.01 (m, 2H), 3.73 (s, 3H), 3.15 – 2.75 (m, 2H), 1.76 – 1.54 (m, 4H), 1.46 (s, 9H). For major rotamer: ^{13}C NMR (126 MHz, $CDCl_3$) δ 155.9, 154.4, 81.1, 53.1, 44.9, 44.7, 28.2, 23.9, 23.5. IR (film cm^{-1}) 2946, 2921, 1709, 1691, 1390, 1282, 1160. HRMS: calcd for $C_{11}H_{20}N_2O_4Na$ [M+Na] 267.1315, found 267.1317.

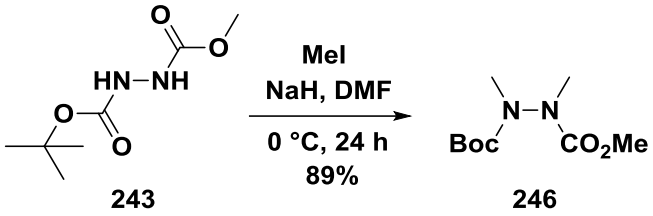

243 246

1-(*tert*-butyl) 2-methyl 1,2-dimethylhydrazine-1,2-dicarboxylate (246): To a suspension of NaH (0.395 g, 9.93 mmol, 2.35 equiv) in DMF (14 mL) cooled at 0 °C in an ice-bath, was added 1-(*tert*-butyl) 2-methyl hydrazine-1,2-dicarboxylate **243** (0.800 g, 4.21 mmol, 1 equiv) in small portions. After evolution of hydrogen had ceased, iodomethane (0.60 mL, 9.7 mmol, 2.3 equiv) was added, and the mixture was stirred for 24 h, gradually warming up to room temperature overnight. Saturated aqueous NH_4Cl (15 mL) was added to the reaction mixture and extracted with EtOAc (3 x 20 mL). The combined organic extracts were washed with water (3 x 25 mL), brine, dried with anhydrous Na_2SO_4 and concentrated under reduced pressure. The residue was purified by chromatography on silica gel using 20% EtOAc:Hexane as eluent to give **246** as a yellow oil (178 mg) in 89% yield. Upon storage at -20 °C, the product crystallized as an off-white solid. ^{1}H NMR (500 MHz, Chloroform-*d*) δ 3.77 – 3.65 (m, 3H), 3.10 – 2.98 (m, 6H), 1.52 – 1.36 (m, 9H). For major rotamer: ^{13}C NMR (126 MHz, $CDCl_3$) δ 156.7, 154.8, 81.0, 53.2, 35.6, 34.9, 28.2. IR (film cm^{-1}) 2956, 1696, 1362, 1145. HRMS: calcd for $C_9H_{18}N_2O_4Na$ [M+Na] 241.1159, found 241.1165.

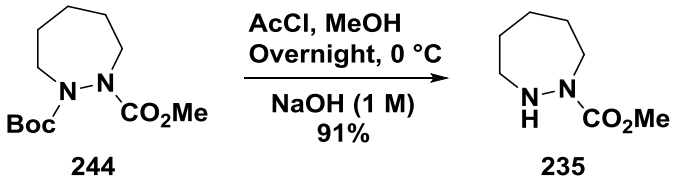

244 235

Methyl 1,2-diazepane-1-carboxylate (235): To a solution of hydrazide **244** (1.73 g, 6.71 mmol, 1 equiv) in MeOH (22 mL) cooled at 0 °C in an ice-bath was added AcCl (4.8 mL, 67 mmol, 10 equiv) dropwise. The reaction was open to air and stirred overnight at room temperature. After evaporation of MeOH under reduced pressure, the residue was dissolved in DCM (20 mL) and washed with aqueous NaOH solution (1M, 20 mL). The aqueous layer was extracted with DCM (3 x 20 mL), and the combined organic extracts were washed with water (25 mL), brine, dried with anhydrous $MgSO_4$ and concentrated under reduced pressure. The crude residue was purified by chromatography on silica gel using 20% EtOAc:Hexane as eluent to give **235** as a light-yellow oil (0.963 g) in 91% yield. ^{1}H NMR (500 MHz, Chloroform-*d*) δ 4.06 (s, 1H), 3.73 (s, 3H), 3.51 (s, 2H), 2.93 (d, *J* = 5.4 Hz, 2H), 1.77 (dq, *J* = 9.7, 5.8 Hz, 2H), 1.62 (m, 4H). ^{13}C NMR (126 MHz, $CDCl_3$) δ 157.1, 52.8, 50.9, 48.3, 29.8, 27.5, 25.3. IR (film cm^{-1}) 3539, 3316, 2926, 1694, 1443, 1380, 1193, 1127. HRMS: calcd for $C_7H_{14}N_2O_2Na$ [M+Na] 181.0947, found 181.0942.

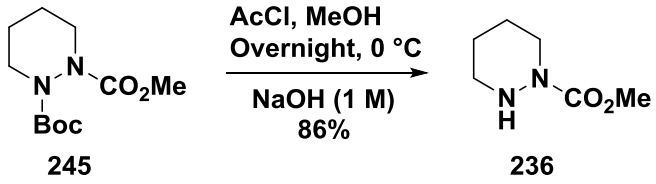

245 236

Methyl tetrahydropyridazine-1(*2H*)-carboxylate (236): To a solution of pyridazine **245** (178 mg, 0.731 mmol, 1 equiv) in MeOH (3.7 mL) cooled at 0°C in an ice-bath was added AcCl (0.52 mL, 7.3 mmol, 10 equiv) dropwise. The reaction was open to air and stirred overnight at room temperature. After evaporation of MeOH under reduced pressure, the residue was dissolved in DCM (10 mL) and washed with aqueous NaOH solution (1M, 10mL). The aqueous layer was extracted with DCM (3 x 10 mL), and the combined organic extracts were washed with water (15 mL), brine, dried with anhydrous $MgSO_4$ and concentrated under reduced pressure. The crude

residue was purified by chromatography on silica gel using 100% EtOAc as eluent to give **236** as a yellow oil (91 mg) in 86% yield. ^{1}H NMR (500 MHz, Chloroform-*d*) δ 3.75 (s, 3H), 3.62 – 3.32 (m, 3H), 3.01 – 2.78 (m, 2H), 1.65 (m, 4H). ^{13}C NMR (126 MHz, $CDCl_3$) δ 156.1, 53.0, 47.9, 45.7, 25.1, 24.2. IR (film cm^{-1}) 3534, 3255, 2936, 2850, 1683, 1438, 1259. HRMS: calcd for $C_6H_{12}N_2O_2Na$ [M+Na] 167.0791, found 167.0791.

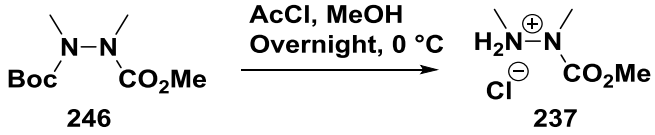

Methyl 1,2-dimethylhydrazine-1-carboxylate HCl salt (237): To a solution of hydrazide **246** (150 mg, 0.678 mmol, 1 equiv) in MeOH (7.5 mL) cooled at 0°C in an ice-bath was added AcCl (0.24 mL, 6.7 mmol, 10 equiv) dropwise. The reaction was open to air and stirred overnight at room temperature. After evaporation of MeOH under reduced pressure, the residue was washed with diethyl ether (3 x 20 mL) and dried under high vacuum (< 0.1 mm Hg) overnight to give **237** as a colorless crystalline solid which was sufficiently pure for use without further purification. ^{1}H NMR (500 MHz, Chloroform-*d*) δ 3.86 (s, 3H), 3.37 (s, 3H), 3.00 (s, 3H). ^{13}C NMR (126 MHz, $CDCl_3$) δ 154.3, 54.5, 34.3, 33.4 IR (film cm^{-1}) 3392, 2957, 1725, 1562. HRMS: calcd for $C_4H_{10}N_2O_2Na$ [M+Na] 141.0634, found 141.0629.

4.3.1 Experimental procedures for ^{13}C kinetic isotope effect measurements

Procedures for Diels-Alder reactions

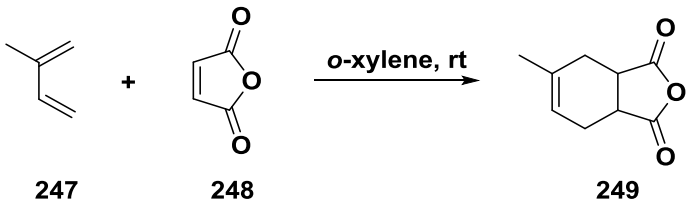

5-methyl-3a,4,7,7a-tetrahydroisobenzofuran-1,3-dione (249)

Excess Isoprene Reaction

To a flame-dried 250 mL round bottom flask was added maleic anhydride (1.18 g, 12.0 mmol, 1 equiv) and *o*-xylene (75 mL) and the solution was sonicated until all maleic anhydride

dissolved. Isoprene (4.1 g, 60 mmol, 5.0 equiv) was added to the solution and the flask was stoppered and sealed with parafilm. The reaction was stirred for 3 d at room temperature, and the resulting mixture was purified directly by chromatography on silica gel using 100% DCM as eluent to give cycloadduct **249** as a white solid (1.10 g) in 55 % yield. The spectroscopic data is in agreement with that published in the literature[77]. 400 mg of this sample was dissolved in 0.65 mL of $CDCl_3$ and the solution was transferred to a screw cap NMR tube and sealed with parafilm. Additional sample was prepared by repeating the procedure above.

Excess Maleic Anhydride Reaction

To a flame-dried 250 mL round bottom flask was added maleic anhydride (2.82 g, 0.0288 mmol, 1.2 equiv), isoprene (1.63 g, 0.0239 mmol, 1 eqiuv) and *o*-xylene (30 mL) and the flask was stoppered and sealed with parafilm. The reaction was stirred at room temperature for 5 d, and the resulting mixture was purified directly by chromatography on silica gel using 1:1:8 DCM:Et_2O:hexane as eluent afford cycloadduct **249** as a white solid (0.788 g) in 20 % yield. The spectroscopic data is in agreement with that published in the literature[77]. 400 mg of this sample was dissolved in 0.65 mL of $CDCl_3$ and the solution was transferred to a screw cap NMR tube and sealed with parafilm. Additional sample was prepared by repeating the procedure above.

Procedure for organocatalytic Cope rearrangement:

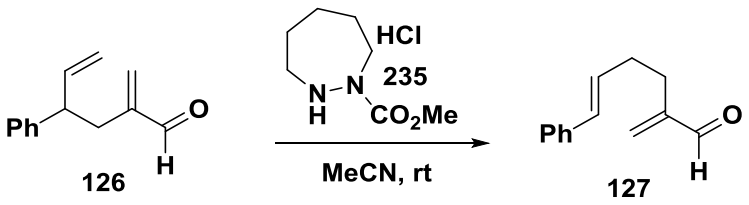

(*E*)-2-methylene-6-phenylhex-5-enal

Partial conversion reaction

To a solution of 2-methylene-4-phenylhex-5-enal (650 mg, 3.49 mmol, 1 equiv) in MeCN (14 mL) was added methyl 1,2-diazepane-1-carboxylate HCl (67.9 mg, 0.349 mmol, 0.1 equiv) and mesitylene (200 μL), and the solution stirred at room temperature. Aliquots were removed

periodically (6 min, 11 min and 17 min) to determine percent conversion by ^{1}H NMR analysis. The reaction mixture was diluted with EtOAc (50 mL) and saturated aqueous $NaHCO_3$ (30 mL). The layers were separated and the aqueous phase was extracted with EtOAc (3 x 25 mL), washed with brine, dried with anhydrous Na_2SO_4 and concentrated under reduced pressure. The crude residue was purified by chromatography on silica gel using 25:1 pentane:Et_2O as eluent to afford **127** as a light-yellow oil (128 mg) in 20% yield. ^{1}H NMR analysis indicated ~25% conversion to the product relative to the starting material. The spectroscopic data is in agreement with that published in the literature[46]. 63.5 mg of this sample was dissolved in 0.65 mL of $CDCl_3$ and the solution was transferred to a screw cap NMR tube and sealed with parafilm. Second sample was prepared by repeating the procedure above on a larger scale (15 % conversion, 190 mg of **127** in 0.65 mL of $CDCl_3$.

Full conversion reaction

To a solution of 2-methylene-4-phenylhex-5-enal (120 mg, 0.644 mmol, 1 equiv) in MeCN (2.6 mL) was added methyl 1,2-diazepane-1-carboxylate HCl (12.5 mg, 0.0644 mmol, 0.1 equiv) and mesitylene (90 μL), and the solution stirred at room temperature for 12 d. Aliquots were removed periodically to determine percent conversion by ^{1}H NMR analysis The reaction mixture was diluted with EtOAc (50 mL) and saturated aqueous $NaHCO_3$ (30 mL). The layers were separated and the aqueous phase was extracted with EtOAc (3 x 25 mL), washed with brine, dried with anhydrous Na_2SO_4 and concentrated under reduced pressure. The crude residue was purified by chromatography on silica gel using 25:1 pentane:Et_2O as eluent to afford **127** as a light-yellow oil (68 mg) in 57% yield. The spectroscopic data is in agreement with that published in the literature[46]. 63.5 mg of this sample was dissolved in 0.65 mL of $CDCl_3$ and the solution was transferred to a screw cap NMR tube and sealed with parafilm. Second sample was prepared by repeating the procedure above on a larger scale.

NMR procedures and calculated ^{13}C KIE data:

^{1}H NMR and distortionless enhancement by polarization transfer (DEPT) spectra were recorded at 25 °C on 500 MHz Bruker spectrometer, and setting for DEPT measurement were done according to Jacobsen et al[77] with the help of Dr. Stein in the nuclear magnetic resonance facility

in the Department of Chemistry, McGill University. After all integrals were obtained, KIEs and the standard errors were calculated using an Excel document.

$$\mathrm{KIE_{PDT}} = \frac{\ln(1-F)}{\ln[(1-F(R_{PDT}/R_0))]}$$

Standard errors for KIEs were calculated using the equation provided by Jacobsen et al[77]:

$$B = \frac{F}{\ln(1-F)} * \frac{R}{R_0} * KIE * \left(1 - \left(F * \frac{R}{R_0}\right)\right); Error = \frac{R}{R_0}\sqrt{\frac{B^2 * ({s_A}^2 + {s_B}^2)}{n}}$$

Table 4.1 integrals for ^{13}C KIE measurement for Diels-Alder reaction

Note: Values shown are average of raw integrals. Sample 1 is the average of raw integrals from 10 blocks of 16 scans each. Sample 2 is the average of raw integrals from 9 blocks of 16 scans each.

Sample name (raw integral)	C1	C3	C4	Methyl
Sample 1 (full conversion 1)	10243.85	9863.36	9833.84	9324.59
Sample 2 (full conversion 2)	10095.80	9698.34	9673.65	9117.63
Sample 3 (partial conversion 3)	10127.75	9903.78	9767.26	9404.98
Sample 4 (partial conversion 4)	9911.69	9706.58	9528.60	9122.81

Sample name (Standard Deviation)	C1	C3	C4	Methyl
Sample 1 (full conversion 1)	37.64	22.90	34.88	50.97
Sample 2 (full conversion 2)	37.38	12.99	23.68	57.53
Sample 3 (partial conversion 3)	31.56	22.37	32.72	32.86
Sample 4 (partial conversion 4)	19.27	13.50	23.42	31.76

Ratios ($^{13}C/^{12}C$)	C1	C3	C4	Methyl
Sample 1 (full conversion 1)	1.0986	1.0578	1.0546	1.0000
Sample 2 (full conversion 2)	1.1073	1.0637	1.0610	1.0000
Sample 3 (partial conversion 3)	1.0768	1.0530	1.0385	1.0000

Sample 4 (partial conversion 4)	1.0865	1.0640	1.0445	1.0000

Experimental KIEs	C1	C3	C4
Measurement 1	1.023(3)	1.005(3)	1.017(3)
Measurement 2	1.021(3)	1.000(3)	1.018(3)

Table 4.2 integrals for ^{13}C KIE measurement for Cope rearrangement

Note: Values shown are average of raw integrals. Sample 1 is the average of raw integrals from 35 blocks of 16 scans each. Sample 2 is the average of raw integrals from 45 blocks of 16 scans each.

Sample name (raw integral)	C1	C3	C4	C5
Sample 1 (full conversion 1)	1682.67	2006.27	1719.80	1695.44
Sample 2 (full conversion 2)	4577.36	5610.69	4673.53	4569.22
Sample 3 (partial conversion 3)	1669.70	2005.42	1722.354	1706.34
Sample 4 (partial conversion 4)	4462.41	5527.53	4623.54	4570.76

Sample name (raw integral)	C6	C7	C8	C9	C10
Sample 1 (full conversion 1)	1695.27	1726.27	3575.83	1724.38	3468.88
Sample 2 (full conversion 2)	4628.82	4608.06	9576.05	4610.73	9282.17
Sample 3 (partial conversion 3)	1677.32	1726.85	3616.30	1741.49	3505.47
Sample 4 (partial conversion 4)	4524.06	4592.06	9600.24	4623.67	9316.38

Sample name (standard deviation)	C1	C3	C4	C5
Sample 1 (full conversion 1)	23.28	18.79	17.90	13.48
Sample 2 (full conversion 2)	21.73	20.19	15.31	21.48
Sample 3 (partial conversion 3)	19.92	19.85	24.08	19.50
Sample 4 (partial conversion 4)	17.85	21.35	18.47	19.26

Sample name (standard deviation)	C6	C7	C8	C9	C10
Sample 1 (full conversion 1)	18.06	16.79	28.52	19.07	27.73
Sample 2 (full conversion 2)	22.15	19.32	32.14	18.93	31.23

Sample 3 (partial conversion 3)	21.11	16.52	26.80	20.98	26.32
Sample 4 (partial conversion 4)	21.02	17.96	23.46	20.14	25.55

Ratios ($^{13}C/^{12}C$)	C1	C3	C4	C5
Sample 1 (full conversion 1)	0.9758	1.1635	0.9973	0.9832
Sample 2 (full conversion 2)	0.9928	1.2169	1.0136	0.9910
Sample 3 (partial conversion 3)	0.9588	1.1516	0.9890	0.9798
Sample 4 (partial conversion 4)	0.9651	1.1955	1.0000	0.9886

Ratios ($^{13}C/^{12}C$)	C6	C7	C8	C9	C10
Sample 1 (full conversion 1)	0.9831	1.0011	2.0737	1.0000	2.0117
Sample 2 (full conversion 2)	1.0039	0.9994	2.0769	1.0000	2.0132
Sample 3 (partial conversion 3)	0.9632	0.9916	2.0766	1.0000	2.0129
Sample 4 (partial conversion 4)	0.9785	0.9932	2.0763	1.0000	2.0149

Experimental KIEs	C1	C3	C4	C5
Measurement 1	1.021(7)	1.012(7)	1.010(8)	1.004(7)
Measurement 2	1.033(4)	1.021(4)	1.016(4)	1.003(4)

Ratios ($^{13}C/^{12}C$)	C6	C7	C8	C10
Measurement 1	1.024(8)	1.011(7)	0.998(6)	0.999(6)
Measurement 2	1.030(4)	1.007(4)	1.000(4)	0.999(4)

4.3.2 Kinetic Analysis of Organocatalytic Cope rearrangement

Representative procedure:

To a solution of 2-methylene-4-phenylhex-5-enal (28 mg, 0.15 mmol, 1 equiv) in CD_3CN (600 µL) was added mesitylene (21 µL) as an internal standard, and ^1H NMR was taken with a relaxation delay of $t_1 = 3$ seconds. Then methyl 1,2-diazepane-1-carboxylate HCl (2.9 mg, 0.015 mmol, 0.1 equiv) was added and ^1H NMR was taken periodically with a relaxation delay of $t_1 = 3$ seconds until reaction completion. Percent conversion was calculated versus the internal standard.

Same procedure above was repeated for employing methyl tetrahydropyridazine-1(*2H*)-carboxylate HCl and methyl 1,2-dimethylhydrazine-1-carboxylate HCl as organocatalyst. Each experiment was performed in duplicate except for methyl tetrahydropyridazine-1(*2H*)-carboxylate HCl.

4.4 Experimental procedures for chapter 3

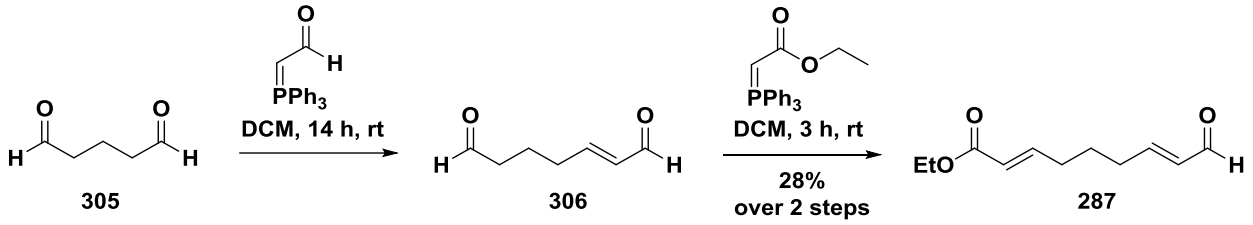

Ethyl (2*E*,7*E*)-9-oxonona-2,7-dienoate (287): To a solution of glutaric dialdehyde (50 wt%, 45 mL, 7.7 equiv) in DCM (100 mL), was added (Triphenylphosphoranylidene)acetaldehyde (10.0 g, 32.8 mmol, 1 equiv) and the reaction mixture was stirred for 20 h at room temperature. The mixture was diluted with water (50 mL), extracted with DCM (3 x 75 mL), and the combined organic extracts were dried with anhydrous $MgSO_4$ and concentrated under reduced pressure. The crude **306** (2.25 g) was used in the next step without further purification.

To a solution of **306** (2.25g, 17.8 mmol, 1 equiv) in DCM (150 mL) was added (carbethoxymethylene)triphenylphosphorane (6.21 g, 17.8 mmol, 1 equiv), and the reaction was stirred for 3h at room temperature. The mixture was diluted with water (50 mL), extracted with DCM (3 x 75 mL), and the combined organic extracts were dried with anhydrous $MgSO_4$ and concentrated under reduced pressure. The crude residue was purified by chromatography on silica gel using 20% EtOAc:Hexane as eluent to give **287** as a light-yellow oil (1.79 g) in 22% yield over two steps. ^{1}H NMR (500 MHz, Chloroform-*d*) δ 9.51 (d, *J* = 7.8 Hz, 1H), 6.93 (dt, *J* = 15.6, 7.0 Hz, 1H), 6.82 (dt, *J* = 15.6, 6.7 Hz, 1H), 6.13 (ddt, *J* = 15.7, 7.9, 1.5 Hz, 1H), 5.84 (dt, *J* = 15.7, 1.6 Hz, 1H), 4.19 (q, *J* = 7.1 Hz, 2H), 2.44 – 2.32 (m, 2H), 2.27 (qd, *J* = 7.2, 1.6 Hz, 2H), 1.70 (p, *J* = 7.5 Hz, 2H), 1.29 (t, *J* = 7.2 Hz, 3H). ^{13}C NMR (126 MHz, $CDCl_3$) δ 193.8, 166.4, 157.2, 147.5, 133.4, 122.3, 60.3, 31.9, 31.4, 26.2, 14.3. IR (film cm^{-1}) 2982, 2936, 1715, 1687, 1653, 1267. HRMS: calcd for $C_{11}H_{16}O_3Na$ [M+Na] 219.0991 found 219.0991.

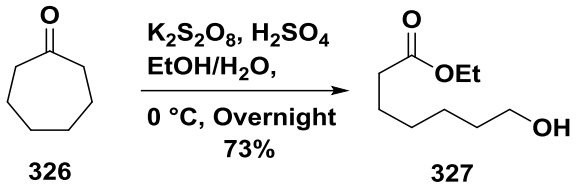

Ethyl 7-hydroxyheptanoate (327): A mixture of 96% sulfuric acid (28.5 mL, 0.532 mmol, 14.2 equiv), water (9.6 mL) and EtOH (40 mL) was cooled at 5 °C in an ice bath. Potassium persulfate (28.9 g, 0.107 mmol, 3.0 equiv) was added gradually with stirring, maintaining internal temperature at 5 °C. A solution of **326** (4.00 g, 0.0356 mmol, 1 equiv) in EtOH (12 mL) was added dropwise and the mixture was stirred overnight. The reaction mixture was diluted with water (250 mL) and extracted with EtOAc (3 x 75 mL). The combined organic extracts were dried with anhydrous Na_2SO_4, concentrated under reduced pressure, and the residue was purified by chromatography on silica gel using 50% EtOAc:Hexane as eluent to give **327** as colorless liquid (4.53 g) in 73% yield. The spectroscopic data is in agreement with that published in the literature[113].

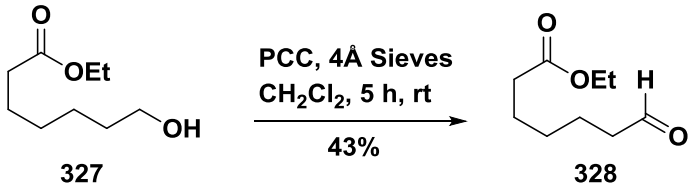

Ethyl 7-oxoheptanoate (328): To a solution of alcohol **327** (4.53 g, 26.0 mmol, 1 equiv) in DCM (75 mL) was added PCC (13.5g, 62.5 mmol, 2.4 equiv) and 4 Å sieves (8.2 g), and the mixture was stirred for 5h at room temperature at which point TLC analysis indicated complete consumption of starting material. The mixture was filtered through a short pad of florisil and rinsed with DCM (250 mL). The filtrate was concentrated under reduced pressure, and the crude residue was distilled under high vacuum (< 0.1 mmHg) to afford **328** as a colorless liquid (1.94 g) in 43% yield. The spectroscopic data is in agreement with that published in the literature[113].

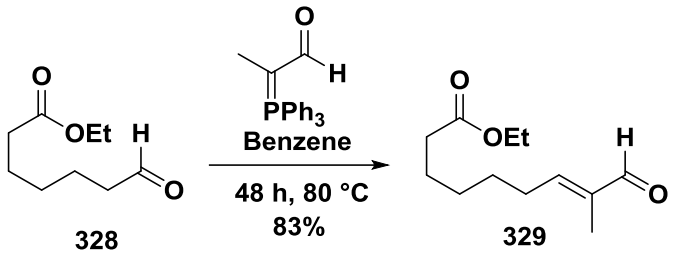

Ethyl (*E*)-8-methyl-9-oxonon-7-enoate (329): To a solution of aldehyde **328** (1.94 g, 11.3 mmol, 1 equiv) in benzene (50 mL) was added 2-(triphenylphosphoranylidene)propionaldehyde (4.30 g, 13.5 mmol, 1.2 equiv), and the mixture was stirred under reflux for 48 h. The reaction mixture was concentrated under reduced pressure and purified directly by chromatography on silica gel using 1:1:6 EtOAc:Et_2O:Hexane as eluent to afford **329** as a colorless oil (1.97g) in 83% yield. ^{1}H NMR (500 MHz, Chloroform-*d*) δ 9.40 (s, 1H), 6.48 (td, *J* = 7.3, 1.4 Hz, 1H), 4.13 (q, *J* = 7.1 Hz, 2H), 2.42 – 2.24 (m, 3H), 1.74 (q, *J* = 1.0 Hz, 2H), 1.71 – 1.57 (m, 2H), 1.58 – 1.45 (m, 3H), 1.45 – 1.34 (m, 2H), 1.26 (t, *J* = 7.1 Hz, 3H). ^{13}C NMR (126 MHz, $CDCl_3$) δ 195.3, 173.6, 154.5, 139.5, 60.3, 34.2, 28.8, 28.8, 28.1, 24.7, 14.3, 9.2. IR (film cm^{-1}) 2934, 2860, 1731, 1684, 1179. HRMS: calcd for $C_{12}H_{20}O_3Na$ [M+Na] 235.1305, found 235.1296.

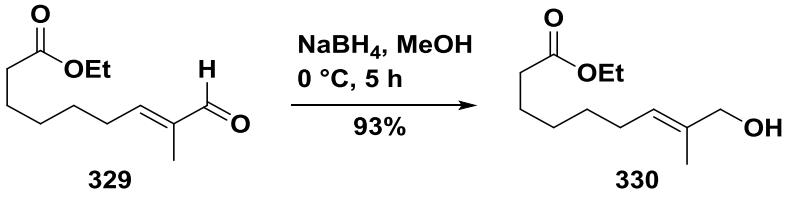

Ethyl (*E*)-9-hydroxy-8-methylnon-7-enoate (330): To a solution of enal **329** (1.96 g, 9.23 mmol, 1 equiv) in MeOH (46 mL) cooled at 0°C was added $NaBH_4$ (0.384 g, 10.2 mmol, 1.1 equiv), and the reaction was stirred for 5h at room temperature. The reaction mixture was quenched with saturated aqueous NH_4Cl (25 mL) and extracted with ethyl acetate (3 x 25 mL). The combined organic extracts were washed with brine, dried with anhydrous Na_2SO_4 and concentrated under reduced pressure. The crude residue was purified by chromatography on silica gel using 25% EtOAc:Hexane as eluent to afford **330** as a colorless oil (1.83g) in 93% yield. ^{1}H NMR (500 MHz, Chloroform-*d*) δ 5.40 (tq, *J* = 7.2, 1.4 Hz, 1H) 4.12 (q, *J* = 7.1 Hz, 2H), 4.00 (dd, *J* = 6.1, 1.2 Hz, 2H), 2.29 (t, *J* = 7.5 Hz, 2H), 2.04 (q, *J* = 6.7 Hz, 2H), 1.70 – 1.58 (m, 5H), 1.43 – 1.27 (m, 5H),

1.25 (t, *J* = 7.1 Hz, 3H). ^{13}C NMR (126 MHz, $CDCl_3$) δ 173.8, 134.8, 126.2, 69.0, 60.2, 34.3, 29.1, 28.8, 27.4, 24.8, 14.3, 13.7. IR (film cm^{-1}) 3409, 2930, 2857, 1733, 1182, 1013. HRMS: calcd for $C_{12}H_{22}O_3Na$ [M+Na] 237.1461, found 237.1456.

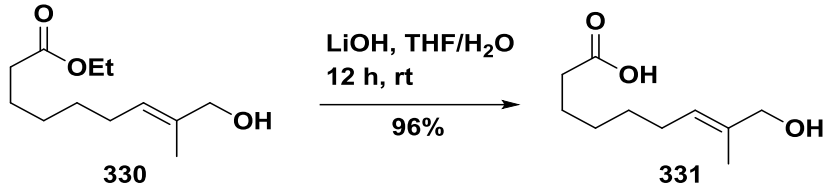

(*E*)-9-hydroxy-8-methylnon-7-enoic acid (331): To a solution of alcohol **330** (1.82 g, 8.52 mmol, 1 equiv) in THF/H_2O (1:1, 40 mL) was added lithium hydroxide monohydrate (0.894 g, 21.3 mmol, 2.5 equiv) and stirred for 12 h at room temperature. The biphasic mixture was separated, and the aqueous layer was washed with Et_2O (30 mL) and made acidic to pH 2~3 with 1M HCl solution. The mixture was extracted with EtOAc (3 x 50 mL), washed with brine, dried with anhydrous Na_2SO_4 and concentrated under reduced pressure to afford **331** as a colorless oil (1.52 g) in 96 % yield which was sufficiently pure for use without further purification. ^{1}H NMR (500 MHz, Chloroform-*d*) δ 5.40 (tp, *J* = 7.1, 1.4 Hz, 1H) 4.00 (d, *J* = 1.2 Hz, 2H), 2.35 (t, *J* = 7.5 Hz, 2H), 2.04 (q, *J* = 6.8 Hz, 2H), 1.74 – 1.51 (m, 5H), 1.49 – 1.25 (m, 5H). ^{13}C NMR (126 MHz, $CDCl_3$) δ 179.2, 134.8, 126.3, 69.0, 33.9, 29.0, 28.6, 27.3, 24.5, 13.7. IR (film cm^{-1}) 3360, 3265, 2930, 2854, 1694, 1234, 1193, 1012. HRMS: calcd for $C_{10}H_{18}O_3Na$ [M+Na] 209.1148, found 209.1145.

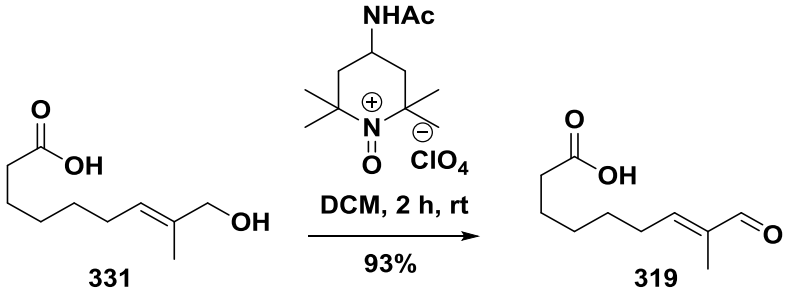

(*E*)-8-methyl-9-oxonon-7-enoic acid (319): To a solution of alcohol **331** (1.48 g, 7.96 mmol, 1 equiv) in DCM (40 mL) was added 4-(acetylamino)-2,2,6,6-tetramethyl-1-oxo-piperidinium perchlorate (3.73 g, 11.9 mmol, 1.5 equiv). The reaction was stirred at room temperature for 2 h

at which point NMR aliquot indicated complete consumption of the starting material. The mixture was filtered through a short pad of sand rinsing with DCM, and the filtrate was concentrated under reduced pressure. The crude residue was purified by chromatography on silica gel using 2:1 Hexane:Acetone as eluent to afford **319** as a light-yellow oil (1.40 g) in 93 % yield. ^{1}H NMR (500 MHz, Chloroform-*d*) δ 11.02 (s, 1H), 9.42 (s, 1H), 6.50 (tq, *J* = 7.5, 1.5 Hz, 1H), 2.46 – 2.34 (m, 4H), 1.77 (q, *J* = 7.4 Hz, 2H), 1.70 (p, *J* = 7.4 Hz, 2H), 1.61 – 1.52 (m, 2H), 1.49 – 1.37 (m, 2H). ^{13}C NMR (126 MHz, $CDCl_3$) δ 195.4, 179.1, 154.4, 139.6, 33.7, 28.8, 28.7, 28.1, 24.4, 9.2. IR (film cm^{-1}) 3250, 2932, 2860, 1706, 1682, 1408, 1215. HRMS: calcd for $C_{10}H_{16}O_3Na$ [M+Na] 207.0992, found 207.0990.

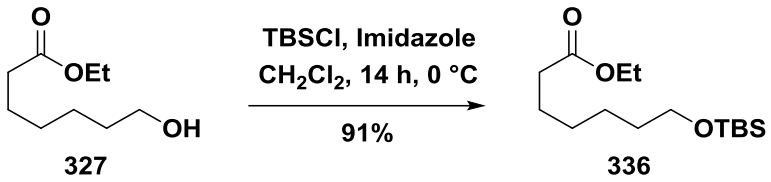

Ethyl 7-((*tert*-butyldimethylsilyl)oxy)heptanoate (336): To a solution of alcohol **327** (4.16 g, 23.9 mmol, 1 equiv) in DCM (40 mL) cooled at 0 °C in an ice-bath was added TBSCl (4.32 g, 28.7 mmol, 1.2 equiv) and imidazole (4.23 g, 62.2 mmol, 2.6 equiv), and the mixture was stirred for 14 h. The reaction mixture was diluted with DCM (50 mL) and water (30 mL), and it was extracted with DCM (3 x 50 mL). The organic extracts were washed with brine (50 mL), dried with anhydrous Na_2SO_4, and concentrated under reduced pressure. The residue was purified by chromatography on silica gel using 3% EtOAc:Hexane as eluent to give **336** as a colorless oil (6.26 g) in 91% yield. ^{1}H NMR (500 MHz, Chloroform-*d*) δ 4.12 (q, *J* = 7.1 Hz, 2H), 3.59 (t, *J* = 6.5 Hz, 2H), 2.29 (t, *J* = 7.6 Hz, 2H), 1.63 (p, *J* = 7.4 Hz, 2H), 1.51 (tq, *J* = 6.8, 3.3 Hz, 2H), 1.33 (p, *J* = 3.7 Hz, 4H), 1.25 (t, *J* = 7.1 Hz, 3H), 0.89 (s, 9H), 0.04 (s, 6H). ^{13}C NMR (126 MHz, $CDCl_3$) δ 173.9, 63.2, 60.2, 34.3, 32.7, 29.0, 26.0, 25.5, 25.0, 18.4, 14.3, -5.3 . IR (film cm^{-1}) 2930, 2857, 1737, 1253, 1096. HRMS: calcd for $C_{15}H_{32}O_3SiNa$ [M+Na] 311.2013, found 311.2016.

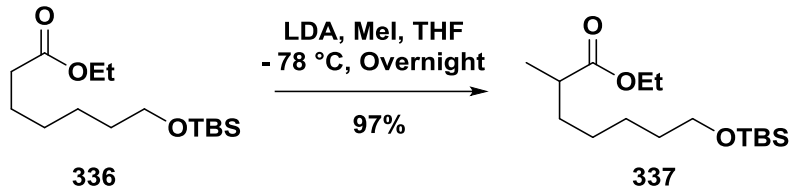

336 337

Ethyl 7-((*tert*-butyldimethylsilyl)oxy)-2-methylheptanoate (337): A solution of *i*-Pr_2NH (1.3 mL, 9.2 mmol, 1.3 equiv) in THF (15 mL) was treated with *n*-BuLi (1.6 M in hexane, 5.2 mL, 8.3 mmol, 1.2 equiv) at -78 °C, then cooled to 0 °C in an ice bath and stirred for 1 h. The solution was cooled back to -78 °C and a solution of ester **336** (2.00 g, 6.93 mmol, 1 equiv) in THF (10 mL) was added dropwise via cannula and stirred for 1h. MeI (0.57 mL, 9.2 mmol, 1.3 equiv) was added, and the reaction was stirred at -78 °C for 15 min then at 0 °C to room temperature overnight. The reaction mixture was quenched with saturated aqueous NH_4Cl (50 mL), extracted with EtOAc (3 x 50 mL). The combined organic extracts were washed with brine (50 mL), dried with anhydrous Na_2SO_4, and concentrated under reduced pressure. The crude residue was purified by chromatography on silica gel using 3% EtOAc:hexane as eluent to afford **337** as a colorless oil (2.03 g) in 97 % yield. ^{1}H NMR (500 MHz, Chloroform-*d*) δ 4.12 (q, *J* = 7.2 Hz, 2H), 3.59 (t, *J* = 6.5 Hz, 2H), 2.41 (h, *J* = 7.0 Hz, 1H), 1.72 – 1.58 (m, 1H), 1.54 – 1.47 (m, 2H), 1.45 – 1.36 (m, 4H), 1.25 (t, *J* = 7.1 Hz, 3H), 1.13 (d, *J* = 7.0 Hz, 3H), 0.89 (s, 9H), 0.04 (s, 6H). ^{13}C NMR (126 MHz, $CDCl_3$) δ 176.9, 63.2, 60.1, 39.5, 33.8, 32.7, 27.0, 26.0, 25.7, 18.4, 17.1, 14.3, -5.3. IR (film cm^{-1}) 2931, 2857, 1735, 1463, 1253, 1161, 1095. HRMS: calcd for $C_{16}H_{34}O_3SiNa$ [M+Na] 325.2169, found 325.2162.

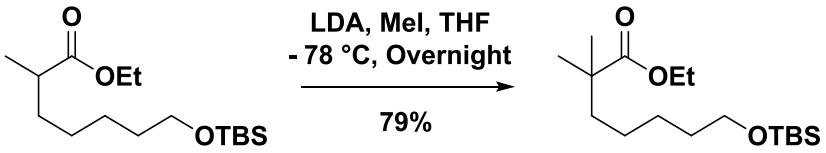

337 343

Ethyl 7-((*tert*-butyldimethylsilyl)oxy)-2,2-dimethylheptanoate (343): A solution of *i*-Pr_2NH (573 µL, 4.05 mmol, 1.4 equiv) in THF (10 mL) was treated with *n*-BuLi (1.6 M in hexane, 235 µL, 3.76 mmol, 1.3 equiv) at -78 °C, then cooled to 0 °C in an ice bath and stirred for 1 h. The solution was cooled back to -78 °C and a solution of ester **337** (0.876 g, 2.89 mmol, 1 equiv) in

THF (8 mL) was added dropwise via cannula and stirred for 1h. MeI (254 µL, 4.08 mmol, 1.41 equiv) was added, and the reaction was stirred at -78 °C for 15 min then at 0 °C to room temperature overnight. The reaction mixture was quenched with saturated aqueous NH_4Cl (25 mL), extracted with EtOAc (3 x 30 mL). The combined organic extracts were washed with brine (30 mL), dried with anhydrous Na_2SO_4, and concentrated under reduced pressure. The crude residue was purified by chromatography on silica gel using 3% EtOAc:hexane as eluent to afford **343** as a colorless oil (0.722 g) in 79 % yield. ^{1}H NMR (500 MHz, Chloroform-*d*) δ 4.11 (q, *J* = 7.1 Hz, 2H), 3.59 (t, *J* = 6.5 Hz, 2H), 1.54 – 1.46 (m, 4H), 1.35 – 1.18 (m, 7H), 1.15 (s, 6H), 0.89 (s, 9H), 0.04 (s, 6H). ^{13}C NMR (126 MHz, $CDCl_3$) δ 178.1, 63.2, 60.2, 42.1, 40.8, 32.7, 26.3, 26.0, 25.1, 24.7, 18.4, 14.3, -5.3. IR (film cm^{-1}) 2931, 2857, 1729, 1472, 1253, 1100. HRMS: calcd for $C_{17}H_{36}O_3SiNa$ [M+Na] 339.2326, found 339.2326.

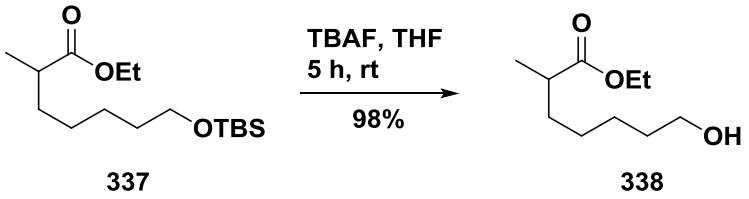

337 338

Ethyl 7-hydroxy-2-methylheptanoate (338): To a solution of ester **337** (900 mg, 2.97 mmol, 1 equiv) in THF (15 mL) was added TBAF (1M in THF, 6.7 mL, 6.7 mmol, 2.3 equiv), and the reaction was stirred at room temperature for 5 h at which point TLC analysis indicated complete consumption of the starting material. The mixture was diluted with EtOAc (50 mL) and water (50 mL), and it was extracted with EtOAc (3 x 30 mL). The combined organic extracts were washed with water (50 mL), brine (50 mL), dried with anhydrous Na_2SO_4, and concentrated under reduced pressure. The crude residue was purified by chromatography on silica gel using 2:1 EtOAc:hexane as eluent to give **338** as a light-yellow oil (535 mg) in 98% yield. ^{1}H NMR (500 MHz, Chloroform-*d*) δ 4.13 (q, *J* = 7.1 Hz, 2H), 3.64 (td, *J* = 6.5, 4.6 Hz, 2H), 2.50 – 2.33 (m, 1H), 1.67 (dddd, *J* = 13.2, 8.6, 7.7, 5.7, 1H), 1.61 – 1.51 (m, 2H), 1.48 – 1.20 (m, 9H), 1.14 (d, *J* = 7.0 Hz, 3H). ^{13}C NMR (126 MHz, $CDCl_3$) δ 176.9, 62.9, 60.1, 39.5, 33.7, 32.6, 27.00, 25.6, 17.1, 14.3. IR (film cm^{-1}) 3370, 2934, 2860, 1731, 1463, 1183, 1158. HRMS: calcd for $C_{10}H_{20}O_3SiNa$ [M+Na] 211.1305, found 211.1299.

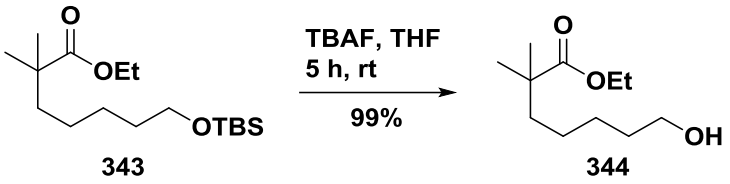

343 344

Ethyl 7-hydroxy-2,2-dimethylheptanoate (344): To a solution of ester **343** (716 mg, 2.26 mmol, 1 equiv) in THF (10 mL) was added TBAF (1M in THF, 5.1 mL, 5.1 mmol, 2.3 equiv), and the reaction was stirred at room temperature for 5 h at which point TLC analysis indicated complete consumption of the starting material. The mixture was diluted with EtOAc (50 mL) and water (50 mL), and it was extracted with EtOAc (3 x 30 mL). The combined organic extracts were washed with water (50 mL), brine (50 mL), dried with anhydrous Na_2SO_4, and concentrated under reduced pressure. The crude residue was purified by chromatography on silica gel using 2:1 EtOAc:hexane as eluent to give **344** as a light-yellow oil (450 mg) in 99% yield. ^{1}H NMR (500 MHz, Chloroform-*d*) δ 4.11 (q, *J* = 7.1 Hz, 2H), 3.63 (td, *J* = 6.6, 5.1 Hz, 2H), 1.61 – 1.48 (m, 4H), 1.38 – 1.29 (m, 2H), 1.29 – 1.19 (m, 6H), 1.16 (s, 6H). ^{13}C NMR (126 MHz, $CDCl_3$) δ 178.0, 62.9, 60.2, 42.1, 40.6, 32.6, 26.2, 25.2, 24.7, 14.3.IR (film cm^{-1}) 3365, 2976, 2935, 1726, 1474, 1175, 1139. HRMS: calcd for $C_{11}H_{22}O_3SiNa$ [M+Na] 225.1461, found 225.1458.

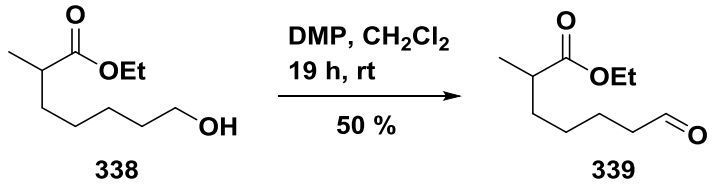

338 339

Ethyl 2-methyl-7-oxoheptanoate (339): To a solution of alcohol **338** (535 mg, 2.84 mmol, 1 equiv) in DCM (15 mL) was added DMP (1.8 g, 4.3 mmol, 1.5 equiv), and the reaction was stirred for 19 h at room temperature. The mixture was filtered through celite and concentrated under reduced pressure. The crude residue was purified by chromatography on silica gel using 20% EtOAc:hexane as eluent to afford **339** as a colorless liquid (266 mg) in 50 % yield. ^{1}H NMR (500 MHz, Chloroform-*d*) δ 9.76 (t, *J* = 1.7 Hz, 1H) 4.12 (q, *J* = 7.1 Hz, 2H), 2.48 – 2.38 (m, 3H), 1.75 – 1.57 (m, 3H), 1.49 – 1.28 (m, 3H), 1.25 (t, *J* = 7.1Hz, 3H), 1.14 (d, *J* = 7.0 Hz, 3H). ^{13}C NMR (126 MHz, $CDCl_3$) δ 202.5, 176.7, 60.2, 43.7, 39.4, 33.4, 26.8, 21.9, 17.1, 14.3. IR (film cm^{-1})

2977, 2938, 1725, 1463, 1377, 1158. HRMS: calcd for $C_{10}H_{18}O_3SiNa$ [M+Na] 209.1148, found 209.1146.

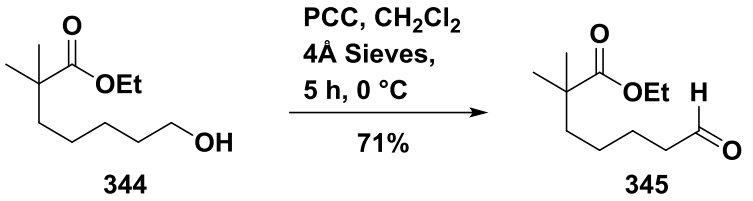

344 345

Ethyl 2,2-dimethyl-7-oxoheptanoate (345): To a suspension of PCC (950 mg, 4.41 mmol, 2 equiv) and 4 Å sieves (950 mg) in DCM (10 mL) cooled at 0 °C was added a solution of alcohol **344** (446 mg, 2.20 mmol, 1 equiv) *via* cannula, and the reaction was stirred for 5h at which point TLC analysis indicated complete consumption of the starting material. The mixture was filtered through a short pad of florisil, rinsed with DCM (100 mL), and the filtrate was concentrated under reduced pressure. The crude residue was purified by chromatography on silica gel using 20% EtOAc:hexane as eluent to afford **345** as a colorless liquid (313 mg) in 71% yield. ^{1}H NMR (500 MHz, Chloroform-*d*) δ 9.76 (t, *J* = 1.8 Hz, 1H), 4.11 (q, *J* = 7.1 Hz, 2H), 2.43 (td, *J* = 7.3, 1.8 Hz, 2H), 1.61 (p, *J* = 7.4 Hz, 2H), 1.57 – 1.49 (m, 2H), 1.31 – 1.21 (m, 5H), 1.15 (s, 6H). ^{13}C NMR (126 MHz, $CDCl_3$) δ 202.5, 177.8, 60.3, 43.7, 42.1, 40.3, 25.2, 24.6, 22.5, 14.3.IR (film cm^{-1}) 2977, 2939, 1722, 1175, 1137. HRMS: calcd for $C_{11}H_{20}O_3SiNa$ [M+Na] 223.1305, found 223.1294.

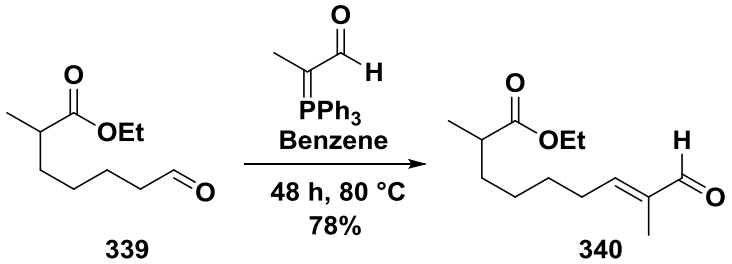

339 340

Ethyl (*E*)-2,8-dimethyl-9-oxonon-7-enoate (340): To a solution of aldehyde **339** (259 mg, 1.39 mmol, 1 equiv) in benzene (9 mL) was added 2-(triphenylphosphoranylidene)propionaldehyde (531 mg, 1.67 mmol, 1.2 equiv), and the mixture was stirred under reflux for 48 h. The reaction mixture was concentrated under reduced pressure and purified directly by chromatography on

silica gel using 1:1:6 EtOAc:Et_2O:Hexane as eluent to afford **340** as a colorless oil (247 mg) in 78% yield. ^{1}H NMR (500 MHz, Chloroform-*d*) δ 9.39 (s, 1H), 6.47 (td, *J* = 7.4, 1.5 Hz, 1H), 4.13 (q, *J* = 7.1 Hz, 2H), 2.47 – 2.28 (m, 3H), 1.77 – 1.63 (m, 4H), 1.55 – 1.30 (m, 5H), 1.25 (t, *J* = 7.1 Hz, 3H), 1.15 (d, *J* = 7.0 Hz, 3H). ^{13}C NMR (126 MHz, $CDCl_3$) δ 195.3, 176.7, 154.5, 139.5, 60.2, 39.5, 33.5, 28.8, 28.3, 26.7, 17.2, 14.3, 9.2.IR (film cm^{-1}) 2976, 2936, 2860, 1730, 1685, 1463, 1181, 1155. HRMS: calcd for $C_{13}H_{22}O_3Na$ [M+Na] 249.1461, found 249.1451.

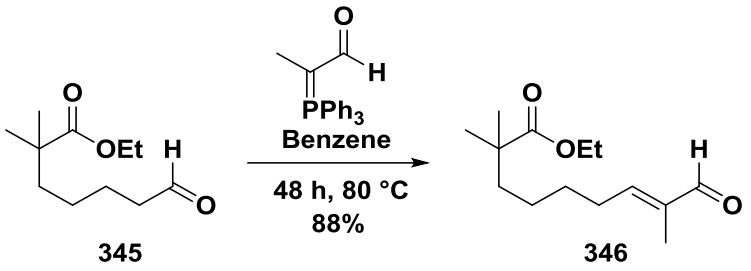

Ethyl (*E*)-2,2,8-trimethyl-9-oxonon-7-enoate (346): To a solution of aldehyde **345** (310 mg, 1.55 mmol, 1 equiv) in benzene (10 mL) was added 2-(triphenylphosphoranylidene)propionaldehyde (591 mg, 1.86 mmol, 1.2 equiv), and the mixture was stirred under reflux for 48 h. The reaction mixture was concentrated under reduced pressure and purified directly by chromatography on silica gel using 1:1:6 EtOAc:Et_2O:Hexane as eluent to afford **346** as a colorless oil (316 mg) in 88% yield. ^{1}H NMR (500 MHz, Chloroform-*d*) δ 9.39 (s, 1H), 6.47 (td, *J* = 7.4, 1.4 Hz, 1H), 4.11 (q, *J* = 7.1 Hz, 2H), 2.44 – 2.23 (m, 2H), 1.74 (q, *J* = 0.9 Hz, 3H), 1.57 – 1.42 (m, 4H), 1.34 – 1.20 (m, 5H), 1.16 (s, 6H). ^{13}C NMR (126 MHz, $CDCl_3$) δ 195.3, 177.9, 154.6, 139.4, 60.3, 42.1, 40.40, 28.9, 28.8, 25.2, 24.7, 14.3, 9.2. IR (film cm^{-1}) 2976, 2937, 1724, 1686, 1173, 1150. HRMS: calcd for $C_{14}H_{24}O_3Na$ [M+Na] 263.1618, found 263.1610.

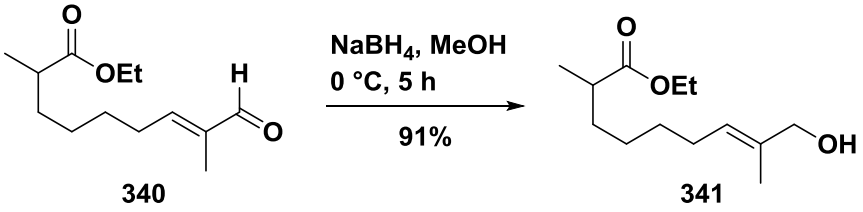

Ethyl (*E*)-9-hydroxy-2,8-dimethylnon-7-enoate (341): To a solution of enal **340** (242 mg, 1.07 mmol, 1 equiv) in MeOH (6 mL) cooled at 0°C was added $NaBH_4$ (44.5 mg, 1.17 mmol, 1.1 equiv), and the reaction was stirred for 5h at room temperature. The reaction mixture was quenched with saturated aqueous NH_4Cl (20 mL) and extracted with ethyl acetate (3 x 20 mL). The combined organic extracts were washed with brine, dried with anhydrous Na_2SO_4 and concentrated under reduced pressure. The crude residue was purified by chromatography on silica gel using 25% EtOAc:Hexane as eluent to afford **341** as a colorless oil (222 mg) in 91% yield. ^{1}H NMR (500 MHz, Chloroform-*d*) δ 5.39 (tq, *J* = 7.2, 1.4 Hz, 1H) 4.13 (qd, *J* = 7.2, 0.8 Hz, 2H), 4.00 (dd, *J* = 6.1, 1.1 Hz, 2H), 2.54 – 2.30 (m, 1H), 2.10 – 1.93 (m, 2H), 1.66 (d, *J* = 1.2 Hz, 4H), 1.47 – 1.23 (m, 9H), 1.14 (d, *J* = 6.9 Hz, 3H). ^{13}C NMR (126 MHz, $CDCl_3$) δ 176.9, 134.8, 126.3, 69.1, 60.1, 39.5, 33.7, 29.3, 27.4, 26.9, 17.1, 14.3, 13.7. IR (film cm^{-1}) 3421, 2976, 2933, 2857, 1732, 1462, 1377, 1181, 1155. HRMS: calcd for $C_{13}H_{24}O_3Na$ [M+Na] 251.1618, found 251.1612.

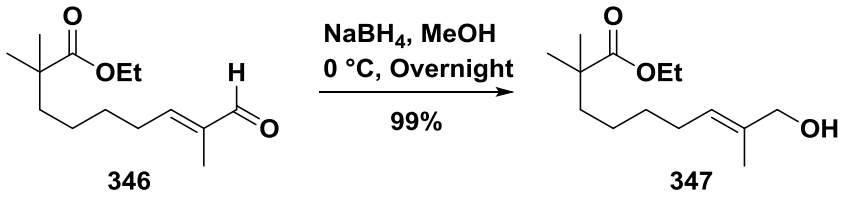

346 347

Ethyl (*E*)-9-hydroxy-2,2,8-trimethylnon-7-enoate (347): To a solution of enal **346** (313 mg, 1.30 mmol, 1 equiv) in MeOH (7 mL) cooled at 0°C was added $NaBH_4$ (54.2 mg, 1.43 mmol, 1.1 equiv), and the reaction was stirred overnight at room temperature. The reaction mixture was quenched with saturated aqueous NH_4Cl (20 mL) and extracted with ethyl acetate (3 x 20 mL). The combined organic extracts were washed with brine, dried with anhydrous Na_2SO_4 and concentrated under reduced pressure. The crude residue was purified by chromatography on silica gel using 25% EtOAc:Hexane as eluent to afford **347** as a colorless oil (312 mg) in 99% yield. ^{1}H NMR (500 MHz, Chloroform-*d*) δ 5.39 (tq, *J* = 7.2, 1.4 Hz, 1H) 4.11 (q, *J* = 7.2 Hz, 2H), 4.00 (dd, *J* = 6.1, 1.2 Hz, 2H), 2.06 – 1.98 (m, 2H), 1.66 (d, *J* = 1.3 Hz, 3H), 1.54 – 1.47 (m, 2H), 1.38 – 1.29 (m, 2H), 1.29 – 1.19 (m, 6H), 1.15 (s, 6H). ^{13}C NMR (126 MHz, $CDCl_3$) δ 178.1, 134.8,

126.3, 69.1, 60.2, 42.2, 40.6, 29.9, 27.5, 25.2, 24.6, 14.3, 13.7. IR (film cm^{-1}) 3431, 2976, 2934, 2858, 1727, 1174, 1149. HRMS: calcd for $C_{14}H_{26}O_3Na$ [M+Na] 265.1774, found 265.1770.

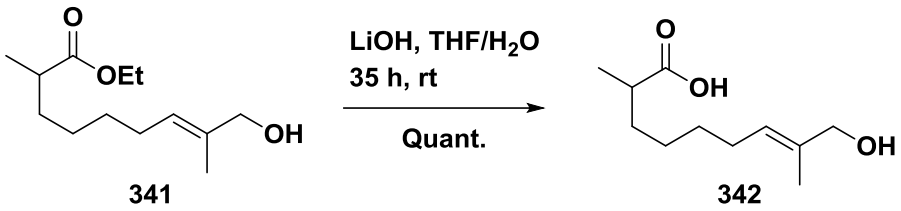

341 342

***(E)*-9-hydroxy-2,8-dimethylnon-7-enoic acid (342)**: To a solution of alcohol **341** (220 mg, 0.964 mmol, 1 equiv) in THF/H_2O (1:1, 4.8 mL) was added lithium hydroxide monohydrate (323 mg, 7.71 mmol, 8.0 equiv) and stirred for 35h at room temperature. The biphasic mixture was separated, and the aqueous layer was washed with Et_2O (30 mL) and made acidic to pH 2~3 with 1M HCl solution. The mixture was extracted with EtOAc (3 x 25 mL), washed with brine, dried with anhydrous Na_2SO_4 and concentrated under reduced pressure. The crude residue was purified by chromatography on silica gel using 2:1 acetone:hexane as eluent to afford **342** as a colorless oil (193 mg) in quantitative yield. ^{1}H NMR (500 MHz, Chloroform-*d*) δ 5.40 (tq, *J* = 7.3, 1.4 Hz, 1H) 4.00 (d, *J* = 1.1 Hz, 2H), 2.47 (h, *J* = 6.9 Hz, 1H), 2.04 (q, *J* = 7.0 Hz, 2H), 1.75 – 1.58 (m, 4H), 1.51 – 1.25 (m, 6H), 1.18 (d, *J* = 7.0 Hz, 3H). ^{13}C NMR (126 MHz, $CDCl_3$) δ 181.1, 134.8, 126.3, 69.1, 39.1, 33.4, 29.2, 27.3, 26.7, 16.9, 13.7. IR (film cm^{-1}). 3250, 2931, 2858, 1703, 1463, 1121. HRMS: calcd for $C_{11}H_{20}O_3Na$ [M+Na] 223.1305, found 223.1292.

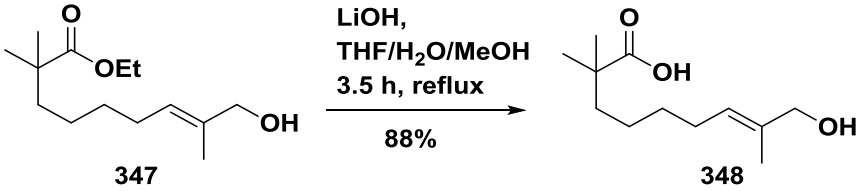

347 348

(*E*)-9-hydroxy-2,2,8-trimethylnon-7-enoic acid (348): To a solution of alcohol **347** (306 mg, 1.26 mmol, 1 equiv) in THF/H_2O/MeOH (2:1:1, 5 mL) was added lithium hydroxide monohydrate (159 mg, 3.79 mmol, 3.0 equiv) and stirred for 3.5h under reflux. The biphasic mixture was separated, and the aqueous layer was washed with Et_2O (30 mL) and made acidic to pH 2~3 with 1M HCl solution. The mixture was extracted with EtOAc (3 x 25 mL), washed with brine, dried

with anhydrous Na_2SO_4 and concentrated under reduced pressure. The crude residue was purified by chromatography on silica gel using 2:1 acetone:hexane as eluent to afford **348** as a colorless oil (237 mg) in 88% yield. ^{1}H NMR (500 MHz, Chloroform-*d*) δ 5.39 (ddq, *J* = 7.2, 5.7, 1.4 Hz, 1H) 4.00 (d, *J* = 1.2 Hz, 2H), 2.04 (q, *J* = 7.2 Hz, 2H), 1.66 (d, *J* = 1.3 Hz, 3H), 1.59 – 1.47 (m, 2H), 1.42 – 1.23 (m, 5H), 1.19 (s, 6H). ^{13}C NMR (126 MHz, $CDCl_3$) δ 183.1, 134.8, 126.3, 69.1, 42.1, 40.4, 29.8, 27.3, 25.0, 13.7. IR (film cm^{-1}) 3254, 2933, 2859, 1697, 1187, 1002. HRMS: calcd for $C_{12}H_{22}O_3Na$ [M+Na] 237.1461, found 237.1452.

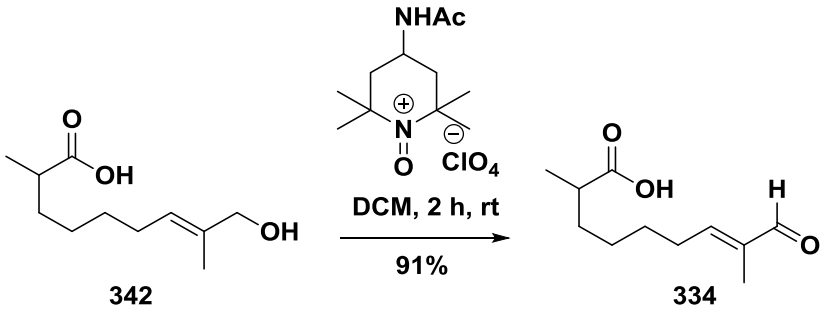

(*E*)-2,8-dimethyl-9-oxonon-7-enoic acid (334): To a solution of alcohol **342** (190 mg, 0.949 mmol, 1 equiv) in DCM (7 mL) was added 4-(acetylamino)-2,2,6,6-tetramethyl-1-oxo-piperidinium perchlorate (445 mg, 1.42 mmol, 1.5 equiv). The reaction was stirred at room temperature for 2 h at which point NMR aliquot indicated complete consumption of the starting material. The mixture was filtered through a short pad of sand rinsing with DCM, and the filtrate was concentrated under reduced pressure. The crude residue was purified by chromatography on silica gel using 2:1 Hexane:Acetone as eluent to afford **334** as a light-yellow oil (171 mg) in 91 % yield. ^{1}H NMR (500 MHz, Chloroform-*d*) δ 10.63 (s, 1H), 9.40 (s, 1H), 6.48 (tq, *J* = 7.4, 1.4 Hz, 1H), 2.48 (h, *J* = 6.9, 6.5 Hz, 1H), 2.41 – 2.31 (m, 2H), 1.80 – 1.65 (m, 4H), 1.59 – 1.35 (m, 5H), 1.20 (d, *J* = 7.0 Hz, 3H). ^{13}C NMR (126 MHz, $CDCl_3$) δ 195.3, 181.6, 154.4, 139.5, 39.1, 33.2, 28.8, 28.3, 26.9, 16.9, 9.2. IR (film cm^{-1}) 2932, 2860, 1703, 1683, 1463, 1233. HRMS: calcd for $C_{11}H_{18}O_3Na$ [M+Na] 221.1148, found 221.1146.

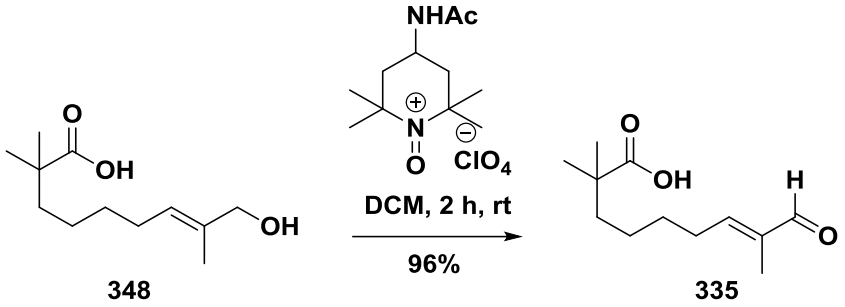

(*E*)-2,2,8-trimethyl-9-oxonon-7-enoic acid (335): To a solution of alcohol **348** (235 mg, 1.09 mmol, 1 equiv) in DCM (10 mL) was added 4-(acetylamino)-2,2,6,6-tetramethyl-1-oxo-piperidinium perchlorate (514 mg, 1.64 mmol, 1.5 equiv). The reaction was stirred at room temperature for 2 h at which point NMR aliquot indicated complete consumption of the starting material. The mixture was filtered through a short pad of sand rinsing with DCM, and the filtrate was concentrated under reduced pressure. The crude residue was purified by chromatography on silica gel using 2:1 Hexane:Acetone as eluent to afford **335** as a light-yellow oil (226 mg) in 96 % yield. ^{1}H NMR (500 MHz, Chloroform-*d*) δ 9.40 (s, 1H), 6.48 (tq, *J* = 7.4, 1.4 Hz, 1H), 2.42 – 2.28 (m, 2H), 1.74 (q, *J* = 1.0 Hz, 3H), 1.61 – 1.45 (m, 4H), 1.40 -1.29 (m, 2H), 1.21 (s, 6H). ^{13}C NMR (126 MHz, $CDCl_3$) δ 195.3, 183.0, 154.5, 139.5, 42.0, 40.2, 28.8, 28.8, 25.0, 24.7, 9.2. IR (film cm^{-1}) 2937, 2862, 1730, 1686, 1475, 1192. HRMS: calcd for $C_{12}H_{20}O_3Na$ [M+Na] 235.1305, found 235.1294.

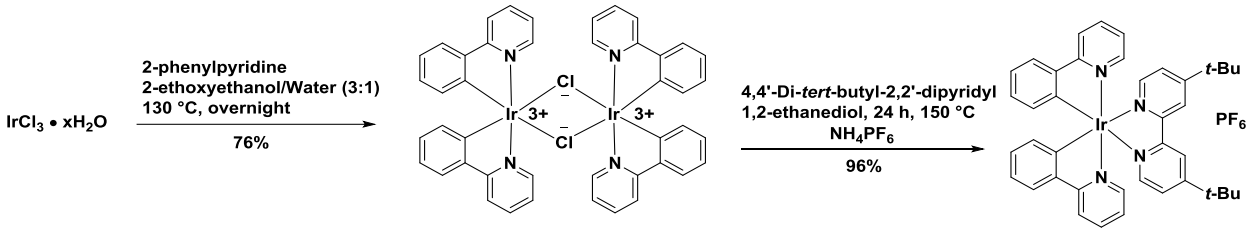

(4,4'-di-*tert*-butyl-2,2'-bipyridine)bis(2-(2-pyridinyl)phenyl)Iridium(III) hexafluorophosphate (307): A solution of iridium trichloride hydrate (0.200 g, 0.567 mmol, 1 equiv) and 2-phenylpyridine (0.220 g, 1.42 mmol, 2.5 equiv) in 2-ethoxyethanol/water (3:1, 16 mL) was refluxed at 130 °C overnight. After the mixture was cooled to room temperature, the yellow filtrate was collected by filtration and rinsed with absolute ethanol (25 mL). The resulting yellow solids were collected and dried under high vacuum (< 0.1 mmHg) overnight to afford $[Ir(ppy)_2Cl]_2$ (0.271 g) in 76% yield which was used for the next step without further purification.

A solution of $[Ir(ppy)_2Cl]_2$ (0.271 g, 0.253 mmol, 1 equiv) and 4,4'-di-*tert*-butyl-2,2'-dipyridyl (0.149 g, 0.556 mmol, 2.2 equiv) in 1,2-ethanediol (12.5 mL) was refluxed for 24 h at 150 °C. After the mixture was cooled to room temperature, water (150 mL) was added. The solution was washed with diethyl ether (3 x 50 mL). The aqueous layer was heated to 70 °C to remove trace diethyl ether, and NH_4PF_6 in water (10 mL) was added to the solution. The mixture was stirred at room temperature for 1h, and the yellow precipitate was collected by filtration, dried in vacuo and recrystallized by vapor diffusion with acetonitrile and diethyl ether to afford **307** as a yellow prism (0.45 g) in 96% yield. The spectroscopic data is in agreement with that published in the literature[114].

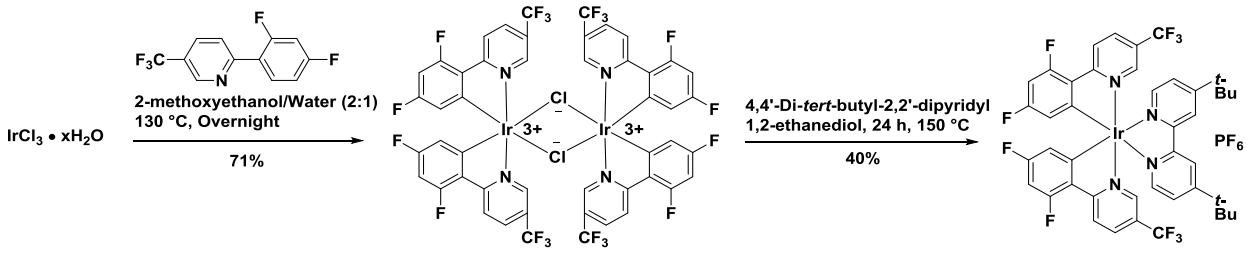

(4,4'-Di-*tert*-butyl-2,2'-bipyridine)bis[3,5-difluoro-2-[5-trifluoromethyl-2-pyridinyl-kN)phenyl-kC]iridium(III) hexafluorophosphate (332):

A solution of iridium trichloride hydrate (0.200 g, 0.567 mmol, 1 equiv) and 2-(2,4-difluorophenyl)-5-(trifluoromethyl)pyridine (390 mg, 1.51 mmol, 2.25 equiv) in 2-methoxyethanol/water (2:1, 13.5 mL) was refluxed at 130 °C overnight. After the mixture was cooled to room temperature, the yellow filtrate was collected by filtration and rinsed with water (3 x 20 mL) and hexane (3 x 10 mL). The resulting yellow solids were collected and dried under high vacuum (< 0.1 mmHg) overnight to afford $[Ir(dF(CF_3)ppy_2Cl]_2$ (0.353 g) in 71% yield which was used for the next step without further purification.

A solution of $[Ir(dF(CF_3)ppy_2Cl]_2$ (0.353 g, 0.237 mmol, 1 equiv) and 4,4'-di-*tert*-butyl-2,2'-dipyridyl (0.142 g, 0.529 mmol, 2.22 equiv) in 1,2-ethanediol (12.5 mL) was refluxed for 24 h at 150 °C. After the mixture was cooled to room temperature, water (250 mL) was added. The solution was washed with hexane (3 x 60 mL). The aqueous layer was heated to 70 °C to remove trace hexane, and NH_4PF_6 in water (10 mL) was added to the solution. The mixture was stirred at

room temperature for 1h, and the yellow precipitate was collected by filtration, dried in vacuo and recrystallized by vapor diffusion with acetone and pentane to afford **332** as a yellow powder (0.236 g) in 40% yield. The spectroscopic data is in agreement with that published in the literature[115].

General procedure (B) for photocatalytic reductive cyclization:

A flame-dried 10 mL Schlenk tube was charged with the enal **287** (50 mg, 0.25 mmol, 1 equiv), photocatalyst ($Ru(bpy)_3Cl_2 \cdot 6H_2O$ or $[Ir(ppy)_2(dtb\text{-}bpy)][PF_6]$, 0.00637 mmol, 0.025 equiv), HCO_2H (2.0 – 5.0 equiv), terminal reductant (1.5 – 10.0 equiv), with or without methyl 1,2-diazepane-1-carboxylate (0.5 equiv) and acetonitrile (0.05 M) and degassed in the dark using three freeze/pump/thaw cycles under argon. Then the reaction was stirred in a water bath at room temperature and irradiated with 26 W compact fluorescent lamp. Upon completion of reaction, the solvent was evaporated under reduced pressure and the residue purified by chromatography on silica gel using 20% EtOAC:Hexane as eluent to give the cyclized product **292** as a colorless oil in mixture of two inseparable diastereomers.

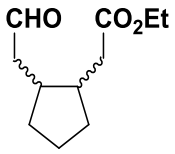

292

Ethyl 2-(2-(2-oxoethyl)cyclopentyl)acetate (292): Prepared according to general procedure using 100 mg (0.509 mmol) ethyl (2*E*,7*E*)-9-oxonona-2,7-dienoate, 11.6 mg (0.0127 mmol) $[Ir(ppy)_2(dtb\text{-}bpy)][PF_6]$, 96 µL (2.5 mmol) HCO_2H, 887 µL *i*-Pr_2NEt (5.09 mmol), 10 mL acetonitrile and irradiated for 3 h. The crude residue was purified by chromatography on silica gel using 20% EtOAc:hexane as eluent to give cycloadduct **292** (64.5 mg) in 64% yield. ^1H NMR (500 MHz, Chloroform-*d*) δ 9.77 – 9.74 (m, 1H), 4.16 – 4.08 (m, 2H), 2.61 (ddd, *J* = 16.6, 4.2, 1.7 Hz, 1H), 2.48 – 2.41 (m, 1H), 2.38 – 2.30 (m, 1H), 2.28 – 2.18 (m, 1H), 2.02 – 1.77 (m, 4H), 1.63 (ddt, *J* = 9.0, 8.1, 5.5 Hz, 2H), 1.38 – 1.22 (m, 5H). For major diastereomer: ^{13}C NMR (126 MHz, $CDCl_3$) δ 202.3, 173.0, 60.3, 49.0, 42.0, 39.6, 39.2, 32.2, 31.9, 23.5, 14.3. IR (film cm^{-1}) 2949, 2871, 1721, 1175, 1029. HRMS: calcd for $C_{11}H_{19}O_3$ [M+H] 199.1328 found 199.1329.

4.5 References

112. Friedrich, M., et al. (2003). European Journal of Organic Chemistry **2003**(11): 2138-2143.

113. Ballini, R., et al. (1991). Synthetic Communications **21**(8-9): 1075-1081.

114. Kim, S., et al. (2016). Chemical Science **7**(1): 85-88.

115. Vasu, D., et al. (2019). Chemical Science **10**(11): 3401-3407.